MIDDLE ATMOSPHERE ELECTRODYNAMICS

Report
of
The Workshop on the Role of the
Electrodynamics of the Middle
Atmosphere on Solar Terrestrial Coupling

Reston, Virginia
January 17-19, 1979

Edited by

Nelson C. Maynard
Electrodynamics Branch
Goddard Space Flight Center
Greenbelt, Maryland 20771

June 1979

NATIONAL AERONAUTICS AND SPACE ADMINISTRATION

CONTENTS

CONTENTS (continued)

MIDDLE ATMOSPHERE ELECTRODYNAMICS (MAE)

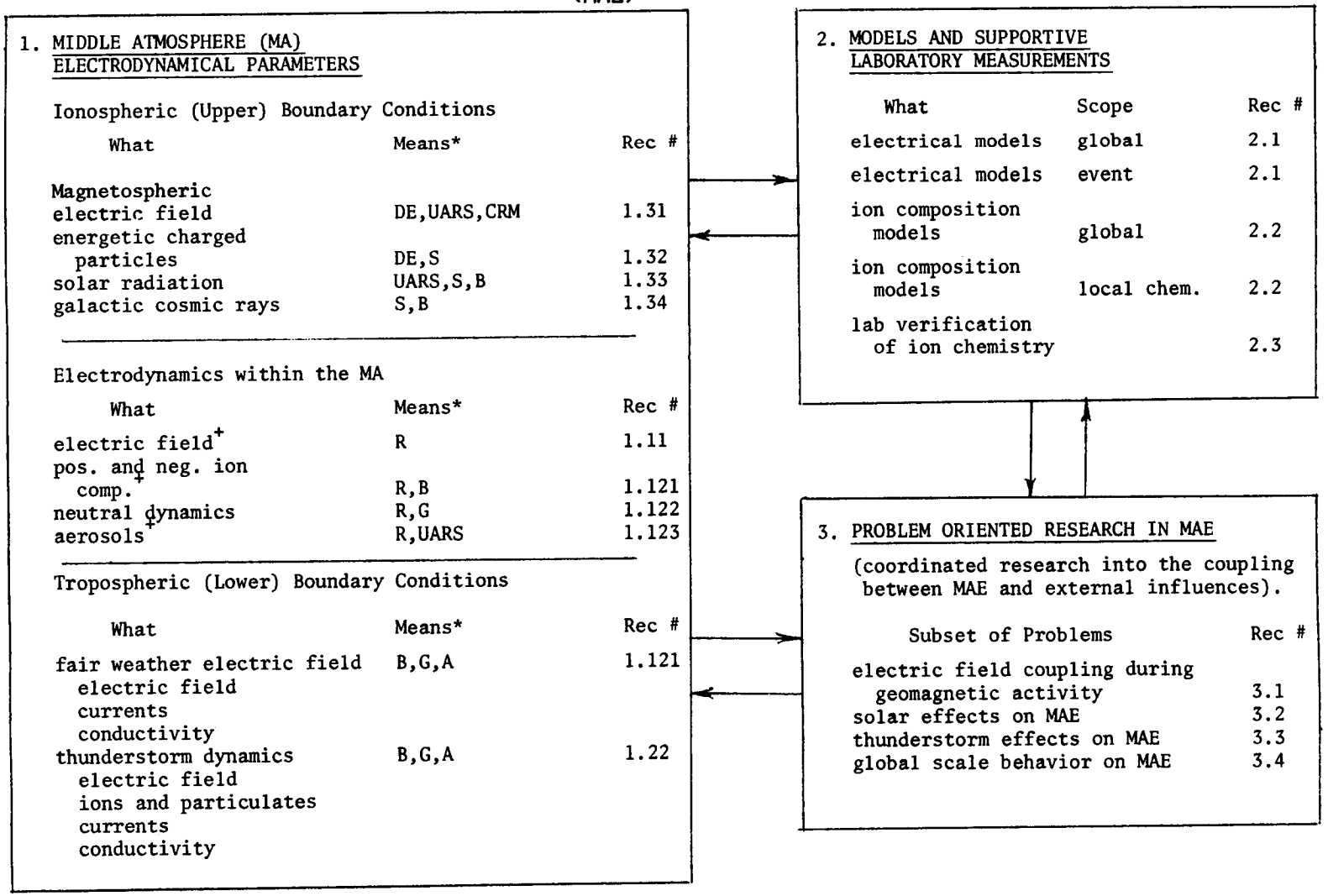

+new measurement techniques or significant improvements in techniques required

*R-sounding rocket, B-balloon, G-ground based, A-aircraft, S-satellite. Specific satellites: DE-Dynamics Explorer, UARS-Upper Atmosphere Research Satellite, CRM-Chemical Release Module.

MIDDLE ATMOSPHERE ELECTRODYNAMICS

Summary

Significant deficiencies exist in our present understanding of the basic physical processes taking place within the middle atmosphere (the region between the tropopause and the mesopause), and in our knowledge of the variability of many of the primary parameters that regulate Middle Atmosphere Electrodynamics (MAE). Knowledge of the electrical properties, i.e., electric fields, plasma characteristics, conductivity and currents, and the physical processes that govern them is of fundamental importance to the physics of the region. Middle atmosphere electrodynamics may play a critical role in the electrodynamical aspects of solar-terrestrial relations. The time is ripe to initiate a coordinated assault on these problems with fresh approaches and renewed vigor. As a first step, the Workshop on the Role of the Electrodynamics of the Middle Atmosphere on Solar-Terrestrial Coupling was held in Reston, Virginia, on January 17-19, 1979, to review the present status and define recommendations for future MAE research.

The interest in this research discipline is rapidly broadening as is evidenced by the participation of more than 80 scientists in the three-day Workshop. A comprehensive and feasible direction is presented in the concensus recommendations. The fact that the middle atmosphere can have significant impact on our environment is exemplified by the recent attention to the ozone balance. The electrodynamics of the middle atmosphere needs to be investigated systematically making best use of the parallel programs.

The summary chart on the opposite page outlines the recommendations. The recommendation numbers (abbreviated as Rec #) refer to sections in Chapter III and the "Means" are the Workshop's choice of the best platforms from which to perform the measurements.

As is indicated in the summary chart, the recommended investigations are grouped into three major parts, all interrelated. Part 1 on middle atmosphere electrodynamical parameters emphasizes measurements that will fill gaps in our basic knowledge. Instrument development is needed in several of these areas. In parallel with the new measurement efforts, models need to be developed and evolved (Part 2). Part 3 requires simultaneous coordinated measurements performed in several different regions to explore coupling phenomena. Only a representative subset of the problems is given in the chart. As the measurement capabilities are developed, more coupling investigations will become practical and scientifically valuable. Implementation of each part will be an iterative process as new information in one area generally places new requirements on other areas.

The next five to seven year period is an auspicious time for augmentation of research in this area. During this period MAP (Middle Atmosphere Program) will extensively study the properties and dynamics of the neutral middle atmosphere, DE (Dynamics Explorer) will investigate magnetosphere-ionosphere-atmosphere coupling, and UARS (Upper Atmosphere Research Satellite) will sense remotely on a global basis middle atmosphere parameters affecting the chemistry, energetics

and dynamics of the region. MAE complements each of these efforts. The present program can be merged with those efforts according to the following schedule:

a. Develop new techniques and improve existing techniques to measure middle atmosphere electrodynamical parameters (1980-1982).

b. Develop models of the coupled electrical system and of the ion composition and chemistry on local event scales and global scales. (1980-1986).

c. Investigate the coupling of middle atmosphere electrodynamics to external influences emphasizing electrical fields. Many of these investigations will be coordinated with DE which will be launched in the summer of 1981. (1981-1983).

d. Examine the role of current carriers in the electrodynamic coupling of the middle atmosphere to external influences, emphasizing ion composition and chemistry in the investigation. Coordination with MAP (1983-1985) and with UARS (planned launches in 1983 and 1984) will be important. (1983-1986).

MIDDLE ATMOSPHERE ELECTRODYNAMICS

Report
of
The Workshop on the Role of the
Electrodynamics of the Middle
Atmosphere on Solar Terrestrial Coupling

I. INTRODUCTION

The middle atmosphere, which is defined as the region bounded below by the tropopause near 10 km and above by the mesopause near 90 to 100 km, has long been regarded as a passive medium through which electric fields and currents are transmitted from sources above and below. However, there are insufficiences in our knowledge of the physical processes and parameters which govern the electrodynamics of this region. Recent attempts to measure electric fields within this region even bring into question the assumption of passivity. These attempts, in conjunction with renewed interest in electrical mechanisms for solar-terrestrial coupling, have created an impetus to understand middle atmosphere electrodynamics (MAE).

The electrodynamics of the middle atmosphere are known to be affected from above and below by solar protons, cosmic rays and other ionization sources, by thunderstorms and the fair-weather electric field, and by magnetospherically and ionospherically generated electric fields. The nature of these effects has to some degree been modeled; however, measurements to verify and improve models are sparce since the bulk of this region is above balloon altitudes and below satellite altitudes and the measurement techniques are difficult. The deficiencies in our understanding of middle atmosphere electrodynamics and its interaction with neighboring regions now limit the scope of solar-terrestrial coupling processes that can be studied. We ought to understand these relationships well enough to determine if they are important in solar-weather relations.

The diversity of inputs across the boundaries to the middle atmosphere that affect middle atmosphere electrodynamics requires the amalgamation of many disciplines in a coordinated effort in order to examine the problems comprehensively. This in turn makes the next five to seven year period a propitious time to attack these questions. During this period under the aegis of MAP (Middle Atmosphere Program), research will be conducted to (1) determine the structure and composition of the atmosphere with special attention being paid to minor species, (2) determine the interaction of radiation from the Sun, the Earth and the atmosphere with the middle atmosphere and (3) investigate motions on all scales within the middle atmosphere and monitor them on a continuing basis (see MAP Planning Document). The DE (Dynamics Explorer) satellites will be launched to study the coupling between the magnetosphere, the ionosphere and the upper atmosphere. In addition under the planned UARS (Upper Atmosphere Research Satellite) program, parameters (especially neutral) in the middle atmosphere and above will be remotely sensed on a global basis from a

series of satellites to study the chemistry, energetics and dynamics of those regions. A study of the electrodynamics of the middle atmosphere complements each of these efforts.

With the above rationale as a foundation, a workshop was convened at Reston, Virginia, on January 17-19, 1979, to establish a consensus on what problems are most important in the area of middle atmosphere electrodynamics and what approaches might best be adopted to solve them.

It was hoped that the MAE workshop would also:

- Determine outstanding research needs in the area of middle atmosphere electrodynamics related to the solar-terrestrial coupling.

- Assess the importance of middle atmosphere electric fields and currents in solar-terrestrial relations.

- Improve communication among researchers knowledgeable about individual aspects of middle atmosphere electrodynamics and associated physics.

The meeting program, program committee, review panel, and attendees are given in Appendix B. The Workshop was sponsored by the National Aeronautics and Space Administration's Space Plasma Physics Programs Office. Participation was open to anyone.

In parallel with this Workshop the Workshop on the need for Lightning Observations from Space was held February 13-15, 1979, under the sponsorship of NASA's Office of Space and Terrestrial Applications (NASA CP-2083). Investigations of lightning are useful to middle atmosphere electrodynamics in that they address the problems of understanding the electric field source at the lower boundary of the middle atmosphere. At the MAE Workshop the topic of lightning observations was therefore referred to their expertise.

Recommendations relative to outstanding research needs in middle atmosphere electrodynamics were discussed, drafted and agreed upon in principle at the MAE Workshop. A select panel was convened at the Workshop to review the recommendations relative to worth, appropriateness, balance and completeness. The recommendations presented in Chapter III of this report are an edited version of the drafts reflecting the meeting concensus. The editing of the recommendations was done with the concurrence and assistance of the select panel and the session chairmen.

In order to acquaint scientists from diverse backgrounds with the manifold scope of middle atmosphere electrodynamics a series of tutorial lectures was presented. Each of these papers is presented in Appendix A as a review of the present status of knowledge. A synopsis of background information most pertinent to the Workshop recommendations is given in Chapter II. For more information and references on any particular topic in Chapter II, the reader is referred to the appropriate review paper in Appendix A.

II. SCIENTIFIC BACKGROUND

1.0 SOURCES OF MIDDLE ATMOSPHERE ELECTRIC FIELDS

The major generators in the Earth's atmosphere are found in the troposphere and in the ionosphere/magnetosphere. In the troposphere, the most important generator is thunderstorm activity, although some contributions are also made by volcanoes, dust storms, blowing snow, etc. An average of about 2000 thunderstorms that are active over the globe at any given time drive electric currents upward into the middle atmosphere and maintain it at an average potential of some 300 kV with respect to the Earth. The current path is closed by downward flow in fair-weather regions and lateral flow along the Earth's surface to the origin. The fair-weather atmospheric electric field associated with the downward current flow is inversely related to the atmospheric conductivity and is typically a few hundred volts per meter near the Earth's surface. In the typical description of the "global circuit", it has been general practice to regard the upper atmosphere above ~60 km altitude as a perfect conductor, since the conductivity there is about 4 orders of magnitude greater than the conductivity at cloud altitudes. In this picture tropospheric electric fields do not penetrate this "perfect" conductor, which has been referred to as the electrosphere or the potential equalizing layer. However, this picture is now known to be incorrect.

For example, recent model calculations using more realistic upper boundary conditions show that horizontal fields up to ~1 mV/m can be expected in the ionosphere over large thunderstorms, as a result of these storms, and also in the conjugate ionosphere. (Above ~90 km, geomagnetic field lines may be regarded as equipotentials transmitting large scale electric fields from hemisphere to hemisphere with little attenuation.) These fields are comparable in magnitude to the fields generated within the ionosphere by dynamo action from neutral winds in the lower thermosphere dragging ions across magnetic field lines and would be important in troposphere/ionosphere coupling. Calculated field strengths, however, are subject to large uncertainties due to uncertainties in the modeling of middle atmosphere parameters.

In the ionosphere, the above dynamo generates electric fields of the order of 1 mV/m, which, when integrated over the characteristic distance, yields a horizontal potential drop of the order of 30 kV. A stronger and more variable source of electric field is the solar wind interaction with the magnetosphere. Horizontal electric fields of 10 to 100 mV/m exist in the polar cap and auroral ionosphere, and the total potential drop across the polar cap ionosphere may vary from 20 to 200 kV. These fields of magnetospheric origin are strongest in the high latitude regions and diminish to 1-10 mV/m in the middle latitudes.

It has long been accepted that the ionosphere and the magnetosphere were closely coupled and that a complete electrical circuit must include generators and loads in both regions. However, coupling of these regions to the middle and lower atmospheres has not been considered important until recently.

It is now recognized theoretically that large scale horizontal electric fields originating in the ionosphere and magnetosphere can map down to ~10 km altitude with little attenuation and that the accompanying variations in the ionospheric potential are directly reflected in the vertical atmospheric electric field all the way down to the Earth's surface. At high latitudes, magnetospheric modulation of fair-weather-atmospheric electric fields may be as large as 50 percent or more. Thus, solar activity induced disturbances can produce large electrical signals down to the ground. These effects need to be investigated carefully for herein may lie the elusive mechanism of coupling between solar activity induced processes and the tropospheric weather.

Although there has been increasing evidence for solar activity-weather correlations, skepticism remains because it is extremely difficult to explain such correlations. Two of the more serious difficulties lie in the facts that (1) the energy in solar activity induced processes is much smaller than the energy in weather processes, and (2) it is difficult for these disturbances to propagate down to the troposphere. The second difficulty can be circumvented by invoking electrical coupling as mentioned previously. The first difficulty, however, still remains in spite of recent attempts to invoke "trigger" mechanisms. For example, it has been suggested that the modulation of the atmospheric electric field by solar activity induced processes might control the initiation of thunderclouds. However, at present there is not even general agreement on the fundamental question of how thunderclouds become electrified.

Observational programs during the past decade have yielded a first-order description of spatial and temporal variations of ionospheric electric fields. There have been no systematic observations of the propagation of these electric fields into and through the middle atmosphere. Knowledge about middle atmosphere conductivity variations during solar activity induced events that are thought to affect electric field and current distributions on a global scale is meager.

In the past and in the above discussion, the middle atmosphere has been regarded as a passive medium through which electric fields and currents are transmitted from the sources above and below. However, there may be important electrodynamical effects within the middle atmosphere that have thus far been ignored. For example, exceptionally energetic thunderclouds are known to penetrate the tropopause. Strong electric fields around the tops of such clouds may have important effects on charged stratospheric aerosols. Recent measurements suggest that during geomagnetically quiet times large vertical electric fields may exist in the lower mesosphere. In addition, strong ionospheric electric fields that reach 100 mV/m during geomagnetic disturbances may produce significant Joule heating not only in the thermosphere as has been observed, but also in the upper mesosphere. These effects have not received much attention because of observational difficulties. A program dedicated to middle atmosphere electrodynamics should provide opportunities to explore these areas.

2.0 MIDDLE ATMOSPHERE PLASMA CHARACTERISTICS

Any understanding of the electrodynamics of the middle atmosphere requires a knowledge of the plasma and its behavior. The plasma is best defined through direct measurements of the positive and negative ion composition, charged particle densities, ionization sources and critical neutral

species. The in situ studies are conducted simultaneously with laboratory measurements of chemical rate constants, each effort driving the other until a self-consistent model is developed which can predict the observed time-dependent plasma behavior as a function of various sources of ionization.

2.1 ELECTRON CONCENTRATION

Electrons are the primary current carriers and constitute the majority of the negatively charged particles in the upper part of the middle atmosphere. The daytime electron concentration profile has a plateau near 500 electrons per cm^3 in the D region between 70 and 82 km and falls off rapidly below 70 km where negative ions start to become dominant. D-region electron densities vary significantly with changes in season, solar elevation, and sunspot activity. Variability in the sources of ionization (Section 2.5) can create up to two orders of magnitude change in the electron density at high latitudes. Those variations are of interest in radio propagation where reflection heights change with changing conditions.

Electron concentrations have been measured by a variety of techniques from both rocket and ground-based instrumentation. The most accurate measurements in the upper middle atmosphere have been derived from a combination of Faraday rotation, differential absorption, and Langmuir probe measurements on rockets. Ground-based radar measurements using partial reflection and incoherent scatter techniques have also been used. Below about 70 km densities are well below 100 electrons per cm^3 and comparison of reflection coefficients of several VLF waves provides the best method of measurement.

2.2 POSITIVE ION COMPOSITION

2.21 MEASUREMENTS

There exists now a body of rocket measurements of positive ion composition in and above the mesosphere between about 60 and 120 km made with pumped ion mass spectrometers. Rocket programs have been conducted to study diurnal variations, latitude effects and a number of disturbances, including solar proton events, aurora, relativistic electron precipitation, winter anomaly, solar eclipses, sporadic E, meteor showers and noctilucent clouds. The measurements have generally shown that the D region consists primarily of water cluster ions, $H_3O^+ (H_2O)_n$, which decrease rapidly above about 83 km in daytime and about 86 km in twilight or nighttime. Above these altitudes NO^+ and O_2^+ are dominant and meteoric ions, mainly Fe^+ and Mg^+, are present in a broad layer near 93 km and in more variable layers at greater heights. During highly disturbed conditions, NO^+ and O_2^+ ions predominate to much lower altitudes. The complexity of the D region may be appreciated by examining Tables I and II which list the species measured in the D region and possible identifications.

There are a number of difficulties associated with the measurements requiring improved instrumentation and techniques in the future. The measured relative abundances of the cluster ions are uncertain because fragmentation of these complex weakly bound ions occurs through thermodynamic breakup in the shock-heated layer or by energetic collisions from large ion draw-in potentials. To overcome these problems, subsonic measurements or the use of the conical sampling probes which

Table I
D-Region Positive Ion Species

AMU	SPECIES	AMU	SPECIES
19	$H_3{}^{16}O^+$	88±1	FeO_2^+
		*90	$FeO^+(H_2O)$
21	$H_3{}^{18}O^+$	91	$H_{11}O_5^+$
30	NO^+	92	$Fe^+(H_2O)_2, NO^+(H_2O)CO_2$
32	O_2^+	94	$Ni^+(H_2O)_2$
34	$^{16}O^{18}O^+$	96	$Ni^+(H_2O)_2$
		99	$H_7O_3^+(CO_2)$
39	$H_5{}^{16}O^{18}O^+$	100	Fe^+CO_2
46	NO_2^+	106	$FeO_2^+(H_2O)$
48	$NO^+(H_2O)$	108	$FeO^+(H_2O)_2$
50	$O_2^+(H_2O)$	109	$H_{13}O_6^+$
55	$H_7O_3^+$	110	$Fe^+(H_2O)_3$
58	$NO^+(N_2)$	112	?
60±1	?	118	$Fe^+(H_2O)CO_2$
63±1	$H_3O^+(CO_2), NO_2^+(H_2O), O_4^+$	124	$FeO_2^+(H_2O)_2$
66±1	$NO^+(H_2O)_2$	126	$FeO^+(H_2O)_3$
68	$O_2^+(H_2O)_2$	127	$H_{15}O_7^+$
72	FeO^+	128	$Fe^+(H_2O)_4$
73	HgO_4^+		
74	NO^+CO_2	137	$Fe^+(H_2O)_2CO_2$
80±2	$H_5O_2^+(CO_2)$, $NO^+(H_2O)(O_2)$		
84±1	$NO^+(H_2O)_3$		

*Masses above 90 amu uncertain by ± 1 or 2 amu.

Table II
Meteoric Atomic Ions

TABLE II: Meteoric Atomic Ions

AMU	SPECIES	AMU	SPECIES
23	Na^+	52	Cr^+
24		54	Fe^+
25	Mg^+	56	
26		55	Mn^+
27	Al^+	58	Ni^+
28	Si^+	60	
39	K^+	59	Co^+
41	K^+, $Na^+(H_2O)$	63	Cu^+
		65	
40			
42	Ca^+		
44			
48	Ti^+, SO^+		
51	Va^+		

attach the shockwave as well as lowered draw-in potentials have been attempted more recently with some success. However, it is still not certain that the problem has been totally solved since the larger cluster ions are so weakly bound. For this reason the upper ion mass limit is currently unknown. The measurements also suffer from inaccurate mass numbers due to insufficient sensitivity and mass resolution so that the ion identities are in doubt. This is seen to some extent in Table I, for masses greater than about 80 amu there is considerable uncertainty in the ion identities. The development of ion chemical models has been further hampered by inaccurate absolute ion concentrations, unknown temperature profiles and critical neutral species distributions.

In the upper stratosphere some preliminary measurements of the positive ion composition have recently been made with cryopumped balloon-borne ion mass spectrometers. In addition to the expected water cluster ions $H_3O^+ (H_2O)_n$, n = 1, 2, 3, 4, species identified as $H^+ (NaOH)_x (H_2O)_y$ where x = 1, 2, or 3 and y = 0, 1, 2, 3, or 4 yielding ten ion clusters from 41 to 139 amu were detected. The mass numbers were uncertain by plus or minus one to two amu and are clearly critical for proper ion identification. More stratospheric measurements are required with higher mass range and resolution and should be extended to include the lower stratosphere.

2.22 POSITIVE ION CHEMISTRY

The current status of D region theory is peculiar in that the highly disturbed D region can be modeled much more accurately (especially for nighttime) than the quiescent normal situation. This is simply because the chemistry of the disturbed case where O_2^+ is the precursor ion is well established and a reasonable model agreement with measurements has been accomplished. In quiet periods when presumably NO^+ is the primary ion it has long been a problem to find a fast reaction path to convert NO^+ to the observed water cluster ions. A scheme of clustering and switching reactions has been proposed (Appendix A: Figure 1, Ferguson) whereby $NO^+ \cdot N_2$ or $NO^+ \cdot CO_2$ is formed leading to $NO^+ (H_2O)$ and through fast switching reactions to $NO^+ (H_2O)_3$ which finally reacts exothermically with water to yield $H_7O_3^+ + HNO_2$. Some evidence for the "intermediate" ions in this reaction path exists from the rocket measurements. However, the identities of these ions are still open to question. Further a number of the chemical rate constants remain to be measured. Thus although this reaction scheme appears attractive, it should be placed on much firmer ground.

In the stratosphere the ion chemistry to explain the observed water cluster ions, $H_3O^+ (H_2O)_n$, is well established (Appendix A: Figure 3, Ferguson). The chemistry to produce the $H^+ (NaOH)_x \cdot (H_2O)_y$ clusters is summarized in Ferguson's paper (Appendix A). There remains to determine whether there is enough neutral sodium in the stratosphere for these species to be generated and indeed if these are the actual species. In general, more stratospheric measurements and laboratory chemistry studies of the meteoric species are required to clarify their ultimate fate in both the mesosphere and stratosphere.

2.3 NEGATIVE ION COMPOSITION

2.31 MEASUREMENTS

Negative ion composition measurements are more difficult to perform and are much fewer in number than positive ion measurements. The electrodynamic problems of sampling from a negatively charged payload and low signal strengths are the major difficulties. Rocket measurements have been made to examine diurnal variations and such disturbances as a solar proton event, aurora, relativistic electron precipitation and solar eclipse. Generally the measurements of one group (e.g., Appendix A: Figure 5, Ferguson) show large cluster ions below 92 km consisting of species tentatively identified as $NO_3^- (H_2O)_n$ n = 0-8, CO_4^- and some possible admixtures of $CO_3^- (H_2O)_n$. Other ions at 55 ± 1 amu and 121 ± 2 amu are unidentified. The upper mass limit is unknown but the high pass transmission mode of the quadrupole mass spectrometers indicates sizable quantities of even more massive ions. The large ion clusters are typically observed in a broad layer peaking at altitudes near 84 km (day) and 88 km (night). During disturbed periods O^- and O_2^- ions predominate in the D region; however, most of the O^- is made in the sampling process when the electron density is enhanced by the reaction $e + O_2 \rightarrow O^- + O$. Some of the O_2^- may also be made by the energetic charge transfer reaction $O^- + O_2 \rightarrow O + O_2^-$, however, this does not appear to account for the large amounts of O_2^- observed. Ions of Cl^- and NO_2^- are detected in the E region but are believed to be due to contaminants.

The single measurement of another group during a weak nighttime auroral event is different in character, showing CO_3^-, Cl^- and NO_3^- below 80 km along with ions tentatively identified as HCO_3^-, $CO_4^- (H_2O)$ or $NO_2^- (HNO_2)$. The heavier clusters of $CO_4^- (H_2O)_2$ and $NO_3^- (HNO_3)$ as well as O_2^- were present above 80 km.

All the measurement difficulties associated with positive ions apply identically for the negative ion measurements. There is clearly a need for better instrumentation and rocket measurements. Special stress should be placed upon improving the mass number accuracy, extending the mass range, obtaining accurate ion concentrations and performing simultaneous measurements of critical neutral species.

Initial measurements of stratospheric negative ions have been reported recently. Nine species with masses from 125 to 295 amu were observed between 33 and 37 km, including cluster ions identified as $NO_3^- (HNO_3)_x (HCl)_y$. With errors of plus and minus 2 to 3 amu the ion species cannot be identified unequivocally. Many more stratospheric measurements are required to establish the negative ion composition and its variations.

2.32 NEGATIVE ION CHEMISTRY

Negative ions are initially formed in the D region primarily by three-body electron attachment to molecular oxygen creating O_2^-. This ion, through the complex scheme depicted in Figure 4 of Ferguson's paper (Appendix A), is converted to the "terminal" ions of NO_3^- or HCO_3^-. The terminal ions are then assumed to undergo further hydration ractions. According to this chemistry

fast associative detachment reactions between atomic oxygen and O_2^- or O^- prohibit negative ion production above 80 km. This is inconsistent with most of the observations which show relatively large concentrations above 80 km. Although the chemistry predicts the $NO_3^-(H_2O)_n$ ions, it cannot explain their excessive hydration as well as their presence at such high altitudes. Similarly the relatively large amounts of O_2^- observed above 80 km cannot be explained. The conflicts between the measurements and the chemistry remain to be resolved.

As is true in the D region, the stratospheric negative ion chemistry is strongly affected by trace species. The core ion predicted is the highly stable NO_3^- ion and this can cluster with trace species forming such complex ions as $NO_3^- \cdot \ell H_2O \cdot m\, SO_2 \cdot n\, HNO_3$. The initial stratospheric measurements have also suggested HSO_4^- cores and H_2SO_4 neutrals as part of the cluster ion. Stratospheric negative ion chemistry is in an early state of development and will very likely improve as more in situ measurements are available.

2.4 AEROSOLS

Various observations in the middle atmosphere indicate aerosols are present at all levels from the tropopause to about 85 km at certain times and geographical locations. Aerosols are arbitrarily defined to cover the size range 10^{-7} to 10^{-2} cm diameter. They are further classified as Aitken particles (of major importance to atmospheric electricity) $\approx 10^{-7}$ to 10^{-5} cm diameter, large particles, 10^{-5} to 10^{-4} cm, and giant particles, $>10^{-4}$ cm. Two distinct "layers" are known: the Junge layer having a rather broad maximum around 20 km and noctilucent clouds which appear at high latitudes within the cold summer mesopause between 80 and 85 km. It can be generally stated that the mechanisms for the formation of the aerosols are not well established. Observations of the Junge layer show concentrations of 0.6 to 5 cm^{-3} for particles larger than 3×10^{-5} cm diameter and $SO_4^=$ as the major constituent. Noctilucent clouds appear in 1-km-thick layers and are thought to be comprised of ice particles in estimated concentrations of between 1 and 50 cm^{-3} and radii of about 1.4×10^{-5} cm. Measurements of the more numerous Aitken particles have been severely restricted because of a lack of adequate instruments.

The role of aerosols in electrical processes in the middle atmosphere is complex. Ions can act as nucleation centers to form aerosols suggesting that a direct link between ionizing radiation and aerosols may exist. The aerosols, in turn, can affect the ionization through heterogeneous chemistry and ion annihilation processes. Although it is unknown, the aerosols may also have a charge distribution. Massive ions, by their large cross sections, influence the conductivity as well as electric fields in the middle atmosphere. Not only are these massive ions present below the mesosphere where expected but there also exists evidence from two areas indicating both their presence and dominance in the mesosphere. Positive ion measurements with Gerdien condensers have shown heavy ion current carriers with mobilities one-tenth that of the light ion carriers. The heavy ion concentrations exceeded those of the light ions by factors of two to ten between 55 and 75 km. Also, several measurements of very heavy negative ion clusters have been made near the mesopause with ion mass spectrometers. This perhaps suggests production by heterogeneous chemistry since these ions cannot be accounted for by current gas-phase chemistry. In fact, one suggested mechanism for noctilucent cloud formation is nucleation of water vapor on ions.

Aerosols present very difficult and challenging problems for the future. Laboratory and theoretical efforts must continue; new in-situ and remote instruments must be developed to determine the size and charge distributions, mobilities, composition and chemistry.

2.5 SOURCES OF IONIZATION

All of the important ionization sources for the middle atmosphere are galactic, solar or magnetospheric in origin. These sources are tabulated in Table I of Rosenberg and Lanzerotti (Appendix A) along with estimates of the incident energy flux from each. These energy fluexes range over 10 orders of magnitude. However, the relative importance of each cannot be judged by merely comparing incident energy fluxes, as many sources are limited to specific height or latitude ranges.

The major quiet time mesospheric ionization source is solar Lyman-alpha radiation at 121.6 nm which ionizes the NO molecule. Lyman-alpha is only weakly absorbed by O_2 and penetrates most of the mesosphere, reaching unit optical depth at about 75 km for an overhead Sun. The chief source of O_2^+ is the ionization of $O_2(^1\Delta)$ from solar radiation in the 102.7 to 111.8 nm range. Solar x-rays are also a significant source of O_2^+ and NO^+. These are the primary ions in the positive ion chemistry chains described in Section 2.22.

In the auroral zones, one routinely encounters high fluxes of precipitated energetic electrons, which will dominate as an ionization source in the upper portions of the middle atmosphere a large fraction of the time (see Appendix A: Figure 14, Rosenberg and Lanzerotti). Even at midlatitudes during highly disturbed periods the ionization produced by precipitated energetic electrons and the associated bremsstrahlung exceeds daytime sources above ~55 km.

In the lower half of the middle atmosphere the particle component of galactic cosmic rays is the dominant ionization source under normal conditions. The existence of the Earth's magnetic field results in a pronounced magnetic-latitude effect on the incoming flux such that the full cosmic ray spectrum reaches the Earth only at latitudes greater than 60° magnetic. This hardening of the spectrum as the latitude decreases results in a lowering of the height of maximum production from 13 km at high latitudes to 10 km near the Equator. The solar wind tends to exclude cosmic ray particles from the Earth, which explains why the cosmic ray flux is lower on the average during solar maximum and more intense during solar minimum.

The various sources of middle atmosphere ionization all display variations on a wide variety of time scales. In addition, anomalously large electron concentrations are known to exist in the mesosphere on certain groups of days each winter at mid-latitudes (known as the D-region winter anomaly). The cause of the enhanced ionization may well be the transport of polar air that is rich in such minor constituents as NO to lower latitudes where it becomes subject to photoionization (see Appendix A: Reid). Changes like this in the neutral composition can greatly affect the resulting ionization levels.

3.0 MIDDLE ATMOSPHERE CONDUCTIVITY AND CURRENTS

Conductivity is dependent upon all the factors discussed in Section 2. In the lower mesosphere conductivity is dominated by the ions. Both the ion densities and ion mobilities (positive and negative) are linearly related to conductivity (see Appendix A: Reid). The mobilities are in turn related to both the ion and neutral masses. For ion masses that are much larger than neutral masses (a condition satisfied by many of the hydrated ions in the middle atmosphere) the mobility should be nearly independent of ion mass.

In the upper mesosphere the principal ions become comparable in mass with the neutrals; however most of the current at these higher levels is carried by the electrons. In this region the geomagnetic field begins to have an important effect on the electron conductivity. Electrons which are constrained to spiral around magnetic field lines can only move transverse to those field lines through collisions creating the directionally dependent conductivity tensor applicable in the ionosphere. Conductivity along magnetic field lines is much greater than that in the directions perpendicular to the magnetic field.

Throughout the whole middle atmosphere the ions are collision-dominated and are not constrained by the magnetic field. Figure 6 of Reid's paper (Appendix A) depicts the ion and electron (both σ_e along **B** and σ_{pe} perpendicular to **B**) conductivities in the middle atmosphere. There is a substantial increase in the gradient of the total conductivity between 60 and 70 km where the electron conductivity begins to exceed the ion conductivitiy. The effect of aerosols on middle atmosphere conductivity is still unknown.

Because the conductivity of the atmosphere increases nearly exponentially with altitude, the bulk of the total columnar resistance occurs below 10 km. Only 10 percent of this total resistance occurs above 10 km. Thus it has generally been assumed that large variations in upper atmospheric conductivity due to solar-activity-induced influences on the middle atmosphere plasma may occur without affecting the global resistance. Recently efforts are being made to model comprehensively the whole global electrical system without the restriction of an equipotential layer in the middle atmosphere (see Appendix A: Roble and Hays). As the scope of the modeling of the Earth's electrical environment necessarily increases, middle atmosphere conductivity and currents must be realistically included into any comprehensive study of the coupled electrodynamical systems.

Current systems in the middle atmosphere, the product of conductivity and electric fields, are presently understood only in terms of model calculations. Vertical currents upward over thunderstorms and downward in fair weather regions in the troposphere must close in the middle atmosphere regions or above. Details of this closure are not known, nor has the question of existence of localized current systems been investigated.

III. RECOMMENDATIONS FOR RESEARCH IN MIDDLE ATMOSPHERIC ELECTRODYNAMICS

1.0 MIDDLE ATMOSPHERE ELECTRODYNAMICAL PARAMETERS

Important deficiencies exist in our present understanding of the basic physical processes and of the variability of many of the primary physical parameters that govern the electrodynamics of the middle atmosphere. This is largely the result of the difficulty of measurement techniques and of the limited in-situ access to the region (sounding rockets being the primary vehicle). Middle atmosphere electrodynamics affects both the ionized and neutral constituents of that region and is an integral part of many mechanisms for coupling the troposphere with the regions above. During the early and mid 1980's ionosphere-magnetosphere coupling will be investigated in the Dynamics Explorer Program (DE) and the neutral properties of the middle atmosphere will be studied by the Middle Atmosphere Program (MAP) and are planned to be remotely sensed by the Upper Atmosphere Research Satellite Program (UARS). A coordinated program to investigate middle atmosphere electrodynamics during this period complements these other efforts and is necessary to understand and evaluate many solar-terrestrial coupling processes.

Recommendations in Section 1 address themselves to basic gaps in our knowledge of parameters related to the electrodynamics. Each recommendation is concerned with an important element of in-situ measurement needs and could be addressed either separately or as part of the coordinated measurements discussed in Section 3. Laboratory and modeling needs will be discussed in Section 2; these discussions include areas requiring theoretical attention.

1.1 Basic Electrodynamics within the Middle Atmosphere

Because of the difficulty of access and of the difficulty of many measurement techniques basic information is lacking on the electric fields, conductivity and neutral motions in the middle atmosphere. All Workshop discussions stressed the need of a coordinated approach to treat the coupled system (to be discussed specifically in Section 3); however, certain individual problem areas need attention as building blocks for a basic understanding of the coupled systems.

1.11 Electric Fields

It is generally believed that electric fields in the middle atmosphere are caused by processes that take place in the troposphere (e.g., thunderstorms) and in the ionosphere-magnetosphere system (e.g., ionospheric dynamo, magnetospheric convection). In theory, the determination of the electrostatic field in the middle atmosphere can be viewed as a boundary value problem that can be solved in a straightforward way if the conductivity distribution throughout the middle atmosphere as well as the upper and lower boundary conditions are known. Several techniques have been developed in recent years to model the electrical structure from the ground up to ionospheric heights and beyond. These models predict strong electrical coupling between the upper, middle and lower regions of the atmosphere that may be an important factor in understanding some of the outstanding problems in solar-terrestrial relations, such as reported sun-weather-climate correlations. However, quantitative predictions from these models are subject to large uncertainties due to our imprecise

knowledge of model input parameters and due to the lack of observational data to compare with model outputs.

Electric field measurements between balloon altitudes and 100 km (above which radar and satellites are useful) are almost non-existent. Those that do exist suggest that the electric field structure is more complex than would be expected from a passive coupling of the fields from magnetospheric and ionospheric sources to those from the tropospheric source. The problems separate into: (i) Are there unexpected sources of electric fields in the middle atmosphere? (ii) To what extent do electric field variations correspond to spatial and temporal variations in conductivity? and (iii) What is the role of temporal and spatial variations in the ionospheric, magnetospheric, and tropospheric sources? The last two will be further treated in Section 3.

RECOMMENDATION: Determine in-situ the structure of the vector electric field in the middle atmosphere, probing the existence of middle atmosphere sources.

Scope and Technique:

Measurements below 100 km will require an extension of present techniques. Double probe measurements appear feasible with special care. Measurements of the vertical electric field have also been attempted with a field-mill. Rockets have to be the principal vehicle. It may also be desirable to utilize parachute-borne payloads ejected from rockets. Measurements should initially be attempted at high latitudes where the electric fields from the magnetospheric source are strong. Measurements should also be made at mid and low latitudes and at different local times and magnetic conditions. Coordination of these measurements with those of other parameters will maximize their usefulness (see Section 3).

1.12 Parameters Affecting Conductivity

Conductivity in the middle atmosphere is dependent predominantly on electron concentrations in the upper middle atmosphere and ion concentrations below. Other influences are ionizing agents (as discussed in 1.3.2), mobility of ions, and factors that affect the ion composition (i.e., ion chemistry, neutral composition effects on ion chemistry, the role of aerosols, etc.). Our knowledge of these parameters has been limited by the means of access and the measuring techniques. Development of or improvement in measurement techniques is needed.

1.121 Ion Composition

Information on the positive and negative ion compositions below 120 km is sketchy. Conductivity in the middle atmosphere is dependent on the ion composition. Also the production of neutral species such as odd hydrogen and odd nitrogen during charged particle precipitation and solar x-ray events is affected by ion-neutral reactions. Models which describe the relationship of ion composition to middle atmosphere electrodynamics are dependent on knowledge of the photochemistry and general circulation of the middle atmosphere.

RECOMMENDATION: Develop a systematic program of ion composition measurements in the mesosphere and stratosphere and coordinate these measurements with other programs for the measurement of neutral composition and temperature.

Scope and Technique:

Ion mass spectrometers have been used for composition measurements from both balloons and rockets. Information, however, is still sparse, especially for negative ions. Current instrumentation needs to be refined to minimize uncertainties and extend the mass range. Experiments need to be developed to identify the core in cluster ions. The data set should be expanded to cover locational, seasonal and solar activity. The feasibility of detecting and identifying ion species using remote sensing techniques such as radar should be explored.

1.122 Neutral Dynamics

It is difficult to formulate a picture of the global electrical circuit without knowing the velocity distribution and spatial distribution of ions. Except near the upper boundary, and in specialized environments such as clouds, the velocity distribution of ions in the middle atmosphere largely mirrors the velocity distribution of the neutrals. Moreover, neutral motions redistribute the ion composition, which further affects the electrical properties in the region of interest, between 10 and 100 km altitudes. Gaps in our knowledge of neutral atmosphere motions can be found on all scales, including tides, planetary waves, gravity waves, and regions of shear.

RECOMMENDATION: Investigate the electrical conductivity response to neutral winds and wave structures in the middle atmosphere.

Scope and Technique:

There is some evidence that temperature and atmospheric neutral waves affect the vertical structure of electrical conductivity profiles. It is important to establish whether or not these variations are a normal occurrence, what classes of atmospheric waves modulate conductivity, and what the physical connections are. Measurements of neutral motions can be made by such techniques as ground based radars and in-situ chemical releases. They need to be made in conjunction with conductivity-related measurements to explore the detailed connections. The theory of neutral wave propagation also needs further development, especially through the use of large-scale numerical modeling to study such specific topics as stratospheric warmings, D-region winter anomalies, and the reflection of planetary waves.

1.123 The Role of Aerosols

The effects of charged aerosols on atmospheric electrical parameters such as mobility and conductivity are very important. There have been some suggestions from rocket measurements with Gerdien condensers and ion mass spectrometers that very massive ions may exist in significant concentrations within the middle atmosphere, some perhaps multiply charged. The processes responsible for these large and heavy ions, which have radii in the range 10 to 10^4 Å, are unknown.

RECOMMENDATION: Develop and apply new techniques to measure in-situ and/or remotely the concentration, size and distribution of aerosols in the 10 to 10^4 Å radius range and conduct laboratory and theoretical studies to establish the physical-chemical characteristics of these aerosols including charge distribution, ion-induced formation, heterogeneous chemistry and ion annihilation processes in order to determine the effect of these aerosols on conductivity.

Scope and Technique:

While no techniques presently exist for in-situ measurements of aerosols in this range two approaches have possible application. One approach is to extend LIDAR techniques for both in-situ and remote sensing of particulates in the specified size range. A time-of-flight drift-tube mass spectrometer can be developed to determine in-situ both the mobilities and composition of the charged aerosol population. These measurements need to be made in unperturbed (or background) conditions and during such distrubances as solar proton events, noctilucent cloud events and the winter anomaly. Simultaneous correlative measurement of ion composition and density, temperature and water vapor content are recommended. It is desirable to include these measurements as part of the coupled system studies in Section 3. Laboratory studies will be similar to those recommended in Section 2.3.

1.13 Intercalibration of Techniques

A number of the above measurements involve advances in present measurement techniques. Also there are questions as to the best and most reliable method. It is necessary to conduct simultaneous comparisons of various techniques for measurement of atmospheric electrical parameters in order to establish the reliability and repeatability of measurements and to provide intercalibrations.

RECOMMENDATION: Establish the reliability, repeatability and accuracy of measurement techniques for middle atmosphere electrical parameters through one or more of

a. *coordinated rocket and balloon flights to intercalibrate instruments making similar measurements on different vehicles,*

b. *simultaneous soundings with identical payloads, and*

c. *laboratory determinations of absolute accuracy.*

Scope and Technique:

These studies are necessary to help reduce the uncertainty and controversy concerning many of the present measurements and measurement techniques. While useful in all measurements, such studies have particular value in the measurement of the basic middle atmosphere parameters recommended in the previous sections.

1.2 Definition of the Lower Boundary

Recognizing that the tropospheric fair-weather electric field, which is generated by thunderstorm activity, is a source of electric fields in the middle atmosphere and that a large body of data exists for this source, our recommendations in this area are specifically directed toward the development of quantitative information about its variability with solar activity and solar induced activity and its penetration into the middle atmosphere.

1.21 Fair-Weather Electric Fields

RECOMMENDATION: Perform synoptic studies of the temporal variations of the tropospheric fair-weather electric field by:

a. *measuring in-stu the "Earth-stratosphere potential" daily or more often.*

b. *monitoring short term changes in the Earth-stratosphere potential and large scale horizontal potential gradients using reliable ground measurements.*

Scope and Technique:

The Earth-stratosphere potential at mid to low latitudes is thought to be a measure of the Earth's overall atmospheric electrification from thunderstorms. The temporal variation of Earth-stratosphere potential can be measured by simple radiosonde class instrumentation and/or a tethered balloon to establish a geoelectric index. The time resolution of the index would be determined by the frequency of balloon soundings. Such instrumentation could also be used to measure horizontal potential differences between judicious locations in the troposphere and stratosphere. The instrumentation should be developed and a minimal program of routine (at least 1 per day, more frequent at times of solar flares, etc.) measurements should be conducted from a suitable launch site for an extended period of time such as one year.

Although such balloon soundings have been made in the past, the results are not suitable for correlation studies of solar-terrestrial effects (solar flares, sector boundary crossings geomagnetic storms), because measurements were made at irregularly spaced times with many days or weeks between soundings. A minimum time span of one year is required even for small sample statistics. Higher time resolution over selected periods can be obtained by continuous monitoring from a tethered balloon.

A long history of ground based measurements of electric fields, air currents, and conductivity exists. It is not suggested to reproduce these measurements. Note that some previous measurements have suffered from excessive weather-related and man-made noise and are not well suited for studies of middle atmosphere and global problems. Thus, judicious choice and use of ground instrumentation in conjunction with middle atmosphere campaign operations and statistical studies should be made.

1.22 Storm-Time Electric Fields

RECOMMENDATION: Study the penetration of electrically active storm systems into the lower stratosphere and obtain quantitative measurements of the electrodynamical effects of these storms.

Scope and Technique:

The mechanism of electrification in electrically active storm systems has not yet been identified. While detailed cloud microphysics is not considered to lie within the scope of middle atmosphere electrodynamics, it is important to relate electrical parameters to the type of cloud, storm intensity, cloud altitude, etc. and thus to develop more quantitative information concerning the lower boundary condition of the middle atmosphere.

There are several coordinated research programs within the United States such as TRIP (Thunderstorm Research International Project) that are directed to studies of severe electrified storms and their local environment. Measurements of storm parameters that are necessary inputs for middle atmosphere studies should be made. Such a program can be implemented more easily as an add-on to existing efforts than by establishing a new independently organized program and will also benefit greatly from having a wealth of supporting meteorological data available. Specifically, high latitude aircraft and/or balloons should fly over and through storms that are selected for intensive study and measure vector electric fields, currents and conductivity as well as ion and particulate concentrations.

1.3 Definition of the Upper Boundary

The second most significant source of electric fields in the middle atmosphere is the magnetospheric electric field as it maps down below the ionosphere. Of smaller total magnitude is the ionospherically generated dynamo electric field. While only limited measurements of the electric fields from these sources presently exist, a detailed study of them is planned in the Dynamics Explorer program (involving two satellites to be launched in 1981). The variability of these sources with solar induced activity is important to the understanding of middle atmosphere electric fields.

Energy is deposited directly into the middle atmosphere across the upper boundary. Galactic cosmic rays, ultraviolet and x-radiation from the Sun including Lyman α, energetic electrons of magnetospheric and solar origin and their bremsstrahlung x-rays, and solar flare particle and x-ray fluxes are principal sources of ionization in the middle atmosphere and thus influence the conductivity. The knowledge of sources of ionization is rarely as precise as desired, even for quiet-Sun conditions. The situation during solar flares and magnetic storms is even less satisfactory and is a focus for particular emphasis. Ionization levels are interrelated to recombination rates and, along with other electrodynamic properties of the middle atmosphere, determine conductivity; hence, they should not be studied in isolation. The overall objective of the ionization measurements is to determine sources of ionization to about 20 percent precision.

Recommendations in this area largely involve satellite monitoring of these parameters. It may not be necessary to generate new satellite programs for this purpose, if these needs are considered along

with the primary mission goals of approved and future programs. Coordinated measurements in the middle atmosphere should be planned to take advantage of available satellite measurements.

1.31 Magnetospheric Electric Fields

RECOMMENDATION: Perform a synoptic study of the spatial extent and the integrated potential of the magnetospheric electric field source, by systematically recording variations in these parameters with solar activity over a solar cycle.

Scope and Technique:

The above measurements can be made using the double probe technique from a polar orbiting satellite at ionospheric altitudes. A minimum of two passes per day are desired over as much of the time period as possible. The study can be started with the approved Dynamics Explorer mission during solar maximum conditions and should be continued on a future polar orbiting mission through solar minimum.

1.32 Energetic Charged Particles

RECOMMENDATION: Measure, using orbiting satellites that can monitor the auroral and polar regions, the energetic electron and ion distribution functions (spectra and pitch angle) supplemented by imaging of the back-scattered x-ray spectrum to determine the variability of these energy sources with solar and solar induced activity.

Scope and Technique:

Particles that deposit significant energy in the mesosphere and below have energies above 50 keV for electrons and 1 MeV for protons. Detection techniques for these particles are well known. Recently techniques for imaging the associated bremsstrahlung x-ray fluxes have also been proposed. The spatial extent, temporal variability, energy spectra and the incident angular distribution of energetic electrons and associated bremsstrahlung are the essential inputs to energy deposition calculations to derive ionization-rate profiles in the middle atmosphere. This ionization source can be significant, and at times the dominant source term, in the upper regions of the middle atmosphere at high and mid latitudes. Both short- and long-term compositional changes in the neutral and ionized constituents of the atmosphere result from these inputs. These measurements will be of primary importance to middle atmosphere electrodynamics when combined with remote and in-situ measurements of the middle atmosphere neutral and ion constituents.

1.33 Solar Radiation

RECOMMENDATION: Utilize data from current and planned solar monitoring spacecraft to define with improved precision the range of variability of non-flare and flare-associated solar x-ray and ultraviolet fluxes (including Lyman α).

Scope and Technique:

Current estimates suggest that the relative importance of x-ray ($\sim$100Å) versus UV (including Lyman α) sources can change appreciably with changes in solar activity. This is a particularly important consideration for ionization levels at altitudes above 60 km. Detection techniques are well known. The study should be limited in scope and should concentrate on events where cause and effect can be investigated.

1.34 Galactic Cosmic Rays

RECOMMENDATION: Encourage continuation of the programs investigating solar modulation of galactic cosmic rays.

Scope and Technique:

Galactic cosmic rays are the principal source of ionization in the region between the tropopause and 40 km altitude. Measurement sets spanning about 2 solar cycles are available. Correlations of changes in cosmic ray flux with solar flare indices are not perfect, although the existence of solar modulation is evident. Continuation of measurements is desirable to establish cyclic solar modulation effects, primarily for long term solar-middle atmosphere response studies.

2.0 MODELS AND SUPPORTIVE LABORATORY MEASUREMENTS

Modeling plays a vitally important role in all atmospheric research. In the specific case of middle atmosphere electrodynamics modeling on a global scale of the coupled electrical system provides predictions of the large scale interactions between electric fields and conductivity that are testable with the measurements recommended here, which in turn provide new inputs to the models. On a local scale, modeling of ion chemistry forms the connecting link between laboratory measurements of ion reactions and predictions of ion composition, and thus of atmospheric electrical parameters. Models and hypotehses of the coupled system behavior under solar-induced perturbation will be the foundation of any solar-terrestrial coupling connection that may exist. It is within this context that recommendations are made in Section 2, which relate to models and laboratory measurements, and in Section 3, which are oriented toward coordinated measurements that will verify or disprove present hypotheses.

2.1 Electrical Models

Through models, the coupled electrical system concept can be developed, tying electric fields, conductivity and currents together with realistic boundary conditions. As this interrelation is understood and proven through measurements, the iterated versions can be applied to study coupling processes through the middle atmosphere.

RECOMMENDATION: Develop models of the middle atmosphere electrical systems, coupling tropospheric and magnetospheric electric field sources on a global scale and on a limited area and/or event scale in order to identify and understand electrical coupling mechanisms through the middle atmosphere.

Scope and Technique:

Global scale models are being developed which attempt to tie together the total electrostatic environment below the ionosphere. Verification and refinement of these models will be possible as we obtain more data on the distribution of thunderstorms and current sources, middle atmosphere electric fields and conductivity, and magnetospheric electric field sources. Activities recommended in Sections 1 and 3 will provide important data for use in this task. More detailed models on a local scale are necessary to understand perturbations to the system. These models should include, as they are identified, the effects of localized middle atmosphere conductivity perturbations and possible middle atmosphere electric field sources.

Related to these models and the interpretation of measurements, we recognize the importance of solar and geophysical activity indices (e.g., Zurich sunspot number, 10.7 cm solar flux and geomagnetic indices Kp, AE, Dst, etc.) and recommend that continued production of these indices be supported.

2.2 Modeling of Ion Composition

Modeling of ion composition is an essential step in increasing our understanding of the important physical mechanisms, and in the development of a predictive capability, in the field of middle atmosphere electrodynamics.

RECOMMENDATION: Develop comprehensive models if ion composition with input from the general circulation models to understand the interaction between ion composition and neutral composition and temperature.

Scope and Technique:

Most ion composition models have utilized a separate model of the minor neutral constituent composition, derived from one-dimensional photochemical models or from direct measurement, and have also used some standard atmospheric temperature profile. Ideally, the ion composition and other chemical parameters should be modeled in conjunction with the neutral composition as an integral part of a photochemical model. Since temperature is a vitally important factor in cluster ion growth, it is essential that the temperature profile used in electrodynamic models be consistent with the minor constituent composition. Thus a better model of the radiative balance of the middle atmosphere is possible. Atmospheric motions are also important, since they lead to changes in both neutral composition and temperature.

2.3 Middle Atmosphere Ion Chemistry

The problem of middle atmosphere ion chemistry has three aspects: (a) observations of ion composition, (b) laboratory determination of ion molecular processes involved in controlling the ion composition and (c) theoretical modeling to rationalize observed ion composition with laboratory measurements and atmospheric parameters. Item (a) has been covered in Section 1.1, and item (c) was discussed in Section 2.2. Laboratory measurements (b), form an important link in this iterative process.

The current approach is to improve and correct D-region positive and negative ion schemes and extend them into the stratosphere. These schemes are discussed in the background section of the report. Problem areas that remain to be solved in order to quantitatively validate these models include:

a. Mesospheric positive ions: Laboratory measurements are needed of the formation and breakup reactions of weak cluster ions, in the chain from NO^+ to the terminal distribution of $H^+ \cdot (H_2O)_n$ ions, (e.g., the reaction $NO^+ \cdot H_2O + CO_2 \overset{M}{\leftrightarrow} NO^+ \cdot H_2O \cdot CO_2$). The measurements are extremely temperature dependent and must be made in the appropriate atmospheric temperature range. In addition, processes such as

$$H^+ \cdot (H_2O)_n + N_2 \overset{M}{\leftrightarrow} H^+ \cdot (H_2O)_n \cdot N_2$$

have not been investigated and may be important. Thermodynamic data are important as well as kinetic (reaction rate) data.

b. Stratospheric positive ions: Uncertainties in this chemistry relate primarily to possible ion reactions with trace neutral species which can be important down to the $10^5/cm^3$ concentration level, i.e., chemistry which has not yet been identified. The recent suggestion of the possible importance of metallic compounds arising from meteorites is a case in point, e.g., the role of MgO, FeO, NaOH and KOH in stratospheric positive ion chemistry. A large number of necessary measurements of reaction processes are not currently available.

c. Mesospheric negative ions. The principal concern at present involves reactions that have yet to be included in the present scheme.

d. Stratosphere negative ions: Certain possible reactions of negative ions with trace atmospheric constituents (and aerosols) have not yet been investigated. For example, recent first observations of stratospheric negative ions suggest that H_2SO_4 becomes involved in the ion chemistry as HSO_4 core ions. This is not encompassed in the present scheme. Species known to be present in significant concentration (e.g., $ClONO_3$, HO_2, NO_3) should be considered for their potential role in the ion chemistry.

RECOMMENDATION: Perform laboratory measurements of ion-molecule reactions potentially important to the ion chemistry responsible for the observed ion species in the middle atmosphere.

Scope and Technique:

The following are representative of measurement needs as seen at this time:

a. Additional laboratory measurements of association reactions of both positive and negative ions with the major species N_2, O_2, and CO_2 at atmospheric temperatures are needed in order to understand the time evolution and steady state distribution of ion composition. Present techniques are available for this.

b. Reactions of the known atmospheric ions ($H^+ (H_2O)_n$, $NO_3^- (H_2O)_n$, etc.) with neutral species of concentrations greater than $10^5/cm^3$ in the middle atmosphere are required as these neutrals become known either from atmospheric measurement or theoretical models. Present experimental technology must generally be extended before such measurements can be carried out.

c. Laboratory studies of the interactions of ions with aerosols are needed. Reasonable experiments of this nature remain to be developed.

d. Laboratory measurements of photodissociation (and photo-detachment) processes of both positive and negative ions are needed.

In addition it will be important to use the in-situ ion composition and correlative data gathered from the coordinated investigations in Sections 1 and 3 to complete the loop in this iterative process of understanding ion composition.

3.0 INVESTIGATION OF SPECIFIC PROBLEMS IN THE COUPLED SYSTEM

The subject of the electrodynamics of the middle atmosphere is a study of a complex, interrelated set of parameters, many of which are driven from outside sources. Coordinated measurements that address specific physical hypotheses are the best attack on the problems involved. In this section we have attempted to define specific problem areas within the overall topic that can be addressed by campaigns of coordinated measurements. Recognizing that this subset is by no means complete, the recommended approach for choice of problem areas is to focus on specific issues and hypotheses rather than employing a shotgun approach. It should be noted that a particular campaign may advantageously attack more than one problem area.

3.1 Electric Field Coupling During Disturbed Geomagnetic Conditions

Large electric fields in the high latitude ionosphere during geomagnetic disturbances and PCA events are expected to spread to lower altitudes and significantly modify the electric field distribution down to the ground. Enhanced horizontal fields can cause significant Joule heating in the upper mesosphere. In the troposphere, the main effect is expected to be in the vertical field. These high latitude disturbances can have global effects through horizontal spreading of electric fields to lower latitudes and through modification of the global current path due to greatly enhanced conductivities down to $\sim$30 km altitude in the polar region. Electric fields may provide an effective mechanism by which high-latitude solar-terrestrial disturbances can affect the middle and lower atmosphere on a global scale.

RECOMMENDATION: Perform on a campaign basis coordinated electric field and conductivity measurements aimed at understanding how high latitude ionospheric/magnetospheric electric fields spread to lower altitudes and to lower latitudes. These measurements should be made under geomagnetic quiet conditions, during substorms, and during PCA events.

Scope and Technique:

Instruments mounted on balloons and rockets would be used to measure vector electric fields and conductivity over a wide range of altitude extending up to the ionosphere in the auroral zone and/or in the polar cap. Existing techniques can be used at balloon altitudes, but further development is needed to insure reliable measurements in the mesosphere. Simultaneous measurements of overhead ionospheric electric fields can be made by a ground-based incoherent scatter radar, a low-altitude satellite, or chemical release experiments. Balloons at sub-auroral latitudes can be used to determine the latitudinal extent of the electric field perturbation. Ground-based measurements of vertical electric field and air-Earth current would also provide important supporting data.

3.2 The Response of the Electrical Conductivity to Solar UV and Geomagnetically Induced Energetic Radiations

Atmospheric electrical conductivity is a function of both ion mobility and concentration. In addition, the mobility can be affected by the presence of charged aerosols and particulates. The changes in conductivity in response to variations in the different types of penetrating radiations must be studied in order to establish whether such changes are induced by mobility or ionization changes.

During periods of sunrise, the conductivity exhibits a rapid increase at altitudes too low for penetration by solar ionizing radiations (<60 km). The assumption has been that conductivity changes must be incurred by non-ionizing solar radiation, causing dissociation of the ions to smaller size. Soundings with Gerdien probes (which give simultaneous measurements of mobility and concentration) have indicated that the change is related to mobility. The details of these processes are essential for us to comprehend the nature and role of ions and charged aerosols within the stratosphere, and to estimate its response to, sensitivity to, and modulation by normal changes in the solar UV radiation reaching the stratosphere. This knowledge can be adapted to studies concerned with the various coupling processes proposed, including photochemical and transport considerations.

In order to evaluate ionic changes it is also necessary to measure variations in O_3 and other trace species. Such measurements should be coordinated with electric field studies, to evaluate the impact of conductivity changes on the electric field.

RECOMMENDATION: Develop integrated rocket and balloon payloads using available instrumentation to permit simultaneous measurements of sources (energetic electrons and protons, x-rays, UV) and responses (electron and ion densities, temperatures, electric fields, neutral dynamics) to evaluate the middle atmosphere conductivity perturbations associated with transient geophysical phenomena and rapid changes in solar UV illumination.

Scope and Technique:

The coordinated measurements stated above are necessary to understand the causes of conductivity changes, separating out changes in ion mobility from ion density changes. This requires the source and response to be measured in the same spatial and temporal frame. Campaigns should be conducted to take maximum advantage of available data from satellite passes and ground based radar for the purpose of obtaining information on the boundary conditions.

The minimum effort to study changes at sunrise should include simultaneous measurements of conductivity and mobility, using Gerdian probes from a rocket. The payload should also monitor the penetrating solar radiation as a function of altitude. A simultaneous flight of a balloon near 40 km could be useful in providing the time structure for these parameters near the lower boundary of the effect. Early campaigns should concentrate on Equatorial sites, where modulations induced by energetic particles, cosmic rays, and galactic x-rays are small. For middle and high latitudes (and also low latitudes if possible) x-ray and cosmic rays can be monitored on the balloon flight, and particle detectors should be included on the rocket payloads to evaluate supplemental energy sources.

3.3 Middle Atmosphere Electrical Coupling Above Tropospheric Thunderstorms

Thunderstorms are generally thought to be the major generators that maintain the global fair-weather electric field. Large storms extend vertically into the stratosphere. It is important to know how much current flows upward and how it spreads out horizontally at higher altitudes. Strong electric fields above thunderclouds may have important local effects on charged aerosols in the middle atmosphere. Furthermore, theory predicts that thundercloud electric fields may have significant effects even in the ionosphere and magnetosphere. However, since calculated field intensities depend critically on conductivity profiles that are not well known at present, it is important to verify theoretical predictions by making direct measurements over active thunderstorms.

Several theories in global electric field coupling and in sun-weather coupling involve severe modification of currents and atmospheric conductivity above thunderstorms. Measurements are needed to evaluate these hypotheses. At the same time the study of neutrals NO_x and O_3 would permit the evaluation of recent proposals concerning stratospheric ozone depletion induced by lightning in thunderstorms.

RECOMMENDATION: Investigate the upward penetration of electrostatic and electromagnetic fields above thunderstorms into the stratosphere, mesosphere and ionosphere with coordinated measurements of electric fields, currents and conductivity. In addition, verify the predicted depletion of the stratospheric ozone layers by thunderstorm electrodynamics.

Scope and Technique:

Instruments on aircraft, balloons and rockets would be used in campaigns to make simultaneous measurements above thunderstorms at suitable locations at middle or low latitudes. Ionospheric measurements can be made with an incoherent scatter radar, a low-altitude satellite, or high-altitude rockets. Measurement of conductivity, electric fields, and neutral parameters in the stratosphere and of electric fields and conductivity in the mesosphere are necessary. Measurements of horizontal gradients in these parameters with respect to the center of the storm should be made.

3.4 Long Duration Monitoring of the Electrodynamics of the Stratosphere on a Quasi-Global Scale

Existing data on parameters relating to middle atmosphere electrodynamics are sparse and often contradictory. As our knowledge in this area is increased it will be important, relative to testing and improving global electrodynamical models, to measure parameters from several platforms at varying

locations simultaneously and over long periods of time spanning changes in troposphere and solar-terrestrial coupled activity. Superpressure balloons have been demonstrated to provide a long-duration platform for making in-situ measurements in the stratosphere. Specific problems include temporal and spatial variations of the conductivity in the middle atmosphere, spatial structure of the middle atmosphere electric fields as they relate to the penetration of continental electrical "plumes" into the middle atmosphere, and the large scale spatial structures created by solar induced geomagnetic activity and meteorological disturbances.

RECOMMENDATION: Measure using long-duration superpressure ballons the large scale spatial structure in the middle atmosphere vector electric field, conductivity (and mobility), ionization rates and aerosols in order to test global electrification models and their response to perturbations.

Scope and Technique:

Under favorable conditions, a single superpressure balloon can cover large portions of the southern hemisphere in the course of a few months. Three simultaneous flights would provide continuous data coverage as well as information on large scale spatial variations of the measurements of the above-mentioned parameters. Balloon tracking and data telemetry can be handled by an available satellite system such as the Tiros-Argos system. These measurements should be made in conjunction with an operational polar orbiting ionospheric satellite that monitors the vector electric field and the incoming energetic particle and x-ray fluxes in order that knowledge of the upper boundary conditions and their variations can be available to aid in the interpretation of the balloon data. Correlative lower boundary information including meteorological conditions is also available.

APPENDIX A

TUTORIAL PAPERS

THE MIDDLE ATMOSPHERE

G. C. Reid
Aeronomy Laboratory
National Oceanic Atmospheric Administration
Boulder, Colorado 80307

1. INTRODUCTION

The term 'middle atmosphere' is a fairly recent one, coined to describe the region lying approximately between the tropopause and the mesopause, with possibly a slight extension into the lowest part of the thermosphere, i.e., the region of the atmosphere lying between about 10 and 100 km altitude. As such, it includes the stratosphere and the mesosphere, both of which are regions about we know comparatively little, although our knowledge has increased greatly as a result of recent concerns with potential damage to the ozone layer. Planning is now underway for a coordinated international attack on the unsolved problems of this region to take place in the early 1980s under the name of the Middle Atmosphere Program (MAP), which makes the present Workshop particularly useful at this time.

There are three major sources of electric fields in the atmosphere: tropospheric thunderstorms, wind action in the dynamo region of the lower thermosphere, and the interaction between the solar wind and the outer magnetosphere. Although the middle atmosphere is not the source of any of these fields, its electrical parameters are bound to play an important role in determining the extent to which the fields can penetrate through in either direction, or can affect the middle atmosphere itself. The main objective of this paper, then, is to provide a quick introduction to some of the important electrical properties, and to the factors that influence them and their variability.

The chemical composition of the middle atmosphere is an important factor, and several of the minor constituents, of which typical profiles are shown in Figure 1, play prominent roles. The temperature structure and the wind systems of the middle atmosphere are determined by a balance between the rates of heating and cooling. The heating is due to the absorption of solar radiation by ozone, and the cooling to infrared radiation, mainly by carbon dioxide, so that these two minor constituents are chiefly responsible for the structure of the middle atmosphere. The other constituents shown in Figure 1 are the recognized chief participants in the production of ionization, or in the ion chemistry that determines the steady-state ion concentration and composition, but our knowledge is not so complete that we can affort to ignore other potential contributors.

During the winter, there is a pronounced equatorward-directed temperature gradient in the middle atmosphere, and the resultant geostrophic winds are westerly, just as in the troposphere. Wind speeds reach their maximum near the stratopause, forming the so-called polar-night jet, surrounding a strong polar vortex. During the summer the situation tends to be reversed, with a poleward-directed temperature gradient caused by the combination of a high-latitude ozone maximum and essentially continuous insolation, giving rise to prevailing easterlies throughout most of the middle

atmosphere. The spring and fall transitions between these two average conditions are periods of particular interest in the middle atmosphere, as are such transient phenomena as the major stratospheric warming events of the late winter.

Vertical transport in the middle atmosphere is usually parameterized through the use of an eddy-diffusion coefficient whose profile is based on observed vertical diffusion rates. Characteristic vertical mixing times are long, varying from years in the lower stratosphere to months in the upper stratosphere and lower mesosphere and to weeks in the upper mesosphere. Since these are much longer than the characteristic lifetimes of ions, the ions are not themselves directly affected by vertical transport. Many of the minor species that determine the ion composition, however, are dominated by transport effects rather than by photochemistry in much of the middle atmosphere.

2. PRODUCTION OF IONIZATION

Ionization is produced in the middle atmosphere by a variety of sources. The extreme ultraviolet and soft x-radiation from the sun that produces the overlying ionospheric layers is almost entirely absorbed before reaching the mesosphere, but there is a small contribution from harder x-rays, particularly during solar flares, when the flux of hard x-radiation can increase by two or three orders of magnitude over its normal value. The metastable O_2 ($^1\Delta$) molecule provides a source of O_2^+ in the upper mesosphere, but its importance remains somewhat uncertain. These excited molecules are produced by photodissociation of ozone, and their long lifetime and excess electronic energy (amounting to 1 ev) make them susceptible to ionization by solar radiation in the wavelength range from 102.7 to 111.8 nm that cannot ionize ground-state O_2. The concentration of O_2 ($^1\Delta$) is large enough that this would provide a major source of ionization were it not for the fact that the wavelength range needed is strongly absorbed by CO_2, reducing the role of O_2 ($^1\Delta$) ionization to a relatively minor one. It remains, however, the chief source of O_2^+ in the mesosphere under undisturbed conditions.

The major source of mesospheric ionization is the NO molecule, which can be ionized by solar Lyman-alpha radiation at 121.6 nm. By chance, the Lyman-alpha line coincides with a window in the O_2 absorption spectrum, and penetrates most of the mesosphere, reaching unit optical depth at about 75 km for an overhead sun. The primary ion species produced by this source is, of course, NO^+. Figure 2 shows the rates of production of both O_2^+ (from the O_2 ($^1\Delta$) source as well as from x-rays during average solar conditions) and NO^+ for a solar zenith angle of 45° and for currently accepted profiles for NO and O_2 ($^1\Delta$).

In the lower mesosphere and throughout the stratosphere the chief source of ionization is provided by galactic cosmic rays under normal conditions. The rate of ion production by cosmic rays is shown in Figure 3 for different geomagnetic latitudes during the solar minimum year of 1965, based on the balloon measurements reported by Neher [1967]. The existence of the geomagnetic field gives rise to a pronounced magnetic-latitude effect in the incoming cosmic-ray flux, in such a sense that the full cosmic-ray energy spectrum reaches the earth only at latitudes higher than about 60° As we move to lower latitudes, successively more and more of the lower-energy particles are excluded, and only particles with energies greater than about 15 Bev have access to the magnetic

equator. The successive hardening of the cosmic-ray spectrum with decrease in latitude is evident in Figure 3 from the lowering in height of the maximum production rate from about 13 km at high latitudes to about 10 km near the equator. The short barred segments indicate the average tropopause level at the different latitudes, and show clearly that the bulk of cosmic-ray ionization lies in the troposphere at low and middle latitudes, and in the stratosphere at high latitudes. Even at high latitudes, however, the tropospheric ion production rate is considerably larger than at low latitudes.

The solar wind tends to exclude cosmic-ray particles from the inner solar system, and thus from the earth, through mechanisms that are not fully understood, but that probably involve the scattering effects of magnetic-field irregularities. The chief result is that the cosmic-ray flux at the earth is lower during solar maximum, when the solar wind is more intense on the average, than during solar minimum. This is illustrated by the broken curve in Figure 3, which shows the high-latitude ion production rate in 1958, again based on measurements by Neher [1961]. There is a considerable reduction in the peak ionization rate, coupled with a slight decrease in the height of the peak caused by the fact that the solar wind preferentially excludes the particles with lower energy. This produces a regular solar-cycle variation in the electrical properties of the middle atmosphere that may have some significant effects.

3. ION CONCENTRATION MOBILITY AND CONDUCTIVITY

The steady-state ion concentration profile of the middle atmosphere is illustrated in Figure 4, which shows the results of a recent model calculation of positive-ion concentrations for a solar-maximum year at geomagnetic latitude 40°, and for a solar zenith angle of 45°. Also shown are the results of direct measurements of small-ion concentrations reported by Widdel et al. [1976] for a similar geomagnetic latitude, but for different phases of the solar cycle. Obviously there is a general agreement in the shape of the profiles, but the sharp enhancements in ion concentration that appeared at 65 km in 1968 and at 45 km in 1975 have no counterpart in the theoretical results. The model results also appear to be higher by about a factor of 3 than the actual observations over most of the range. Since our knowledge of the ion production rate is unlikely to be seriously in error, at least below 60 km, the discrepancies must reflect our lack of knowledge of the full details of the ion chemistry of the stratosphere.

Figure 5 shows the results of a similar model calculation of the concentrations of the negatively charged species—negative ions and electrons—for the same conditions of solar illumination, but for polar and equatorial latitudes. The very sharp transition between the overlying electron-dominated region and the underlying negative-ion-dominated region is the most obvious feature, and there is a certain amount of observational confirmation that the transition occurs at about 70 km during quiet daytime conditions, as predicted by the model.

The ion concentration is related to the conductivity through the mobility. The current density, $\underline{j}$, is given by

$$j = n_i \, e(V^+ - V^-)$$

where n_i is the concentration of ions of either sign, e is the electronic charge, and $\mathbf{V}^+$ and $\mathbf{V}^-$ are the velocities of positive and negative ions respectively. Expressing the velocities as $\mathbf{V} = k\mathbf{E}$, where k is the mobility, and using the Ohm's Law relationship $\mathbf{j} = \sigma\mathbf{E}$ between current density and electric field, where σ is the conductivity, we have

$$\sigma = n_i e(k^+ + k^-)$$

The simplified Langevin theory of ionic mobility predicts that

$$k = B(1 + m_n/m_i)^{1/2}$$

where m_n and m_i are the masses of the gas molecules and of the ions respectively, and B is a constant of the gas. This relationship is borne out reasonably well in practice for small molecular ions, and indicates that if the dominant ions are much lighter than the parent gas the mobility should be proportional to $m_i^{-1/2}$. If the ions are much heavier than the gas molecules, on the other hand, the mobility should be nearly independent of the ion mass. In the middle atmosphere, as we shall see, the latter is generally true, since most ions will be hydrated, i.e., will be surrounded by several water molecules, leading to characteristic masses several times greater than those of the air molecules. Toward the lower thermosphere, the principal ions become comparable in mass with the air molecules, but most of the current at these higher levels will be carried by electrons rather than by ions.

Figures 6a and 6b show theoretical profiles of conductivity for equatorial and polar latitudes, again for solar maximum conditions and for a solar zenith angle of 45°. The solid lines represent the ionic component and the broken lines the electronic component of the conductivity, with the crossing points marking a sudden increase in the gradient of total conductivity. Below this altitude, substantial horizontal potential differences can be maintained, but the conductivity at greater heights is large enough to allow only relatively small potential variations on a global scale. The 'fair-weather' electric field exists between this conducting layer and the surface of the earth, each of which can be regarded as one plate of a spherical-shell capacitor whose charge is determined by a balance between the charging effect of global thunderstorm activity and the discharging effect of vertical leakage currents.

In the upper mesosphere the geomagnetic field begins to have an important effect on the electron conductivity. The electrons are forced to spiral around the direction of the magnetic field, and if the collision frequency is low enough they can no longer move freely along the direction of an applied electric field that has a component perpendicular to the magnetic field. Collisions with gas molecules, however, break up this organized spiralling motion, and allow some movement along the electric field direction, thereby preventing the electron conductivity along the direction of the electric field from vanishing entirely. The residual electron conductivity perpendicular to the magnetic field is known in ionospheric terminology as the Pedersen conductivity, and is shown in Figures 6a and 6b by the broken line labeled σ_{Pe}. The conductivity along the direction of the magnetic field is unaffected by the spiralling motion of the electrons, and is identical to the uniform conductivity that would exist if there were no magnetic field. It is shown by the broken line

labeled σ_e. Since the electrons drift along a direction perpendicular to both the magnetic and electric fields between collisions, there is a third component of the conductivity, known as the Hall conductivity, but it differs in character from the other components by virtue of its vanishing power dissipation (since $\mathbf{j}_H \cdot \mathbf{E} = 0$).

Throughout the middle atmosphere the ions remain collision-dominated, and are just as free to move perpendicular to the magnetic field as they would be in the absence of a magnetic field. The total current is thus carried to an increasing extent by the ions in the upper mesosphere and lower thermosphere, and the total Pedersen conductivity reaches its peak value in the upper E region of the ionosphere.

4. ION COMPOSITION

The nature of the ions is a matter of some interest since it has a direct bearing on the electrical properties of the middle atmosphere. The paper by Ferguson will provide an overview of the ion chemistry that determines the steady-state ion composition, but I shall show some examples taken from a series of calculations based on our present understanding of the ion chemistry. I shall discuss only the 'small ions', i.e., ions of molecular dimensions. The role of large aerosol-size ions in the middle atmosphere is still an open question that will probably be aired at some stage in this Workshop.

Throughout most of the middle atmosphere, hydrated protons were until recently thought to be the dominant positive ions. Figure 7 shows a typical set of profiles of the hydrated protons of the chemical form $H^+(H_2O)_n$ (often written, perhaps more properly, as $H_3O^+(H_2O)_{n-1}$), with each of the curves labeled with n, the number of clustered water molecules. Since the clustering bonds are relatively weak for the higher members of the series, they are subject to collisional breakup, and the ambient temperature is a very important factor in determining the detailed height distributions. In the lower stratosphere temperatures are low, and the heavier clusters can survive, but as we go upward the characteristic mass becomes smaller, reaching a minimum near the stratopause, where the temperature is highest. At greater heights, the heavier clusters again try to form as the temperature drops, but the decreasing pressure leads to slower formation rates, and eventually the reactions leading to formation of the heavier clusters cannot compete with loss of the ions by recombination. Above this point the hydrated protons lose their dominance, and are replaced by other species.

The few existing measurements of positive-ion composition in the stratosphere have shown that the hydrated protons are indeed dominant above about 40 km, but that they tend to be replaced at lower heights by other species, many of which can be explained as hydrates of a core ion of mass 41 [Arnold et at., 1978; Arijs et al., 1978]. Ferguson [1978] has recently proposed that this core ion is $H^+(NaOH)$, and it appears that this explanation is consistent with estimates of the sodium content of the middle atmosphere arising from meteors and with the known proton affinity of NaOH. This development is too recent to have been included in the model calculations shown, and implies a significant revision at heights below 40 km. At greater heights, the dominance of the hydrated protons has been shown by a large number of rocket mass-spectrometer flights, beginning with that of Narcisi and Bailey [1965] carried out in 1963.

The primary positive ions formed in the middle atmosphere are NO^+, O_2^+, and N_2^+, with traces of other minor species. N_2^+ is very rapidly converted by charge exchange into O_2^+, so that the only important primary species are NO^+ and O_2^+. These are both converted into the proton hydrates by a series of chemical reactions, the details of which remain somewhat obscure, at least in the case of NO^+. Figure 8 shows height profiles for some of the intermediate species involved in one model of NO^+ chemistry [Reid, 1977]. Appreciable concentrations are reached only at heights above those at which the proton-hydrate spectrum is fully developed, but they become of major importance in the 70-85 km height range, and only above the mesopause does NO^+ itself become the dominant species. Figure 9 shows the height profiles for the O_2^+ intermediates, which never become major constituents in the middle atmosphere under normal conditions. During intense particle ionization events such as major solar-proton events, however, O_2^+ becomes the principal primary ion species, and the O_2^+-series intermediates assume more importance.

The negative-ion composition of the middle atmosphere is much less certain, since the number of direct in-situ measurements is very small. Figure 10 shows the results of a model calculation based on the presently accepted ion chemistry, and using the same conditions as the positive-ion model. The most notable feature is the overwhelming dominance of the nitrate ion, NO_3^-, at all heights at which negative ions have significant concentrations. Hydration processes for these ions have been omitted from the model, but they will in fact be hydrated. Narcisi et al., [1971] report observations of the appropriate ion masses for $NO_3^-(H_2O)_n$ with n = 1 to 5.

Above about 70 km in daytime conditions negative-ion formation, which takes place through three-body attachment to O_2, can no longer compete with dissociative recombination as a sink for free electrons, and the negative-ion concentration rapidly drops to quite small values. At night, when positive-ion concentrations are greatly reduced, dissociative recombination is much slower, and the negative-ion region extends to greater altitudes.

The rates of most of the important atmospheric negative-ion reactions have been measured in the laboratory, and they will be described in outline in Ferguson's paper in these proceedings. One important negative-ion process about which we still know very little, however, is photodetachment of the principal terminal species, NO_3^-. The reason for the predominance of NO_3^- is its large electron affinity, which prevents it from undergoing any further exothermic reactions with atmospheric species. The electron affinity has recently been measured as 3.91 ± 0.24 ev [Davidson et al., 1977], so that photodetachment requires light in the 299 to 339 nm wavelength range, i.e., in the near ultraviolet. Each successive hydration of the ion will add to the energy needed for detachment, since the binding energy of the water molecule will also have to be supplied. Since the flux of protons with energies above these limits is much less than the flux of visible-light photons required for photodetachment of such ions as O_2^- and O^-, whose rates are known, the photodetachment rate of NO_3^- will be much smaller than those of the simpler atmospheric ions.

In order to estimate the possible importance of photodetachment, calculations were carried out with a photodetachment rate (reciprocal lifetime) of 0.002 s^{-1}, following Turco and Sechrist [1972], who based this value on a uniform cross section of 10^{-18} cm^2 for all wavelengths shorter than the threshold given by the electron affinity. The computed profiles of electron and negative-ion concentrations are shown in Figure 11, and indicate that the major effect of photodetachment

on the negative-ion concentration is confined to a small range of heights near the top of the distribution. At lower heights, the electrons released by photodetachment quickly become attached again, and the reduction in negative-ion concentration is negligible. Photodetachment also enhances the electron concentration, but only in regions where they are very few free electrons.

The influence of photodetachment is thus likely to be fairly insignificant, at least during undisturbed conditions. Sunlight will have a more serious effect in an indirect way, however, through the production of atomic oxygen in the middle atmosphere. Atomic oxygen takes part in associative detachment reactions such as

$$O_2^- + O \rightarrow O_3 + e$$

which effectively reduce the rate of formation of negative ions.

5. VARIABILITY

The various sources of middle-atmosphere ionization all display variability on a wide variety of time scales, and a corresponding variability in the electrical parameters must exist. In the mesosphere, the solar x-ray flux varies with the 27-day solar rotation period, with the 11-year solar cycle, and most dramatically of all with individual flares, when its intensity can increase by at least three orders of magnitude above the normal value in the case of the more energetic x-rays. Except during intense solar flares, however, x-rays remain a fairly negligible ionization source.

The major mesospheric ionization source, Lyman-alpha ionization of NO, must certainly have a variability that reflects the known variability of the solar Lyman-alpha flux. The latter increases by nearly a factor of two in going from solar minimum to solar maximum [Weeks, 1967], and by about 30% in the course of a solar rotation [Hall and Hinteregger, 1970]. The concentration of NO itself in the mesosphere may also be variable, reflecting a variability in the production of NO in the lower thermosphere by energetic particles. Auroral ionization is known to be accompanied by the production of large quantities of NO near 100 km altitude, but the extent to which this NO survives to diffuse down into the mesosphere is still unknown.

Anomalously large electron concentrations are known to exist in the mesosphere on certain groups of days each winter at mid-latitudes. This phenomenon has long been known as the D-region winter anomaly, and is closely associated with stratospheric warming events, marking a major breakdown in the winter polar circulation. The cause of the enhanced ionization may well be the transport of polar air that is rich in such minor constituents as NO to lower latitudes, where it becomes subject to photoionization.

In the stratosphere, cosmic-ray ionization undergoes a regular solar-cycle variation, as noted above, and this should produce a corresponding variation in conductivity by 30% or so. The most dramatic changes in middle-atmosphere electrical properties, however, are undoubtedly those that occur as a result of intense solar-proton events. As an illustration, Figure 12 shows the calculated rate of production of O_2^+ (and N_2^+) at the peak of the major solar-proton event of September 1966, together with the rate of production by the normal sources. Obviously there is an increase in ion production

by several order of magnitude, and there must be a corresponding increase in conductivity at all heights. A simple calculation shows that during this particular event the height of the transition between negative ions and electrons as the principal current carriers dropped by about 20 km, from 60 km to 40 km.

Intense solar-proton events represent very major disturbances in all aspects of middle-atmosphere electrical properties, and they can also produce significant changes in neutral composition through the molecular dissociation that accompanies the intense ionization. Direct effects on global atmospheric electric fields have now been reported for the case of the August 1972 event [Holzworth and Mozer, 1977], but much remains to be learned.

In conclusion, we have seen that the electrical properties of the middle atmosphere are both complex and variable. The middle atmosphere responds to driving forces from above and from below, and is subject to electric fields of both tropospheric and magnetospheric origin. It is likely that any mechanism for solar-terrestrial coupling that reaches down into the lower atmosphere must intimately involve the middle atmosphere in some way, and possible mechanisms involving atmospheric electricity have been suggested in the past. If we are ever to be in a position to evaluate such proposals, we need to acquire a more detailed and less superficial knowledge of the electrical parameters of the middle atmosphere than we presently possess. One of the chief purposes of the present Workshop is to plan activities that will lay the foundation for moving forward in this somewhat neglected area of atmospheric physics.

REFERENCES

Arijs, E., J. Ingels, and D. Nevejans, Mass spectrometric measurements of the positive ion composition of the stratosphere, *Nature*, **271**, 642, 1978.

Arnold, F., H. Böhringer, and G. Henschen, Composition measurements of stratospheric positive ions, *Geophys. Res. Letters*, **5**, 653, 1978.

Davidson, J. A., F. C. Fehsenfeld, and C. J. Howard, The heats of formation of NO_3^- association complexes with HNO_3 and HBr, *Int. J. of Chem. Kinetics*, **9**, 17, 1977.

Ferguson, E. E., Sodium hydroxide ions in the stratosphere, *Geophys. Res. Letters*, **5**, 1035, 1978.

Hall, L. A. and H. E. Hinteregger, Solar radiation in the extreme ultraviolet and its variation with solar rotation, *J. Geophys. Res.*, **75**, 6959, 1970.

Holzworth, R. H. and F. S. Mozer, Direct evidence of solar flare modification of weather related atmospheric electric fields, Space Sciences Laboratory Report, University of California, Berkeley, July 1977.

Narcisi, R. S., and A. D. Bailey, Mass spectrometric measurements of positive ions at altitudes from 64 to 112 kilometers, *J. Geophys. Res.*, **70**, 3687, 1965.

Narcisi, R. S., A. D. Bailey, L. Della Lucca, C. Sherman, and D. M. Thomas, Mass spectrometric measurements of negative ions in the D- and lower E-regions, *J. Atmos. Terr. Phys.*, **33**, 1147, 1971.

Neher, H. V., Cosmic-ray knee in 1958, *J. Geophys. Res.*, **66**, 4007, 1961.

Neher, H. V., Cosmic-ray particles that changed from 1954 to 1958 to 1965, *J. Geophys. Res.*, **72**, 1527, 1967.

Reid, G. C., The production of water-cluster positive ions in the quiet daytime D region, *Planet. Space Sci.*, **25**, 275, 1977.

Turco, R. P., and C. F. Sechrist, An investigation of the ionospheric D region at sunrise, 2, Estimation of some photodetachment rates, *Radio Sci.*, **7**, 717, 1972.

Weeks, L. H., Lyman-alpha emission from the Sun near solar minimum, *Astrophys. J.*, **147**, 1203, 1967.

Widdel, H. U., G. Rose, and R. Borchers, Experimental results on the variation of electric conductivity and ion mobility in the mesosphere, *J. Geophys. Res.*, **81**, 6217, 1976.

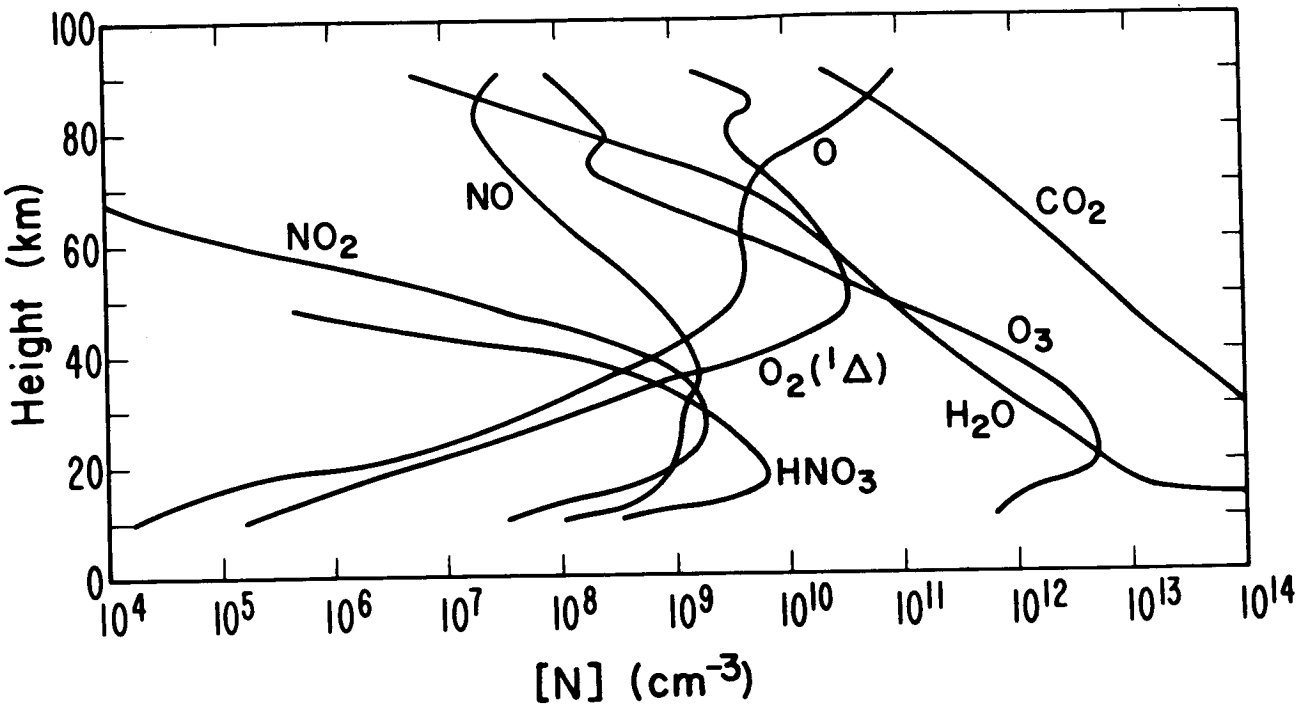

Figure 1. Typical daytime concentration profiles of some minor constituents of the middle atmosphere.

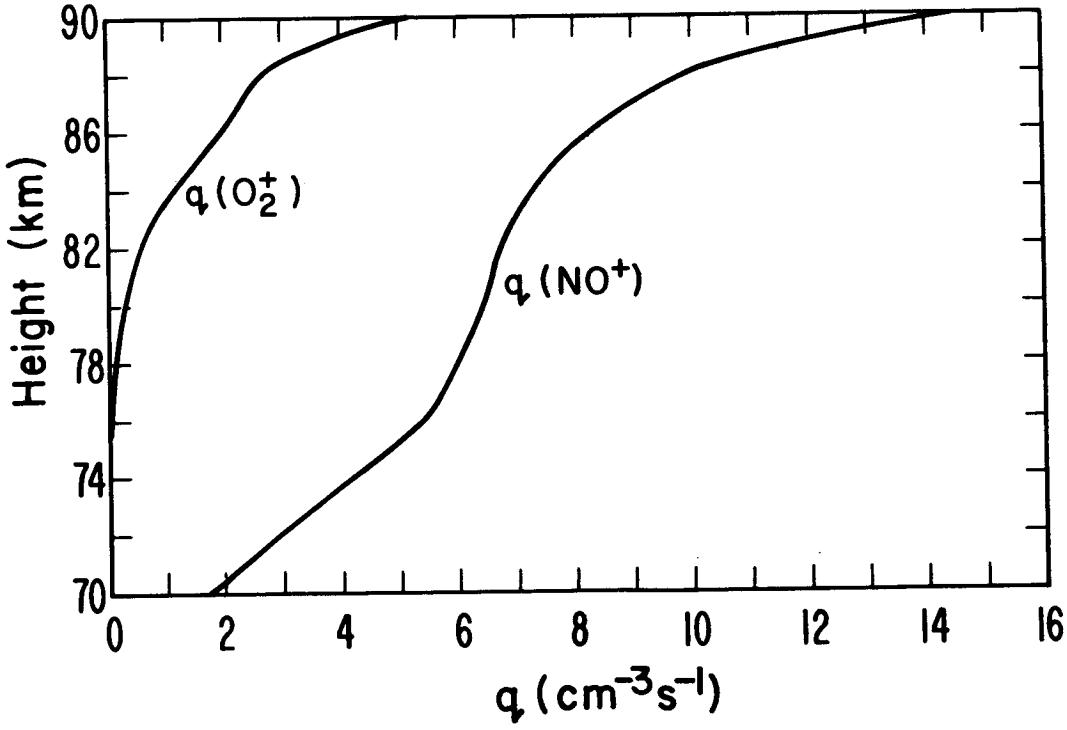

Figure 2. Rate of ion production for a solar zenith angle of 45° and undisturbed conditions.

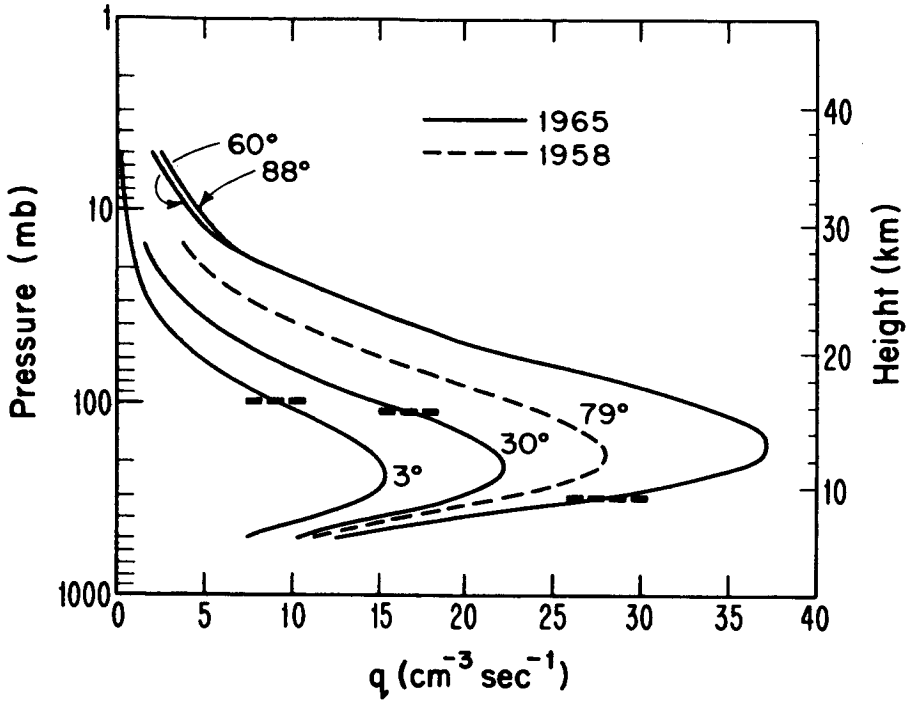

Figure 3. Rate of production of ions by cosmic rays for solar minimum (1965) and solar maximum (1958) conditions at the indicated geomagnetic latitudes. Heavy barred lines indicate tropopause height.

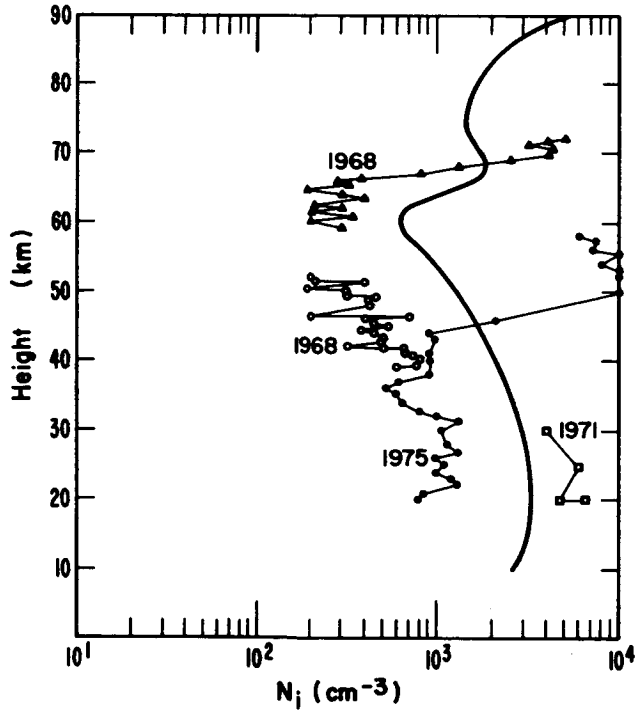

Figure 4. Positive-ion concentration profile from model calculation (solid line) and observed (from Widdel et al., [1976]).

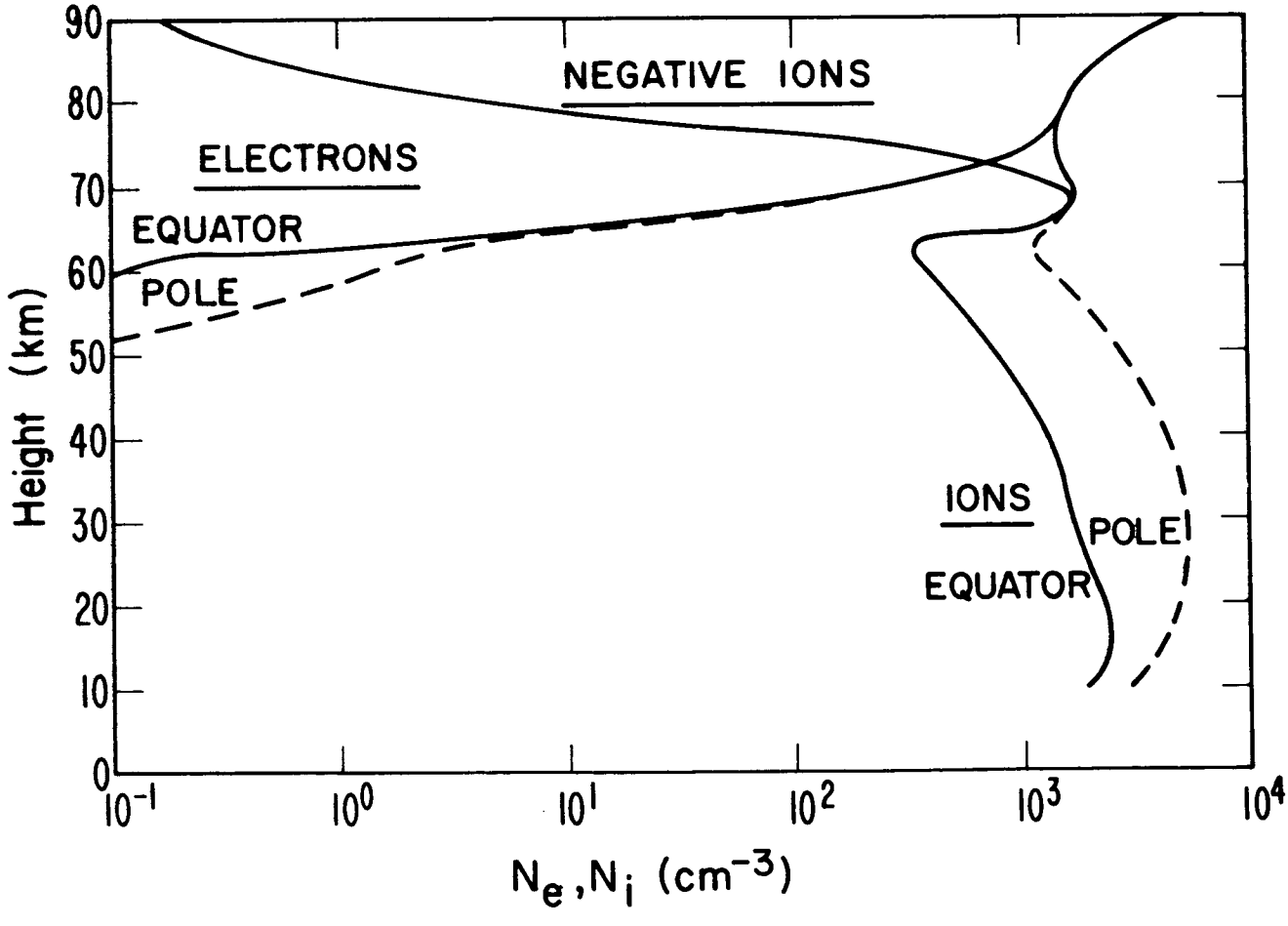

Figure 5. Negative-ion and electron concentration profiles at the pole and equator from model calculation.

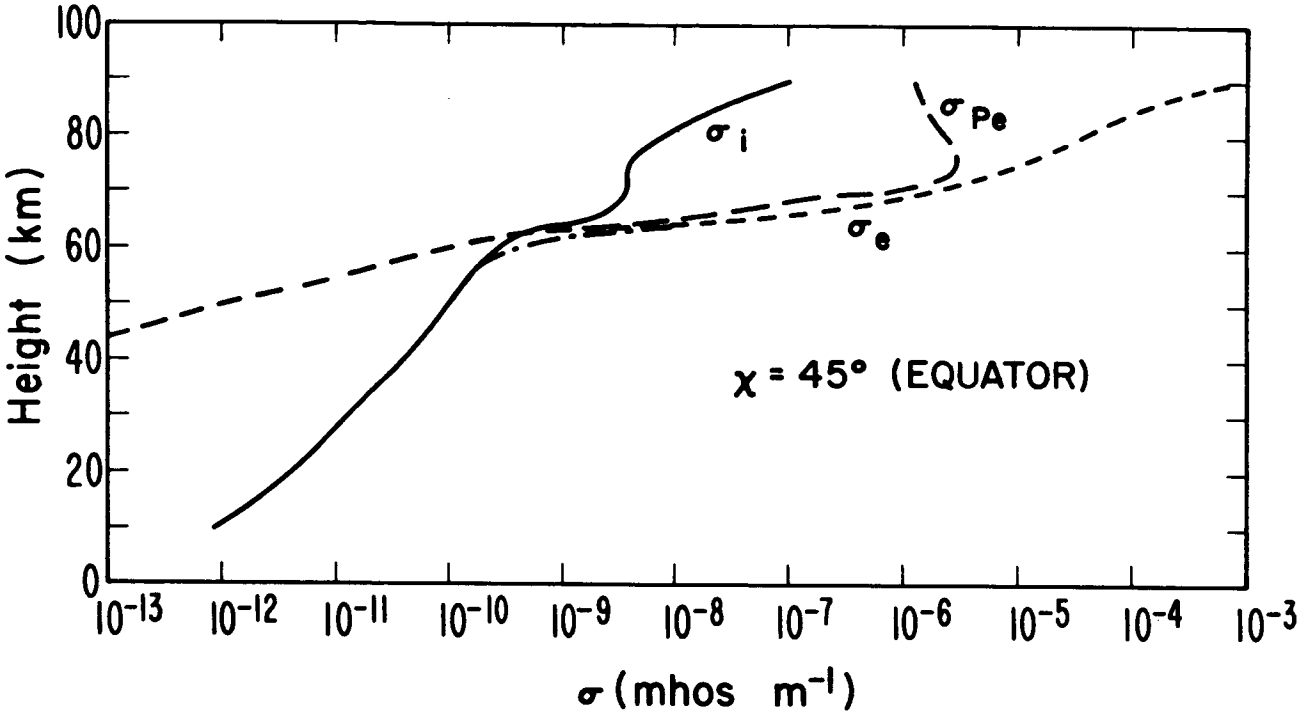

Figure 6a. Calculated profiles of electron and ion conductivity at the equator.

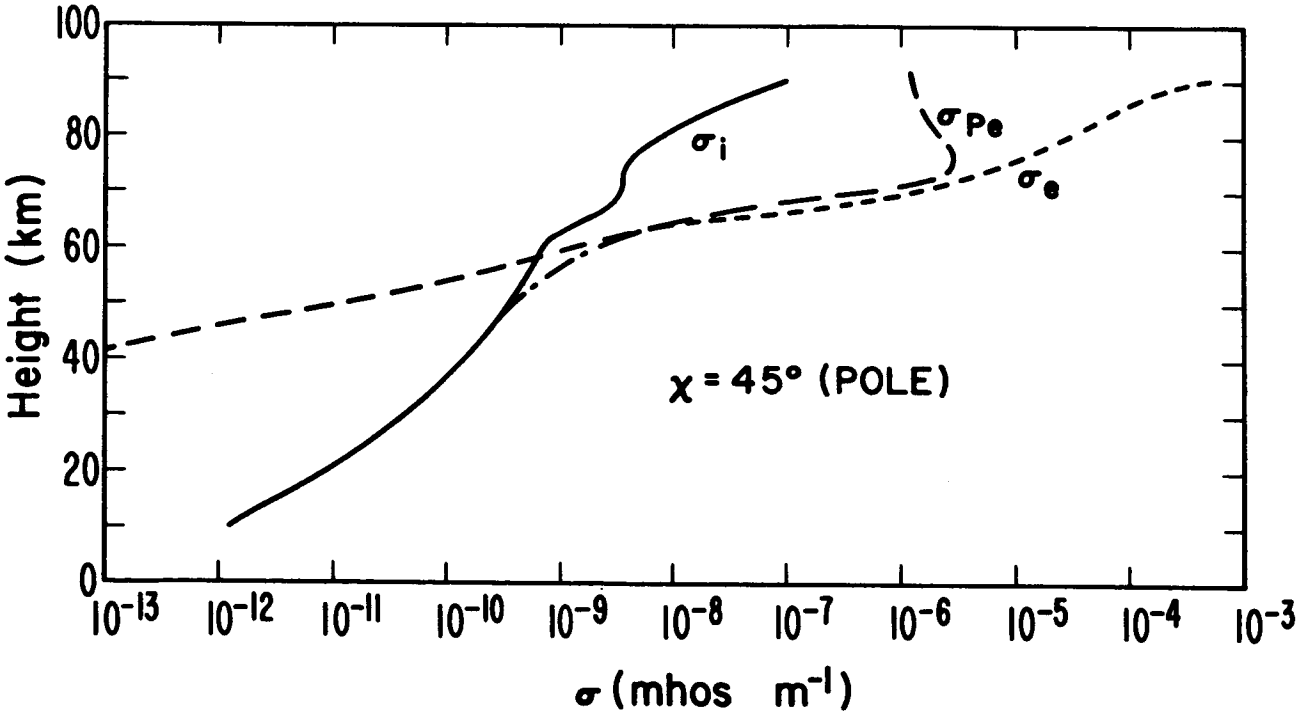

Figure 6b. Calculated profiles of electron and ion conductivity at the poles.

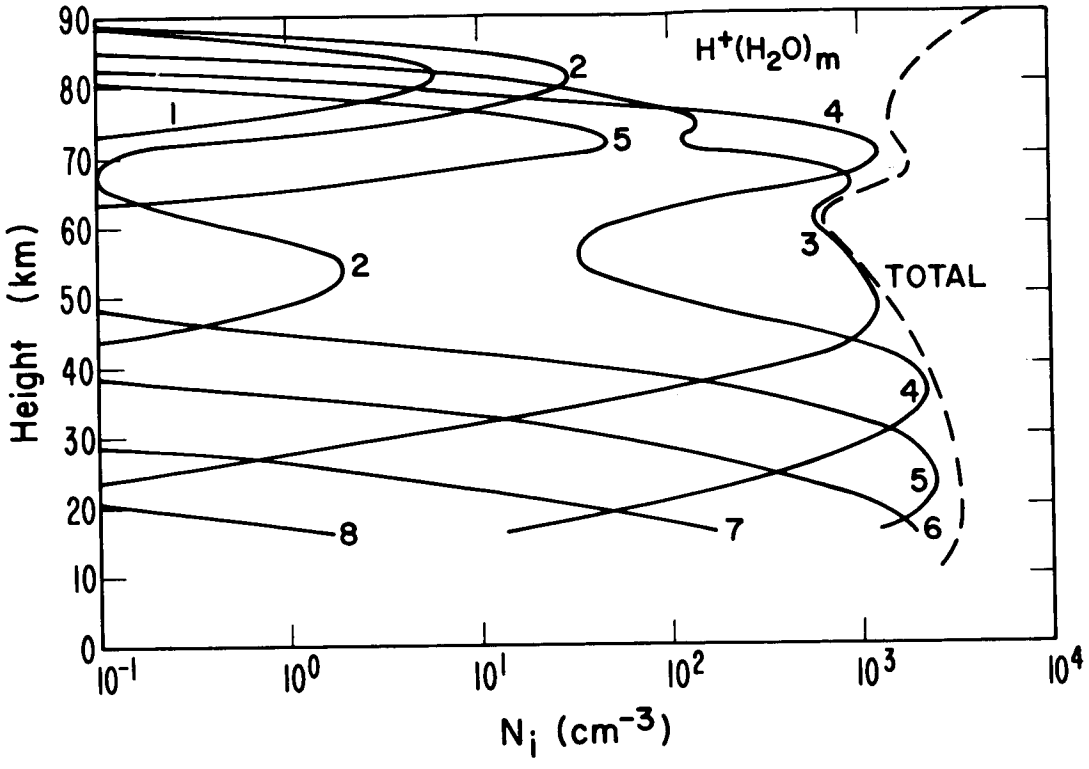

Figure 7. Altitude profiles of hydrated protons in the middle atmosphere from model calculation.

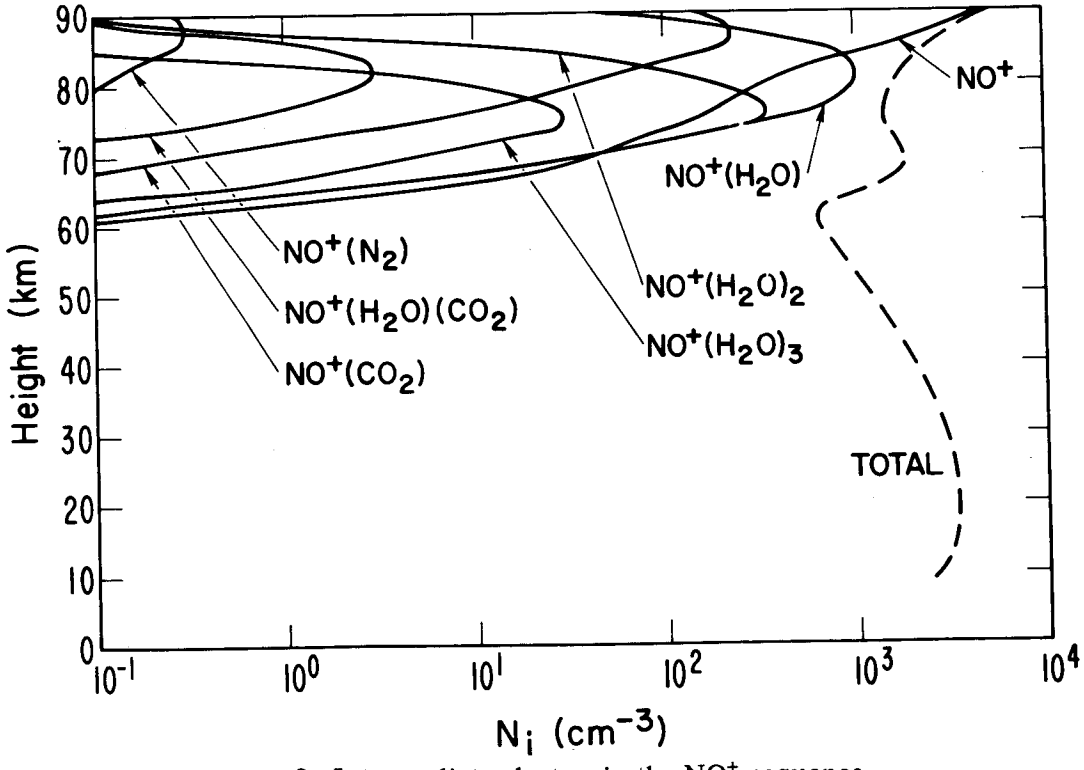

Figure 8. Intermediate clusters in the NO^+ sequence.

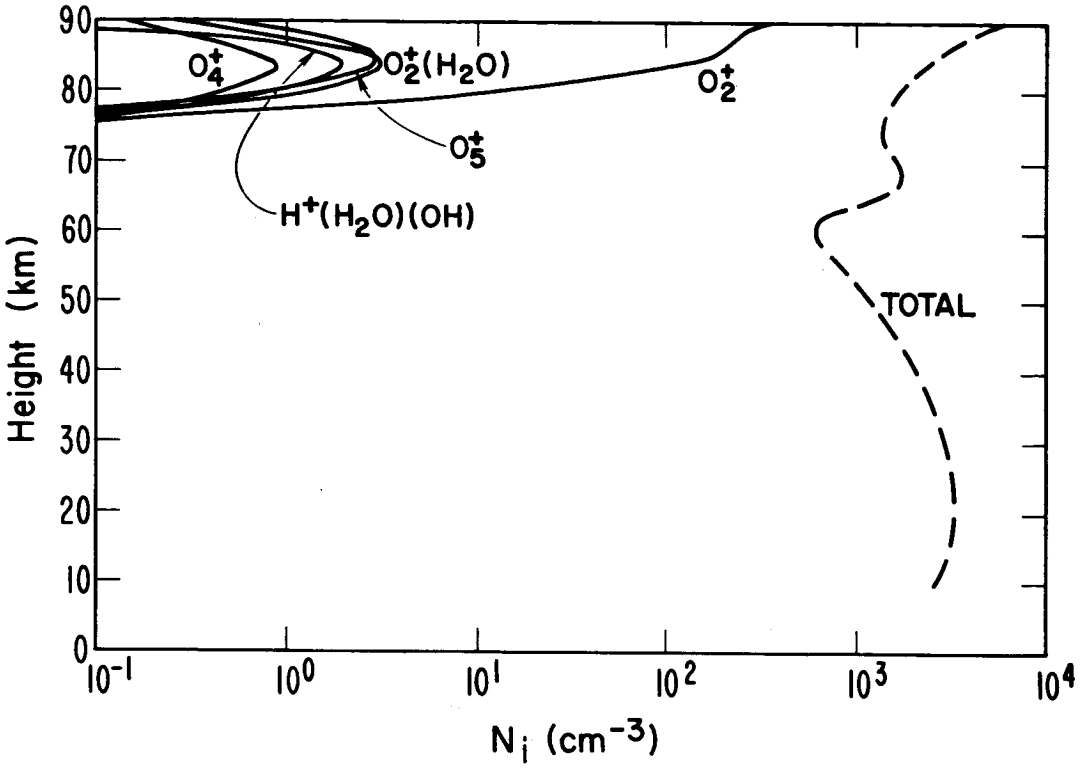

Figure 9. Intermediate clusters in the O_2^+ sequence.

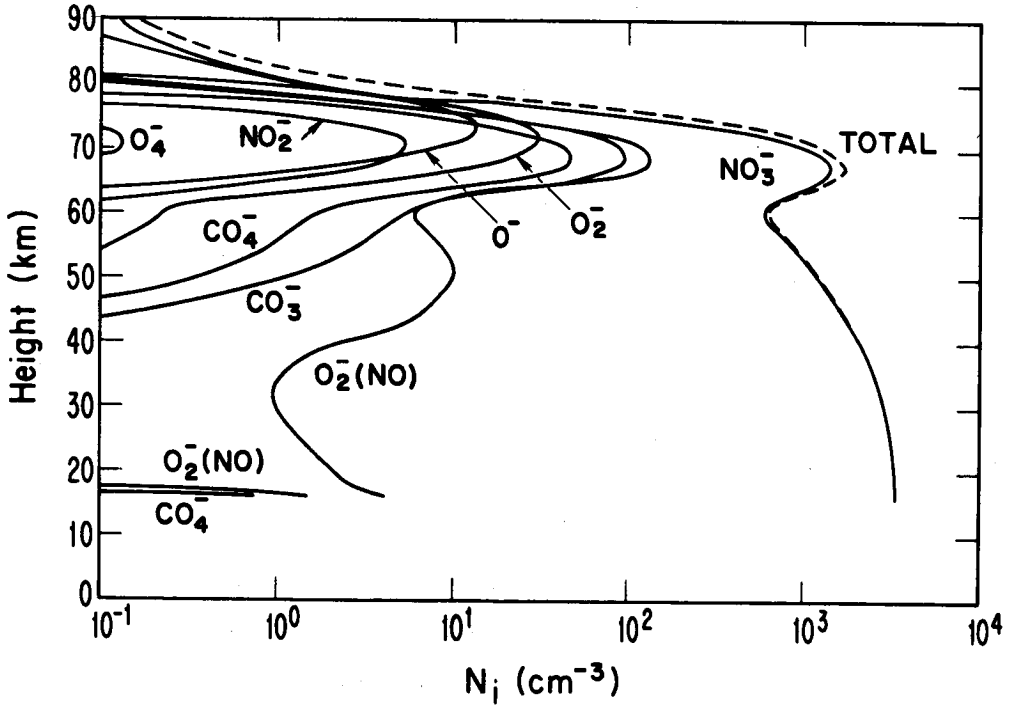

Figure 10. Negative-ion concentration profiles from model calculation (note: labels for CO_3^- and O_2^- (NO) are interchanged).

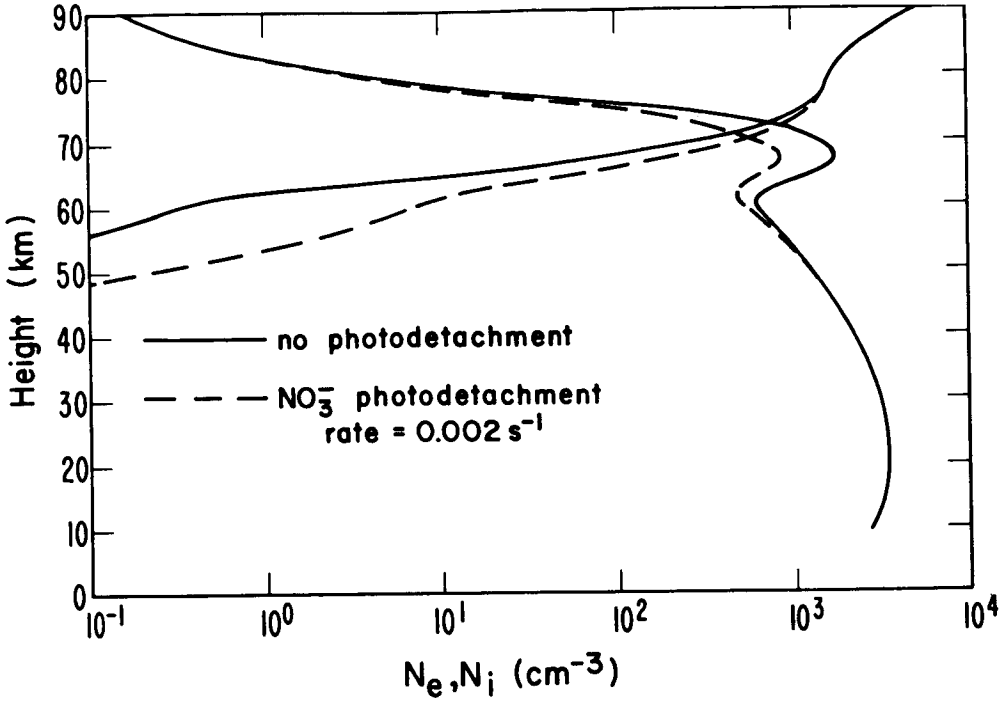

Figure 11. Effects of including NO_3^- photodetachment on negative-ion and electron profiles.

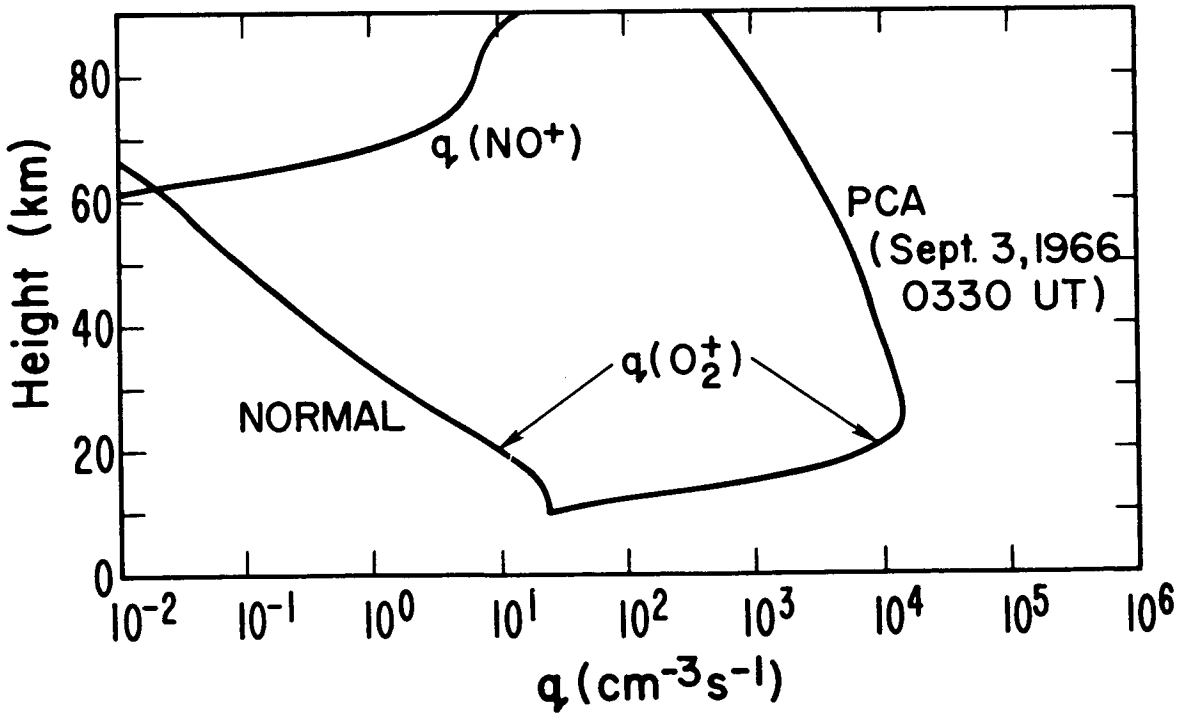

Figure 12. Ion production rate at the peak of the solar-proton event of September 1966 compared with undisturbed rates.

DIRECT ENERGY INPUTS TO THE MIDDLE ATMOSPHERE

T. J. Rosenberg
Institute for Physical Science and Technology
University of Maryland
College Park, Maryland 20742

L. J. Lanzerotti
Bell Laboratories
Murray Hill, New Jersey 07971

1. INTRODUCTION

The purpose of this review is to examine direct energy inputs to the middle atmosphere. As a working definition of the extent of the middle atmosphere we have adopted the height range from 30 to 100 km, a more restricted range than that used by Dr. Reid in his introductory lecture. The neutral and ionic composition and the dynamics within this height range are, for the most part, poorly understood. This is because of the sparsity of in situ measurements by rocket or balloon techniques. We assess, from available information, the importance of various particle and photon energy sources, including their variability, for ionization of the neutral atmosphere in this height range.

Knowledge of middle atmosphere ionization sources is important for a variety of reasons. For example, large variations in the ionizing input may play a role in aerosol formation (Mohnen and Kiang, 1978) and a role in altering the concentrations of minor neutral species (Crutzen et al., 1975; Thorne, 1977; Reagan et al., 1978). Variations in the ionization input can also modulate atmospheric electricity via the influence of conductivity variations on the mapping of electric fields and current flow (Markson, 1978). Thus, for the middle atmosphere at all geomagnetic latitudes, it is important to determine the relative importance of the ionization rates from the various background (quiet-time) energy sources; it is also important to evaluate the atmospheric response to transient solar-geophysical phenomena.

2. PENETRATION OF THE MIDDLE ATMOSPHERE BY PARTICLE AND ELECTROMAGNETIC ENERGY

Figure 1 pictorially presents the atmospheric penetration depth for various particle and electromagnetic energy sources. Of particular interest for ionization of the middle atmosphere is the wavelength range from the ultraviolet (UV) through x-rays, electrons > 0.01 MeV and protons > 0.3 MeV. Higher energy heavy nuclei (not illustrated here) can also penetrate to the middle atmosphere. Although it is not accurately depicted here, portions of the solar UV spectrum are absorbed above 100 km and, in the extreme ultraviolet (EUV), some solar line emissions (e.g., hydrogen Ly α) can penetrate below 100 km and can be the dominant source of ionization at altitudes above $\sim$ 60-70 km.

A more conventional view of particle and x-ray penetration of the atmosphere is shown in Figure 2. This figure defines more precisely the energy and wavelength limits of interest for this review. The curve for x-rays gives the 50% transmission height for a given energy. Thus, x-rays with wavelength $\lambda < 10$ Å (energy $E > 1$ keV) would deposit more than half of their energy below 100 km. However, x-rays of longer wavelengths may contribute significantly to the ionization of the middle atmosphere if, as in the case of solar x-rays, the incident flux is sufficiently large. Note that only relativistic electrons can affect directly the lower half of the middle atmosphere (below $\sim$ 60 km). The high proton energies required for penetration below 100 km, and particularly below $\sim$ 60 km, effectively precludes a significant contribution from precipitating magnetospheric protons. At high latitudes, of course, solar proton events become important, as will be discussed below.

3. IONIZATION SOURCES FOR THE MIDDLE ATMOSPHERE

All of the important ionization sources for the middle atmosphere are galactic, solar, or magnetospheric in origin. Previous reviews of ionization sources for the lower ionosphere (e.g., see Potemra and Zmuda, 1970; Potemra, 1973, 1974; Reagan, 1977) have emphasized different aspects of the subject (for example, application to VLF propagation, maintenance of the midlatitude nighttime ionosphere).

Table I lists the energy sources that contribute to the ionization of the middle atmosphere, together with estimates of the incident energy fluxes. In the table the various sources have been separated according to whether they contribute to the background (quiet-time) ionization levels, or are associated with specific events. Event sources can have durations ranging from a few minutes, as in the case of solar flare x-rays, to several days as in the case of solar cosmic ray events or for the midlatitude precipitation of energetic electrons following a geomagnetic storm (Spjeldvik and Thorne, 1975).

The contributions of auroral or ring current protons are not shown in the table because penetration to middle altitudes does not occur. In addition, two of the penetrating sources listed in the table have been shown to be of negligible importance. These include the 1-10 Å cosmic x-rays from both the diffuse background and from discrete sources including SCO X-1 (Potemra, 1973). These sources will not be discussed further here.

Direct energy deposition by auroral electrons is not a major factor for most of the middle atmosphere, in spite of the high fluxes indicated in the table. This is because the dominant fluxes of auroral electrons have energies < 10 keV. However, the lower fluxes of higher energy electrons which often accompany auroras, and which can precipitate on the dayside of the Earth as well as considerably equatorward of the nominal auroral regions, may at times be dominant ionization sources.

The x-ray bremsstrahlung produced by precipitating electrons will be deposited much deeper in the atmosphere than the primary electrons themselves. Since the bremsstrahlung production efficiency is of order 0.01% to 1% at the energies of interest, (Evans, 1955), the flux values listed in the table for magnetospheric electrons should be reduced by 10^{-4} - 10^{-2} to obtain associated x-ray energy fluxes.

The energy fluxes of the various sources listed in Table I range over 10 orders of magnitude. Because the energy deposited in the atmosphere by many of the sources is specific to some limited height or latitude range, the relative importance of different sources as ionizing agents cannot be judged merely by comparing the magnitudes of the incident fluxes. Consequently, as a quantitative measure for comparison, we have used the height profiles of the ionization rates of the sources. The computations of the energy deposition or ionization rates require the use of appropriate atmospheric density models, absorption coefficients, and range-energy relationships for each specific source. The details of these calculations are not considered here.

4. GALACTIC COSMIC RAYS

The charged particle component of the galactic cosmic rays is the dominant ionization source for the lower half of the middle atmosphere. Figure 3 shows the integral incident particle energy spectra of galactic cosmic rays before encountering the Earth's magnetic field, as a function of particle energy/nucleon. The minimum particle energy in this plot corresponds to 100 MeV protons, which can reach $\sim$ 30 km altitude in the absence of geomagnetic cutoff effects.

The data for protons and alpha particles are plotted for both solar maximum and solar minimum and the total intensity ($\sim 10^{-2}$ ergs $cm^{-2}\,sec^{-1} > 0.1$ GeV/nucleon) is given for solar minimum conditions. In this representation the effect of solar modulation over a solar cycle is seen to be $< 10\%$. This is due mainly to the fact that galactic cosmic ray spectra at the orbit of Earth have broad peaks at proton and alpha particle energies of about 200-300 MeV/nucleon. Thus, although the solar cycle modulation for particles of energies $\lesssim$ 200 MeV/nucleon may reach a factor of 5 or more, the relative contribution of these energy particles to the total incident energy flux is small (Lanzerotti, 1977). In spite of the fact that protons and alphas dominate the composition of the primary cosmic rays ($\sim$ 98.5%), they contribute only $\sim$50% to the rate of production of ionization (Velinov, 1968).

Two factors, the latitudinal (i.e., geomagnetic cutoff) effect and the solar cycle modulation, as just mentioned, substantially affect the cosmic ray flux incident on the atmosphere. The latitudinal effect enters through the dependence of the particle's cutoff rigidity on the magnitude of the Earth's magnetic field. The effect is illustrated in Figure 4 which plots the relative intensity of cosmic rays at $\sim$10 km altitude as a function of geomagnetic latitude. At this height the variation is almost a factor 2 between the equator and the auroral zone. Beyond $\lambda_m \simeq 70°$, essentially all cosmic rays have access to the top of the atmosphere and the effective cutoff is only atmospheric.

The solar cycle dependence of the ionization rate is illustrated in Figure 5. This figure shows the ionization rate at 20 g cm^{-2} altitude ($\sim$ 20 km, or near the base of the middle atmosphere) over 4 solar cycles, corrected to polar latitudes. Also plotted are the annual sunspot numbers. The atmosphere cutoff corresponds to protons of $\sim$ 500 MeV. The ionization rate at this altitude is seen to vary by about a factor 2 within one solar cycle and from one cycle to another (Pomerantz and Duggal, 1974; Lanzerotti, 1977).

Summarizing, we show in Figure 6 the altitude profile of the ionization rate for 3 geomagnetic latitudes and for solar maximum and minimum conditions at the higher latitudes, adopting values determined by Velinov (1968) and Webber (1962). The solar cycle dependence at the equator is very small and is not differentiated here. The ionization rate varies by 5 orders of magnitude over the middle atmosphere. Above $\sim$ 60-70 km, and depending on day/night conditions, the rate falls below the rates contributed by other background sources, most notably the photoionization of nitric oxide (NO) by solar H Ly α.

5. SOLAR H Ly α, OTHER EUV, AND X-RAYS

As was illustrated above in Figure 6, in the upper portion of the middle atmosphere the ionization from solar H Ly α overwhelms the galactic cosmic ray ionization. The energy flux of solar H Ly α incident directly on the atmosphere, and the time variability of this source, has been a topic of some debate. For example, Smith and Gottlieb (1974) adopted the incident energy value 8.5 ergs $cm^{-2}\,sec^{-1}$ for moderate solar activity. They attributed to this line a variability of $\leqslant 20\%$ over a solar cycle, including solar flare activity. More recently, Vidal-Madjar (1977) concluded that the Lyman α irradiance of the quiet sun increases by nearly a factor of 2 in going from solar minimum to solar maximum conditions. Typical values range from approximately 4.5 to 6 ergs $cm^{-2}\,sec^{-1}$ (as listed in Table I). The absolute accuracy of these determinations is now believed known to better than $\pm$ 30%. Enhancements associated with solar flares are negligible ($< 20\%$) except for very unusual flares (Vidal-Madjar, 1977; Smith and Gottlieb, 1974).

The flux of scattered solar H Ly α on the nightside is more uncertain. Measurements tend to show it to range from 10^{-3} to 10^{-2} that of the direct flux (Donahue, 1966; Tohmatsu, 1970). The higher figure has generally been adopted by most researchers.

The photoionization of nitric oxide by solar H Ly α in the height range 70-100 km is usually computed using the nitric oxide densities obtained by Meira (1971) from daytime midlatitude rocket measurements of the resonance fluorescence of NO. However, Strobel (1972) has argued that lower NO densities below $\sim$ 80 km are also consistent with the data. The ionization rates for both the Meira (1971) data and the Strobel (1972) interpretation are shown in Figure 6. These two density estimates illustrate the critical dependence of the rates on the NO concentration and, in turn, on the altitude at which cosmic ray ionization becomes dominant.

Smith and Gottlieb (1974) reviewed the solar photon flux and its variations at all wavelengths. The measurements are summarized in Figure 7 according to the level of solar activity. For solar photon wavelengths $\lambda < 100$ Å there are order of magnitude variations, even in the absence of pronounced flare activity. For $\lambda > 100$ Å there is little variation, except during major flares.

The solar x-ray fluxes in several wavelength ranges are further summarized in Table II (from data in Smith and Gottlieb, 1974), for different solar activity levels. Quiet sun refers to sunspot numbers R $\sim$ 10-40 and the absence of large plage regions (a solar minimum condition). Active refers to R $\sim$ 100 with no flares present (a solar maximum condition - essentially the present (1979) situation). Slowly - varying refers to the growth and decay of large active regions and their appearance and disappearance as the sun rotates. The photon energy flux increase is a factor of 20 for $\lambda < 10$ Å, 3 for 10-30 Å, and $\sim$ 1.5 for 30-100 Å for a change from quiet to active conditions.

Although the x-ray flux increase during solar flares can be spectacular, the energy deposition in the atmosphere from an x-ray flare occurs within a time interval of only $\sim$ 15 min. Thus x-ray flares are less likely to be important in the long term than the general non-flare background. However, whether or not solar x-ray flare ionization can serve as a "trigger" source for some geophysical process under some conditions remains a matter of pure speculation.

The ionization rates from solar x-rays, compared to UV and H Ly α, are shown in Figure 8. The heavy solid curves labeled MIN and MAX? refer to calculations performed by Thrane (1972) for a solar zenith angle of 50° and are based on pre-1970 measurements of the non-flare solar x-ray flux. His results for solar minimum conditions seem reasonable still in view of the Smith and Gottlieb (1974) estimates. However, Thrane's (1972) results for solar maximum seem to be based upon a considerable overestimate of the solar cycle flux increase. The thin solid line (labeled MAX) in the figure is our estimate based upon the average values suggested in the tabulation of Smith and Gottlieb (1974). Figure 8 suggests that ionization by non-flare solar x-rays may dominate over the H Ly α contribution above $\sim$ 85 km on the dayside during the active years of the solar cycle. The ionization rates for solar UV (other than H Ly α), taken from a previous review (Potemra, 1973), are seen to be of secondary importance compared to the x-rays, except near the very top of the middle atmosphere during solar minimum.

6. MAGNETOSPHERIC ELECTRONS AND BREMSSTRAHLUNG X-RAYS

A picture of the geographical distribution of observations of trapped 100 keV electrons at altitudes of 250-400 km from measurements obtained on a polar-orbiting satellite during a several-day interval in 1961 is shown in Figure 9 (Seward, 1973; Paulikas, 1975). This figure graphically illustrates the presence and approximate extent of the auroral zones as well as the regions of trapped fluxes extending to quite low latitudes, including the magnetic anomaly region in the South Atlantic.

These measurements, although of trapped electrons, were among the first to suggest that energetic electrons probably also precipitate into the atmosphere over a similarly extensive region. Later satellite, rocket, and balloon measurements have, of course, largely supported this view. Most of the precipitation occurring over this vast area is believed to be driven by wave-particle interactions occurring in the magnetosphere. The particle energy spectra are complex, as are the pitch angle distributions, and the precipitating flux levels are dependent on latitude, longitude, and the level of geomagnetic activity.

Interest in the precipitation of energetic electrons at low and middle latitudes arose because of their possible importance in the maintenance of the undisturbed nighttime D region and for their possible production of magnetic storm after-effects which are observed on VLF communication signals. Potemra and Zmuda (1970) reviewed the available midlatitude satellite and rocket data on precipitated > 40 keV electron fluxes. They parameterized the ranges of flux levels with power law energy spectra and computed the ionization rates assuming isotropic pitch angle distributions. Their results, compared with some measurements and other ionization rates already discussed, are shown in Figure 10 (Potemra, 1973). Curves A, B, and C refer to energy fluxes and power law exponents of $\sim 5 \times 10^{-3}$ (-3), 2×10^{-4} (-3), and 1.5×10^{-3} (-5), respectively. Spectra B and C correspond to relatively undisturbed conditions, whereas spectrum A corresponds to a more active period. The

quiet time ionization rates by the electrons exceed the scattered H Ly α contribution between $\sim$ 70 and 90 km, depending upon the spectrum chosen. The A spectrum is also comparable to or exceeds the direct H Ly α contribution on the dayside (compare with Figure 8, for example). Thus, energetic electron precipitation at middle latitudes can be a significant ionization source for the lower ionosphere for both nighttime and daytime conditions.

The importance of midlatitude electron precipitation to the ionization of the middle atmosphere has also been discussed by Gough and Collin (1973), Larsen et al., (1976), and Spjeldvik and Thorne (1975).

Gough and Collin (1973) compared 13 rocket measurements of $>$ 40 keV electron precipitation from the L = 3.6 site of South Uist, Scotland, with the K_p sum for the 24-hr interval centered at the launch times. They found the relationship illustrated in Figure 11. Clearly, larger fluxes were encountered with increased magnetic activity. Electron fluxes sufficient to produce ionization equivalent to the nighttime and daytime levels from other sources (the "threshold" level) were estimated as 10^2 and 10^4 $cm^{-2}\,sec^{-1}\,ster^{-1}$, respectively, on the basis of the measured energy spectra. The lower horizontal axis scale in Figure 11 show the percentage of days at solar maximum and solar minimum when the magnetic activity exceeds the corresponding K_p sum. Gough and Collin (1973) concluded that the nighttime threshold was reached on 35 $\pm$ 20% of the nights at solar maximum and 15 $\pm$ 11% of the nights at solar minimum. Corresponding percentages for reaching the daytime threshold were estimated at 1% - 5% at solar maximum and $\sim$ 0.1% at solar minimum.

Most estimates of the electron-produced ionization at low and middle latitudes have been based on rather imprecise knowledge of the actual energy and pitch angle distributions of the precipitated electrons. More recently, Larsen et al., (1976) used detailed energy spectra obtained by satellite to evaluate the ionization produced at L = 3.6 during moderately disturbed periods. A sample spectrum from their work is shown in Figure 12. Electron energy information was available from 10-40 keV and $>$ 130 keV. Using the spectral form given by the dashed/solid curve, and an isotropic pitch angle distribution, Larsen et al., derived the ion pair production rates shown in Figure 13 for both the direct electron impact ionization and the ionization produced by the associated electron bremsstrahlung x-rays.

Figure 13 indicates that direct electron production rates far exceed other daytime sources at altitudes above $\sim$ 55 km. In contrast, the production rates from bremsstrahlung were negligible at all altitudes. Energy spectra measured for a number of other events also gave rates that exceeded those from non-precipitation sources in the 60-70 km altitude range and were competitive with these sources at higher altitudes.

Finally, Spjeldvik and Thorne (1975) have shown that electron precipitation fluxes sufficient to produce ionization rates similar to those shown in Figure 13 can be derived from midlatitude observations, during magnetic storms, of trapped electron energy and pitch angle distributions. Their model is based on resonant pitch angle scattering of trapped electrons with extremely low frequency ($<$ 1 kHz) electromagnetic waves within the plasmasphere.

Considerably higher fluxes of precipitated energetic electrons are routinely encountered in the auroral zones than in middle latitudes. There seems little question that ionization produced by substorm electrons will dominate the upper reaches of the middle atmosphere a large fraction of the time, in the narrow latitude strip ($\lesssim 10^\circ$) defining the auroral zone. According to estimates by Davis et al., (1978), the Earth experiences substorm conditions (as defined by auroral electrojet index (AE) values exceeding 100γ) from $\sim$ 24% to $\sim$ 36% of the time, depending on the phase of the solar cycle.

The spectrum of precipitated electrons in the auroral zone is characterized by the relatively low energy ($<$ 10 keV) electrons that produce the visible aurora at night and the higher energy electrons ($\gtrsim$ 40 keV) that are principally responsible for the radiowave absorption recorded on the dayside by riometers. Rees (1969), Boyd (1975), and Bailey (1968) have reviewed the characteristics of auroral zone electron precipitation and the related ionospheric effects. Calculations of the energy deposition by electrons have been performed by Rees (1963), Berger et al., (1974), and Banks et al., (1974). Rees (1964), Berger and Seltzer (1972), and Newkirk et al., (1974) have also calculated the bremsstrahlung energy deposition from precipitated electrons. We show here, in Figure 14, two representative examples of the electron and bremsstrahlung ionization rates for exponential electron energy spectra and isotropic pitch angle distributions, using the calculations of Berger et al., (1974), and Berger and Seltzer (1972).

For the nightside spectrum (ionization rate curve 1) a flux and spectrum was chosen sufficient to produce $\sim$ 10 kR of auroral luminosity and $\sim$ 1 dB of auroral 30 MHz radio absorption. For this spectrum, 60% of the total energy flux is in electrons with energies $<$ 10 keV. For the daytime precipitation, a flux and spectrum was chosen sufficient to produce a 4 dB 30 MHz radio absorption event (corresponding to the average peak absorption on the dayside found by Berkey et al., (1974) in a study of 60 substorms). For each spectrum, the electron-induced ionization rates dominate over the nonprecipitation sources, above an altitude of $\sim$ 85 km for spectrum 1, and above $\sim$ 60 km for spectrum 2. It is interesting to note that, in the absence of high energy precipitation at night, the bremsstrahlung x-ray contribution from the low-energy spectrum could dominate the ionization rate to altitudes as low as 50 km.

Electron precipitation with energies sufficiently high ($\gtrsim$ 200 keV) to perturb daytime HF forward scatter radar or VLF propagation circuits is known to occur during some geomagnetic storms and substorms (Bailey, 1968; Bailey et al., 1970; Rosenberg et al., 1972; Larsen and Thomas, 1974; and Thorne and Larsen, 1976). Such events have been called relativistic electron precipitation (rep) events. However, it is not clear that this precipitation differs from the more typical substorm precipitation in any way other than being somewhat more intense (but not necessarily more energetic). The frequency of occurrence, spatial extent, and intensity levels of truly relativistic electron precipitation have yet to be thoroughly investigated.

Energy deposition by electrons or bremsstrahlung x-rays has been speculated as possibly influencing the mechanisms for cirrus cloud formation (Roberts and Olson, 1973 a,b) and for thunderstorm generation (Markson, 1978). However, these energy sources have been rejected as an important agent for solar-weather coupling on the basis of energy flux considerations (Johnson and Imhof, 1975; Willis, 1976).

7. SOLAR COSMIC RAYS

Although the Sun seems to be a more or less continuous emitter of low fluxes of MeV particles, these fluxes have relatively little impact on the ionization of the middle atmosphere. In contrast, the discrete solar flare events that produce large fluxes of $>$ 10 MeV particles can dominate the ionization levels of the polar caps over the entire range of the middle atmosphere for several days at a time.

As for auroral electron precipitation, a measure of the extent and effect of solar particle bombardment of the atmosphere can be obtained by observing the absorption of galactic radio noise. The normal geographical distribution of polar cap radiowave absorption effects (pca) is illustrated for both hemispheres in Figure 15. Inside the inner curve, which corresponds approximately to a geomagnetic cutoff energy of 1 MeV, pca effects are observed at their maximum intensity. On the other hand, regions outside the outer curve, which corresponds to a cutoff of $\sim$ 100 MeV, are normally not affected. The locations in invariant latitude of these energy limits correspond to about 65° and 60°. These latitudes change with geomagnetic disturbances, decreasing by a few degrees with increased magnetic storm intensity.

In addition to protons, the composition of solar flare particle events includes alpha particles and other heavy nuclei as well as electrons. With certain few exceptions, these other components are of secondary importance as regards their contribution to the ionization of the middle atmosphere. One important exception can occur at the onset of a solar event, when, for the first hour or so, electron bombardment of the atmosphere will be predominant. At these times, the cosmic noise absorption can be attributed solely to high energy electrons arriving promptly from a flare (e.g., Lanzerotti and Maclennan, 1972).

Solar proton fluxes incident on the atmosphere have been measured indirectly over the last two solar cycles by the use of riometers to record the cosmic radio noise absorption in the ionosphere. Figure 16 (top) presents the number of pca events per year from 1965 through 1973 for which the equivalent 30 MHz peak absorption was greater than 2.5 dB (Pomerantz and Duggal, 1974; Lanzerotti, 1977). Also shown is the yearly sunspot number. The number of pca events is seen to roughly track the sunspot cycle. Figure 16 (bottom) shows the average peak absorption for the pca events in each year. The righthand scale gives an estimate of the incident flux of $>$ 7 MeV protons based upon an empirical relationship derived by Potemra (1972), $J(E> 7\ \text{MeV}) = (0.083)^{-2} A^2$, which relates the particle flux $J(\text{cm}^{-2}\text{sec}^{-1})$ to the radiowave absorption A (dB).

Except for the two periods of extreme absorption (1959, 1972), both of which occurred during the declining phase of each solar cycle, the average absorption does not show a pronounced dependence on either the phase of the cycle or the relative magnitude of the cycle as given by the maximum sunspot numbers. However, the yearly incidence of solar protons as measured by the total absorption does roughly follow the sunspot cycle (Pomerantz and Duggal, 1974; Lanzerotti, 1977).

Direct measurements of solar proton fluxes by satellites outside the magnetosphere became routinely available after 1965 (i.e., during solar cycle 20). Figure 17 illustrates the event-integrated solar proton fluxes ($>$ 10 MeV and $>$ 30 MeV) measured by satellite after 1965 and estimates of

the >30 MeV fluxes from indirect measures available during the previous cycle (King, 1974; Lanzerotti, 1977). Included in this figure are all events (intervals of time of about a week) for which the time-integrated flux of protons above 30 MeV exceeded 10^6 cm^{-2}. For protons >10 MeV the event of 4 August 1972 had a total integrated intensity about 20 times that of any of the other events in solar cycle 20.

On occasion the sun produces cosmic rays with energies as high as several GeV, which can be recorded at ground level by detectors such as neutron monitors and (for the most energetic events) meson telescopes. The peak intensities of the individual ground level events since their discovery in 1942 are shown in Figure 18 (Pomerantz and Duggal, 1974). For an hour or so for each event, the events can exceed, by several tens to several hundreds of percent, the galactic cosmic ray intensity levels. Most (but not all) ground level events are followed by the regular, long (several days) pca events produced by the lower energy proton fluxes.

The importance of ground level events for middle atmosphere processes and dynamics, other than for producing intense, short-lived atmospheric ionization, may lie in any "triggering" process they may initiate. Such considerations are purely speculative at this time.

Solar flare γ-rays were observed for the first (and only) time in the solar flare events of August 4 and 7, 1972 (Chupp et al., 1973). Gamma rays probably accompany all flares that produce large, ground-level events. The γ-ray fluxes probably last no longer than, or shorter than, the normal x-ray bursts from a flare ($\lesssim 15$ minutes). Their ionization effects and possible significance must be considered in the light of these short time scales.

Zmuda and Potemra (1972) computed, from the proton fluxes and energy spectra measured by several satellites, the ionization rates for a number of solar proton events that occurred between 1965 and 1969. These rates, corresponding to the peak proton fluxes observed during each event, are shown in Figure 19. Also included are the ionization rates for the peak of the August 4, 1972 event, the largest on record. The incident energy fluxes for all but the August 1972 event lie in the range 10^{-2} - 10^{0} ergs cm^{-2}-sec^{-1}. For the August 1972 event, the energy flux reached 50 ergs cm^{-2} -sec^{-1}.

The ionization rates during "average" pca events far exceed those from any other source at altitudes below $\sim$ 80-90 km and above $\sim$ 20-30 km. However, as the curves in Figure 19 show, it is obviously difficult to "typify" the ionization situation during solar particle events. For example, the rates maximize at altitudes varying from 40 to 80 km, depending on the event, indicating that the spectra of individual events can vary widely.

8. SUMMARY

Ionization of the middle atmosphere is controlled, to a degree strongly dependent on altitude and latitude, by direct energy inputs in the form of galactic and solar cosmic rays, solar H Ly α (and solar UV and EUV radiation), non-flare and flare-associated solar x-rays, and magnetospheric electron precipitation with its associated x-ray bremsstrahlung. Of these sources, only galactic and solar cosmic rays and high energy solar x-rays and x-ray bremsstrahlung can contribute to the ionization

at altitudes below $\sim$ 50 km; the x-ray sources appear to be non-competitive at altitudes below $\sim$ 30-40 km.

Computational methods are available for evaluating rates of energy deposition (and ionization) to sufficiently high accuracies for most purposes if particle source characteristics (flux, energy spectrum, pitch angle distributions, and time dependencies) can be specified. Ionization rates represent a starting point for the calculations of ultimate interest for middle atmosphere electrodynamics, namely equilibrium ion and electron densities and conductivities, and their time rates of change. These quantities depend on other factors, such as details of the atmospheric chemistry, which have not been considered here.

REFERENCES

Bailey, D. K., Some quantitative aspects of electron precipitation in and near the auroral zone, *Revs. Geophys.*, **6**, 289, 1968 (see also Correction, *Revs. Geophys.*, **7**, 666, 1969).

Bailey, D. K., R. R. Brown, and M. H. Rees, Simultaneous forward-scatter, riometer, and bremsstrahlung observations of a daytime electron precipitation event in the auroral zone, *J. Atmos. Terr. Phys.*, **32**, 149, 1970.

Banks, P. M., C. R. Chappell, and A. F. Nagy, A new model for the interaction of auroral electrons with the atmosphere: spectral degradation, backscatter, optical emission and ionization, *J. Geophys. Res.*, **79**, 1459, 1974.

Berger, M. J., and S. M. Seltzer, Bremsstrahlung in the atmosphere, *J. Atmos. Terr. Phys.*, **34**, 85, 1972.

Berger, M. J., S. M. Seltzer, and K. Maeda, Some new results on electron transport in the atmosphere, *J. Atmos. Terr. Phys.*, **36**, 591, 1974.

Berkey, F. T., V. M. Driatskiy, K. Henriksen, B. Hultqvist, D. H. Jelly, T. I. Schuka, A. Theander, and J. Yliniemi, A synoptic investigation of particle precipitation dynamics for 60 substorms in IQSY (1964-1965) and IASY (1969), *Planet Space Sci.*, **22**, 255, 1974.

Boyd, J. S., Rocket-borne measurements of auroral electrons, *Revs. Geophys. Space Phys.*, **13**, 735, 1975.

Chupp, E. L., D. J. Forrest, R. R. Higbie, A. N. Suri, C. Tsai, and P. P. Dunphy, Solar gamma ray lines observed during the solar activity of August 2 to August 11, 1972, *Nature*, **241**, 333, 1973.

Crutzen, P. J., I. S. A. Isaksen, and G. C. Reid, Solar proton events: stratospheric sources of nitric oxide, *Science*, **189**, 457, 1975.

Davis, T. N., O. Royrvik, and T. J. Hallinan, Reply, *J. Geophys. Res.*, **83**, 5327, 1978.

Donahue, T. M., The problem of atomic hydrogen, *Ann. Geophys.*, **22**, 175, 1966.

Evans, R. D., *The Atomic Nucleus*, McGraw-Hill Publ. Co., New York, 1955.

Gough, M. P., and H. L. Collin, Energetic electron precipitation as a source of ionization in the nighttime D region over the midlatitude rocket range, South Uist, *J. Atmos. Terr. Phys.*, **35**, 835, 1973.

Johnson, R. G., and W. L. Imhof, Direct satellite observations on bremsstrahlung radiation as a technique to investigate its role in meteorological processes, in *Possible Relationships Between Solar Activity and Meteorological Phenomena*, NASA SP-366, 89, 1975.

King, J. H., Solar proton fluences for 1977-1983 space missions, *J. Spacecraft and Rockets*, **11**, 401, 1974.

Lanzerotti, L. J., Measures of energetic particles from the Sun, in *The Solar Output and Its Variation*, edited by O. R. White, p. 383, Colorado Associated University Press, Boulder, Colorado, 1977.

Lanzerotti, L. J., and C. G. Maclennan, Relative importance of solar electrons, protons, and alphas in the November 1969 PCA event, in *Proc. COSPAR Symp. Solar Particle Event of November 1969*, AFCRL-72-0474, 85, 1972.

Larsen, T. R., and G. R. Thomas, Energy spectra measured during a relativistic electron precipitation event on 2 February 1969, *J. Atmos. Terr. Phys.*, **36**, 1613, 1974.

Larsen, T. R., J. B. Reagan, W. L. Imhof, L. E. Montbriand, and J. S. Belrose, A coordinated study of energetic electron precipitation and D region electron concentrations over Ottawa during disturbed conditions, *J. Geophys. Res.*, **81**, 2200, 1976.

Markson, R., Solar modulation of atmospheric electrification and possible implications for the Sun-weather relationship, *Nature*, **273**, 103, 1978.

Meira, L. G., Jr., Rocket measurements of upper atmospheric nitric oxide and their consequences to the lower ionosphere, *J. Geophys. Res.*, **76**, 202, 1971.

Mohnen, V. A., and C. S. Kiang, Ion-Molecule interactions of atmospheric importance, ASRC-SUNY Publ. No. 681, 1978.

Newkirk, L. L., W. E. Francis, and M. Walt, Bremgat - A code for the generation and transport of bremsstrahlung through the atmosphere, *Rep. LMSC/D407007*, Lockheed Palo Alto Res. Lab., Palo Alto, Calif., 1974.

Paulikas, G. A., Precipitation of particles at low and middle latitudes, *Revs. Geophys. Space Phys.*, **13**, 709, 1975.

Pomerantz, M. A., and S. P. Duggal, the Sun and cosmic rays, *Revs. Geophys. Space Phys.*, **12**, 343, 1974.

Potemra, T. A., The empirical connection of riometer absorption to solar protons during pca events, *Radio Sci.*, **7**, 571, 1972.

Potemra, T. A., Precipitating energetic electrons in the mid-latitude lower ionosphere, in *Physics and Chemistry of Upper Atmosphere*, edited by B. M. McCormac, p. 67, D. Reidel, Dordrecht, Netherlands, 1973.

Potemra, T. A., Ionizing radiation affecting the lower ionosphere, in *ELF-VLF Radio Wave Propagation*, edited by J. A. Holtet, p. 21, D. Reidel, Dordrecht, Netherlands, 1974.

Potemra, T. A., and A. J. Zmuda, Precipitating energetic electrons as an ionization source in the mid-latitude nighttime D region, *J. Geophys. Res.*, **75**, 7161, 1970.

Reagan, J. B., Ionization processes, in *Dynamical and Chemical Coupling Between the Neutral and Ionized Atmosphere*, edited by B. Grandal and J. A. Holtet, p. 145, D. Reidel, Dordrecht, Netherlands, 1977.

Reagan, J. A., R. W. Nightingale, R. E. Meyerott, R. C. Gunton, R. G. Johnson, J. E. Evans, and W. L. Imhof, Effects of the August 1972 solar particle events on stratospheric ozone, *Tech. Report LMSC-D630455*, Lockheed Palo Alto Res. Lab., Palo Alto, Calif., 1978.

Rees, M. H., Auroral ionization and Excitation by incident energetic electrons, *Planet. Space Sci.*, **11**, 1209, 1963.

Rees, M. H., Auroral electrons, *Space Science Revs.*, **10**, 413, 1969.

Rees, M. H., Ionization in the Earth's atmosphere by aurorally associated bremsstrahlung x-rays, *Planet. Space Sci.*, **12**, 1093, 1964.

Reid, G. C., Polar cap absorption-observations and theory, in *Fundamentals of Cosmic Physics*, p. 167, Gordon and Breach, Great Britain, 1974.

Roberts, W. O., and R. H. Olson, Geomagnetic storms and wintertime 300-mb trough development in the North Pacific-North America area, *J. Atmos. Sci.*, **30**, 135, 1973a.

Roberts, W. O., and R. H. Olson, New evidence for effects of variable solar corpuscular emission on the weather, *Rev. Geophys. Space Phys.*, **11**, 731, 1973b.

Rosenberg, T. J., L. J. Lanzerotti, D. K. Bailey, and J. D. Pierson, Energy spectra in relativistic electron precipitation events, *J. Atmos. Terr. Phys.*, **34**, 1777, 1972.

Sandström, A. E., *Cosmic Ray Physics*, North-Holland Publ. Co., Amsterdam, 1965.

Seward, F. D., The geographical distribution of ~ 100 keV electrons above the Earth's atmosphere, *Rep. UCRL-51456*, Univ. of Calif., Lawrence Livermore Lab., Livermore, Oct. 1973.

Smith, E. V. P., and D. M. Gottlieb, Solar flux and its variations, *Space Science Revs.*, **16**, 771, 1974.

Spjeldvik, W. N., and R. M. Thorne, The cause of storm after effects in the middle latitude D region, *J. Atmos. Terr. Phys.*, **37**, 777, 1975.

Strobel, D. F., Nitric oxide in the D region, *J. Geophys. Res.*, **77**, 1337, 1972.

Thorne, R. M., Energetic radiation belt electron precipitation: a natural depletion mechanism for stratospheric ozone, *Science*, **195**, 287, 1977.

Thorne, R. M., and T. R. Larsen, An investigation of relativistic electron precipitation events and their association with magnetospheric substorm activity, *J. Geophys. Res.*, **81**, 5501, 1976.

Thrane, E. V., On the diurnal and seasonal variations of the D and E regions above Kjeller, in *Magnetosphere-Ionosphere Interactions*, edited by K. Folkestad, p. 29, Universitetsforlaget, Oslo, Norway, 1972.

Tohmatsu, T., The hydrogen and helium ultraviolet glow, its origin and aeronomical significance, *Space Res.*, **10**, 608, 1970.

Velinov, P., On ionization in the ionospheric D region by galactic and solar cosmic rays, *J. Atmos. Terr. Phys.*, **30**, 1891, 1968.

Vidal-Madjar, A., The solar spectrum at Lyman-alpha 1216 Å, in *The Solar Output and Its Variation*, edited by O. R. White, p. 213, Colorado Associated University Press, Boulder, Colorado, 1977.

Waddington, C. J., Chemical composition and energy content of the energetic cosmic radiation, in *Proc. Symp. Natural and Manmade Radiation in Space*, edited by E. W. Warman, NASA publication TM-X-2440, 209, 1972.

Webber, W. R., The production of free electrons in the ionosphere D layer by solar and galactic cosmic rays and the resultant absorption of radio waves, *J. Geophys. Res.*, **67**, 5091, 1962.

Willis, D. M., The energetics of Sun-weather relationships: magnetospheric processes, *J. Atmos. Terr. Phys.*, **38**, 685, 1976.

Zmuda, A. J., and T. A. Potemra, Bombardment of the polar cap ionosphere by solar cosmic rays, *Revs. Geophys. Space Phys.*, **10**, 981, 1972.

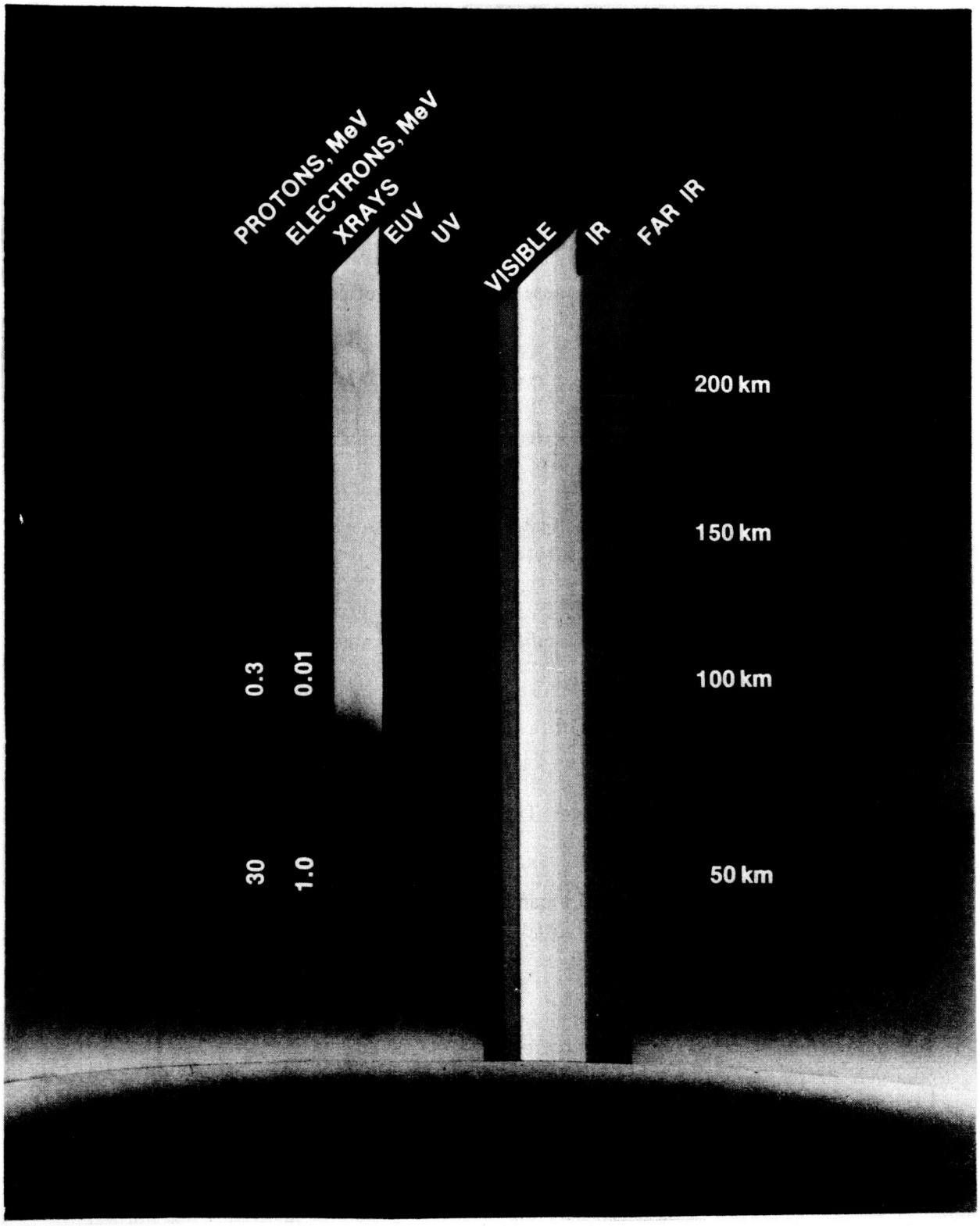

Figure 1. Pictorial representation of penetration depths of particle and electromagnetic radiation incident on the atmosphere.

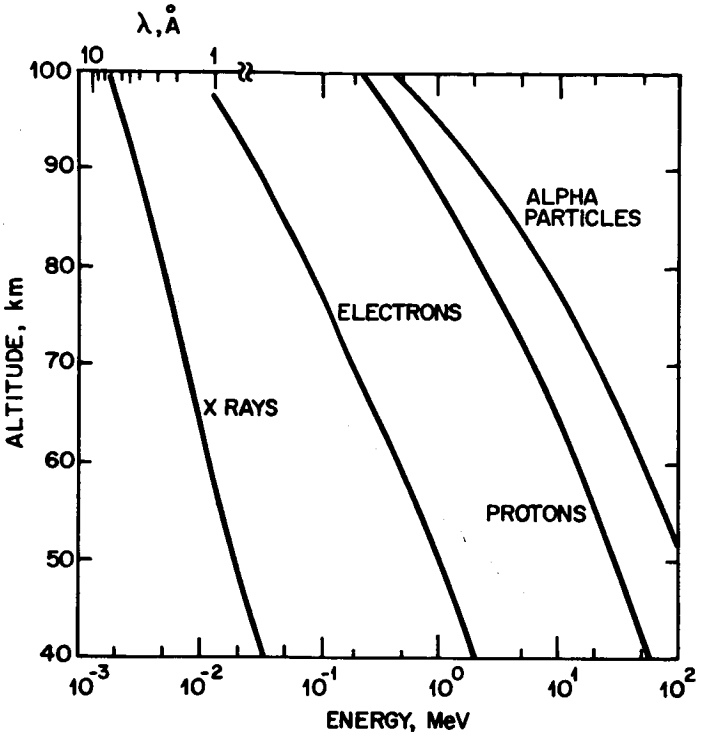

Figure 2. Penetration depth as a function of energy for particles and x-rays capable of ionizing the middle atmosphere. From Potemra (1974).

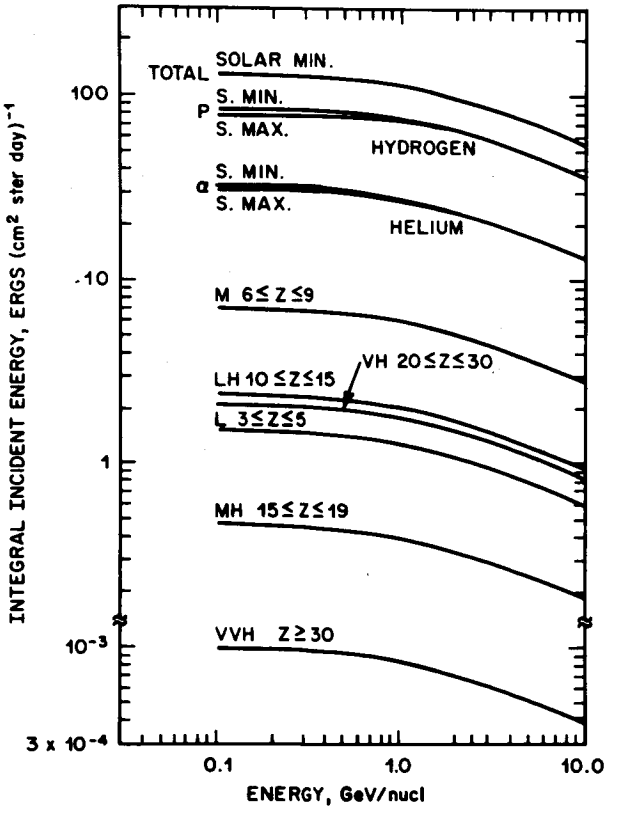

Figure 3. Integral energy intensities for galactic cosmic ray nuclei. From Waddington (1972).

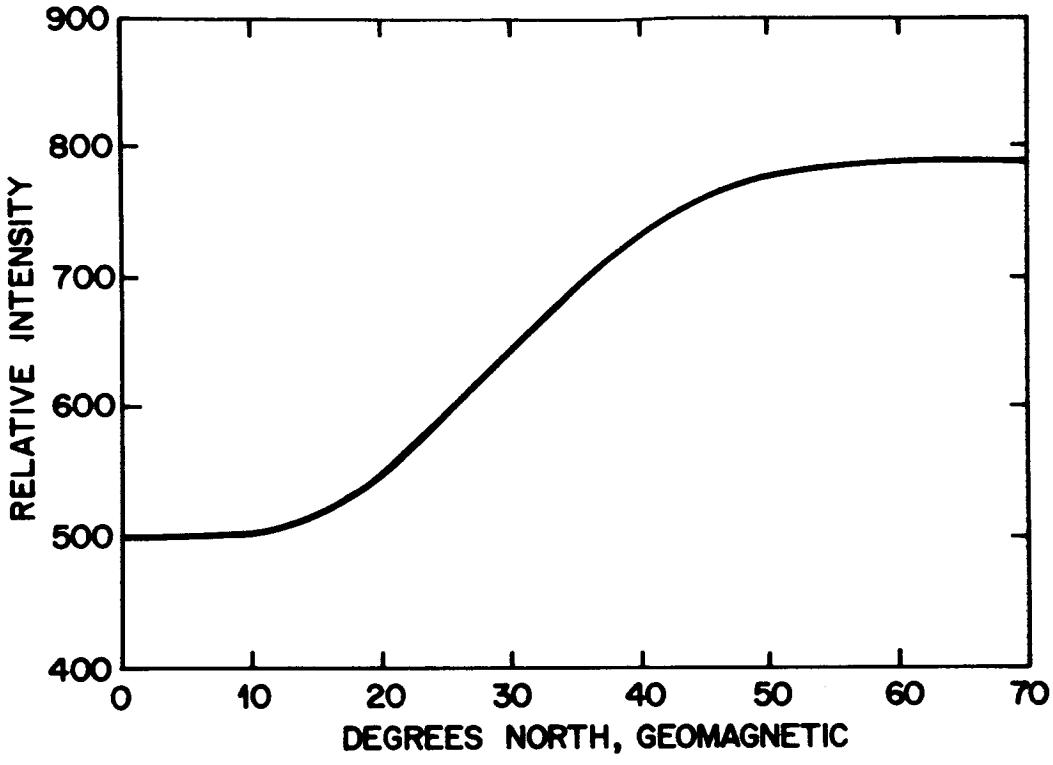

Figure 4. Relative intensity of galactic cosmic rays at 10 km altitude as a function of geomagnetic latitude. Adapted from Sandström (1965).

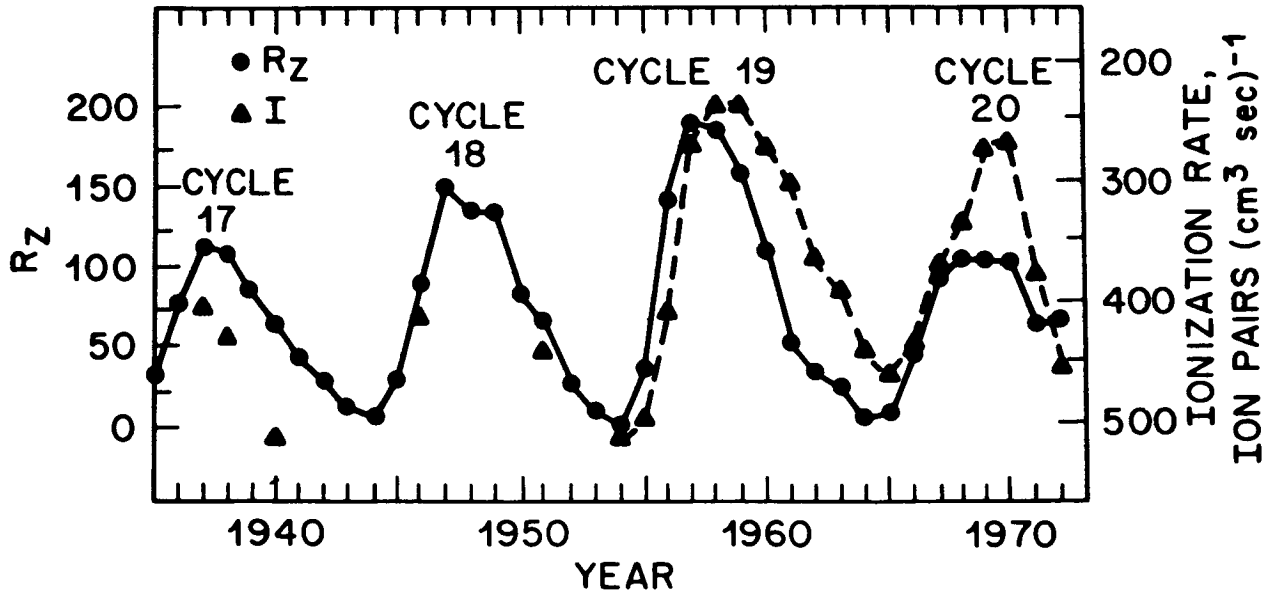

Figure 5. Ionization rate at an altitude of 20 g cm^{-2} for the last four solar cycles. All of the data have been normalized to geomagnetic location of Thule, Greenland. From Pomerantz and Duggal (1974).

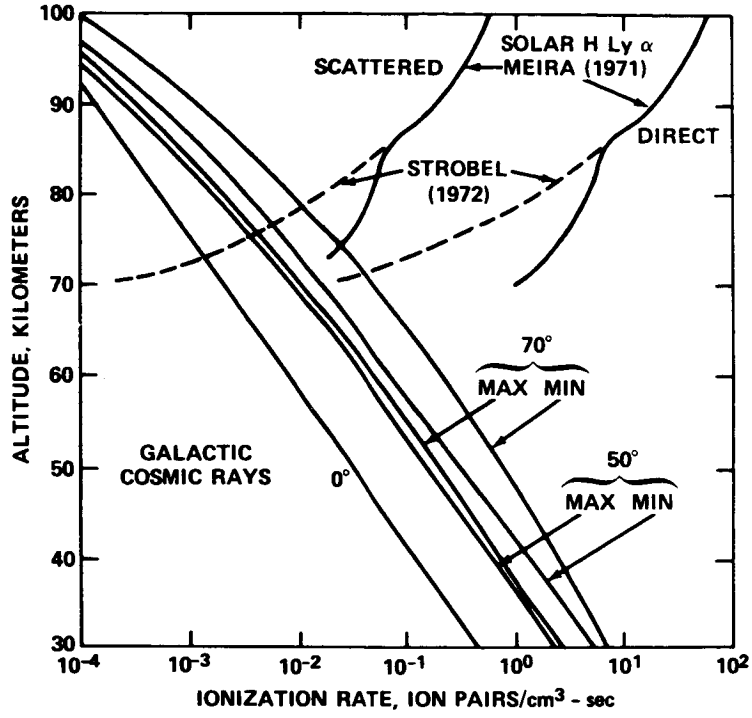

Figure 6. Altitude dependence of ionization rate due to galactic cosmic rays and solar H Ly α.

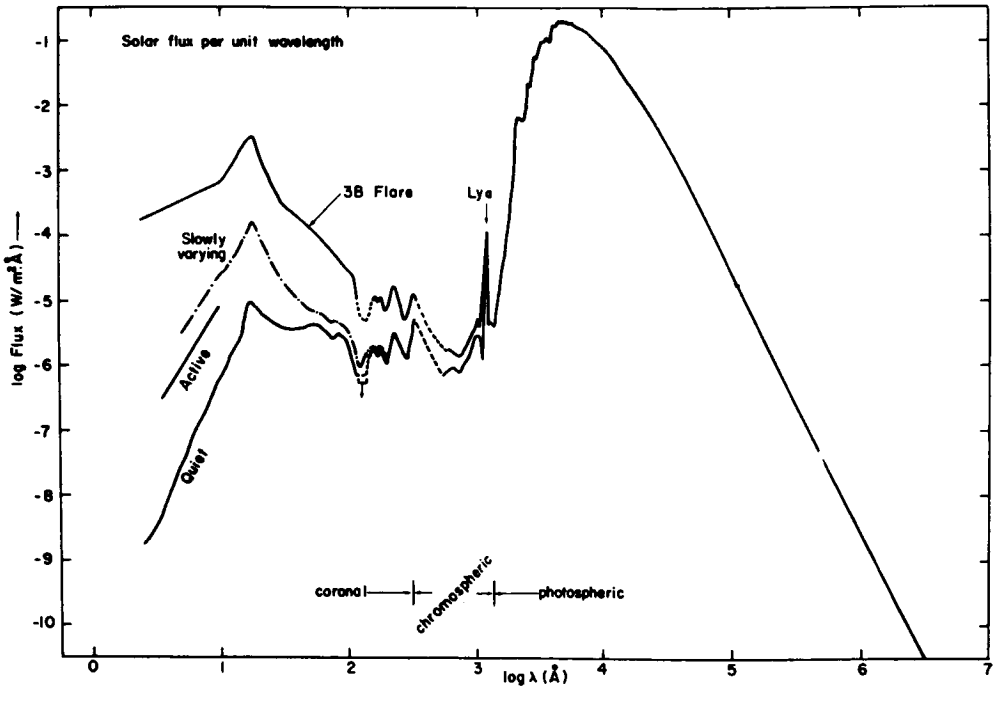

Figure 7. Summary of solar irradiance at all wavelengths. From Smith and Gottlieb (1974).

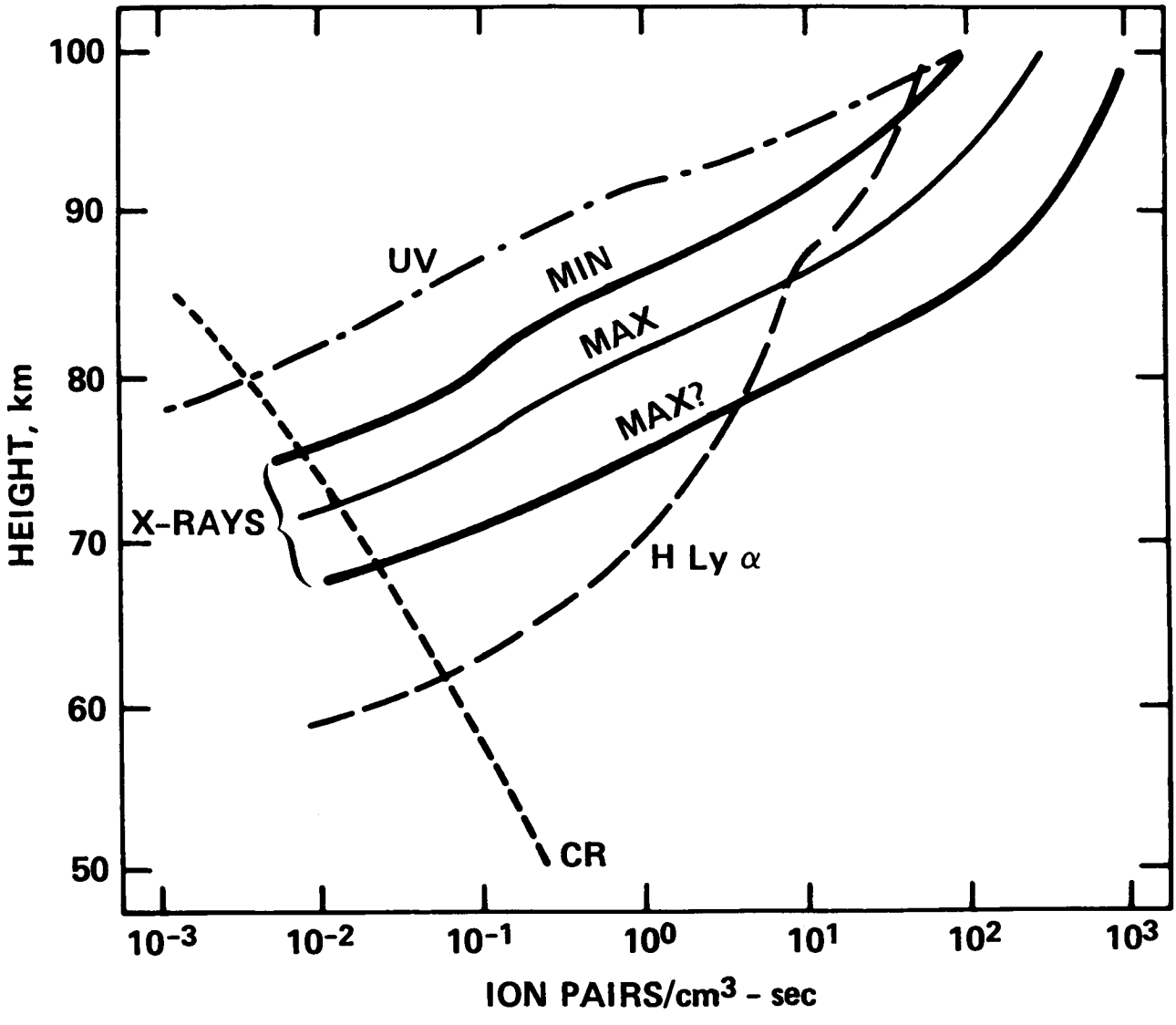

Figure 8. Altitude dependence of ionization rate due to solar x-rays compared with other rates discussed in text. The curves labeled MIN and MAX? are from Thrane (1972).

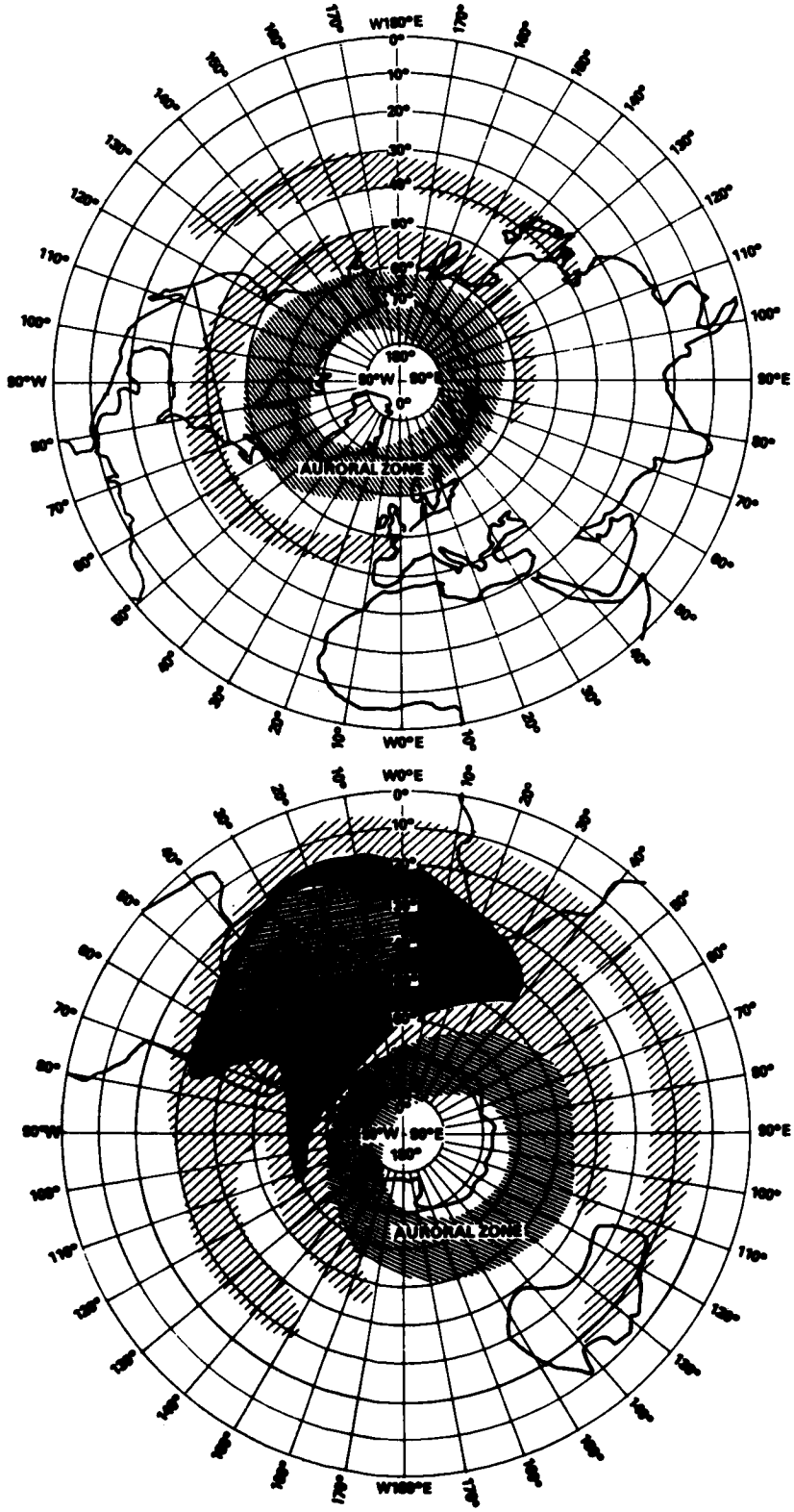

Figure 9. Geographical distribution of the observations of 100 keV electrons at altitudes between 240 and 410 km. From Seward (1973).

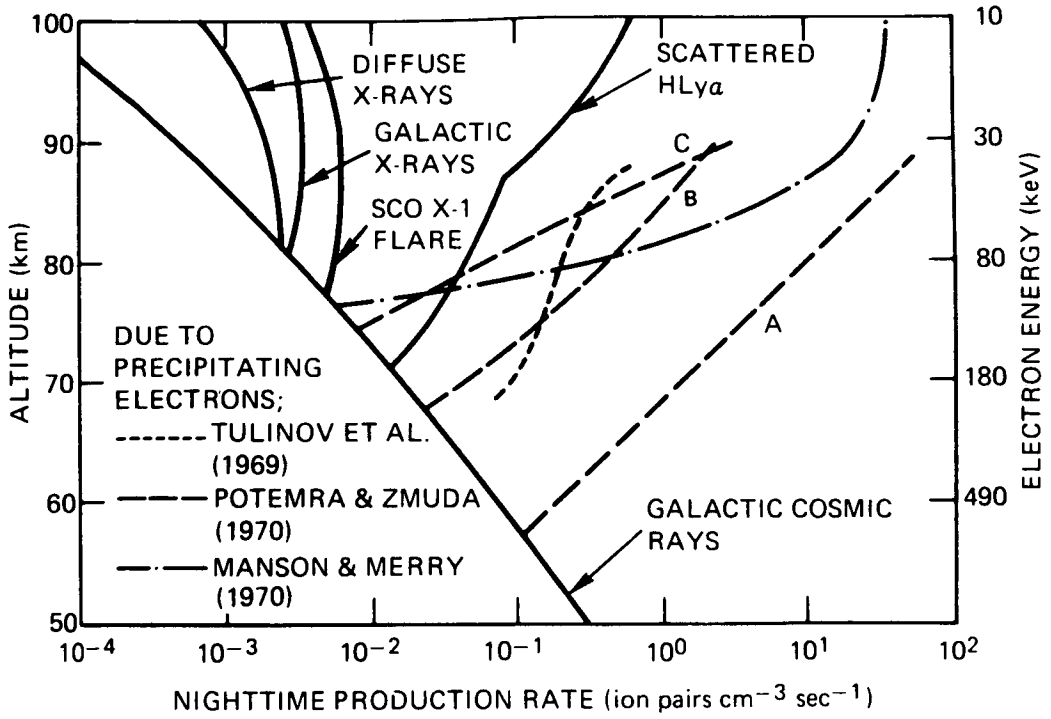

Figure 10. Ionization rates in the midlatitude nighttime ionosphere emphasizing the rates due to precipitating electrons. Consult Potemra (1973), from which this figure is adapted, for references.

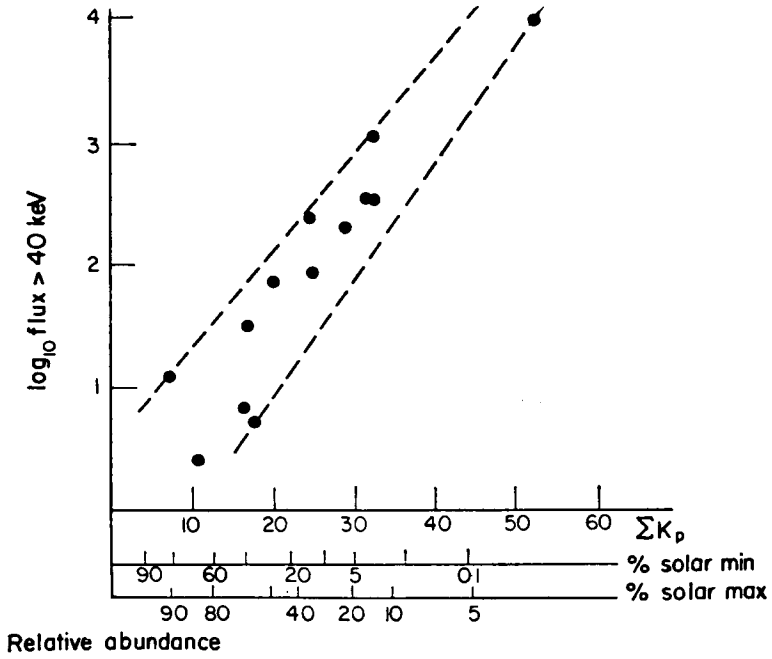

Figure 11. Correlation of measurements of precipitated electron fluxes > 40 keV with magnetic activity expressed by the K_p sum from 12 hr before to 12 hr after the launch of 13 rockets from South Uist. From Gough and Collin (1973).

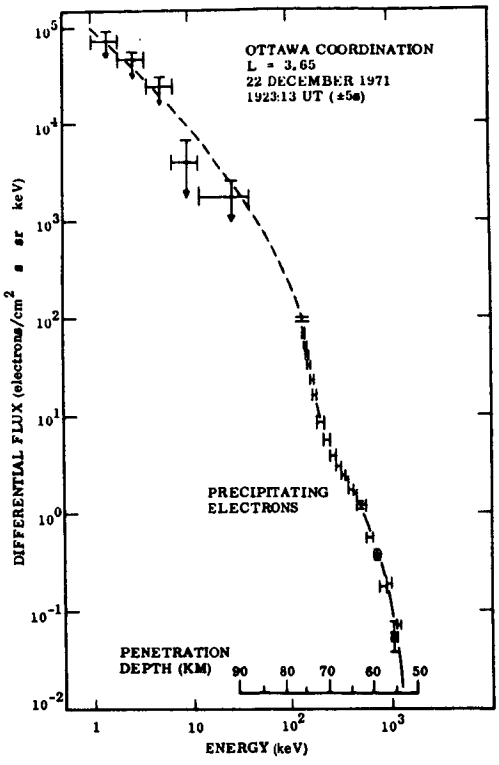

Figure 12. Differential energy spectrum of precipitating electrons measured over Ottawa (L = 3.65) on December 22, 1971. From Larsen et.al., (1976).

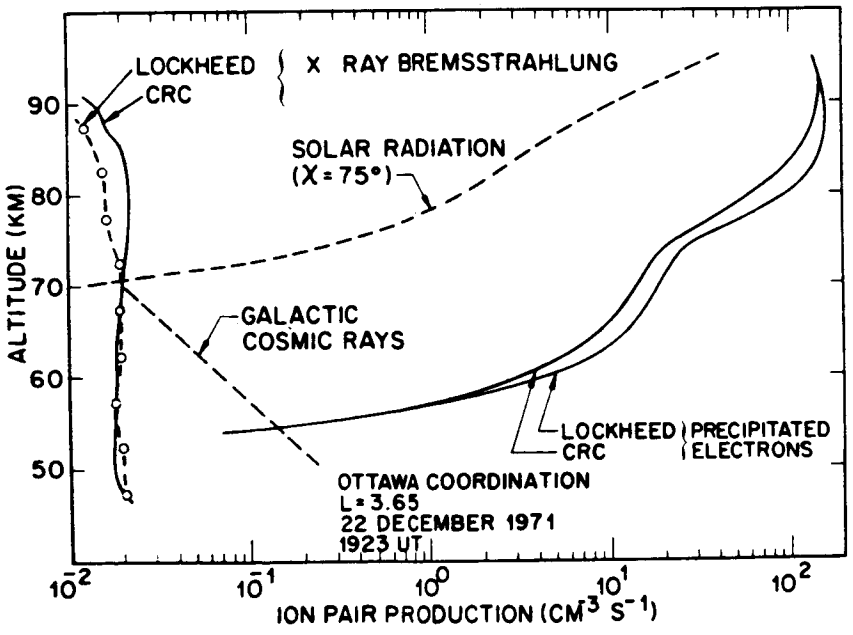

Figure 13. Altitude dependence of ionization rates due to precipitated electrons using the electron energy spectrum of Figure 12 with an isotropic pitch angle distribution, and for the associated bremsstrahlung x-rays (see Larsen et.al., 1976 for details.

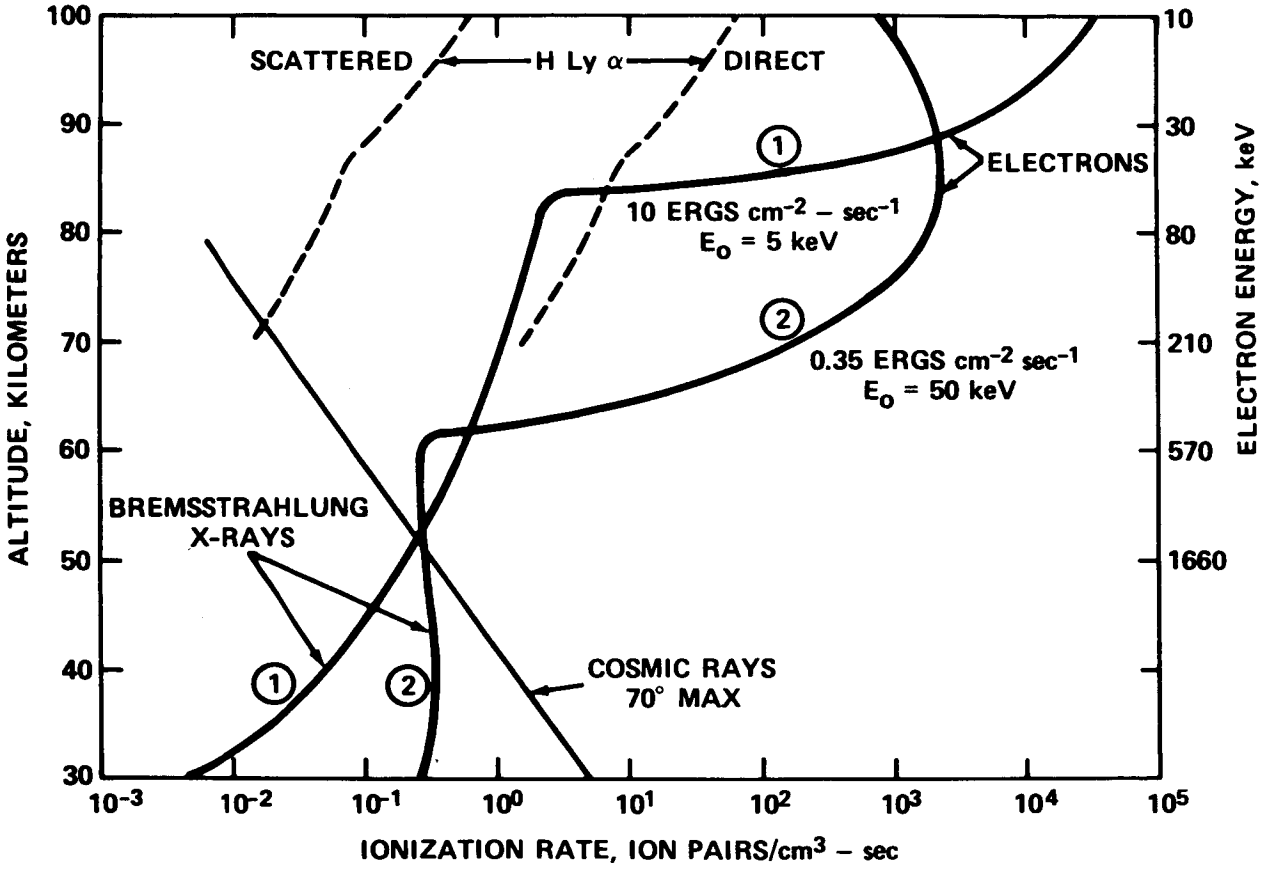

Figure 14. Altitude dependence of ionization rates due to precipitated electrons and associated bremsstrahlung x-rays for cases representative of moderate nighttime visual aurora (curve 1) and average peak dayside auroral radio absorption (curve 2).

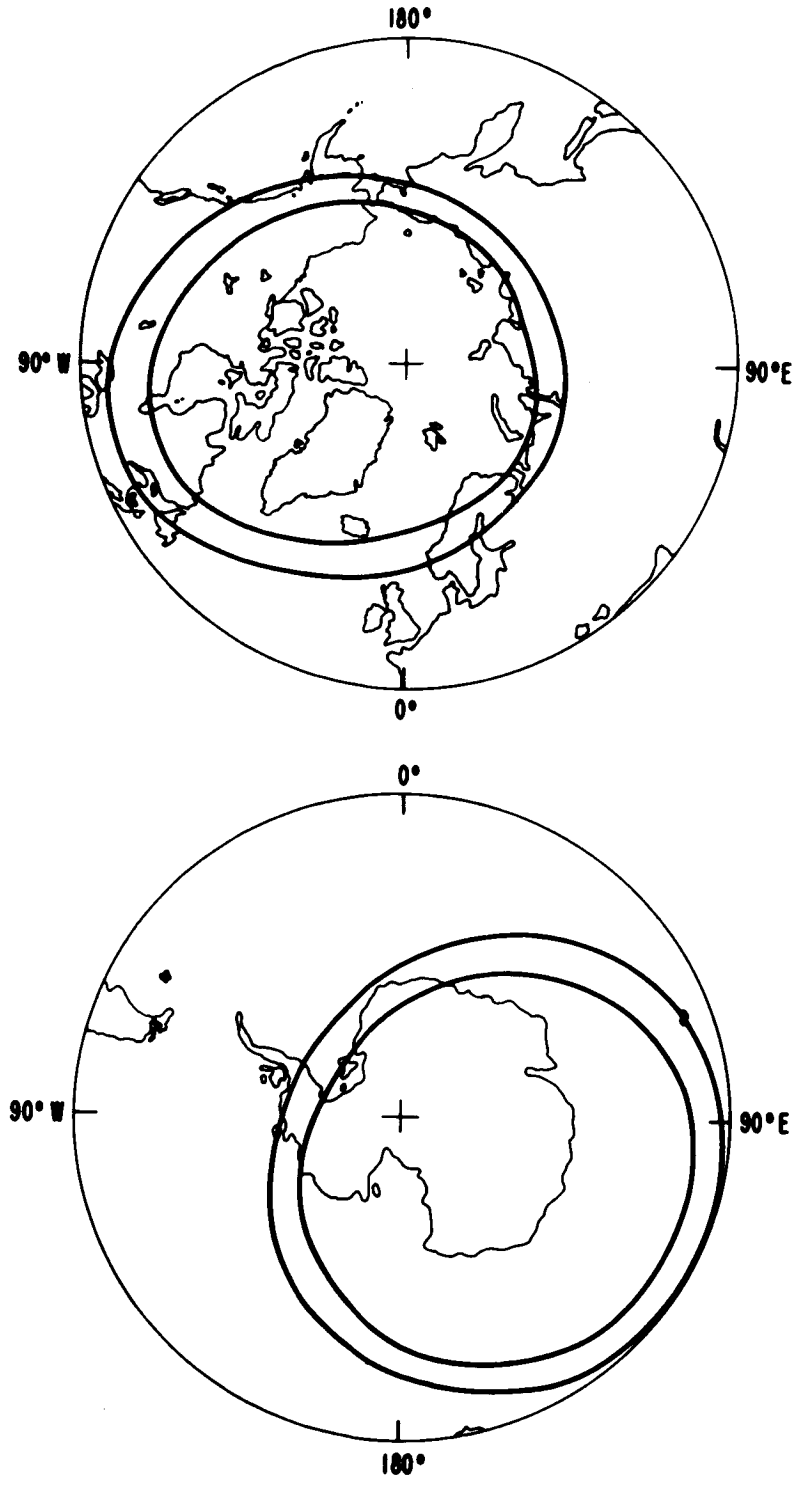

Figure 15. The normal distribution of polar cap absorption (pca) effects in the northern and southern hemispheres. The regions inside the inner curves experience the full intensity, while regions outside the outer curves are normally unaffected, except during geomagnetic disturbances. From Reid (1974).

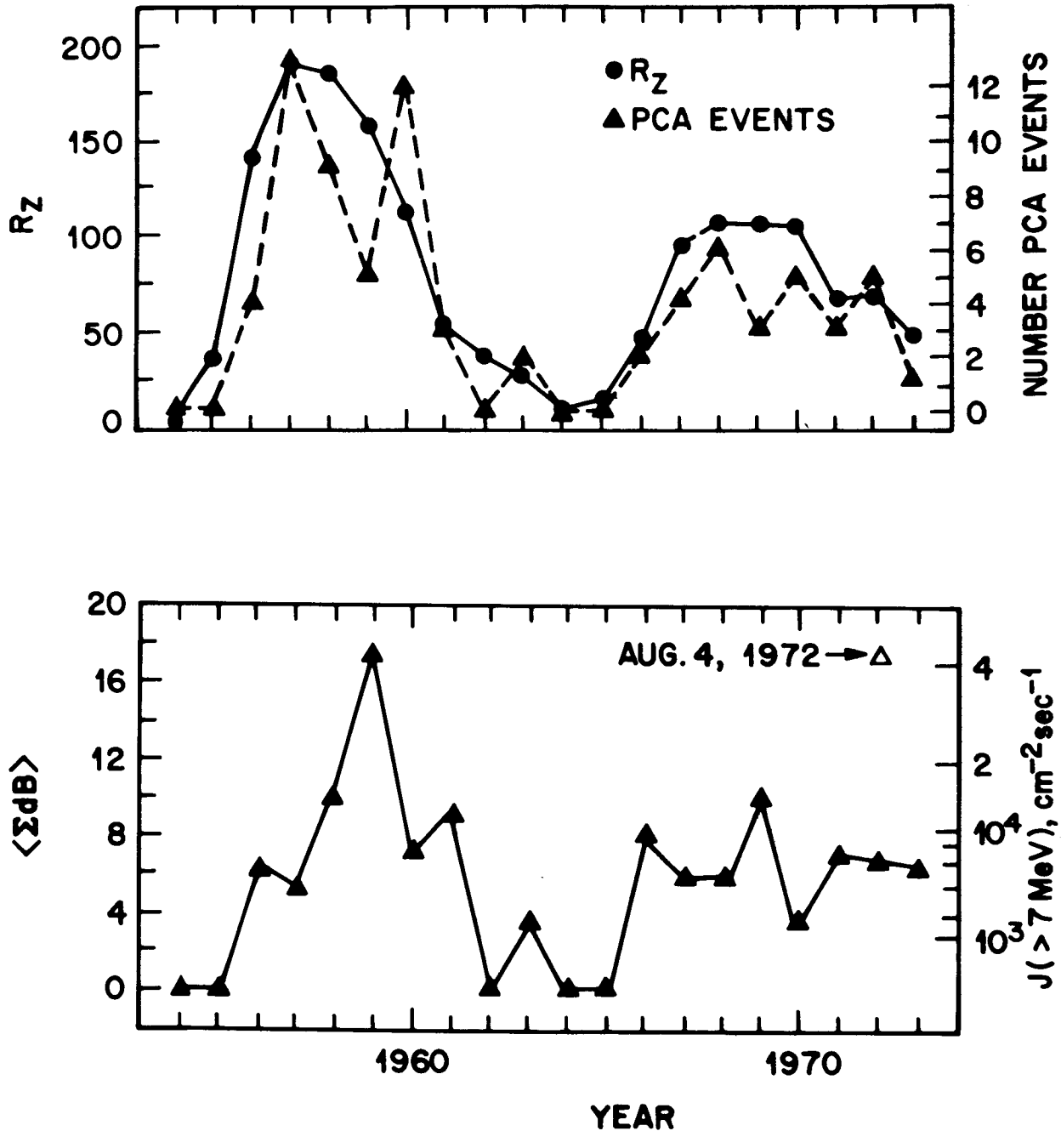

Figure 16. Top, annual number of pca events > 2.5 dB and annual sunspot numbers during two solar cycles. Bottom, average pca magnitude. The righthand scale gives an estimate of the solar proton flux from an empirical relationship of Potemra (1972). Adapted from Pomerantz and Duggal (1974).

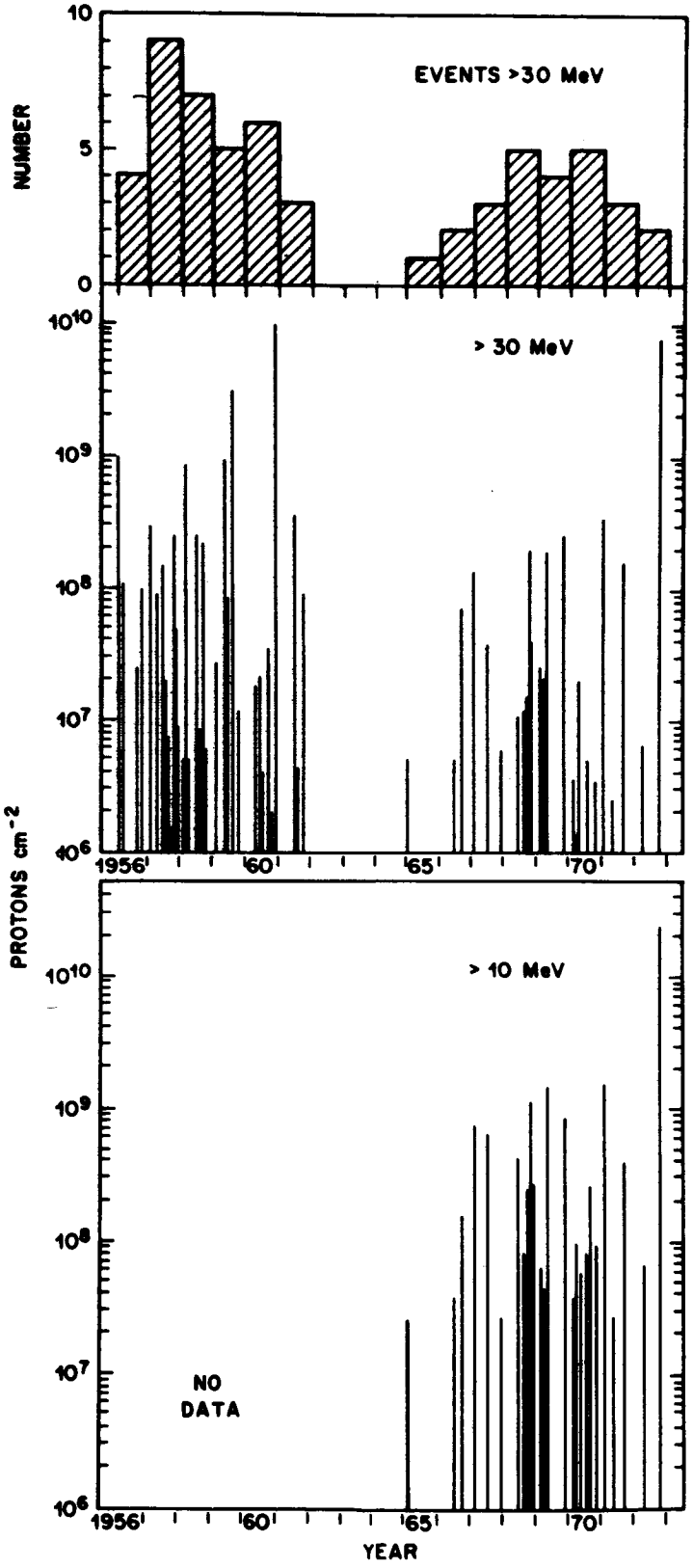

Figure 17. Event-integrated solar proton fluxes > 10 MeV and > 30 MeV for the major solar events of the last two solar cycles. From King (1974).

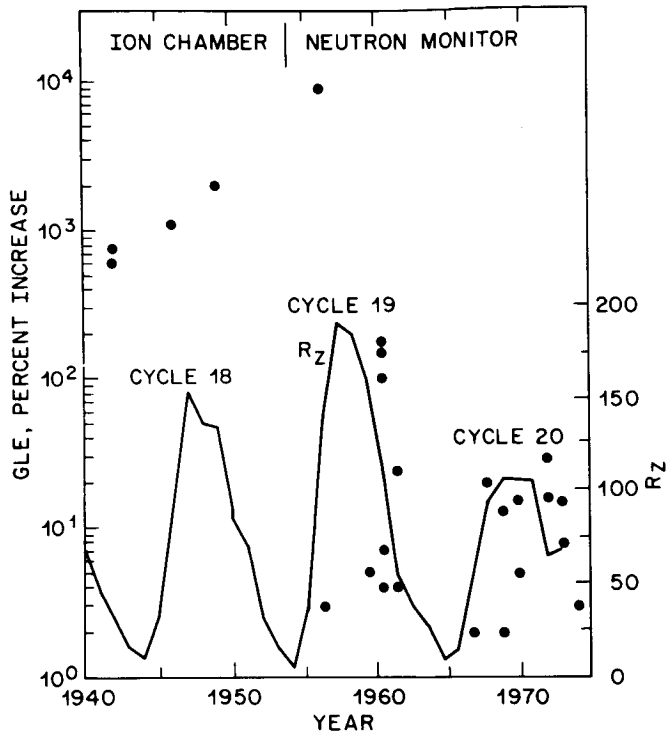

Figure 18. Intensities of individual ground level solar cosmic ray events since their discovery. From Pomerantz and Duggal (1974).

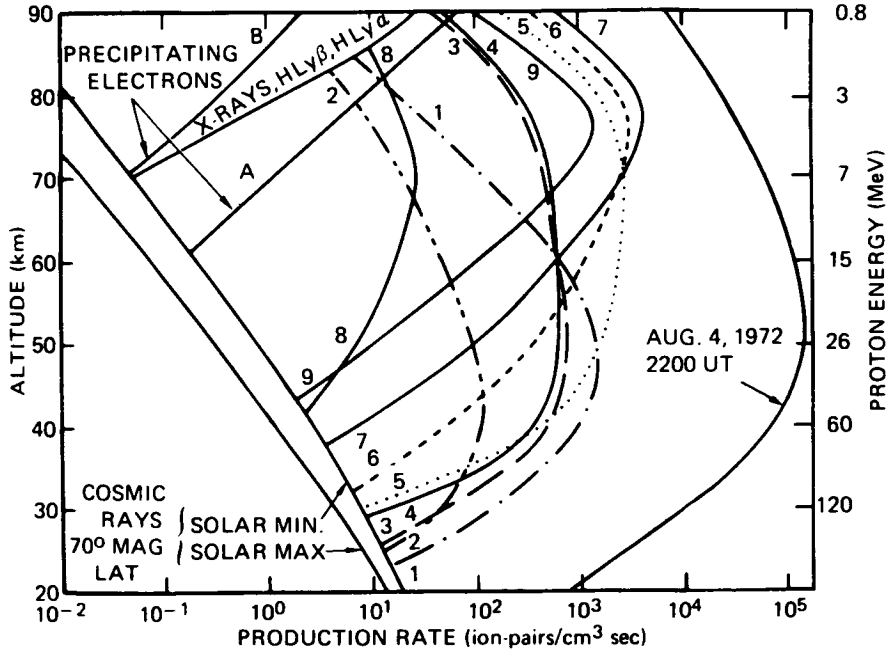

Figure 19. Ionization rates during pca's. Consult Potemra (1974) and Zmuda and Potemra (1972) for details.

Table I
Ionization Sources for the Middle Atmosphere

BACKGROUND ENERGY SOURCES

SOURCE		FLUX, ERGS cm^{-2}-sec^{-1}
Galactic Cosmic Rays		$10^{-3} - 10^{-2}$
Cosmic x-rays:	Diffuse, 1-10 Å	4×10^{-9}
Solar x-rays:	Nonflare, < 10 Å	$10^{-3} - 10^{-1}$
	10-100 Å	$10^{-1} - 10^{0}$
Solar H Ly α:	Direct	6
	Scattered (Nightside)	$6 \times 10^{-3} - 6 \times 10^{-2}$
Magnetosphere Electrons:	Auroral Zone	$10^{-1} - 10^{0}$
	Midlatitude	$10^{-4} - 10^{-3}$

EVENT SOURCES

Solar Cosmic Rays		$10^{-3} - 10^{0}$, 50 (8/2/72)
Solar x-rays: Flare, < 10 Å		< 3
	10-100 Å	< 35
Cosmic x-rays: SCO x-1, 1-10 Å		4×10^{-7}
Magnetosphere Electrons:	Auroral Zone	$10^{0} - 10^{3}$
	Midlatitude	$10^{-3} - 10^{-2}$

Table II
Solar Irradiance Erg cm^{-2} $-sec^{-1}$

WAVELENGTH RANGE, Å	QUIET SUN R ∿ 10-40	ACTIVE SUN R ∿ 100	SLOWLY VARYING SUN	3B FLARE
2-10	1.24 (-3)*	2.32 (-2)	6.16 (-2)	3.10
10-30	1.02 (-1)	3.04 (-1)	1.37	27.8
30-100	2.31 (-1)	3.15 (-1)	4.50 (-1)	6.7

ION CHEMISTRY OF THE MIDDLE ATMOSPHERE

Eldon E. Ferguson
Aeronomy Laboratory
National Oceanic Atmospheric Administration
Boulder, Colorado 80307

1. INTRODUCTION

The ion chemistry of the middle atmosphere is a more difficult subject than that of the upper atmosphere; i.e., the ionosphere. It is more difficult to make *in situ* ion composition measurements because of the relatively high pressure which necessitates vacuum pumps associated with mass spectrometers. The measurement platforms are less satisfactory in the middle atmosphere as well; there are no middle atmosphere platforms of comparable utility to the AE satellites for example which have been used for comprehensive and precise E and F-region ion chemistry studies.

Laboratory studies of the relevant ion chemistry are also much more difficult for middle atmosphere ion chemistry, the relatively high pressure and low temperature leads to the importance of weakly bound cluster ions which are difficult to measure in the laboratory (as well as to sample in the atmosphere). The high pressure also leads to electron attachment which initiates a complex negative ion chemistry.

Our approach to middle atmosphere ion chemistry is to start with the positive ions of the D-region, which have been extensively studied, and extend this down to stratospheric altitudes where the first ion composition measurements have only recently been obtained. Then we do the same for the negative ion chemistry, starting with the D-region, which has been much less extensively measured for negative ions that for positive ions, and extend down to the stratosphere where the first ion composition measurements are only now being carried out. In each case the theoretical and laboratory extension of the ion chemistry from the D-region to the higher pressure stratosphere is primarily a matter of enquiring into the role of the minor constituents whose absolute concentrations become large enough to allow them to become involved in the ion chemistry.

The ion chemistry of the ionosphere and middle atmosphere have recently been reviewed in some detail (Ferguson, 1979; Ferguson et al., 1979).

2. D-REGION POSITIVE ION CHEMISTRY

Middle atmosphere ion chemistry was initiated with the rocket-borne mass spectrometer positive ion flights of Narcisi and Bailey (1965). Subsequently there have been numerous *in situ* measurements of the D-region positive ions (for examples, Goldberg and Aikin, 1971; Narcisi et al., 1972; Arnold and Krankowsky, 1974; and Zbinden et al., 1975). Although there is considerable variation among the various flights, corresponding almost certainly to large atmospheric ion composition variations, these measurements conclusively show that the dominant ions of the lower E-region, O_2^+ and NO^+, are replaced by the water cluster ions, $H_3O^+ \cdot nH_2O$, in the D-region. Considerable

laboratory, theoretical, and *in situ* efforts have been directed toward identifying the D-region reaction paths that convert the primary O_2^+ and NO^+ ions into the observed $H_3O^+ \cdot nH_2O$ ions. The reaction scheme that has emerged is given in Figure 1. Laboratory data are available for the rate constants and/or equilibrium constants for the reactions represented by solid lines and are currently unavailable for those represented by dashed lines. The details of this chemistry have been reviewed recently by Reid (1976). In addition, the hydration of $H_3O^+(H_2O)_n$ ions via intermediate $H_3O^+ \cdot (H_2O)N_2$ and $H_3O^+(H_2O)CO_2$ clusters undoubtedly occurs (Chakrabarty, et al., 1978).

There has been no problem in explaining the conversion of the primary O_2^+ ions into the water cluster ions via the laboratory-verified paths shown in Figure 1 (Fehsenfeld and Ferguson, 1969). However, the major source of ionization in the undisturbed daytime D-region is photoionization of NO by solar Lyman-α radiation. The understanding of the conversion of the NO^+ ions into the water cluster ions has proven to be a more difficult problem. Because of the low mixing ratio of water in the D-region and the relatively low D-region pressures, it is necessary to invoke reactions of the type,

$$NO^+ \cdot nH_2O + X + M \rightarrow NO^+ \cdot nH_2O \cdot X + M, \tag{1}$$

where n = 0, 1, 2 and X = N_2, CO_2 for the conversion process (Ferguson, 1971). The weakly bound association complexes thus formed would then undergo a series of fast switching reactions,

$$NO^+ \cdot nH_2O \cdot N_2 + CO_2 \rightarrow NO^+ \cdot nH_2O \cdot CO_2 + N_2 \tag{2}$$

$$NO^+ \cdot nH_2O \cdot CO_2 + H_2O \rightarrow NO^+ \cdot (n+1)\, H_2O + CO_2 \tag{3}$$

that would greatly accelerate such hydration steps and hence the eventual production of the water cluster ions. These reaction paths are shown in the lower part of Figure 1. However, measurements of these reactions in the laboratory, or the detection of the key ions in the atmosphere, have presented a formidable experimental problem, since the intermediate $NO^+ \cdot nH_2O \cdot X$ ions are extremely fragile.

Arnold and Krankowsky (1974, 1977) have had considerable success in solving the problem of sampling such weakly bound cluster ions in rocket-borne mass spectrometers. As a result, some key ions in this reaction scheme now have been observed *in situ,* for example $NO^+ \cdot N_2$, $NO^+ \cdot CO_2$, and $NO^+ \cdot H_2O \cdot CO_2$. A sample of these results is shown in Figure 2. Progress has also been made in the laboratory. The rate constant and thermodynamic data for the clustering of N_2 to NO^+ (Reaction 1 with X = N_2, n = 0) are now available.

Although very few of these switching reactions have been measured in the laboratory, such reactions are known to be fast, $k \sim 10^{-9}\,cm^3\,s^{-1}$. Thus, this sequence of reactions seems to offer an efficient mechanism for the formation of $NO^+ \cdot H_2O$ ions, particularly around 80 km where the D-region temperatures are the lowest. Reid (1977) has devised a reasonable extension of this cycle that can account for most of the observed D-region positive ion features. The nonpolar neutrals that are clustered to NO^+ are so weakly bound that these neutrals are collisionally dissociated to

some extent even at D-region temperatures. This is the case for $NO^+ \cdot N_2$, which has a bond dissociation energy of 5 kcal/mole. Accordingly, when the temperature is above about 215 K, the collisional decomposition of $NO^+ \cdot N_2$ will be larger than the switching reaction with CO_2.

For this reason, the conversion of NO^+ ion to the observed water cluster ions is extremely sensitive to temperature, and the D-region positive ion composition will, therefore, manifest strong seasonal, latitudinal, and even irregular variations as a result of variations in the atmospheric temperature. Moreover, electron-ion recombination coefficients for these weakly bound cluster ions may be considerably larger than those for the unclustered NO^+ and O_2^+ ions, which may explain, at least in part, the strong variations in the electron density that are observed at about 80 km. While many of the details still await quantitative verification, the reaction scheme shown in Figure 1 has been shown (Reid, 1977) to qualitatively solve the long-standing D-region problem of the conversion of the primary NO^+ ions into the observed water cluster ions.

3. STRATOSPHERIC POSITIVE ION CHEMISTRY

A positive ion reaction scheme for the stratosphere and troposphere is given in Figure 3 (Ferguson, et al., 1979). It is essentially the O_2^+ reaction sequence of the D-region positive ion chemistry (Figure 1), augmented by reactions that involve some of the minor constituents of the lower atmosphere.

Galactic cosmic rays are the primary source of ionization in the stratosphere and upper troposphere. Radioactive decay is the primary source of ionization near the Earth's surface. Cole and Pierce (1965) have given a typical ionization production-rate altitude profile. Values of less than 1 to more than 20 ion pairs cm^{-3} s^{-1} occur in the stratosphere. The ambient concentration of positive ions is determined by the recombination rate with negative ions. Measurements of the ion concentration have been typically about 5×10^3 cm^{-3} in the lower stratosphere (Cole and Pierce, 1965; Paltridge, 1965, 1966). Positive ion lifetimes are on the order of a few thousand seconds.

As shown in Figure 3 the initial products of the ionization below 60 km are predominantly N_2^+ and O_2^+, with lesser amounts of O^+ and N^+. These ions are rapidly converted to O_2^+, as well as an inconsequential amount of NO^+, by well-established reactions. Once formed, the O_2^+ ions associate with O_2:

$$O_2^+ + O_2 + M \rightleftarrows O_2 \cdot O_2^+ + M, \qquad (4)$$

The formation of $O_2^+ \cdot O_2$ begins a series of fast switching reactions (Figure 1) that involve H_2O and leads to the formation of the water cluster ions, $H_3O^+ \cdot nH_2O$.

In the troposphere, where the H_2O mixing ratio is about 10^{-2}, the conversion of $O_2^+ \cdot O_2$ to $O_2^+ \cdot H_2O$ proceeds so rapidly that there is no conceivable alternative to the path described above that leads to the water cluster ions. However, in the stratosphere, where the H_2O mixing ratio is only on the order of 10^{-6}, other neutral constituents have comparable abundances. CO_2 has a much larger concentration and O_3 and CH_4 comparable with that of H_2O. If $O_2^+ \cdot O_2$ reacts with any of these neutrals, then the ion chemistry outlined in Figure 3 might be significantly altered.

These $O_2^+ \cdot O_2$ reactions have been examined recently (Dotan et al., 1978) and the results are given in Table I. The first entry is the fast reaction against which the alternative paths must compete. In contrast to it, the reaction of $O_2^+ \cdot O_2$ with CH_4 is very slow. The reactions of $O_2^+ \cdot O_2$ with CO_2 and O_3 were studied in equilibrium and the thermochemical constants are given. For CO_2, the equilibrium constant is about unity. The ratio of O_2 to CO_2 in the atmosphere is about 600; thus, the equilibrium will always strongly favor $O_2^+ \cdot O_2$ rather than $O_2^+ \cdot CO_2$. However, the exothermicity for the reaction involving O_3 is much larger; hence, the $O_2^+ \cdot CO_2$ and $O_2^+ \cdot O_3$ ion concentrations will be more comparable. The $O_2^+ \cdot O_3$ ion concentrations are estimated to never drop below one-tenth of the $O_2^+ \cdot O_2$ concentration and even equal it at 30 km. This means that the $O_2^+ \cdot O_3$ chemistry must also be considered. The mass 80 ion in Figure 2, incidentally, almost certainly represents O_5^+ rather than $NO^+ \cdot H_2O \cdot O_2$.

The reaction of $O_2^+ \cdot O_3$ with CH_4 was found to be slow, $k < 5 \times 10^{-13}$ cm^3 s^{-1} (Dotan et al., 1978). In contrast, the reaction

$$O_2^+ \cdot O_3 + H_2O \rightarrow O_2^+ \cdot H_2O + O_2 \qquad (5)$$

is fast, $k_5 = 1.2 \times 10^{-9} cm^3 s^{-1}$. However, the product of this reaction is $O_2^+ \cdot H_2O$, which is the same ion produced by the reaction of $O_2^+ \cdot O_2$ with H_2O, the reaction for which competitors were being sought. Therefore, as Figure 3 shows, the $O_2^+ \cdot O_3$ chemistry simply represents a side excursion that loops the stratosphere positive ion chemistry back on the path involving $O_2^+ \cdot H_2O$.

Lastly, it was observed that $O_2^+ \cdot H_2O$ does not react with CH_4, $k < 5 \times 10^{-13} cm^3 s^{-1}$. Thus, the neutrals CO_2, O_3, and CH_4 do not appear to disrput the ion chemistry that leads to the water cluster ions and we assume that $H_3O^+ (H_2O)_n$ ions are formed in the stratosphere as well as in the D-region. With regard to possible reactions of neutrals with $H_3O^+ (H_2O)_n$ ions, we must now concern ourselves with much lower concentration species, since the lifetimes of $H_3O^+ (H_2O)_n$ ions greatly exceed the time it takes for O_2^+ to lead to $H_3O^+ (H_2O)_n$ ions, ($\sim 10^3$ sec compared to $\sim 10^{-3}$ sec). Rather than ppm concentrations we must be concerned with ppt concentrations. HNO_3 is one such species of interest, it is known to exist in both the stratosphere and troposphere. Its mixing ratio at 25 km is expected to be greater than 10^{-9} (Crutzen et.al., 1978). Furthermore, the reaction

$$H_3O^+ + HNO_3 \rightarrow H_2NO_3^+ + H_2O \qquad (6)$$

is fast, $k_6 = 1.6 \times 10^{-9} cm^3 s^{-1}$ (Fehsenfeld et al., 1975). However, HNO_3 does not create a new reaction path that leads away from the ultimate formation of the water cluster ions. A rather remarkable situation exists in that protonated nitric acid, $H_2NO_3^+$, is chemically equivalent to hydrated NO_2^+, i.e., $NO_2^+ \cdot H_2O$ as has been established by chemical reactivities (Fehsenfeld et al., 1975). When this ion is further hydrated in the atmosphere

$$NO_2^+ \cdot H_2O + H_2O + M \rightarrow NO_2^+ \cdot 2H_2O + M, \qquad (7)$$

the product ion does not undergo additional hydration, but instead reacts via a fast binary reaction with H_2O,

$$NO_2^+ \cdot 2H_2O + H_2O \rightarrow H_3O^+ \cdot H_2O + HNO_3. \qquad (8)$$

Thus, the $NO_2^+ \cdot H_2O$ chemistry only leads back to the water cluster ions. As is shown in Figure 3, the same is also true for the possible path involving the trace constituent N_2O_5 (Davidson et al., 1978).

As indicated in Figure 3, both NH_3 and CH_3OH would destroy $H_3O^+ (H_2O)_n$ ions if present in sufficient concentrations. CH_2O on the other hand would not (Fehsenfeld, et al., 1978).

Recently the first stratospheric ion composition measurements have been made in rocket-borne mass-spectrometer flights (Arnold et al., 1977). Three high-latitude studies sampled the positive ions during descent through the altitudes 55 to 35 km, the lower of which is well into the stratosphere. Above 45 km, the substantial signal levels permitted high-resolution identification of the water cluster ions $H_3O^+ \cdot nH_2O$, with n = 0, 1, 2, and 3, as the dominant species in this region. Arnold and coworkers reported a rather sharp transition at about 45 km from the water cluster ions to ions with e/m ratios of 29 ± 2, 42 ± 2, 60 ± 2, and 80 ± 2. In the region below this altitude the non-water-cluster ions become the dominant species. More recently, balloon flights by Arijs et al., (1978) indicate that the water cluster ions are major species at 35 km. Other ions were observed in appreciable concentration, in particular, an ion with an e/m ratio of 96 ± 2.

The observation of the water cluster ions as the dominant species down to altitudes of 45 km or below, having been formed undoubtedly by the chemistry described in Figure 3, places useful upper limits on neutral molecules that react rapidly with $H_3O^+ \cdot nH_2O$ ions. For example, laboratory studies (Fehsenfeld et al., 1978) find that these water cluster ions proton transfer rapidly with methanol with rate constants that are independent of temperature in the stratospheric range. Since Arnold et al. found no masses that could be associated with protonated methanol ions or their hydrates, an upper limit of 10^{-11} on the CH_3OH mixing ratio could be deduced for this region of the atmosphere. This upper limit is several orders of magnitude less than might be inferred from the methane-oxidation chemistry with its present uncertainties.

The situation with ammonia appears to be quite similar. The reactions

$$H_3O^+ \cdot nH_2O + NH_3 \rightarrow NH_4^+ \cdot mH_2O + (n + 1 - m)\, H_2O \qquad (9)$$

(where m = 0, 1, . . . , n) have been found (Fehsenfeld and Ferguson, 1973) to be very fast for n = 0, 1, and 2. No detailed atmospheric profiles of NH_3 have been obtained. The concentration in the lower troposphere is believed to be significant, but is expected to fall off rapidly with altitude because of the large solubility of ammonia and its consequent rain-out of the atmosphere. Presumably $NH_4^+ \cdot nH_2O$ ions do exist in the lower part of the troposphere and indeed may even be the dominant ions, but no ion composition measurements exist yet in this region.

Arnold et al., (1977) have tentatively identified the non-water-cluster ions that were observed in their flights as arising from reactions of the $H_3O^+ \cdot nH_2O$ ions with formaldehyde and used their observations to deduce a CH_2O altitude profile. The reasonable choice of CH_2O as the trace neutral with which the water cluster ions were reacting was based on the fact that the proton affinity of CH_2O is greater than that of H_2O and that CH_2O is expected to be present in the atmosphere from the oxidation of methane. However, recent laboratory studies (Fehsenfeld et al., 1978) of the

CH_2O-H_2O ion chemistry do not support this interpretation. Unclustered H_3O^+ ions do indeed proton transfer with CH_2O but the reactions of the higher-order water cluster ions with CH_2O become endothermic. Even if the protonated formaldehyde ions were produced in some way in the stratosphere, they would be rapidly converted to $H_2O^+ \cdot nH_2O$ ions by reaction with H_2O.

The nonproton hydrates reported below about 40 km by Arnold et al. (1978) have recently been interpreted (Ferguson, 1978) as being due to the presence of protonated sodium hydroxide ions. The interpretation is given in Table II. It has been well known for over seventy years that a layer of atomic sodium exists in the atmosphere from its resonant scattering of sunlight which has been detected spectroscopically. This sodium exists in a layer near 90 km and is due to the ablation of meteorites in the atmosphere upon entry. It is argued that the sodium will be in the form of NaOH below about 40 km in the atmosphere. The proton affinity of NaOH is exceedingly high, $\sim$ 248 kcal mol^{-1} (Kebarle, 1977). It is presumed therefore that reactions

$$H_3O^+(H_2O)_n + NaOH \rightarrow NaOH_2^+(H_2O)_m + (n-m+1)\,H_2O \qquad (10)$$

would occur at the collision rate, $k_{10} \sim 2 \times 10^{-9}\,cm^3\,s^{-1}$. A concentration of NaOH $\sim 10^5\,cm^{-3}$ at 40 km is required for (10) to compete with positive ion - negative ion recombination and this agrees well with calculations of Liu and Reid (1979) on the total expected sodium concentration in this altitude range. It is also predicted that at somewhat lower altitudes KOH_2^+ clusters will become dominant since the proton affinity of KOH $\sim$ 263 kcal mol^{-1} (Kebarle, 1977) exceeds that of NaOH. The atmospheric abundance of K is an order of magnitude or more less than that of Na so that at 40 km the K concentration is too low to be involved in the ion chemistry. MgO has a large proton affinity, $\sim$ 212 kcal mol^{-1} and it may well be that $MgOH^+$ clusters are formed by

$$H_3O^+(H_2O)_n + MgO \rightarrow MgOH^+(H_2O)_m + (n-m+1)H_2O \qquad (11)$$

since Mg is an order of magnitude more abundant than Na in meteorites. However, the $MgOH^+$ hydrates would presumable proton transfer to NaOH,

$$MgOH^+ + NaOH \rightarrow NaOH_2^+ + MgO \qquad (12)$$

so that Mg, while relatively abundant, probably does not contribute to the ion composition. Mixed clusters involving both NaOH and KOH will also occur at some concentration level.

There is a clear need for more detailed measurements of stratospheric positive ions, including measurements at higher mass resolution. There is also a need for measurements of the critical neutral constituents for the ion chemistry, such as NaOH.

4. D-REGION NEGATIVE ION CHEMISTRY

In contrast to the D-region positive ion chemistry, where *in situ* measurements discovered the unexpected water cluster ions, the negative ion chemistry of the D-region has been derived predominantly from laboratory studies. This chemistry is shown schematically in Figure 4. The arrows represent reactions whose rate constants have been measured in the labortory. Many of the details of D-region negative ion chemistry have been reviewed recently by Reid (1976).

The primary negative ion of the D-region is largely O_2^-, which is formed by the termolecular attachment of electrons to O_2. To a much less extent, O^- is formed by dissociative attachment to O_3. The relatively unstable O_2^- ions undergo a series of ion-molecule reactions with the D-region minor *molecular* neutral constituents to form progressively the more stable ions shown in Figure 4. In competition with this progression at each intermediate step are reactions with the minor D-region *atomic* neutral constituents that lead back eventually to the release of the electrons. The terminal ions NO_3^- and HCO_3^- are sufficiently stable to resist attack by the atomic species. For example, the electron affinity of NO_3 is 4.0 eV, one of the largest known for simple molecules.

The first few steps in the reaction sequence of Figure 4 are fast in comparison to the conversion of CO_3^- to NO_2^- by reaction with NO. The relatively small rate constant for this reaction and the low NO concentration implies that this is the limiting step in the NO_3^- production sequence in Figure 4. However, this CO_3^- bottleneck does not mean that there will be a large CO_3^- concentration in the D-region, but rather it implies an overall low negative ion concentration. The rapid conversion of CO_3^- back to O_2^- via reaction with O and thence detachment of the electron by reaction with O holds the CO_3^- concentration in check. The rate constants and densities involved in this loop are such that it will occur many times before a CO_3^- ion is converted to an NO_2^- ion. The step from NO_2^- to NO_3^- is fast compared to the preceding one, thus the steady-state NO_3^- concentration is determined largely by the ratio of the NO_2^- production rate, and the NO_3^- loss by ion-ion recombination. Hence, this model predicts a rather large $[NO_3^-]/[CO_3^-]$ ratio in the D-region.

Thus, to a large extent the negative ion chemistry of the D-region is controlled by the neutral composition, and its variability is linked directly with the large variations in the minor species O, O_3, NO, and H. It is clear from Figure 4 that high pressure, hence lower altitude, favors the attachment of electrons to O_2, thereby initiating the negative ion chemistry, and the termolecular reactions that lead toward more-stable negative ions. Furthermore, the increasing concentrations of O_3 and NO and the decreasing concentration of O at the lower altitudes all imply a rather sharp upper boundary for the D-region negative ions at 75 to 80 km, with the free electrons showing a complementary variation with altitude. Diurnal effects are expected to be large, since the O atom concentration, for example, increases throughout the D-region during the day. At the same time, the less-stable negative ions are subject to photodestruction (Huber et al., 1977).

The temperature of the D-region and lower atmosphere is less than 300 K and varies with time, place, and altitude and particularly with season and latitude. It is therefore also necessary to have temperature dependences for the reaction rate constants in order to understand the negative ion chemistry in detail.

Figure 4 does not include the effects of neutral molecules clustering to the negative ions. The rate constants of such termolecular association reactions typically increase with decreasing temperature and the breakup rates of weakly bound cluster ions decrease. Thus, at the relatively low D-region temperatures, all of the negative ions are subject to clustering, which is not very chemically specific. The terminal, i.e., long-lived, ions like NO_3^- are certainly expected to be hydrated, hence $NO_3^- \cdot nH_2O$ ions are predicted to be the dominant ions in the D-region. If the intermediate ions cluster in their shorter lifetimes, the question arises as to whether this would significantly alter their subsequent chemistry. A limited study carried out a few years ago (Fehsenfeld and Ferguson, 1974)

indicated that water clusters would not significantly effect the reaction scheme of Figure 4. For example, one and two water molecules do not significantly alter the rate of O_2^- charge transfer with O_3. One water molecule does not significantly effect the rate of O_3^- reaction with CO_2 but two water molecules quenches this reaction, probably by making the reaction effectively endothermic. However, because of the large abundance of CO_2, the O_3^- ions will not have time to cluster twice, so that this should have little effect. Clustering to CO_3^- may somewhat alleviate the CO_3^- bottleneck if it inhibits the reaction of CO_3^- with O relative to that with NO. At D-region temperatures, there could be important negative-ion association reactions with O_2, N_2, CO_2, and H_2O, followed by switching, exactly analogous to the D-region NO^+ association sequence proposed in the lower part of Figure 1. Only one such D-region negative-ion reaction path has been studied in the laboratory, namely, the one involving $CO_3^- \cdot H_2O$ shown in Figure 4. With the improved ability to study individual cluster ions that now exists, more extensive studies of the effects of clustering on chemical reactivity are being undertaken.

The first *in situ* measurements of the D-region negative ion composition were made by Narcisi et al., (1971) and Arnold et al., (1971). Figure 5 shows the ion concentration recorded in a later flight by Narcisi and coworkers. The dominant ions below 90 km are those with e/m ratios of 62 + n18 (n = 1-5). An interpretation of these ions as $NO_3^- \cdot nH_2O$ is consistent with the model shown in Figure 4. However, the persistence of e/m ratios of 16 and 32, which are presumably O^- and O_2^-, at the higher altitudes is not in accord with the chemistry of Figure 4 which predicts an upper boundary for the negative ions at lower altitudes. The flights of Arnold and coworkers found somewhat different results. Namely, they report a rather sharp upper boundary to the D-region negative ions, in accord with the predictions based on laboratory measurements, but the $NO_3^- \cdot nH_2O$ sequence was not observed. The major ion species in these flights were identified as CO_3^-, Cl^-, and HCO_3^-.

In view of the sparcity and differences between the atmospheric negative ion measurements, the substantial uncertainties in the concentrations of certain critical minor neutral species, and the need for more laboratory reaction studies, a quantitative understanding of D-region negative ion chemistry cannot be claimed at the present.

5. STRATOSPHERIC NEGATIVE ION CHEMISTRY

The negative ion chemistry of the stratosphere and troposphere are even more speculative than the positive ion chemistry of these regions. In addition to there being few measurements of the trace neutrals involved, only one negative ion composition measurement has so far been reported (Arnold and Henschen, 1978). Furthermore, the D-region measurements, from which one could draw guidance, are relatively sparse and somewhat ambiguous at present, as pointed out above. Thus, our present understanding of the negative ion processes in the stratosphere stems largely from laboratory studies.

The approach here has been to start with the D-region negative ion chemistry given in Figure 4 and modify it to be in accord with the expected differences in neutral composition of the two regions. These considerations fall into two classes. First, to look for possible changes in the chemistry that leads to the NO_3^- ions and secondly to consider whether these ions would react with trace neutral species that are suspected in the lower atmosphere to form even more stable ions.

The first necessary modification of the D-region scheme is to disregard the reactions of atomic oxygen, whose concentration below 50 km is negligible in comparison to that of O_3. In addition, NO will no longer play a role. Furthermore, the rapid formation of cluster ions can strongly alter the evolution of ion chemistry. For example, the reaction of O_3^- with CO_2 is known to decrease rapidly with O_3^- hydration (Fehsenfeld and Ferguson, 1974). Because H_2O bonds more strongly to O_3^- than to CO_3^-, this reaction may become endothermic when O_3^- becomes heavily hydrated (Dotan et al., 1977). In the lower atmosphere, O_3^- hydration is likely to occur before the reaction of O_3^- with CO_2.

The reaction scheme based on these considerations is shown in Figure 6. The dashed lines represent places of considerable uncertainty. For example, it is not clear whether $O_2^- \cdot nH_2O$ ions will react with O_3, as do the unclustered O_2^- ions. The situation with $O_3^- \cdot nH_2O$, O_3^-, and CO_2 is the same; namely, the hydrated ions may not follow the same reaction paths as the unhydrated ions.

However, even if the paths that lead to NO_3^- are somewhat uncertain, its eventual formation does not appear to be in doubt. Both HNO_3 and N_2O_5 provide effective NO_3^- production routes. Some of these reactions are listed in Table III. Furthermore, it has been shown that HNO_3 exothermically displaces H_2O in hydrated negative ions (Fehsenfeld et al., 1975); therefore, the agent for NO_3^- formation can always enter the cluster.

The high stability of NO_3^- seems to insure its role in the terminal negative ions of the lower atmosphere. At the present, no neutral species expected to have a significant atmospheric concentration has been found to react with NO_3^-. The ion will, of course, hydrate and it is known that there are several molecules that can displace H_2O from a hydrated NO_3^- cluster. The molecules SO_2 (Fehsenfeld and Ferguson, 1973) and HNO_3 (Fehsenfeld et al., 1975; Davidson et al., 1978) are examples. Thus, it is likely that the terminal negative ions of the lower atmosphere are complex cluster ions, like $NO_3^- \cdot \ell H_2O \cdot mSO_2 \cdot nHNO_3$, with NO_3^- as the core ion. Recently, Arnold and Henschen (1978) have reported the first stratospheric negative ion observations. They report ions which are tentatively identified as $NO_3^-(HNO_3)_n$ and $NO_3^-(HCl)(HNO_3)_n$ with n = 1, 2, 3 in each case, as well as some ions which may possibly involve HSO_4^- cores and H_2SO_4 neutrals. The negative ion chemistry of the Middle Atmosphere is clearly in a rather elementary state of understanding. This can only be improved by more extensive *in situ* ion composition measurements.

REFERENCES

Arijs, E., J. Ingles, and D. Nevejans, Mass spectrometric measurements of the stratosphere, *Nature*, **271**, 642-644, 1978.

Arnold, F., and D. Krandowsky, A new concept for the D-region ion chemistry as inferred from a mass spectrometer measurements, paper presented at the 4th Int. COSPAR Symp. Solar-Terrestrial Phys. June 17 - July 1, Sao Paulo, Brazil, 1974.

Arnold, F., D. Krandowsky and K. M. Marien, First mass spectrometric measurements of positive ions in the stratosphere, *Nature*, **267**, 30-32, 1977.

Arnold, F., H. Bohringer and G. Henschen, Composition measurements of stratospheric positive ions, *Geophys. Res. Letters*, **5**, 653-656, 1978.

Arnold, F., and G. Henschen, First mass analysis of stratospheric negative ions, *Nature*, **275**, 521, 1978.

Arnold, F., J. Kissel, D. Krankowsky, H. Wieder, and J. Zahringer, Negative ions in the lower ionosphere: A mass spectrometric measurement, *J. Atm. Terr. Phys.*, **33**, 1169-1175, 1971.

Arnold, F., and D. Krankowsky, Ion composition and electron and ion loss processes in the Earth's atmosphere, in *Dynamical and Chemical coupling of the Neutral and Ionized Atmosphere*, B. Grandal and J. A. Holtet, editors, D. Riedel, 1977.

Chakrabarty, D. K., P. Chakrabarty and G. Witt, An attempt to identify the obscured paths of water cluster ions buildup in the D-region, *J. Atm. and Terr. Phys.*, **40**, 437-442, 1978.

Cole, R. K., and E. T. Pierce, Electrification in the Earth's atmosphere for altitudes between 0 and 100 kilometers, *J. Geophys. Res.*, **70**, 2735-2749, 1965.

Crutzen, P. J., I. S. A. Isaksen and J. R. McAfee, The impact of the chlorocarbon industry on the ozone layer, *J. Geophys. Res.*, **83**, 345-363, 1978.

Davidson, J. A., A. A. Viggiano, C. J. Howard, I. Dotan, F. C. Fehsenfeld, D. L. Albritton and E. E. Ferguson, Rate constants for the reactions of O_2^+, NO_2^+, NO^+, H_3O^+, CO_3^-, NO_2^- and halide ions with N_2O_5 at 300 K, *J. Chem. Phys.*, **68**, 2085-2087, 1978.

Dotan, I., J. A. Davidson, G. E. Streit, D. L. Albritton, and F. C. Fehsenfeld, A study of the reaction $O_3^- + CO_2 \leftrightarrows CO_3^- + O_2$, *J. Chem. Phys.*, **67**, 2874-2879, 1978.

Dotan, I., J. A. Davidson, F. C. Fehsenfeld and D. L. Albritton, Reactions of $O_2^+ \cdot O_2$ with CO_2, O_3, and CH_4 and $O_2^+ \cdot O_3$ with H_2O and CH_4 and their role in stratospheric ion chemistry, *J. Geophys. Res.*, **83**, 4036-4038, 1978.

Fehsenfeld, F. C., I. Dotan, D. L. Albritton, C. J. Howard and E. E. Ferguson, Stratospheric positive ion chemistry of formaldehyde and methanol, *J. Geophys. Res.*, **83**, 1333-1336, 1978.

Fehsenfeld, F. C. and E. E. Ferguson, Laboratory studies of negative ion reactions with atmospheric trace constituents, *J. Chem. Phys.*, **61**, 3181-3193, 1974.

Fehsenfeld, F. C. and E. E. Ferguson, Origin of water cluster ions in the D-region, *J. Geophys. Res.*, **74**, 5743-5751, 1969.

Fehsenfeld, F. C., and E. E. Ferguson, Thermal energy positive ion reactions in a wet atmosphere containing ammonia, *J. Chem. Phys.*, **59**, 6272-6276, 1973.

Fehsenfeld, F. C., C. J. Howard, and A. L. Schmeltekopf, Gas phase ion chemistry of HNO_3, *J. Chem. Phys.*, **63**, 2835-2841, 1975.

Ferguson, E. E., Ion Molecule Reactions in the Atmosphere, in *Kinetics of Ion-Molecule Reactions*, P. Ausloos, Editor, Plenum Press, 1979.

Ferguson, E. E., F. C. Fehsenfeld and D. L. Albritton, Ion Chemistry of the Earth's Atmosphere, in *Gas Phase Ion Chemistry, Vol. 1*, M. T. Bowers, Editor, Academic Press, 1979.

Ferguson, E. E., Sodium hydroxide ions in the stratosphere, *Geophys. Res. Lett.*, **5**, 1035-1038, 1978.

Goldberg, R. A., and A. C. Aikin, Studies of positive-ion composition in the equatorial D-region ionosphere, *J. Geophys. Res.*, **76**, 8352-8364, 1971.

Huber, B. A., P. C. Cosby, J. R. Peterson, and J. T. Moseley, Photodetachment and de-excitation of excited NO_2^-, *J. Chem. Phys.*, **66**, 4520-4562, 1977.

Kebarle, P., Ion thermochemistry and solvation from gas phase ion equilibria, *Ann. Rev. Phys. Chem.*, **28**, 445-476, 1977.

Liu, S. C., and G. C. Reid, Sodium and other minor constituents of meteoric origin in the atmosphere, *Geophys. Res. Lett.*, in press, 1979.

Narcisi, R. S., and A. D. Bailey, Mass spectrometric measurements of positive ions at altitudes from 64 to 112 kilometers, *J. Geophys. Res.*, **70**, 3687-3700, 1965.

Narcisi, R. S., A. D. Bailey, L. E. Wlodyka, and C. R. Philbrick, Ion composition measurements in the lower ionosphere during the November 1966 and March 1970 solar eclipses, *J. Atmos. Terr. Phys.*, **34**, 647, 1972.

Narcisi, R. S., A. D. Bailey, L. Della Lucca, C. Sherman and D. M. Thomas, Mass spectrometric measurements of negative ions in the D- and lower E-regions, *J. Atm. Terr. Phys.*, **33**, 1147, 1971.

Paltridge, G. W., Experimental measurements of the small-ion density and electrical conductivity of the stratosphere, *J. Geophys. Res.*, **70**, 2751-2761, 1965.

Paltridge, G. W., Stratospheric small-ion density measurement from a high-altitude jet aircraft, *J. Geophys. Res.*, **71**, 1945-1952, 1966.

Reid, G. C., Ion chemistry in the D-region, *Adv. At. Mol. Phys.*, **63**, 375-411, 1976.

Reid, G. C., The production of water-cluster positive ions in the quiet daytime D-region, *Planet. Space Sci.*, **25**, 275-290, 1977.

Zbinden, P. A., M. A. Hidalgo, P. Eberhardt, and J. Geiss, Mass spectrometer measurements of the positive ion composition in the D- and E-regions of the ionosphere, *Planet. Space Sci.*, **23** 1621-1642, 1975.

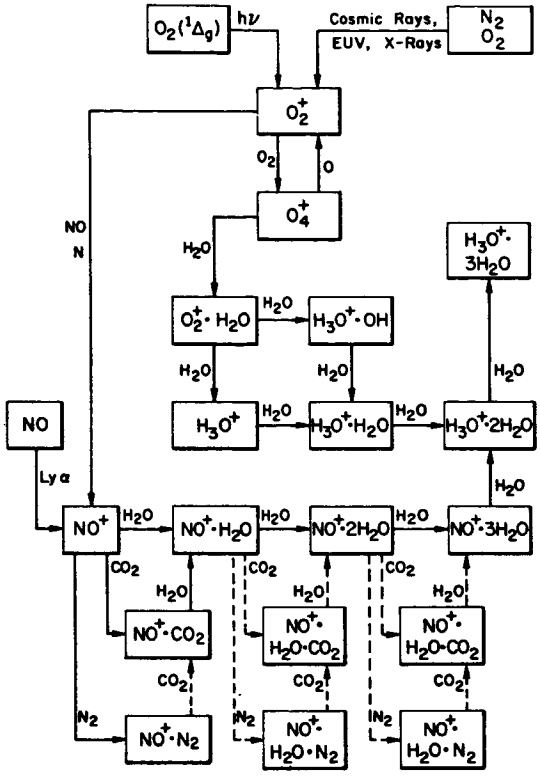

Figure 1. D-region positive ion chemistry.

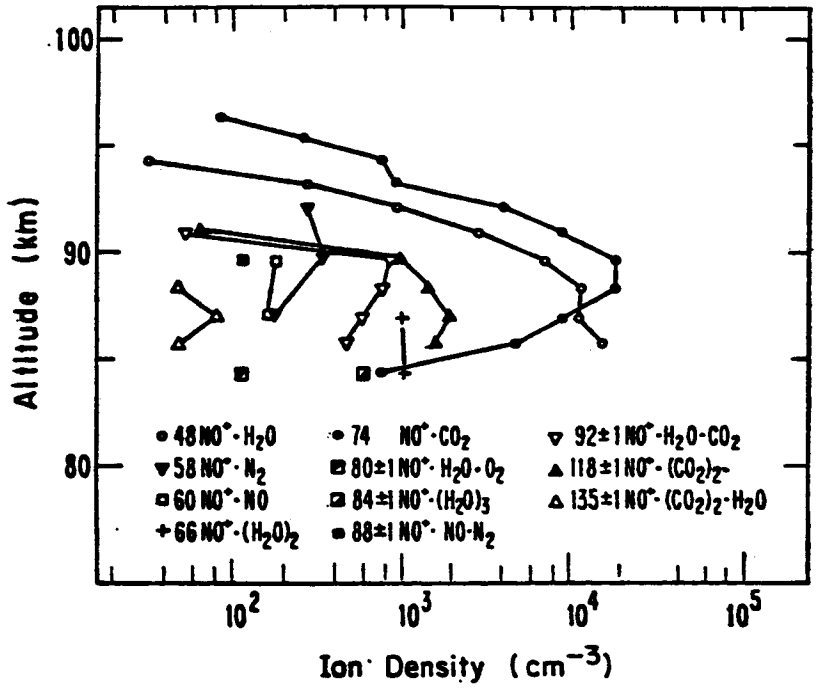

Figure 2. Altitude profiles of NO^+ cluster ions (from Arnold and Krankowsky, 1974). The identification of mass 80 ± 1 and 88± 1 amu are less certain.

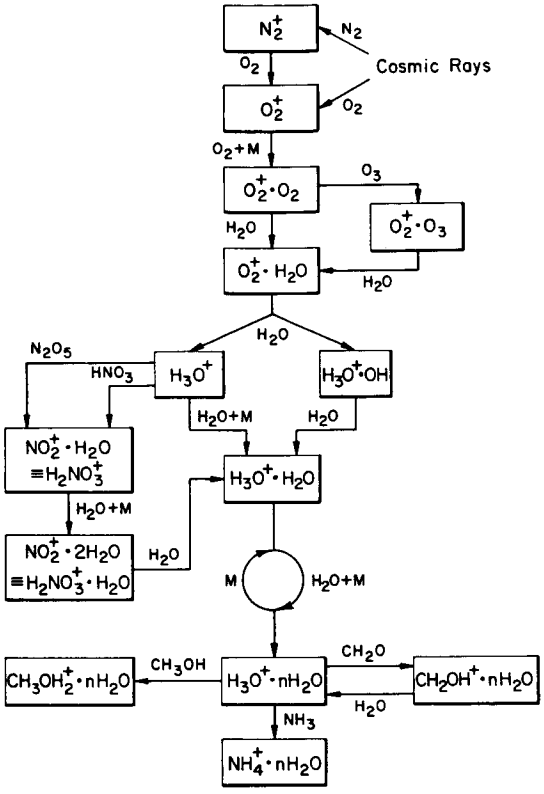

Figure 3. Stratospheric positive ion chemistry.

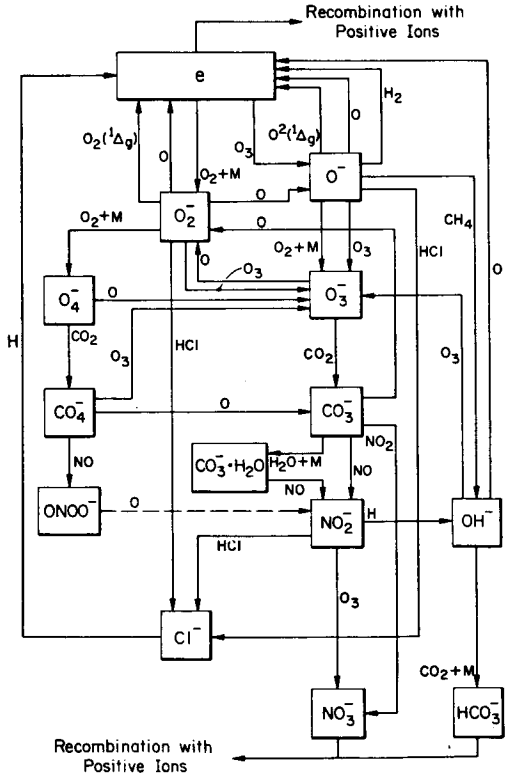

Figure 4. Reaction scheme for D-region negative ion chemistry.

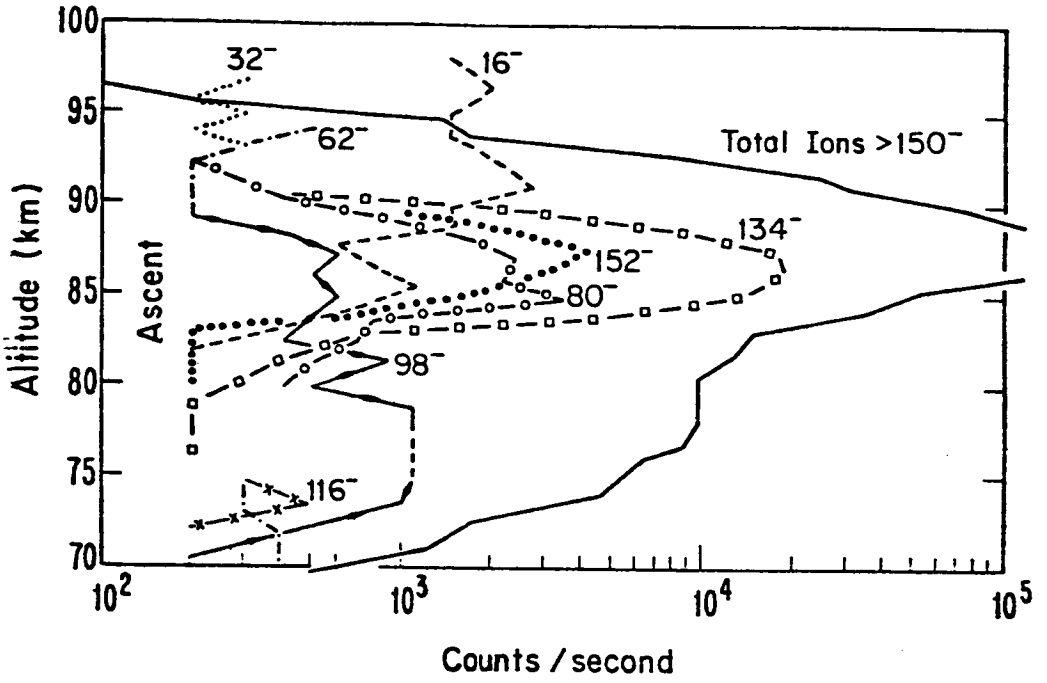

Figure 5. D-region negative ion composition measurements during total eclipse (from Narcisi et.al., 1972).

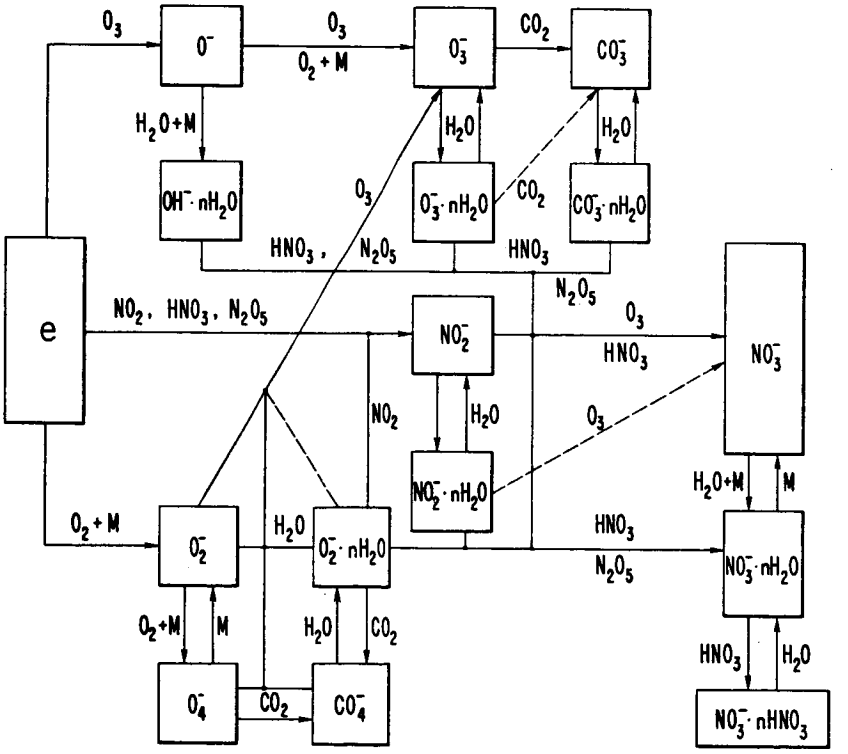

Figure 6. Stratospheric and tropospheric negative ion chemistry.

Table I

$O_2^+ \cdot O_2$ Reactions with H_2O, CH_4, CO_2, and O_3 (300 K)

	Reactions	Result[a]	Source
1.	$O_2^+ \cdot O_2 + H_2O \rightarrow O_2^+ \cdot H_2O + O_2$	$k = 1.5(-9)$ cm^3 s^{-1}	Howard et al. (1972)
2.	$O_2^+ \cdot O_2 + CH_4 \rightarrow$ products	$k < 3(-12)$ cm^3 s^{-1}	Dotan et al. (1978)
3.	$O_2^+ \cdot O_2 + CO_2 \rightleftarrows O_2^+ \cdot CO_2 + O_2$	$\Delta H = 0.3 \pm 1.0$ kcal mole^{-1}	Dotan et al. (1978)
		$\Delta S = 4.3 \pm 2.6$ cal mole^{-1}K^{-1}	
4.	$O_2^+ \cdot O_2 + O_3 \rightleftarrows O_2^+ \cdot O_3 + O_2$	$\Delta H = -3.7 \pm 1.0$ kcal mole^{-1}	Dotan et al. (1978)
		$\Delta S = 4.5 \pm 2.6$ cal mole^{-1} K^{-1}	

[a] 1.5(-9) implies 1.5×10^{-9}.

Table II
Mass Spectra of Stratospheric Positive Ions

Observed			Proposed NaOH Ion Clusters		KOH Ion Clusters	
(1)	(2)	(3)		(4)		
29±2						
42±2			41	$NaOH_2^+$		
60±2	60±2		59	$NaOH_2^+ \cdot H_2O$	57	KOH_2^+
80±2	78±2	78±2	77	$NaOH_2^+ \cdot 2H_2O$	75	$KOH_2^+ \cdot H_2O$
	82±2		81	$NaOH_2^+ \cdot NaOH$		
	96±2	96±1	95	$NaOH_2^+ \cdot 3H_2O$	93	$KOH_2^+ \cdot 2H_2O$
	99±2	100±1	99	$NaOH_2^+ \cdot NaOH \cdot H_2O$		
		114±2	113	$NaOH_2^+ \cdot 4H_2O$	111	$KOH_2^+ \cdot 3H_2O$
					113	$KOH_2^+ \cdot KOH$
		118±1	117	$NaOH_2^+ \cdot NaOH \cdot 2H_2O$		
					129	$KOH_2^+ \cdot 4H_2O$
		136±1	135	$NaOH_2^+ \cdot NaOH \cdot 3H_2O$	131	$KOH_2 \cdot KOH \cdot H_2O$
		140±1	139	$NaOH_2^+ \cdot 2NaOH \cdot H_2O$		

(1) Arnold, Krankowsky and Marien, Nature, 267, 39 (1977).

(2) Arijs, Ingels and Nevejans, Nature, 271, 642 (1978)
Arijs, private communication

(3) Arnold, Bohringer and Henschen, Geophys. Res. Letters 5, 653 (1978)

(4) Ferguson, Geophys. Res. Letters, 5, 1035 (1978).

Table III
Negative Ion Reactions with HNO_3 and N_2O_5 (300 K)

	Reactions	Rate Constant[a] ($cm^3\ s^{-1}$)	Source
1.	$CO_3^- + HNO_3 \rightarrow NO_3^- + HCO_3(?)$	8.0(-10)	Fehsenfeld et al. (1975)
2.	$NO_2^- + HNO_3 \rightarrow NO_3^- + HNO_2$	1.6(-9)	Fehsenfeld et al. (1975)
3.	$Cl^- + HNO_3 \rightarrow NO_3^- + HCl$	1.6(-9)	Fehsenfeld et al. (1975)
4.	$CO_3^- + N_2O_5 \rightarrow NO_3^- + NO_3 + CO_2$	2.8(-10)	Davidson et al. (1978)
5.	$NO_2^- + N_2O_5 \rightarrow NO_3^- + 2NO_2$	7.0(-10)	Davidson et al. (1978)
6.	$Cl^- + N_2O_5 \rightarrow NO_3^- + ClNO_2$	9.4(-10)	Davidson et al. (1978)

[a] 8.0(-10) implies 8.0×10^{-10}.

SOLAR-TERRESTRIAL COUPLING THROUGH ATMOSPHERIC ELECTRICITY

R. G. Roble
National Center for Atmospheric Research*
P. O. Box 3000
Boulder, Colorado 80307

P. B. Hays
Department of Atmospheric and Oceanic Sciences
Space Physics Research Laboratory
University of Michigan
Ann Arbor, Michigan 48105

1. INTRODUCTION

Since the earliest atmospheric electricity studies, there have been many attempts to establish a solar-terrestrial relationship in the correlation of ground currents, electric fields, and thunderstorm frequency with the aurora and variations in solar activity. Ground-based and balloon-borne instruments have detected certain atmospheric electrical responses to solar flares, solar cycle variations, solar magnetic sector boundary crossings, geomagnetic activity, and even visual auroral displays. Often these solar- and upper-atmosphere-induced variations of the global atmospheric electrical circuit are difficult to identify because they are superimposed upon complex electrical variations associated with meterological and anthropogenic processes in the lower atmosphere.

Recently, atmospheric electricity has received renewed interest as a solar-terrestrial coupling mechanism, because it may bypass many of the theoretical difficulties associated with dynamic coupling mechanisms between the upper and lower atmosphere (Markson, 1971). For example, atmospheric heating due to solar flares and auroral activity produces very large global dynamic responses in the neutral thermosphere, as discussed by Roble (1977) in the National Academy of Sciences Study, *The Upper Atmosphere and Magnetosphere*; however, a few scale heights below the thermosphere, the heating is believed to be too small to produce any dynamic perturbations. Upper atmospheric electrical effects, on the other hand – such as the generation of large horizontal scale potential differences by the magnetosphere, particularly at high latitudes, and changes in electrical conductivity by enhanced ionization – may perturb both the electric current and the field patterns of the global circuit that is mainly established by thunderstorms. If these perturbations in lower atmospheric electrical properties could affect cloud microphysical processes, thunderstorm charging mechanisms, or thunderstorm current output, then there may exist a way in which solar-terrestrial variations could modulate the internal energy of thunderstorms (Sartor, 1965; Markson, 1971, 1978a; Herman and Goldberg, 1978). Furthermore, a modulation of large-scale convective systems could drive the tropospheric circulation changes that are required to produce changes in the

*The National Center for Atmospheric Research is sponsored by the National Science Foundation.

vorticity area index. The entire chain from solar-terrestrial electrical effects to changes in tropospheric forcing is very complex and difficult to establish. This report considers the evidence of a solar-terrestrial effect through changes in atmospheric electrical currents and fields, but not the connection to cloud microphysics or possible changes in tropospheric forcing.

2. GLOBAL ELECTRICAL CIRCUIT

According to the "classical picture" of atmospheric electricity (Dolezalek, 1972), the totality of thunderstorms acting together at any given time charges the ionosphere to a potential of several hundred-thousand volts with respect to the earth's surface. This potential difference drives a vertical electric current downward from the ionosphere to the ground in all nonthunderous or fair weather regions. The fair weather electric current varies according to the ionospheric potential and the total columnar resistance between the ionosphere and the ground. A schematic of the global electrical circuit is shown in Fig. 1. Dolezalek (1972) indicated that the vagueness in the words "classical picture" is deliberate because, as yet, there is no experimental proof for the concept. The fundamental problem of atmospheric electricity is determining the origin of the electric current flowing in the atmosphere. The consensus of most atmospheric scientists is that the world-wide network of thunderstorms does act so as to maintain the global fair weather electric current; however, this concept has not been proven and there are still many difficulties associated with it, as described by Dolezalek (1972).

In the "classical picture" the thunderstorm acts as a generator in the global circuit and provides a net positive current which in the average flows upward from a cloud top toward the ionosphere and upward from the ground into a cloud base. The positive current flowing upward from the top of a thundercloud is all conduction current because ionization due to cosmic rays maintains a relatively high conductivity in the upper atmosphere.

Our knowledge of the magnitude of these upward-directed conduction currents is not too reliable. Estimates based on aircraft measurements over thunderstorms indicate that currents of 0.1 A up to 6 A per thunderstorm, with an average value of 0.5 to 1 A per thunderstorm, are flowing upward toward the ionosphere.

The number of thunderstorms acting simultaneously at any given time is also uncertain but recent estimates are between 1500 and 3000. From the number of thunderstorms and a mean value of current from a thunderstorm cell, 0.5-1 A, an estimate of the global current is 750-3000 A. There may be secondary local and regional current generators also acting at any given time, such as showers, continuous rain, sandstorms and snowstorms. These secondary generators produce local effects and are not believed to be coupled to the upper atmosphere.

The estimates of currents flowing from the ground into the bases of thunderstorms are even more uncertain on a global scale. The electric charge released from the ground by point or corona discharge (e.g., from trees, bushes, grass, buildings, etc.) underneath a thunderstorm plays a dominant role in the transfer of charge between the earth and thunderstorms. In addition, lightning and precipitation currents, which can be either in the same direction or in opposite directions, are important charge transfer mechanisms. One recent estimate by Mühleisen (1977) is that global corona currents carry about 700 A and the total lightning current at any time is about 400 A.

These upward-directed currents are counteracted by a downward-directed precipitation current of about 200 A, leaving a net upward current of about 900 A due to all sources. The total currents into thunderstorms should balance the currents flowing back to the earth in fair weather regions. Mühleisen (1977) emphasizes that all of these values are questionable and should be updated continuously as new information becomes available as well as subdivided for moderate, tropical and subtropical climates. He also emphasizes the need to determine the number of lightning flashes on a global scale. Beyond this, do lightning-intensive tropical thunderstorms have more or less current output than thunderstorms in moderate latitudes? Is there a greater current output for mountain thunderstorms compared to, say, oceanic thunderstorms? These are only two of the many questions associated with the current output of thunderstorms, which is one of the most important parameters in the global atmospheric circuit.

It is easier to estimate the local power of the global circuit outside of the generator area. The current density over land varies greatly with local terrain; however, measurements indicate a current density of 10^{-12} A m^{-2} over inhabited and industrialized areas and 2-4 x 10^{-12} A m^{-2} over vegetated grounds and deserts. The values over the oceans have been estimated to be 2.5 x 10^{-12} A m^{-2} for the Pacific Ocean and 1.6 x 10^{-12} A m^{-2} for the Atlantic Ocean, with the difference attributed to an increase of air pollution over the Atlantic. The current density into high mountain peaks should be much greater than that at sea level. The columnar resistance over mountainous areas is much smaller than over flat land and as much as 20% of the global current may stream toward high mountain peaks.

An important element in the global atmospheric electrical circuit, especially with respect to possible solar-terrestrial effects, is the columnar resistance. The conductivity of the atmosphere is primarily maintained by the ionization of atmospheric gases by galactic and solar cosmic radiation. Near the earth's surface over land, there is an additional component due to ionization associated with the radioactive decay of certain crustal materials. The columnar resistance is the vertical integral of the specific resistivity at any given location between the ground and ionosphere. Because the conductivity of the atmosphere increases nearly exponentially with altitude, the bulk of the total columnar resistance occurs in the lower atmosphere, with 90% of the total resistance below 10 km. Fig. 2a shows the percentage of columnar resistance in different atmospheric layers, and Fig. 2b shows the percent of variation of ionospheric potential with altitude (Markson, 1976). Only 10% of the total columnar resistance and ionospheric potential occur above 10 km, where large variations in ion production may result from known solar-terrestrial influences, such as polar cap absorption (PCA) events and auroral ionization. Because the stratospheric and mesospheric conductivity affects less than 10% of the total columnar resistance it is generally believed that large variations in upper atmospheric conductivity due to solar-terrestrial influences may occur without greatly affecting the global resistance. A typical value for the global resistance is 270 Ω when mountains are considered. The resistance of the earth without mountains would be 70 Ω greater.

On the basis of these estimates of the global current and total global resistance, the ionospheric potential would vary between 70 kV and 800 kV. The average of the measurements reported by Markson (1976) and Mühleisen (1977) is 240 kV. Markson's measurements show considerable variation from day to day and even hour to hour, indicating the workings of very complex generators and loads in the global electrical circuit.

All of the atmospheric elements of the global circuit have some type of diurnal variation. The global ionospheric potential, air-earth current, and potential gradient in the free atmosphere above the exchange layer all have a diurnal variation in universal time (GMT) (e.g., Anderson, 1969; Markson, 1976). A universal time variation of atmospheric electrical parameters was first defined by measurements aboard the Carnegie Magnetic Survey Ship expedition in 1928/29. Statistically, the minimum values occur near 0400 UT, whereas the maximum values occur near 1900 UT. This diurnal variation is difficult to measure from the ground because of temporal variations in space charge and conductivity in the air near the Earth's surface. Whipple and Scarse (1936) have shown that the global diurnal variation of the number of thunderstorms in universal time has a similar shape to the Carnegie measurements, as shown in Fig. 3. The peak in "thunderstorm area" occurs near 1900 UT, when the combined effect of thunderstorms on the American and African continents maximize during the local afternoon hours. The corresponding minimum occurs when maximum heating occurs over the Pacific Ocean, where the effects of intense continental heating are absent. The correspondence between the universal diurnal variation of measured electrical parameters and "thunderstorm area" has been considered the strongest argument for the theory that thunderstorms act as generators in the "classical picture" of atmospheric electricity.

A common measurement in atmospheric electricity is the potential gradient or electric field at the earth's surface. This parameter is highly variable and is dependent upon such factors as meterological influences, air pollution, clouds and orography. Under thunderstorms, the electric potential decreases with altitude, suggesting a current flow into the storm. In fair weather regions away from local influences, the electric potential increases with altitude, indicating a current flow to the ground. Near the equator at sea level the Carnegie Ship in 1928/29 measured a potential gradient of 120 V m^{-1} which increased in latitude to values near 155 V m^{-1} at 60° north and south latitude. This variation in latitude is consistent with what one expects from variations in conductivity due to the magnetic latitude shielding effect of cosmic ray production (Israël, 1973). The potential gradient also decreases with altitude, so that at the South Pole station (2800 m) the potential gradient reported by Cobb (1977) has a mean value of 71 V m^{-1} .

Another important parameter of the global electric circuit is the relaxation time at various altitudes; this is the "switch-on" time for the establishment of a final steady state from an arbitrary initial state. In the upper atmosphere near 70 km, it is 10^{-8} s, at 18 km about 4 s, and near the Earth's surface $\sim$ 20 m. The relaxation time of the Earth is about 10^{-5} s so that atmosphere is considered a spherical capacitor with the atmosphere as a dielectric between two highly conducting plates, the ionosphere and the Earth's surface. If all thunderstorms suddenly ceased operating the global circuit would discharge to 1/e in 20 min. Since this has never been observed to happen and variations are only about 20% of the mean, thunderstorms must be operating continuously over the Earth's surface.

These and other properties of the global circuit are summarized in Table 1.

3. MEASUREMENTS OF SOLAR-TERRESTRIAL INFLUENCES ON ATMOSPHERIC ELECTRICITY

The possibility that the aurora may affect the earth's atmospheric electrical circuit has been considered since the early days of atmospheric electricity studies. Wijkander (1874) at Spitzbergen indicated that the onset of the northern lights caused the air to become negatively charged, and Andrée (1890) reported that the fair weather electric field first was reduced during active auroral periods and then recovered to initial values a few hours later. Israël (1973) reviewed the evidence for solar-terrestrial influences in measurements of the ground electric field. The results show that "terrestrial periods", which include diurnal and annual periods, are strongly evident but "cosmic periods", such as the 27-day and 11-year periods, are evident only weakly if at all. Many of the statistical studies correlating thunderstorm frequency with solar flares, solar magnetic sector boundary crossings, etc., have been reviewed recently by Markson (1971, 1978a).

There are a number of measurements of electrical variations that suggest a solar-terrestrial influence on the global atmospheric electrical circuit. The measurements show variations associated with (a) solar flares, (b) solar magnetic sector boundary crossings, (c) geomagnetic activity, (d) aurorae, (e) differences between ground current and potential gradients at high and low latitudes, and (f) solar cycle variations. The evidence for each variation is examined separately below.

3.1 Solar Flares

One of the earliest investigations of effects of solar activity on atmospheric electricity was that of Bauer (1924), who found that the electric field at the ground increased during periods of increased "sun-spottedness." Reiter (1969) reported that the daily means of the ground potential gradient, E, and air-earth current, i, increased from the day a solar flare first appeared until the fourth day later, when they attained maxima. Reiter's measurements were made from a mountain station at Zugspitze, Switzerland (2964 m), where 70-80% of the columnar resistance between the ionosphere and the earth's mean sea level surface is below the station. Therefore, measurements of E and i are not greatly influenced by variations in columnar resistance, and influences due to solar events can be studied. Measurements made over the past 20 years have consistently shown a significant increase (about 50-60% on the average in both the air-earth current and the potential gradient at the station following solar flares. Fig. 4 shows a superposed epoch analysis of the potential gradient, E, and air-earth current, i, following Hα solar flares occurring near the central meridian of the sun (between 20° west and 20° east) from February 1967 to May 1969. They clearly show an increase in both quantities. Also, from individual case studies, Reiter (1977) shows that following solar flares and solar wind velocity, the product E x i measured at Zugspitze, the solar proton density, x-ray intensity, and geomagnetic index, C_p, all increase. The beryllium 7 concentration measured at the mountain station also increases, which Reiter attributes to an injection of stratospheric air into the troposphere following solar flare events.

Cobb (1967) making measurements from the low-latitude station on Mauna Loa, Hawaii (4170 m), also found evidence of solar influence on the atmospheric electric elements. During a one-year measurement period beginning in September 1960, there were times of considerable solar activity, with 28 solar flares of Class 3 or greater and 42 magnetic storms. Following a solar flare eruption,

the air-earth current increased from its established normal values. Fig. 5 shows an increase in the measured air-earth current following solar flare events, averaging 11.7% above normal. In approximately 80% of the cases, this increase occurred in the first 24 hours after a flare.

These measurements suggest a solar influence on the parameters of the global electrical circuit. Through the years there have also been many reports relating increased thunderstorm frequency to solar flares (e.g., see Markson, 1978a, 1978b for a review).

Recent balloon measurements in the high-latitude stratosphere have also shown electrical responses to solar activity. Holzworth and Mozer (1979) have shown that solar controlled ionizing radiation can have large effects on the electrical conductivity down to at least 15 km at mid-geomagnetic latitudes. The large measured increase in electrical conductivity corresponded with a decrease in the vertical electric field measured during the August 1972 PCA event. Cobb (1978) has made balloon measurements of the air-earth current density at the South Pole before and after a solar flare. Balloon borne sensors were released at approximately 0300 UT each day for five consecutive days during the period 22-27 November 1977. The measured air-earth current density profiles are shown in Fig. 6. The first balloon was released at 0255 UT, 22 November 1977, 7 h before a solar flare occurred, and the measured air-earth current density was typical of other balloon flights made by Cobb (1977). The second balloon was released about 17 h after the solar flare, and through the first 25 km the current was nearly identical with the first flight. However, above 25 km the measured air-earth current was much higher. It is not clear whether the abrupt increase is due to a space charge encountered or a temporal effect, since the balloon takes time to rise through the layer. The following day the entire air-earth current density profile was enhanced by 70% from pre-flare conditions. Two days later the measured air-earth current density profile returned to pre-flare conditions. Mühleisen (1971) has also shown that the ionospheric potential difference inferred from measurements made at widely separated mid- and low-latitude stations is generally small. However, during one strong solar event he found a 60 kV ionospheric potential difference between two stations.

3.2 Solar Magnetic Sector Boundary Crossings

Markson (1971) first called attention to solar magnetic sector boundary crossing effects on atmospheric electric parameters and possible increases in thunderstorm frequencies. Since then Park (1976a) and Reiter (1977) have both reported variations in the measured air-earth current and potential gradient at the ground during solar magnetic sector boundary crossings. Park's measurements of the atmospheric electric field were made during the period March-November 1974 at Vostok, Antarctica (78°S, 107°E, which is at the south geomagnetic pole. Although he had only 17 measurements during solar magnetic sector boundary crossings, his results show that the electric field is depressed by $\sim 15\%$ one to three days following the passage of solar magnetic sector boundaries, and the effect is more pronounced in the austral winter, when Vostok is in continuous darkness (Fig. 7). The figure also shows a large seasonal variation, with the field being much stronger in winter than during equinoxes. No significant difference was found between the away-to-toward sector boundaries and the toward-to-away sector boundaries.

Reiter's measurements were made from the high mountain observatory at Zugspitze, Switzerland over a period of one solar cycle. The results show that in cases when the magnetic field polarity

changes from toward the sun to away from the sun, the ionospheric potential significantly decreases on the day before and on the day of the sector boundary passage. However, on the first and second day after the passage it increases by about 20%. If the magnetic polarity changes from away from to toward the sun the ionospheric potential is again observed to change: on the first and second days prior to the passage it is clearly decreased whereas on the day of the passage it is already back to normal. The amplitude of the variation for this case is 10%. Fig. 8 summarizes the E and i variations during a sector boundary passage along with various parameter variations determined from other studies such as the beryllium 7 concentration at Zugspitze, the vorticity area index, and the K_p variations inferred during passage of magnetic sector boundaries.

3.3 Geomagnetic Activity

Cobb (1967) has shown that the monthly variation of the air-earth current from mean values at Mauna Lao, Hawaii, is well correlated with Bartel's magnetic character index, C_p. This correlation from September 1960 to September 1961 is shown in Fig. 9. There is good correlation between the most "magnetically disturbed" months of October and July and the least disturbed months of January and August. Cobb also compares the daily variation of C_p and measured air-earth current density; although the overall correlation is not as good as for the monthly variations, there appear to be interesting upper atmospheric effects.

Märcz (1976) also has reported a measured increase of the ground electric field for several days following high ionospheric absorption events associated with geomagnetic activity. Measurements made from observatories near Nagycenk, Hungary, and Swider, Poland, showed an increase of 12-46% (depending upon the time of day) in the potential for several days following high absorption events.

Tanaka *et al.* (1977), making stratospheric balloon measurements of electric fields and currents at Syowa station, Antarctica (69°S, 39°E geographic), found that the electric field and current both increased by 30% of their normal values during the initial stage of a magnetic substorm. Simultaneous electric field measurements at the ground also showed an increase of 30% of the normal value at the same time that the electric field and current measurements increased at balloon altitudes (~30 km). To account for these increases they required an increase of 80 kV in the ionospheric potential over the station during the magnetic substorm. Although this effect is somewhat confused by the size of the substorm and the onset of the katabatic wind near the observing site, it is suggestive, and the experiment should be repeated to establish whether magnetic substorms cause a perturbation in the atmospheric electrical circuit either at high latitudes or globally.

3.4 Aurorae Effects

As a whole, the available data on the influence of aurorae upon ground potential gradient and air-earth current are inadequate and contradictory. During the International Polar Year, 1932/1933, certain studies (Israël, 1973) found that the potential gradient and air-earth current both experience a fluctuating variation with an aurora: a peak of approximately 155% of the mean value 6-8 min. before the aurora, and a minimum value of some 65% occurs 10 min. after onset. More recently, Freier (1961), Olson (1971), and Lobodin and Paramonov (1972) have reported auroral effects on

vertical electric fields measured on the ground. In general, they report a decrease in the electric field which later recovers to pre-auroral conditions. Fig. 10 shows the results of Lobodin and Paramonov (1972), who examined electric field data from eight high-latitude stations. Seven of the stations were in the Northern Hemisphere between 41°41'N and 80°37'N and 30°18'E and 158°E. The results from the Northern hemisphere stations show that appreciable variations of electric field begin 3 to 4 h before the onset of an aurora and last up to 3 h after its appearance. The mean decrease of E during the aurora is 23-32% for continental stations and 8% for the eastern Siberia sea. In the Southern Hemisphere the potential gradient increased by 36% of the mean. In the Northern Hemisphere the decrease averaged 4% for weak, 6% for medium, 14% for strong, and 20% for very strong aurorae.

Shaw and Hunsucker (1977), on the other hand, analyzed measurements of the ground electric field and found no auroral effects at College, Alaska (65°N), even when the ionosphere is disturbed and there is violent visual auroral activity.

3.5 Differences at High and Low Latitudes

Kasemir (1972) examined the atmospheric electric field, current, and conductivity data recorded during the IGY in 1958 at Thule, Greenland (78°N), which is near the north magnetic pole. He also examined atmospheric electric field measurements made during IQSY in 1964 at the Amundsen-Scott station at the South Pole. The diurnal UT variation averaged over the year of the normalized current at Thule and the normalized field at the South Pole show surprisingly good agreement. Compared with the oceanic diurnal UT variation at low and midlatitudes measured during the Carnegie Ship cruises, the polar curve shows a very similar shape but a much reduced amplitude, as shown in Fig. 11. The maximum and minimum in the polar regions are 1.07 and 0.92 of the mean, whereas the corresponding values on the oceans are 1.20 and 0.85. The cause of the approximately 30% reduction in the diurnal amplitude is not known; however, Kasemir suggests that there is a strong possibility that another agent besides worldwide thunderstorm activity may modulate the global circuit.

Cobb (1977) also has reported on potential gradient and air-earth current density measurements at the South Pole station during the period November, 1972, through March, 1974. The average potential gradient during this period was 71 V m^{-1} and the air-earth current density was 2.5×10^{-12} A m^{-1} . The percent of variation of the air-earth current density measured at the South Pole followed very closely the diurnal UT percent of variation measured earlier at the Mauna Loa low-latitude station, although the mean values at the two stations are different. The diurnal UT variation of the potential gradient at the South Pole, however, is displaced by several hours compared to the Mauna Loa measurements.

Cobb also made balloon measurements to as high as 35 km at the South Pole station. Two aspects of the soundings have emerged. First, the current is usually not constant with altitude even in the stratosphere, and second, the average current in the stratosphere may vary by an order of magnitude from day to day.

3.6 Solar Cycle Variations

There is a long-period variation in cosmic ray radiation that is inversely correlated with sunspot activity (Forbush, 1966; Neher, 1971). At 15 km the ionization rate may vary by 51% (conductivity by 23%) while at 20 km the ionization rate varies by about 76% (conductivity by 33%) at high latitudes. At 20 km, the average conductivity variation through a solar cycle is about 18% at midlatitudes and about 10% near the equator. There are probably significant variations of conductivity day by day.

Mühleisen (1977) has derived the ionospheric potential variation of the global circuit over an 11-year solar cycle by balloon radiosonde ascents. His results suggest a solar cycle variation of ionospheric potential opposite to solar activity as characterized by the relative sunspot number. Olson (1977) has shown the solar cycle variation of air-earth conduction current density depicted in Fig. 12. The maximum current density occurs near solar cycle minimum, as determined by the sunspot number, and minimum current density occurs near solar cycle maximum. The data were divided into two sets: one for the hours near the maximum in the UT diurnal variation and one for the minimum (Markson, 1978b). The scatter plots in the lower portion of Fig. 12 show a negative correlation between air-earth current density and sunspot number for both data sets.

4. UPPER ATMOSPHERE ELECTRICAL COUPLING

In the earth's atmosphere, where electrical conductivity increases exponentially with altitude above the exchange or atmospheric boundary layer, downward field mapping is much more effective than upward field mapping (Park 1976b). Several studies have shown that large horizontal scale electrical fields of ionospheric origin map effectively downward with little attenuation to 20 km and perturbations can occur even at the earth's surface. Because of the high conductivity of the earth's surface, the horizontal electric field cannot be maintained and it produces vertical perturbations in the potential gradient at the ground.

There are at least two ionospheric electrical generators that can produce large horizontal scale potential differences within the ionosphere that effectively couple into the global electrical circuit. These are (a) the ionospheric dynamo and (b) the magnetospheric generator associated with plasma convection at high latitudes.

4.1 The Ionospheric Dynamo

Above about 70 km solar EUV radiation ionizes certain atmospheric constituents more efficiently with increasing altitude; this produces the ionosphere. Below about 80 km, the mobility of solar-produced electrons and ions is dominated by collisions with neutral gas. Above 80 km, however, collisions become less frequent so that electrons gyrate around the geomagnetic field line several times before successive collisions with neutrals, and the electrons are essentially bound to the geomagnetic field line. For ions this process happens above 140 km. This difference in behavior between the electrons and ions makes the electrical conductivity anisotropic. Three conductivities exist: a parallel conductivity along the geomagnetic field line, a Pedersen conductivity that is perpendicular to the geomagnetic field line but in the direction of an applied electric field, and a Hall conductivity which is also perpendicular to the geomagnetic field line but at right angles to

the applied field. The dynamo region is defined as that region in the Earth's atmosphere where most of the Pederson and Hall currents flow; it lies between 100 and 200 km. Outside of this region, the Pedersen and Hall conductivities decrease to 10% of their maximum values. All of the electrical conductivities in the dynamo region are subject to large diurnal, seasonal, and geographic variations due to the varying electron number density which is maintained primarily by solar ionizing radiation. At nighttime, these conductivities drop to very small values. Solar flares and auroral particle precipitation can greatly increase the electron density, thus increasing conductivity and also temporarily shifting the boundary of the dynamo region to lower altitudes.

Global atmospheric tides are generated in the upper atmosphere by the diurnal variations of solar heat input and gravitational forces of the sun and moon. The winds in the dynamo region force plasma across the geomagnetic field line and produces a $\mathbf{v} \times \mathbf{B}$ Lorentz force. Due to ambipolar diffusion of electrons and ions, charge separation occurs, which produces an electric polarization field. Electric currents in the dynamo region flow under the combined influence of the polarization field and the Lorentz force. The magnetic effects of these electric currents, as observed on the ground, are known as S_q (solar quiet) and L (lunar gravitational) geomagnetic variation. Volland (1972, 1977) has shown that the large horizontal scale potential differences generated in the ionospheric dynamo region ($\sim$ 10 kV) map into the lower atmosphere. The ionospheric dynamo perturbs the low-latitude potential and electric field at the ground by about 6% of the tropospheric fair weather potential and electric field established by thunderstorm charging. An empirical model of the ionospheric dynamo potential determined by Richmond (1976) from incoherent scatter radar data is shown in Fig. 13. The values are valid between 0 and 60° in latitude. At higher latitudes potentials due to the magnetospheric generators must be considered. During geomagnetic storms the dynamo potential differences may be enhanced somewhat, but in general the perturbations to the atmospheric potential and fair weather field in the lower atmosphere should be small ($< 10\%$).

4.2 MAGNETOSPHERIC DYNAMO

The interaction of the solar wind with the earth's geomagnetic field and the magnetospheric effects of this interaction have been described by Hill and Wolf (1977) and Burch (1977), respectively, in the National Academy of Sciences study *The Upper Atmosphere and Magnetosphere.* This interaction gives rise to a large-scale flow of plasma across both magnetically conjugate polar caps; this flow is associated with a dawn-to-dusk potential drop across both caps. Heppner (1977), primarily using satellite data, has constructed empirical models of potential distribution around the polar magnetic cap. Fig. 14 shows the potential pattern for both a geomagnetically quiet and a disturbed period. During quiet times the potential drop is typically 50-70 kV and the pattern is generally confined to magnetic latitudes greater than 60°. During geomagnetic storms and substorms, and possibly during solar flare activity, this pattern expands equatorward and the potential drop increases to 150-250 kV. This potential pattern is maintained by pairs of field-aligned current systems, each carrying approximately a million amperes, with current densities of 10^{-6} A m^{-2}, it is also dependent upon the ionospheric conductivity. There are variations of this potential pattern with the direction of the interplanetary magnetic field and it appears that the negative perturbation of the ionospheric potential on the dusk side is greater than the positive perturbation on the dawn side of the polar cap. There is still much uncertainty associated with the time-dependent behavior of the potential pattern; however, it is anticipated to be highly varible. Park (1976b) has discussed mapping this

potential pattern to the ground and has shown perturbations of ±20% in the ground electric field under the pattern during geomagnetic quiet times.

5. NUMERICAL MODEL OF THE GLOBAL ELECTRICAL CIRCUIT

Another method of determining possible solar-terrestrial effects on the global atmospheric electrical circuit is numerical modeling. By imposing variations of electrical conductivity known to occur during solar flares or variations in potential generated by the upper atmospheric generators it is possible to calculate the effects on the global circuit parameters, such as changes of current density or potential gradient, and compare the calculated variations to measurements. A schematic diagram of a global quasi-static model formulated by Hays and Roble (1979) is shown in Fig. 1. Within the model it is assumed that thunderstorms act as dipole current generators, each with a positive center at the top of the cloud and a negative center a few kilometers lower than the positive center. In fair weather regions far away from the storm centers, the distribution of the electrostatic potential above the earth is determined by the current return from the sources to the earth's surface. The geometry of the model is based upon an atmosphere broken into four coupled regions. Region 0 represents the lower troposphere, which has a variable conductivity in the horizontal and vertical; it also includes the earth's orography. Region 1 represents the upper troposphere below the negative current source region within the thunderstorm, and Region 2 represents the stratosphere and mesosphere above the positive current source region of the thunderstorm. For regions 0, 1, and 2 the electrical conductivity is assumed to be isotropic. Region 3 represents the ionosphere and magnetosphere above the dynamo region, where the electrical conductivity is anisotropic and where magnetic conjugate regions are connected along geomagnetic field lines through the magnetosphere. The mathematical details of the model, the boundary conditions, and the matching between various regions are described by Hays and Roble (1979).

The height and latitudinal distribution of electrical conductivity used for model calculations are shown in Fig. 15. The electrical conductivity above the exchange layer in the lower atmosphere is maintained by cosmic ray activity, which in the troposphere varies by about a factor of two between the equator and the poles. Since the conductivity is maintained primarily by small mobile ions, it varies as the square root of the cosmic ray ion production rate. Also shown in Fig. 15 are the variations of electrical conductivity assumed to occur with a sudden increase in cosmic ray ionization resulting from a solar flare and a subsequent Forbush decrease.

On a global scale there is no net current source within the model and the thunderstorms act as pumps, recirculating current from the lower to the upper atmosphere. Two thousand individual thunderstorms occurring at 1900 UT are distributed randomly in latitude and longitude in accordance with the hourly probability of thunderstorm occurrence defined by Crichlow *et al.* (1971). These thunderstorm regions are similar to the observed pattern of lightning flashes during the period 10 September - 11 October, 1977, as determined by the DSMP satellite in a dawn-dusk polar orbit, shown in Fig. 16 (Edgar, 1979). Each dot indicates an observed lightning flash for either the dawn or the dusk pass. The maximum thunderstorm occurrence observed by the satellite is primarily over the continental land masses. For the model calculations, Northern Hemisphere summer months are assumed; therefore at the 1900 UT maximum in ionospheric potential, thunderstorm activity occurs over Central America, Florida, and the Rocky Mountains, in addition to the Amazon basin and parts of Central Africa. It is assumed that at 1900 UT, 600, 100, 1000, 280, and 20

thunderstorms are randomly distributed in latitude and longitude in the vicinity of Africa, Asia, Central America, Argentina, and the Alps, respectively. The actual regions of thunderstorm distribution have been given in Fig. 4 of Hays and Roble (1979). The storm centers are also randomly distributed in the vertical. The model also includes the effects of orography, which is shown as a perspective illustration in Fig. 17. The height of the land above sea level is averaged over a 5°grid in latitude and longitude. The solutions presented in the next sections are obtained on an effective 5°grid in latitude and longitude; therefore it is not possible to resolve the detailed potential distribution around individual mountains or thunderstorms that have a much smaller spatial scale. The model primarily describes global variations, and smaller features can be resolved by coupling a fine-mesh numerical model with the global model through appropriate boundary conditions.

6. MODEL SOLUTION FOR THE LOWER ATMOSPHERE

The calculated electric potential along the $\sigma = 7.3 \times 10^{-12}$ mho m^{-1} constant conductivity surface, which occurs at approximately 25 km at the equator and slopes downward to 23 km in both polar regions, is shown in Fig. 18c. The calculated fair weather ionospheric potential is $\Phi_\infty = 291{,}000$ V and the quantity $(\Phi - \Phi_\infty)$ is plotted along the constant conductivity surface. Over the thunderstorm regions of Central America, Africa, and Argentina, the value of $(\Phi - \Phi_\infty)$ is positive and electric current flows upward from the thunderstorm region to ionospheric heights; the maximum value of $(\Phi - \Phi_\infty)$ is 16,000 V. Minimum values occur over the mountainous fair weather regions, with -5700 V over Tibet and Antarctica. The calculated value of $(\Phi - \Phi_\infty)$ along the $\sigma = 4.74 \times 10^{-10}$ mho m^{-1} surface near 50 km in the equatorial region is shown in Fig. 18b. The potential distribution has spread considerably from the concentrated regions over the thunderstorms at 25 km to a more uniform distribution at 50 km. The calculated value of $(\Phi - \Phi_\infty)$ along the $\sigma_m = 4.54 \times 10^{-6}$ mho m^{-1} conductivity surface, which is the base of the magnetosphere in Region 3 of the model at roughly 105 km, is shown in Fig. 18a. Φ_∞ is the global mean average along this surface. The maximum value of $(\Phi - \Phi_\infty)$, which occurs over the thunderstorms in Africa, is 975 V and the minimum value is -600 V over the central Pacific.

For these model calculations the geomagnetic and geographic poles are assumed to be coincident. At the geomagnetic equator the field lines are horizontal and the vertically directed electric current is restricted from spreading laterally. The maximum potential develops in this region. In Central America, the thunderstorm region is displaced from the geomagnetic equator and therefore currents flow from the storm region along the geomagnetic field line into the conjugate hemisphere. The potential perturbation then attenuates as it penetrates to lower altitudes in the conjugate hemisphere.

The calculated potential, Φ, along the constant conductivity surface $\sigma_1 = 4.3 \times 10^{-13}$ mho m^{-1}, which is approximately 8 km in the equatorial regions, is shown in Fig. 18d. Under each thunderstorm region the potential is strongly negative. The minimum value of several million volts occurs under the Central America thunderstorm region. In the fair weather region away from the thunderstorms the calculated potential is positive with respect to the ground, indicating a current returning to ground. The calculated potentials at 4 km and 2 km are shown in Figs. 18e and 18f, respectively. They are similar to the potential calculated on the 8 km surface, but at these lower altitudes the distortion by the earth's orographic features becomes evident. The potential becomes zero when a surface intersects a high mountain that protrudes above the altitude, and the potential becomes

greatly distorted when the surface is near an orographic feature such as Antarctica, Greenland, or the Himalayas. On the 2 km surface the outline of continental features begins to appear. The subgrid-scale potential distribution around each thunderstorm is on the order of 10 km (Holzer and Saxon, 1952), negative under the thunderstorm and positive in the fair weather regions away from the storm. We cannot resolve the subgrid-scale potential distribution with our global model and thus the solutions are 5° grid area averages of the subgrid-scale distributions.

The calculated electric field and the ground current along the earth's orographic surface are shown as perspective illustrations in Figs. 19a and 19b, respectively. The highest fair weather electric field and electric current flow occur in Antarctica and other high mountainous regions, because there is high conductivity at mountaintop level and because orography distorts the electric potential and amplifies the electric field. The current into the ground in the fair weather regions is balanced by a current from the ground into the thunderstorm regions, leaving no net current flow on a global scale. The electric field at sea level is 134 V m^{-1} at the equator and 173 V m^{-1} in the polar regions, which compares well with the Carnegie expedition's measurements of 120 V m^{-1} near the equator and 155 V m^{-1} at 60° latitude. Table 2 compares the parameters of the model with the estimate of global circuit parameters made by Mühleisen (1977). There are considerable uncertainties in these global estimates, yet the similarity of the parameters is encouraging.

7. COUPLING OF IONOSPHERIC POTENTIALS WITH THE GLOBAL CIRCUIT

At high geomagnetic latitudes, the interaction of the solar wind with the earth's geomagnetic field establishes a dawn-to-dusk electric potential drop across the polar cap. During geomagnetic quiet periods this potential drop is typically 50-70 kV, whereas during disturbed periods it may increase from 150-250 kV.

The empirical model of Heppner (1977), Fig. 14, gives the ionospheric potential distribution in the high-latitude ionosphere for both geomagnetic quiet and disturbed periods. This potential distribution is used as an upper boundary condition above the dynamo region and is incorporated in the global model of atmospheric electricity described by Roble and Hays (1979). Their calculations consider the effects of the earth's orography and the tilted geomagnetic and geographic poles.

The variations in the ground electric potential gradient at sea level calculated using Heppner's magnetically averaged period model are shown in Fig. 20 for various high-magnetic-latitude circles. They are plotted as functions of magnetic local time. For early magnetic local times the ionospheric potential perturbations to the earth's potential gradient are positive. For later magnetic local times the perturbations are negative. The Carnegie expedition showed that at low and middle latitudes there is a universal time variation of potential gradient at the earth's surface due to the diurnal variation of thunderstorm frequency. The maximum electric potential gradient occurs at 1900 UT, and the minimum occurs near 0400 UT.

In Fig. 20, this potential pattern is plotted in magnetic local time for the Atlantic and Pacific sectors; different diurnal variations in magnetic local time are obtained for the two sectors. The total ground potential gradient variation for a station in the Pacific sector is determined by the difference between the variation of the upper curve for the latitude and the lower solid curve, as indicated

by the vertical line with arrows giving $\delta\Phi/\delta z$. The same variation for an Atlantic sector station is obtained from the difference between the appropriate upper curve and the lower dashed curve. The results show that the diurnal variation of potential gradient is small for an Atlantic sector station, but much larger for a Pacific sector station. Thus, measurements at high latitudes should be interpreted in terms of variations of inospheric potential as well as in terms of thunderstorm frequency variations. Kasemir (1972) has reported that the diurnal UT variation of potential gradient at both the Thule, Greenland, and South Pole stations is about 30% less than the global low-latitude UT variation attributed to variations in thunderstorm frequency, which may indicate the influence of the ionospheric generators. For Heppner's magnetically disturbed model the dawn-to-dusk ionospheric potential drop across the polar cap is 140 kV. A similar calculation using the disturbed model gives a larger magnitude to the potential perturbations and also the effects of the generator extend to lower latitudes, indicating a greater upper atmospheric influence during magnetically disturbed periods.

The calculated potential gradient and air-earth current along the earth's orographic surface, due to coupling Heppner's (1977) geomagnetic quiet model into the global electrical model, are shown as perspective illustrations in Figs. 21a and 21b respectively. These 1900 UT patterns must be added to the patterns in Figs. 19a and 19b to obtain the total potential gradient and air-earth current due to the combined effect of worldwide thunderstorm activity and the coupling of the ionospheric potential pattern into the global electrical circuit. The maximum positive ionospheric potential perturbation of +32 kV maps downward and produces a +20 V m^{-1} perturbation in the earth's fair weather electric field. The maximum negative ionospheric potential perturbation produces about -20 V m^{-1} at the earth's surface. Similarly, the positive ionospheric potential perturbation causes a current to flow downward from the ionosphere into the earth surfaces and similarly the negative ionospheric potential perturbations cause a current to flow upwards from the ground toward the ionosphere. As seen in Figs. 21a and 21b, the magnitude of the potential gradient and air-earth current are influenced by the earth's orography.

The magnetospheric potential pattern remains sun-aligned in geomagnetic coordinates. Therefore, as the earth rotates around its geographic pole, the ionospheric potential which maps directly downward moves over the earth's surface in a complex but systematic fashion during the day. The pattern shown in Figs. 21a and 21b is constantly moving.

The positive and negative potential perturbations of the ionospheric potential on the dawn and dusk sides of the polar cap, respectively, cause a downward and upward current to flow from the ionosphere to the ground. The model requires that the divergence of the current must be zero; therefore, any imbalance in the downward and upward current system must be compensated for by the global circuit, which changes the global ionospheric potential between the ground and ionosphere. Such an imbalance may occur when the positive/negative current is aligned over Antarctica, where the surface conductivity on the high mountain plateau is large, and when the negative/positive current is aligned over a cloud-covered ocean, where the surface conductivity is low. For certain large geomagnetic substorms with the upper boundary potential pattern properly aligned over the continent and ocean the current imbalance may require as much as a 5-10% change in the potential between the ground and ionosphere that is maintained primarily by thunderstorms. This dependency upon substorm intensity may help explain the dependence of ground potential gradient and air-earth current on geomagnetic activity observed by Märcz (1976) and Cobb (1967), respectively, as well as the balloon measurements of Cobb (1977)

and Tanaka *et al.* (1977). Fig. 22 shows the potential fields at various altitudes due to the combined action of thunderstorms and ionospheric geomagnetic quiet dawn-dusk potential distribution across the polar cap at a given time at 1900 UT.

In Fig. 22a, the potential difference ($\Phi - \Phi_\infty$) along the $\sigma = 4.54 \times 10^{-6}$ mho^{-1} surface shows the positive and negative perturbations due to the dawn-dusk potential drop across the polar cap. The maximum positive perturbation is 32 kV and the minimum negative perturbation is -40 kV. This pattern maps downward almost unattenuated to the constant conductivity surface at approximately 50 km, Fig. 22b, and even to the 25 km constant conductivity surface, Fig. 22c. The potential perturbations due to thunderstorms are evident along this surface. The calculated potential, Φ, along the 8, 4, and 2 km constant height surfaces are shown in Figs. 22d, 22e, and 22f, respectively. Although the perturbation of the potential field is still present at high latitudes, it is small compared to the very large perturbations near the thunderstorm regions; therefore, the approximately 20% variation from fair weather regions is not easily visible on these perspective illustrations.

8. VARIATIONS DURING SOLAR FLARES AND SECTOR BOUNDARY CROSSINGS

During solar flares the intensity of the cosmic ray flux bombarding the earth changes near the earth's surface in the two-phase manner that has been discussed by Forbush (1966). During the solar flare there is a sudden increase in the cosmic ray intensity which generally lasts from one-half to one hour. The intensity increase at the ground is generally small ($< 5\%$) during this period, depending upon the flux magnitude and energy spectrum of the particle distribution. This increase near the ground is also latitudinally dependent, being largest in the polar regions and smallest near the equator. Following the sudden increase in conductivity, the Forbush effect sets in and worldwide cosmic ray intensity decreases by 5-10% of normal values; this can last from one to several days.

At higher altitudes, the increases in ionization during solar flares are much greater. Also, while the ground-level cosmic ray intensity decreases by the Forbush effect, the ionization at stratospheric altitudes may increase by one or two orders of magnitude. Most solar flares have an energy spectrum so steep that even though large increases in the ionization rate occur at balloon altitudes ($\sim$ 30 km) they are not detected by sea-level cosmic ray monitors (Winckler, 1960). In sum, the solar-controlled changes in ion production in the 20 to 30 km height range are larger than, more frequent than, and generally in the opposite sense (increases) of those near the earth. The magnetic field imposes a cutoff latitude on the equatorward side of which solar protons cannot reach the lower atmosphere. The cutoff is sharp, within a degree or two of latitude in a typical event, but the cutoff latitude moves equatorward as the event intensifies. In large events the cutoff may move to as low as 50° geomagnetic latitude. With certain flares, the solar proton flux enhancement may begin within an hour or two after a solar flare eruption and it gradually intensifies to a maximum several hours later. There is then a gradual decay to normal. The duration is variable from flare to flare but can be from about an hour to four or five days, and the proton flux maximum intensity can vary widely from one event to another. These events are frequently associated with polar cap absorption (PCA) events because the relativistic solar protons impinging on the ionospheric D-region produce intense ionization that causes radio blackouts at high latitudes. The ion production rates calculated for several solar flares and their variation with altitude are shown in Fig. 23. These events are geographically confined to regions within the polar cap as illustrated in Fig. 24.

During solar magnetic sector boundary crossings there are also changes in certain geomagnetic properties. In general, the solar wind velocity and geomagnetic activity increase to maximum values a few days after a sector boundary crossing, whereas the solar wind density may decrease. The cosmic ray activity near the ground first increases a day before the sector boundary crossing and then decreases for several days following the crossing, with minimum values near three days. The variations near the ground, however, are generally small (< a few percent).

The effect of high-latitude conductivity changes on the global circuit can be examined with the numerical model. It is assumed that the conductivity above 8 km at geomagnetic latitudes greater than ± 60° first increases from the normal factor of 1.4 times to 1.6 times the unperturbed equatorial value shown in Fig. 15b. This increase in conductivity crudely simulates the solar flare increase in ionization rate at high latitudes. To simulate a high-latitude Forbush decrease above 60° geomagnetic latitude the latitudinal conductivity factor in Fig. 15c decreases from 1.4 times to 1.2 times the unperturbed equatorial values above 60° geomagnetic latitude. In both of these cases the increases in conductivity were deliberately confined to high latitudes away from the assumed thunderstorm region so as not to affect the thunderstorm current output. These numerical experiments are designed to investigate the response to conductivity changes alone. In the next section, the effect of conductivity changes over thunderstorms is examined. The results of the calculation are summarized in Table 3.

The major calculated global electrical parameters for the solar flare increase and the Forbush decrease, as well as the base 1900 UT case, are given in Table 3 for comparison. The calculated global electrical resistance decreases from 310 to 298 Ω during the solar flare (cosmic ray intensity increase) and increases to 321 Ω during the Forbush decrease. The calculated ionospheric potential decreases from 410,900 V to 394,900 V during the cosmic ray increase but then increases to 425,000 V during the subsequent Forbush decrease. The total global electric current remains constant at 1325 A during this sequence because the thunderstorm current output remains the same and only its redistribution due to global scale changes in conductivity occurs. The ground electric field at both the equator and the pole is also modulated. At low latitudes the electric field first decreases from 192 V m^{-1} to 186 V m^{-1} and then increases to 198 V m^{-1} At high latitudes the field increases from 238 V m^{-1} to 260 V m^{-1} and then decreases to 217 V m^{-1} giving an effect opposite that at low latitudes. These results may explain why Reiter (1977) and Park (1976) detect different variations during the passage of a sector boundary. The calculations indicate that changes in electrical conductivity due to solar flares and perhaps to magnetic sector boundary crossings are capable of altering the electric circuit on a global scale. There is much uncertainty in the actual global representation of conductivity during these events and we stress that these calculations were made to illustrate a possible solar-terrestrial influence on the electrical structure of the atmosphere. This study is not a critical evaluation of a specific event.

9. SOLAR-TERRESTRIAL MODULATION OF THUNDERSTORM CURRENT OUTPUT

Markson (1975, 1978a) proposed a mechanism to explain the observed solar modulation of currents and fields in the global atmospheric electric circuit. The results presented in the previous sections give model calculations of electric current and electric field adjustment to conductivity variations in the global circuit without considering the possible effects of modifying the generator output. Markson's model of the global electrical circuit is shown in Fig. 25. The load portion of the circuit

deals with the ionospheric return current in the fair weather regions and the global resistance is typically 100-200 Ω. He assumes that there are about 1500 thunderstorms operating over the earth's surface at any given time. The current output of a thunderstorm is typically 1 A, giving a total global current on the order of 1500 A. The tops of thunderclouds are at potentials of 10^8-10^9 V, giving a charging or generator resistance of 10^5-10^6 Ω over the thunderstorm generator considering all thunderstorms are acting in parallel. The high generator resistance makes the thunderstorm act as a current generator in the global electrical circuit. Ordinarily, the resistance between the thunderstorm generator and the earth would be greater than the resistance between the cloud top and ionosphere except for the effect of point discharge ions. Because of the strong electric fields under thunderstorms, pointed objects beneath the storms go into corona discharge. While it has been estimated that the conductivity under thunderstorms may increase by several orders of magnitude due to this effect, Markson makes a conservative estimate of a factor of 20. Thus, the resistance under thunderclouds is of the order of 10^4-10^5 Ω. Because of the effect of corona discharge decreasing the resistance beneath thunderstorms, the controlling resistance in the global electrical circuit is the resistance between the top of the cloud and the ionosphere. This is important for solar-terrestrial effects because an appreciable portion of the total global circuit resistance is accessible to solar-controlled ionizing radiation. Thus, a solar modulation of the earth's fair weather electric field and current can be effected without changing the thunderstorm generator itself. Markson (1978a) points out that it may seem strange that the resistance over most of the earth's surface is much lower than that of the air mass over thunderstorms. But he shows that it is essentially a function of area. The atmosphere can be considered as an array of vertical parallel columnar resistances. In fair weather regions all of the resistances in parallel result in a small total resistance; dividing a columnar resistance by a large cross-sectional area gives a small resistance. Over thunderstorms, the charging current flows through a resistor of relatively small cross-sectional area and the resistance is large. With most of the global circuit resistance in this element, Markson argues that it in effect is a valve regulating the current flow in the entire circuit. The ionospheric potential and fair weather electric field over most of the world would adjust in proportion to the variation in charging current flowing upward from the thunderstorms. Thus, any increase in stratospheric ionization over thunderstorms due to solar flares could cause a global increase in electric field intensity which would account for observations of enhanced electric fields following solar flares.

Model calculations of the type performed in the previous section and of a regional numerical model that is coupled to the global model support Markson's mechanism for causing global-scale readjustments in electric field and current. Without affecting the thunderstorm generator itself, decreasing the columnar resistance over the thunderstorm allows more current to flow to the ionosphere, increasing the ionospheric potential, the global current, and the ground electric field and air-earth current on a global basis. This response differs from the variation calculated where conductivity changes occurred only at high latitudes and not over any thunderstorm region as discussed in the previous section. For those calculations a different air-current density and electric field variation would occur between high and low latitudes.

Markson also suggests that these solar-induced variations of the global circuit may affect cloud microphysics, precipitation processes, and thunderstorms electrification and development; however, the precise mechanisms are unknown. He furthermore suggests that if these processes were influenced, atmospheric dynamics could be affected.

10. DISCUSSION

Both the experimental evidence and the calculations made with a global model of atmospheric electricity indicate that there is solar-terrestrial coupling through atmospheric electricity which operates by altering the global electric current and field distribution. A global redistribution of currents and fields can be caused by large-scale changes in electrical conductivity, by alteration of the columnar resistance between thunderstorm cloud tops and the ionosphere, or by both. If the columnar resistance is altered above thunderstorms, more current will flow in the global circuit, changing the ionospheric potential and basic circuit variables such as current density and electric fields. The observed variations of currents and fields during solar-induced disturbances are generally less than 50% of mean values near the earth's surface.

The model calculations suggest that it is necessary to consider the entire electrical circuit from the magnetopause to the ground when analyzing ground-based and satellite data. One segment of the "classical picture" of atmospheric electricity suggests that there is an equalizing layer at 60 km, where upper atmospheric electrical effects are shielded from lower atmospheric electrical effects; this needs to be modified to account for the observed coupling.

The observational evidence presented in the previous sections suggests solar-terrestrial coupling, but a well-coordinated observational program is necessary to establish the nature and characteristics of the global response. Such a program should include coordinated measurements from satellites, rockets, aircraft, balloons, and ground-based stations. Perhaps such a program could be established as part of the international Middle Atmosphere Program (MAP) that is planned for the 1980's or as part of the 10-year plan for atmospheric electricity (Dolezalek, 1972).

Whether atmospheric electricity represents a link between the sun and weather is not clear. Several mechanisms by which thunderstorm cloud development and electrification might be affected by changes in the properties of the global circuit have been proposed, but geophysical data to support them are lacking. Global satellite measurements of lightning frequency and optical power output may be a key in identifying a global thunderstorm response to solar activity. If satellite measurements of lightning activity can establish a statistically significant increase or decrease in thunderstorm frequency correlated with solar flares, solar magnetic sector boundary crossings, geomagnetic activity, aurorae, or the solar cycle, then atmospheric electricity is an intriguing possibility for the physical mechanism in a sun-weather relationship. There are many uncertainties in the chain of physical processes leading to a change in weather systems but the evidence appears to warrant further consideration.

Finally, it should be emphasized that progress in understanding solar-terrestrial coupling requires a collaborative effort between observation and theoretical modeling. For example, by requiring agreement between theory and observations, it may be possible to derive information from a numerical model, such as the global distribution of electrical conductivity variations during a solar flare, that would be very difficult and expensive to obtain experimentally. Likewise, numerical experiments with a global theoretical model of atmospheric electricity may suggest certain experimental efforts to examine solar-terrestrial coupling mechanisms. The search for solar-terrestrial coupling mechanisms through atmospheric electricity should give us a better understanding of the earth's natural electrical environment (Fig. 26).

REFERENCES

Anderson, R. V., Universal diurnal variation in air-earth current density, *J. Geophys. Res.*, **74**, 1697, 1969.

Andrée, S. A., Observations faites au Cap Thordsen, 2. Electricité Atmospherique, Stockholm, 1887, *Meteor. Z.*, 7, 29, 1890.

Bauer, L. A., Cosmic effects in terrestrial magnetism and atmospheric electricity, *Phys. Rev.*, **23**, 303, 1924.

Burch, J. L., The magnetosphere, in *The Upper Atmosphere and Magnetosphere*, Studies in Geophysics, National Academy of Sciences, Washington, D.C., 1977.

Chalmers, J. A., *Atmospheric Electricity*, 2nd ed., Pergamon, London, 1967.

Crichlow, W. Q., R. C. Davis, R. T. Davis and M. W. Clark, Hourly probability of world-wide thunderstorm occurrance, Office of telecommunication/ITS research report 12, Boulder, Colorado, April, 1971.

Cobb, W. E., Balloon measurements of the air-earth current density at the south pole before and after a solar flare, *Conference on Cloud Physics and Atmospheric Electricity*, preprints, American Meteorological Soc., 31 July - 4 August, Issaquah, Washington, 1978.

Cobb, W. E., Evidence of a solar influence on the atmospheric electric elements at Mauna Lao Observatory, *Mon. Weather Rev.*, **95**, 905, 1967.

Cobb, W. E., Atmospheric electric measurements at the south pole, in *Electrical Processes in Atmospheres*, H. Dolezalek and R. Reiter, eds., Steinkopff Verlag, Darmstadt, 161, 1977.

Dolezalek, H., Discussion of the fundamental problem of atmospheric electricity, *Pure Appl. Geophys.*, **100**, 8, 1972.

Edgar, B. C., Global lightning distribution at dawn and dusk for August-December 1977 as observed by the DMSP lightning detector, *J. Geophys. Res.*, in press, 1979.

Freier, G. D., Auroral effects on the earth's electric field, *J. Geophys. Res.*, **66**, 2695,1961.

Forbush, S. E., Time variation of cosmic rays, in *Handbuch der Physik, Geophysik III*, J. Bartels, ed., Springer-Verlag, New York, 1966.

Hays, P. B., and R. G. Roble, A quasi-static model of global atmospheric electricity I. The lower atmosphere, *J. Geophys. Res.*, in press, 1979.

Heppner, J. P., Empirical models of high-latitude electric fields, *J. Geophys. Res.*, **82**, 1115, 1977.

Herman, J. R., and R. A. Goldberg, Initiation of non-tropical thunderstorms by solar activity, *J. Atmos. Terr. Phys.*, **40**, 121, 1978.

Hill, T. W., and R. A. Wolf, Solar-wind interaction, in *The Upper Atmosphere and Magnetosphere,* Studies in Geophysics, National Academy of Sciences, Washington, D.C., 1977.

Holzer, R. E. and D. S. Saxon, Distribution of electrical conduction currents in the vicinity of thunderstorms, *J. Geophys. Res.*, **57**, 207, 1952.

Holzworth, R. H. and F. S. Mozer, Direct evidence of solar flare modification of stratospheric electric fields, *J. Geophys. Res.*, **84**, 363, 1979.

Israël, H., *Atmospheric Electricity,* Vol. 1 and Vol. 2, translated from German, Israël Program for Scientific Translations, Jerusalem, 1978.

Kasemir, H. W., Atmospheric electric measurements in the Arctic and Antarctic, *Pure Appl. Geophys.*, **100**, 70, 1972.

Lobodin, T. V., and N. A. Paramonov, Variation of atmospheric electric field during aurorae, *Pure Appl. Geophys.*, **100**, 167, 1972.

Märcz, F., Links between atmospheric electricity and ionospheric absorption due to extraterrestrial influences, *J. Geophys. Res.*, **81**, 4566, 1976.

Markson, R., Considerations regarding solar and lunar modulation of geophysical parameters, atmospheric electricity and thunderstorms, *Pure Appl. Geophys.*, **84**, 188, 1971.

Markson, R., Solar modulation of atmospheric electrification through variation of the conductivity over thunderstorms, in *Possible Relationships between Solar Activity and Meteorological Phenomena,* symposium held at Goddard Space Flight Center, Greenbelt, Maryland, 7-8 Nov., 1973, NASA SP-366, 1975.

Markson, R., Ionospheric potential variations obtained from aircraft measurements of potential gradient, *J. Geophys. Res.*, **81**, 1980, 1976.

Markson, R., Solar modulation of atmospheric electrification and possible implications for the sun-weather relationship, *Nature,* **273**, 103, 1978a.

Markson, R., Atmospheric electricity and the sun-weather problem, *Proceedings of the Symposium/ Workshop-Solar-Terrestrial Influences on Weather and Climate,* Ohio State University, 24-28 July, 1978b.

Mühleisen, R., Neue Ergebuisse und Probleme in der Luftelektrezutät, *Z. Geophys.*, **37**, 759, 1971.

Mühleisen, R., The global circuit and its parameters, in *Electrical Processes in Atmospheres*, H. Dolezalek and R. Reiter, eds., Steinkopff Verlag, Darmstadt, 467, 1977.

Neher, H. V., Cosmis rays at high latitudes and altitudes covering four solar maxima, *J. Geophys. Res.*, **76**, 1637, 1971.

Olson, D. E., The evidence for auroral effects on atmospheric electricity, *Pure Appl. Geophys.*, **84**, 118, 1971.

Olson, D. E., Symp. Influence of solar activity and geomagnetic changes on weather and climate, IAGA/IAMAP Joint Assy., Seattle, 1977.

Park, C. G., Solar magnetic sector effects on the vertical atmospheric electric field at Vostok, Antarctica, *Geophys. Res. Lettrs.*, 3, 475, 1976a.

Park, C. G., Downward mapping of high-latitude electric fields to the ground, *J. Geophys. Res.*, **81**, 168, 1976b.

Reid, G. C., Polar-Cap Absorption – Observations and Theory, *Fundamentals of Cosmic Phys.*, 1, 167, 1974.

Reiter, R., Solar flares and their impact on potential gradient and air-earth current characteristics at high mountain stations, *Pure Appl. Geophys.*, 72, 259, 1969.

Reiter, R., The electric potential of the ionosphere as controlled by the solar magnetic sector structure. Result of a study over the period of a solar cycle, *J. Atmos. Terr. Phys.*, **39**, 95, 1977.

Richmond, A. D., Electric field in the ionosphere and plasmasphere on quiet days, *J. Geophys. Res.*, **81**, 1447, 1976.

Roble, R. G., The thermosphere, in *The Upper Atmosphere and Magnetosphere*, Studies in Geophysics, National Academy of Sciences, Washington, D.C., 1977.

Roble, R. G., and P. B. Hays. A quasi-static model of global atmospheric electricity II. Electrical coupling between the upper and lower atmosphere, *J. Geophys. Res.*, submitted 1979.

Sartor, D., Induction charging thunderstorm mechanism, in *Problems of Atmospheric and Space Electricity*, S. C. Coronite, ed., Elsevier Pub. Co., Amsterdam, 307, 1965.

Shaw, G. E., and R. D. Hunsucker, A study of possible correlation between fair-weather electric field and auroral activity, *Electrical Processes in Atmospheres*, H. Dolezalek and R. Reiter, eds., Steinkopff Verlag, Darmstadt, 576, 1977.

Tanaka, Y., T. Ogawa and M. Kodama, Stratospheric electric fields and currents measured at Syowa Station Antarctica-1, The vertical component, *J. Atmos. Terr. Phys.*, **39**, 523, 1977.

Volland, H., Mapping of the electric field of the Sq current into the lower atmosphere, *J. Geophys. Res.*, 77, 1961, 1972.

Volland, H., Global quasi-static electric fields in the earth's environment, in *Electrical Processes in Atmospheres*, H. Dolezalek and R. Reiter, eds., Steinkopff Verlag, Darmstadt, **507**, 1977.

Whipple, F. J. H., and F. J. Scarse, Point discharge in the electric field of the earth, *Geophysical Memoirs VII*, No. **68**, 3-20, 1936.

Wijkander, A., Beobachtungen über Luftelektrezutät in Spitzbergen 1872-1873, *Arch. Sci.*, 1874. (Abstract in *Z. Meteorol.* **11**, 255-256, 1876.

Winckler, J. R., Balloon study of high-altitude radiations during the International Geophysical Year, *J. Geophys. Res.*, **65**, 1331, 1960.

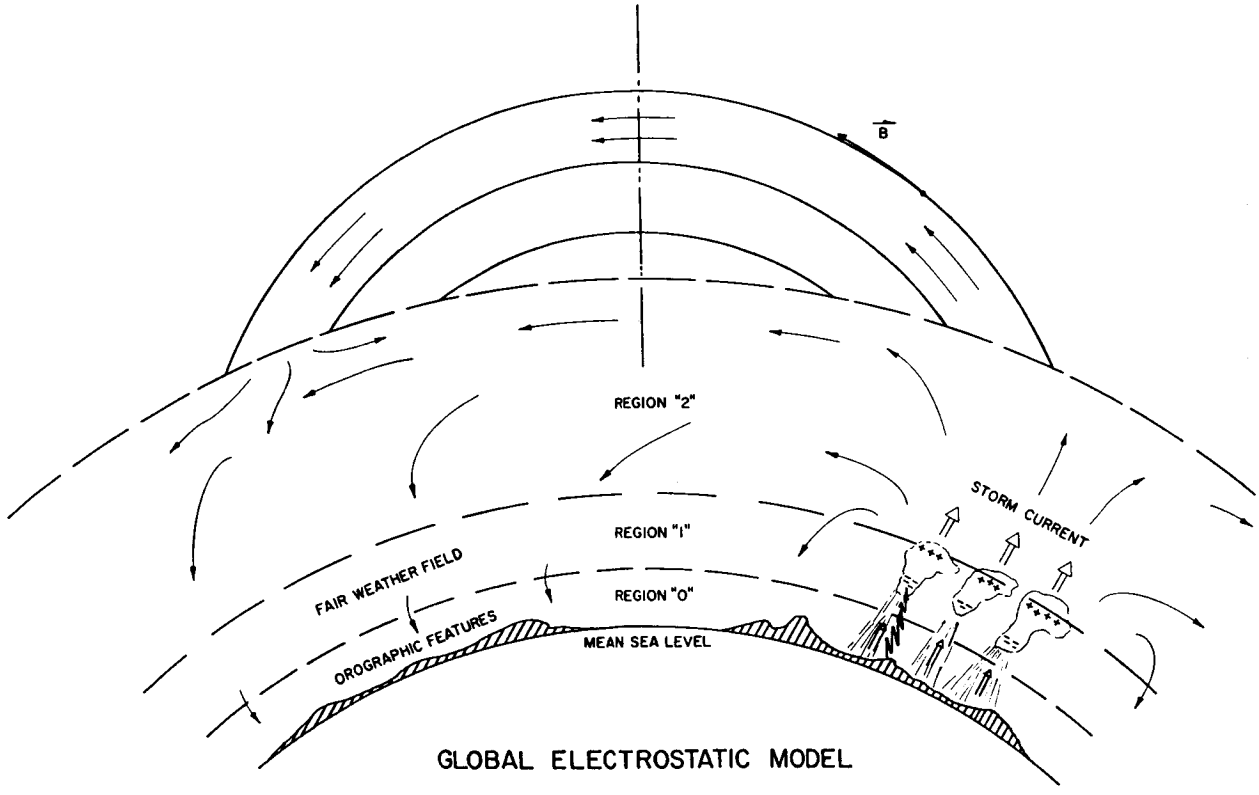

Figure 1. Schematic diagram of global electrostatic model of atmospheric electricity. The vector B illustrates the Earth's geomagnetic field line.

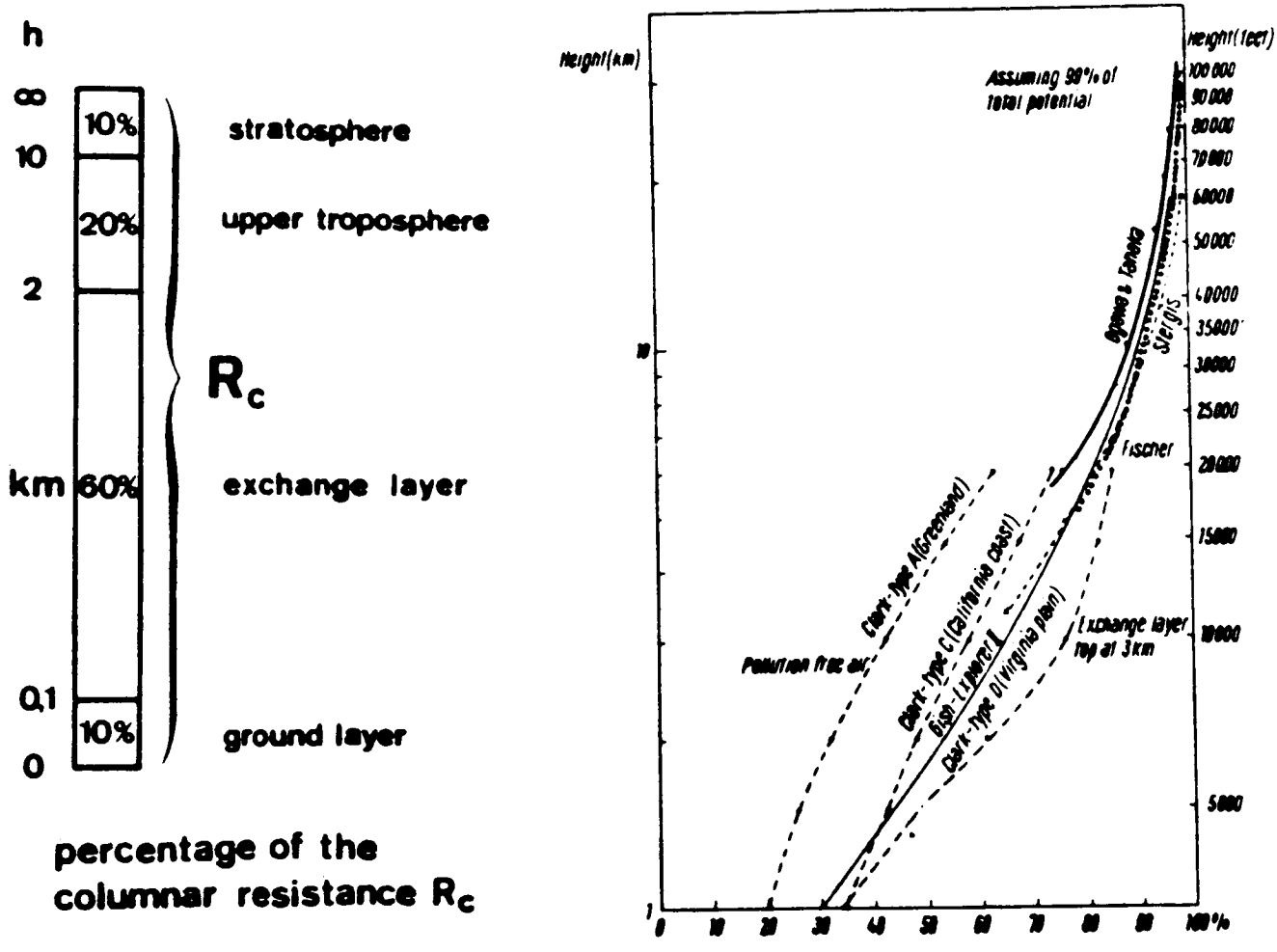

Figure 2. (a) Percentage of the total columnar resistance, R_c, in various altitude intervals (Mühleisen, 1977). (b) Percent of variation of ionospheric potential with altitude (Markson, 1976).

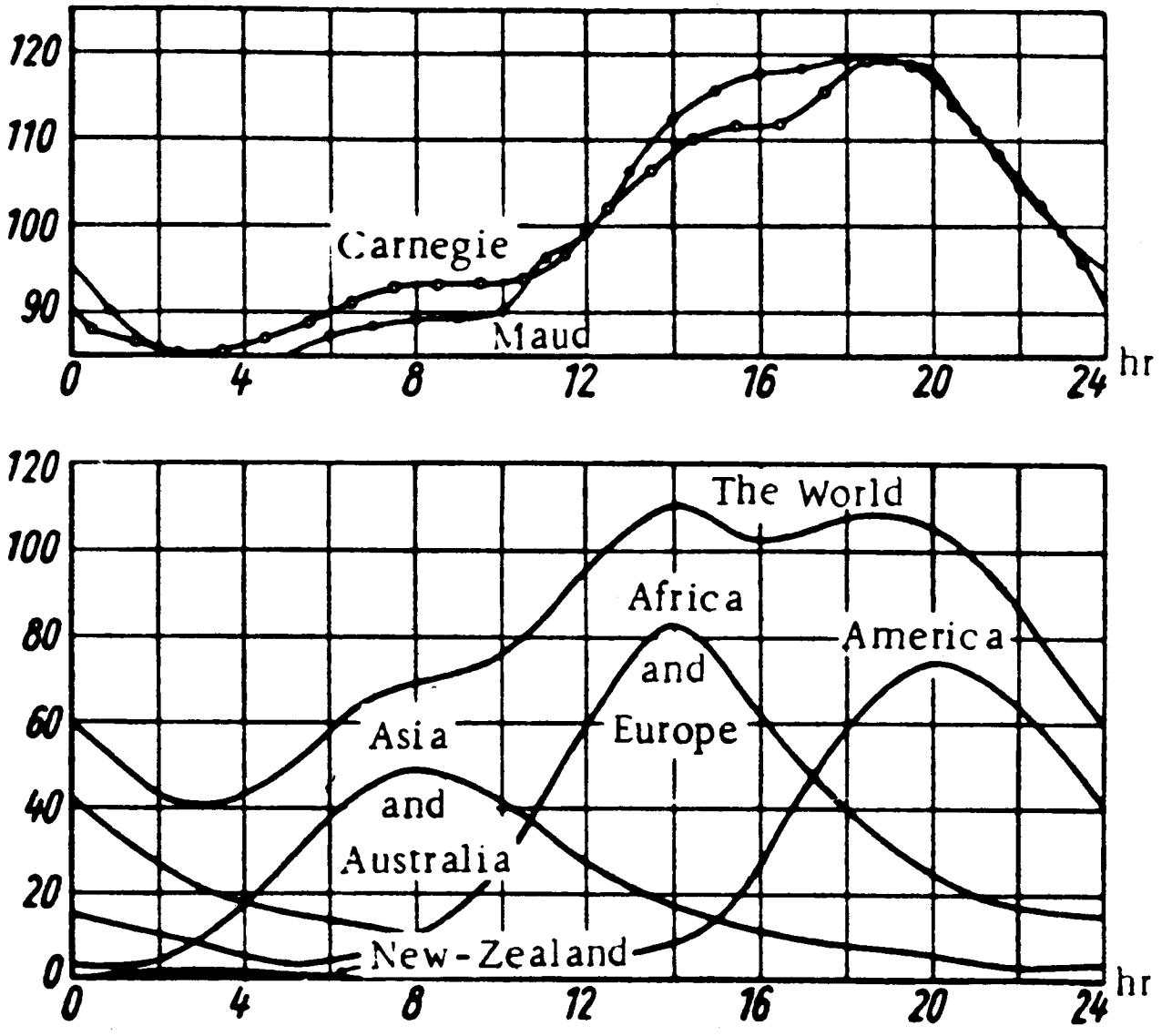

Figure 3. Diurnal UT variation of normalized electric field intensity over oceans, percent variation (upper figure) and diurnal UT variation of land thunder area ($X10^4$ km^2) (lower figure). (Chalmers, 1967.)

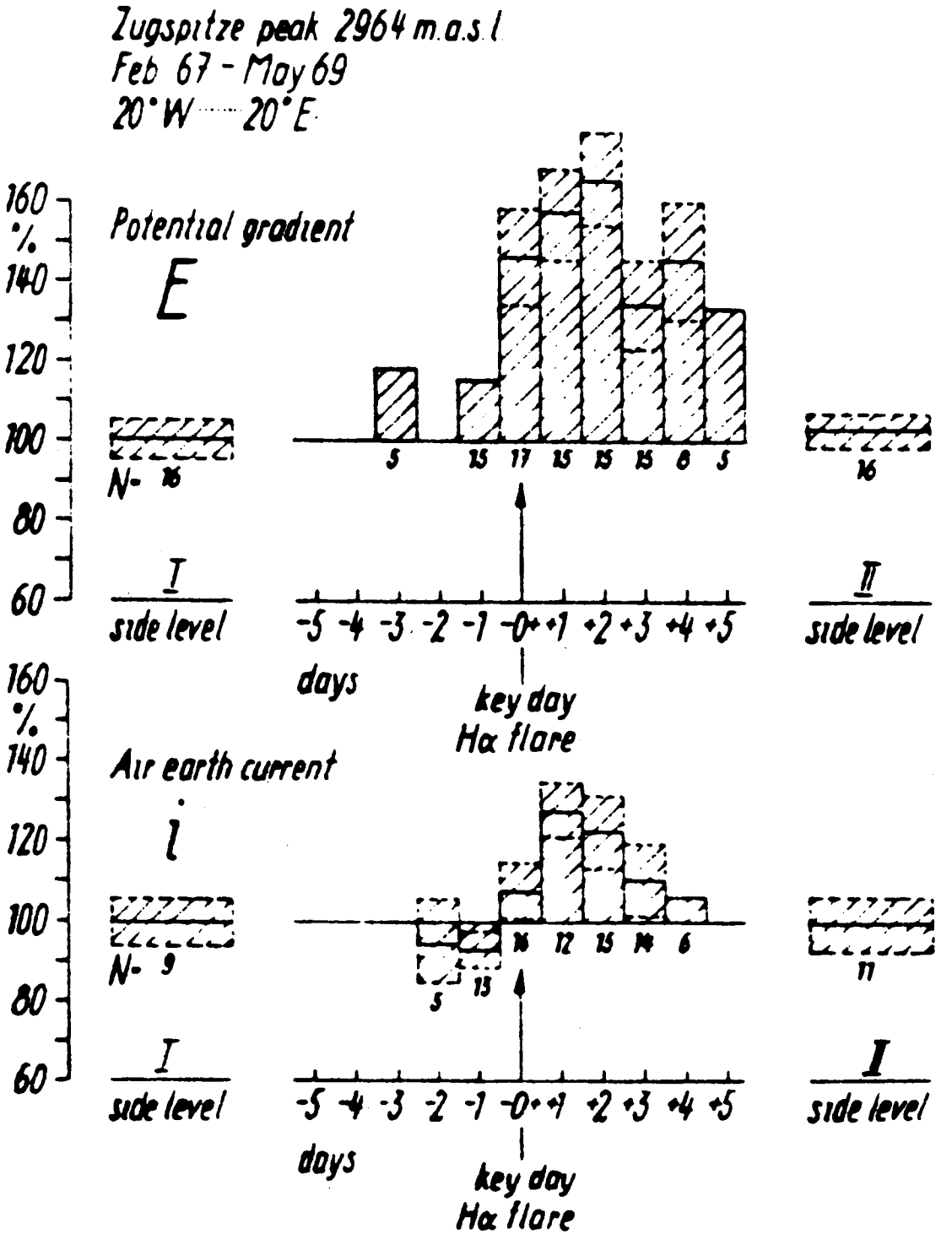

Figure 4. Grouping of hourly means of (a) electric field (%) and (b) air-Earth current (%) around flare days during three years of generally low solar activity levels (1964-1967) as measured at the Zugspitze stations (Reiter, 1969).

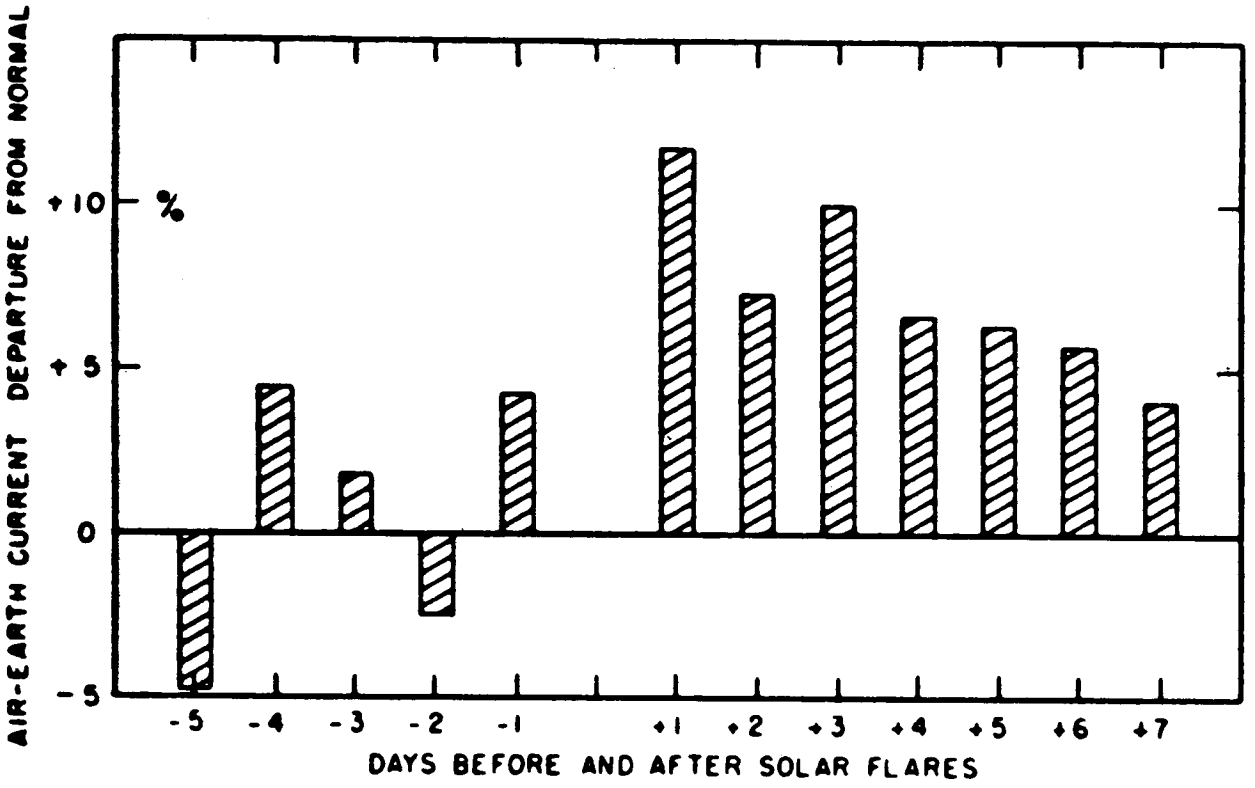

Figure 5. Average daily departure from normal of the fair weather air-Earth current before and after solar flares (Cobb, 1967).

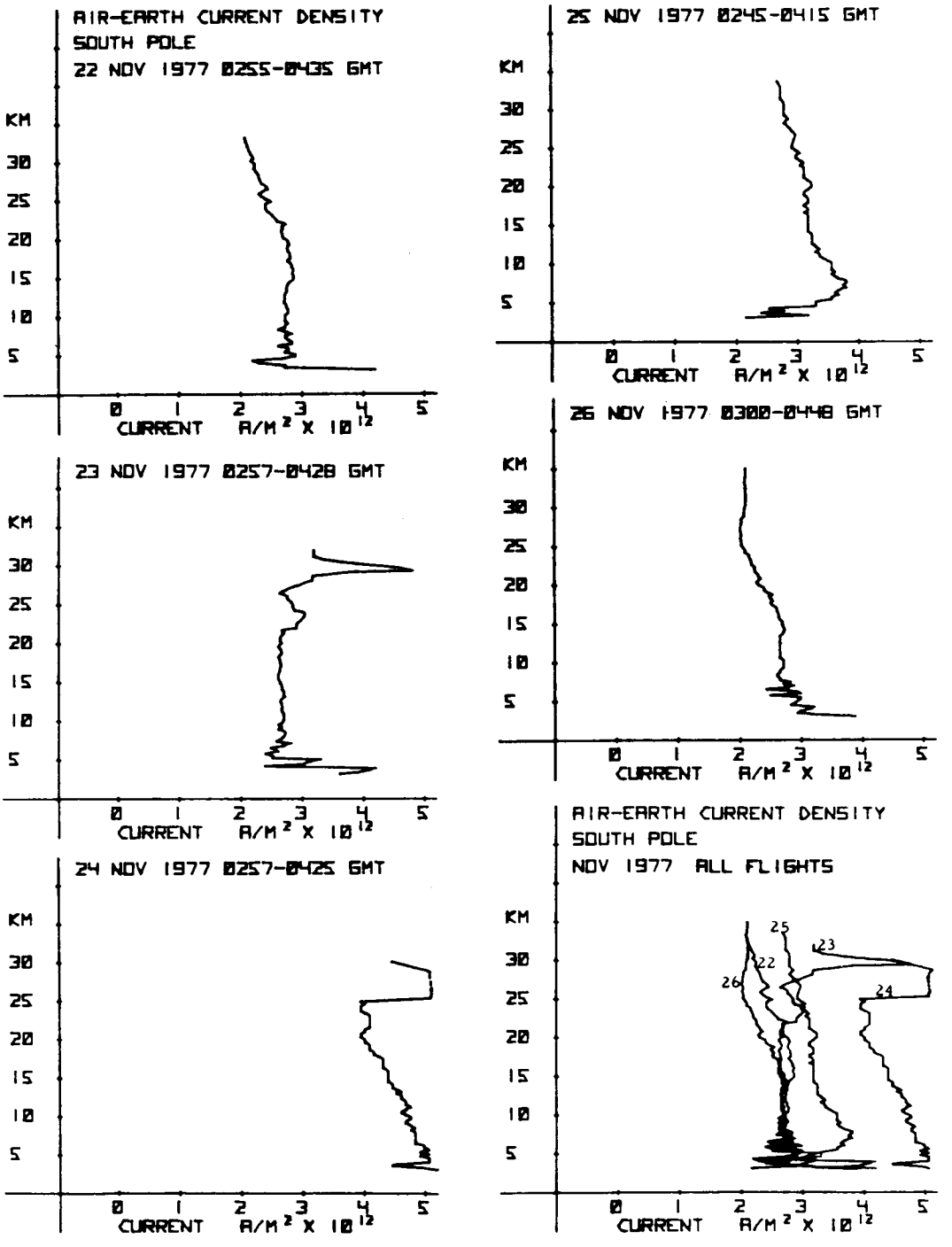

Figure 6. Air-Earth current densities measured during balloon flights from the South Pole, 22-26 November, 1977. A solar flare occurred at 0945 UT, 22 November (Cobb, 1978).

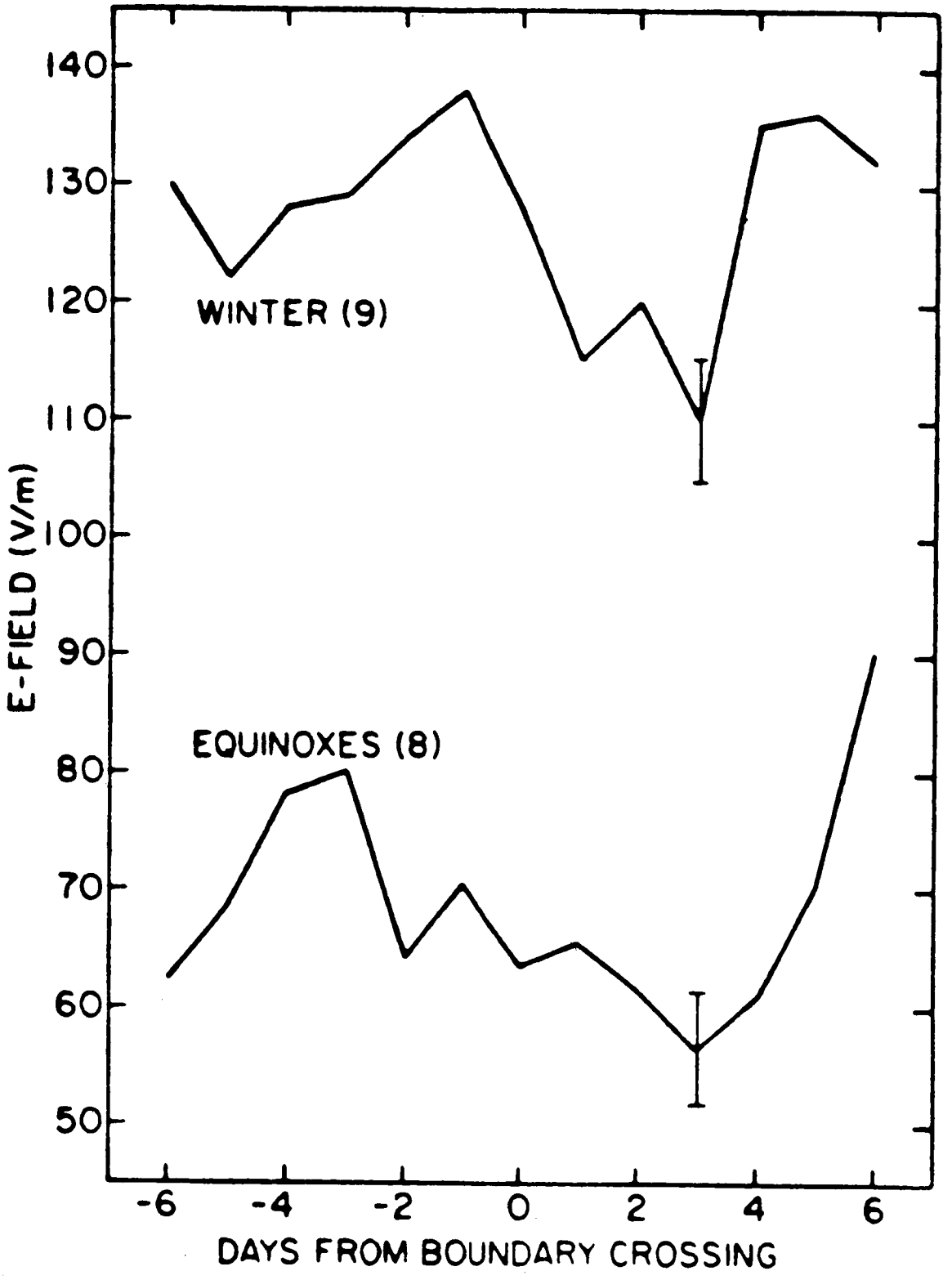

Figure 7. Average behavior of the Vostok electric field about the times of solar magnetic sector boundary crossings for winter and equinox data. The numbers in parentheses indicate the number of cases (Park, 1976a).

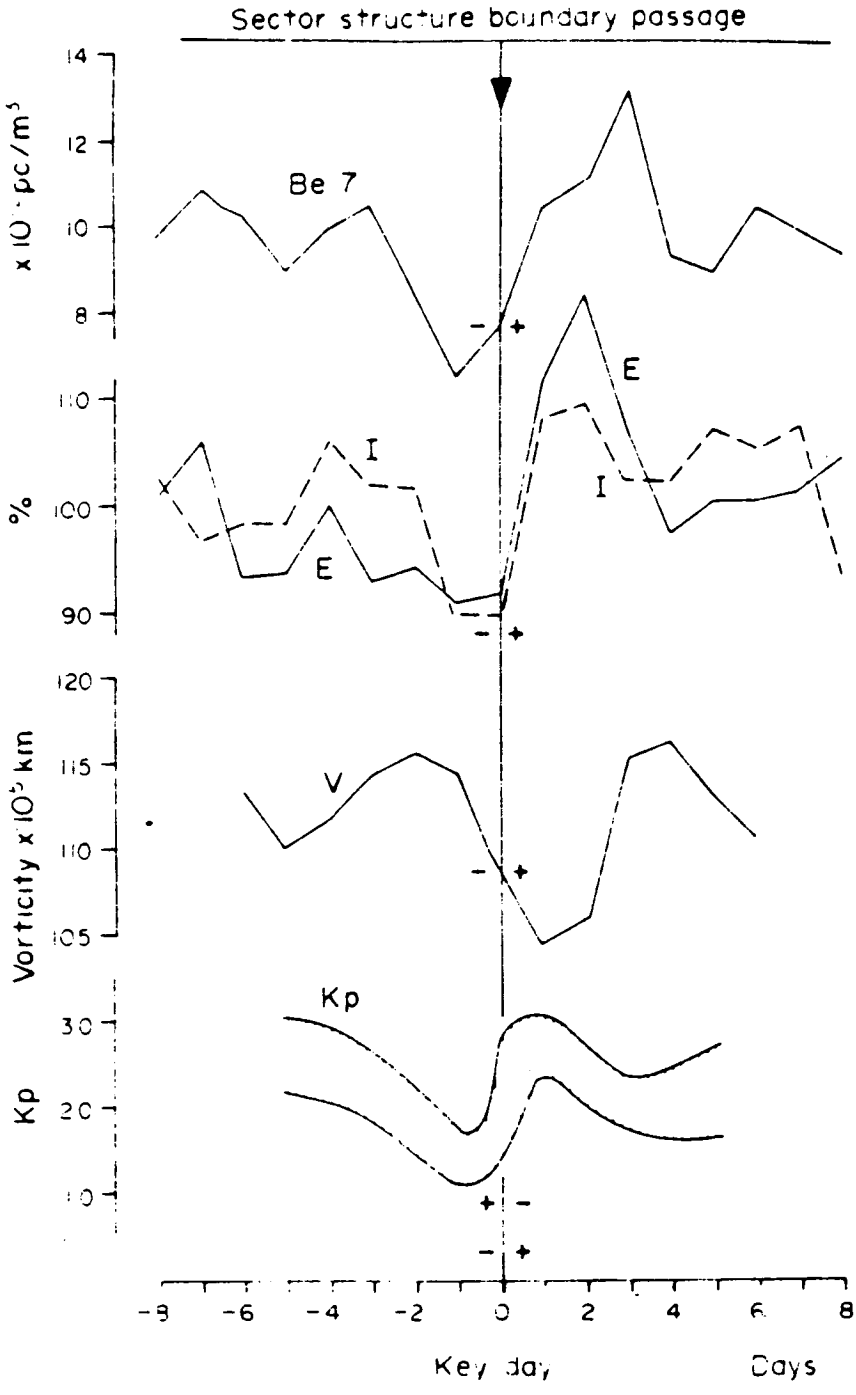

Figure 8. Comparison of several superposed epoch analyses against each other: (a) concentration of beryllium 7 in air at 3 km above sea level, key day -/+ period 1973-1974; (b) electric field, E, and air-Earth current density, I, at 3 km above sea level, key day -/+, period 1967-1971 with maximum solar activity; (c) northern hemispheric vorticity area index, V, key day -/+, period 1964-1970, (d) planetary magnetic field index, K_p, sector boundary passage, irrespective of polarity, period 1967-1969 (Reiter, 1977).

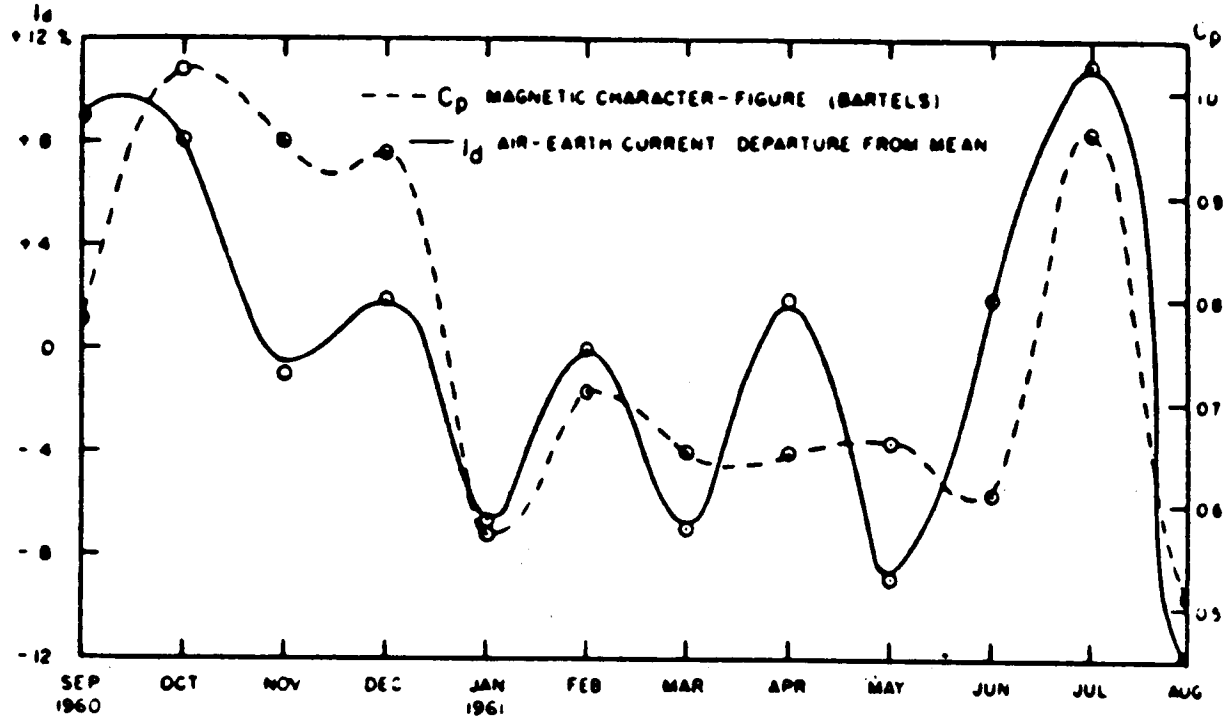

Figure 9. Monthly variation of air-Earth current departure from mean at Mauna Loa, Hawaii, and the Bartels magnetic character-figure from September 1960 to September 1961 (Cobb, 1967).

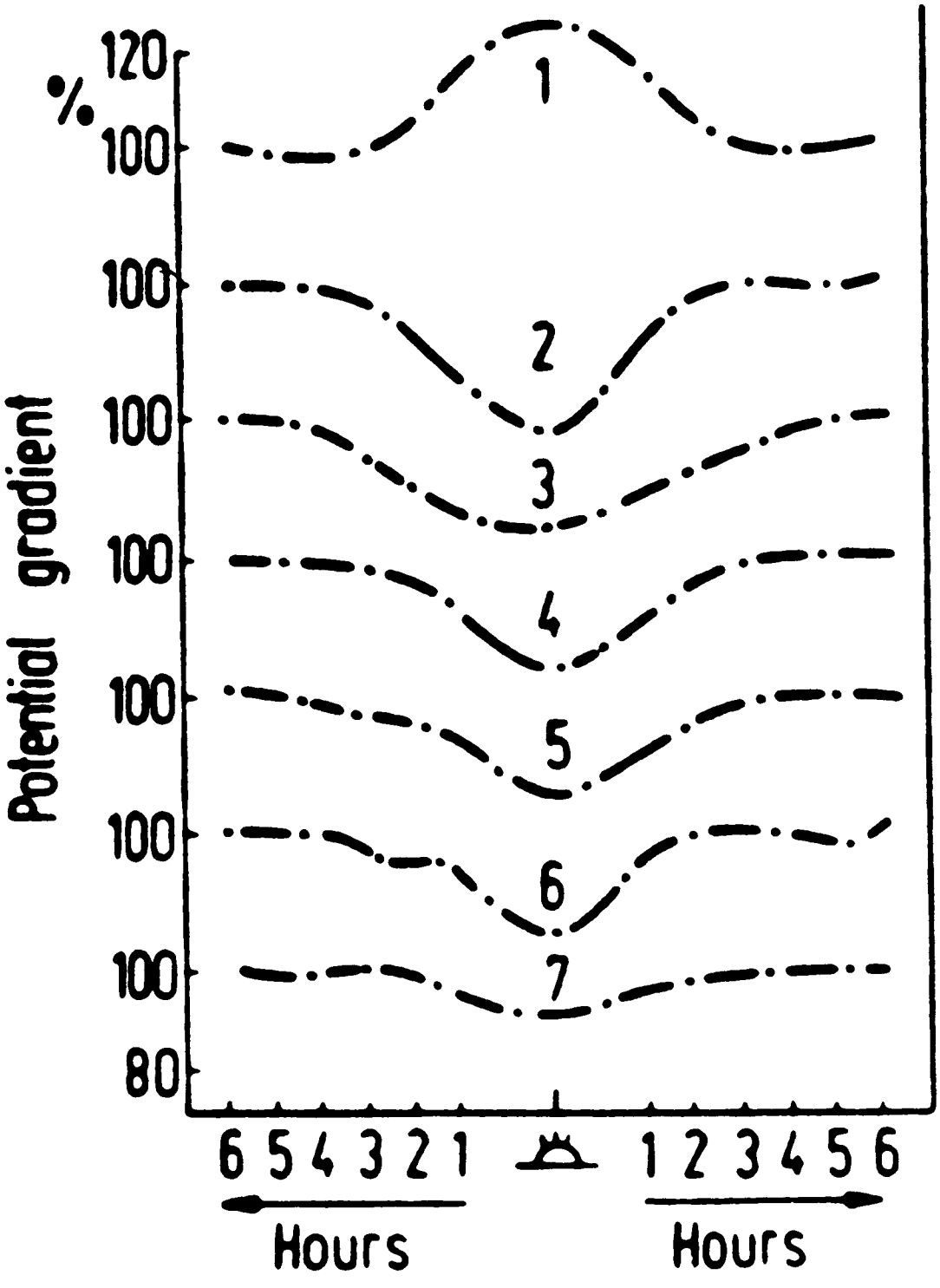

Figure 10. Potential gradient variation during aurorae: 1-Mirny Observatory (66°33′S, 93°00′E), 2-Kheis Island (80°37′N, 58°03′E), 3-Cheluskin Cape (77°43′N, 104°17′E), 4-Yakutsk (62°05′N, 125°45′E) 5-Leningrad (59°48′N, 30°18′E), 6-Vysokaya Dubrava (56°44′N, 61°04′E) and 7-Tbilisi (41°41′N, 44°57′E) (Lobodin and Paramonov, 1972).

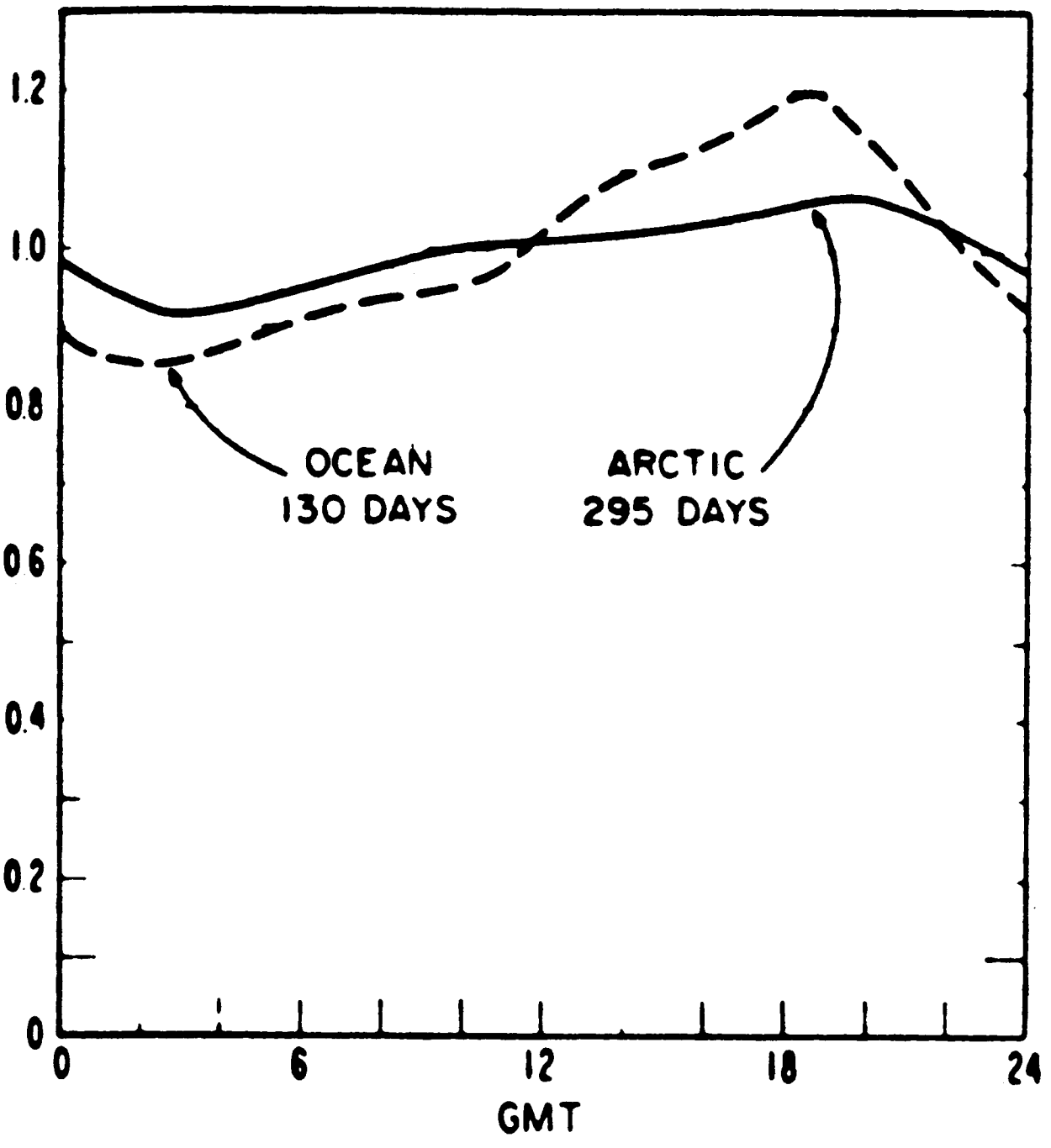

Figure 11. Normalized diurnal variation of the air-Earth current density and electric field in the Arctic and Antarctic, 1958 and 1964 (solid line). Normalized diurnal variation of the atmospheric electric field on the oceans (dashed line) (Kasemir, 1972).

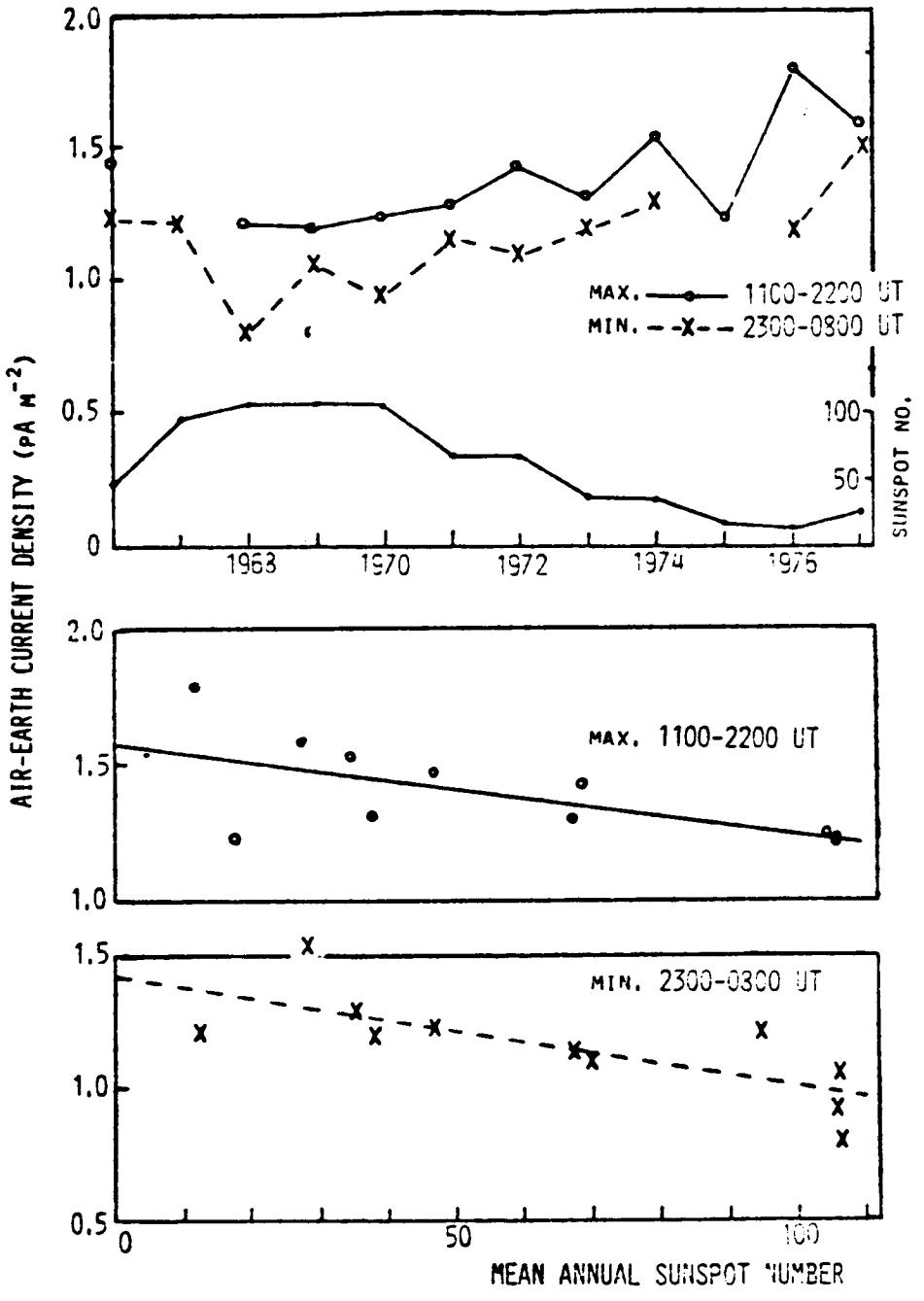

Figure 12. The variation of air-Earth conduction current density through the period of a solar cycle, as determined from balloon measurements of D. E. Olson (1977). The data are divided into two sets, one corresponding to the hours of maximum electric field and the other to the hours of minimum electric field of the "unitary" diurnal variation. Scatter diagrams showing the inverse correlation between current density and sunspot number have been made for each data set (Markson, 1978b).

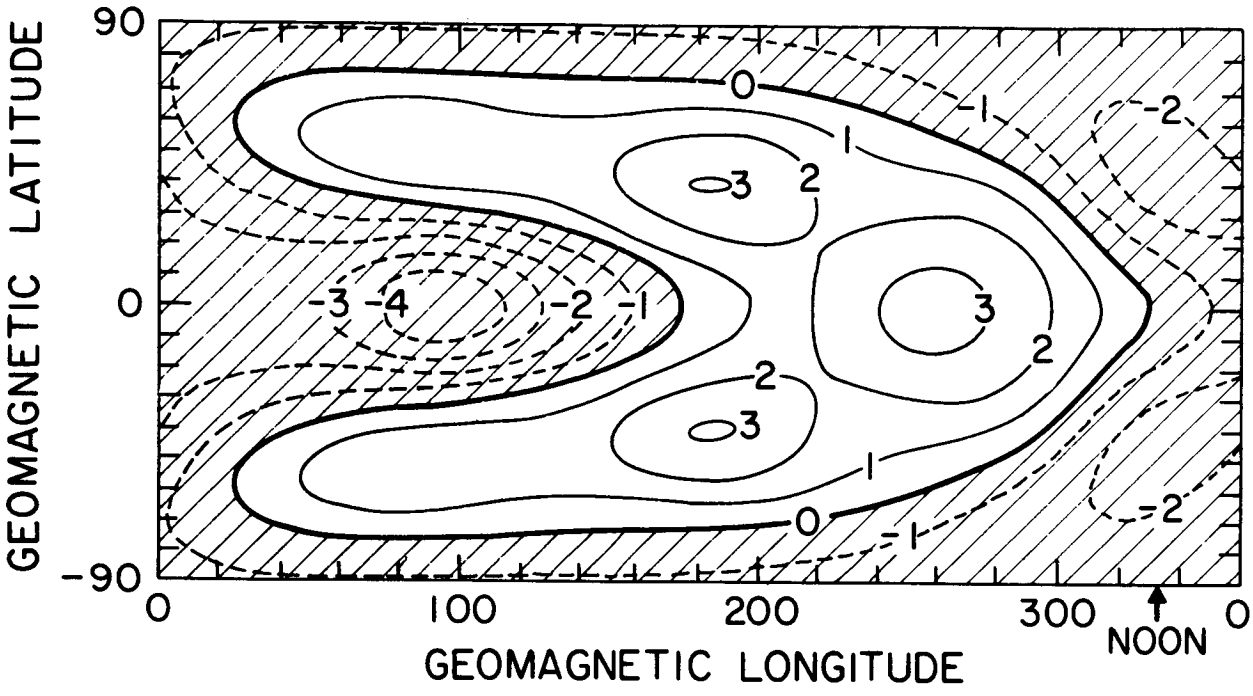

Figure 13. Quiet-day F region electrostatic potential pattern (kV) in apex latitude-local time coordinates. Values above 65° in latitude have no significance (Richmond, 1976).

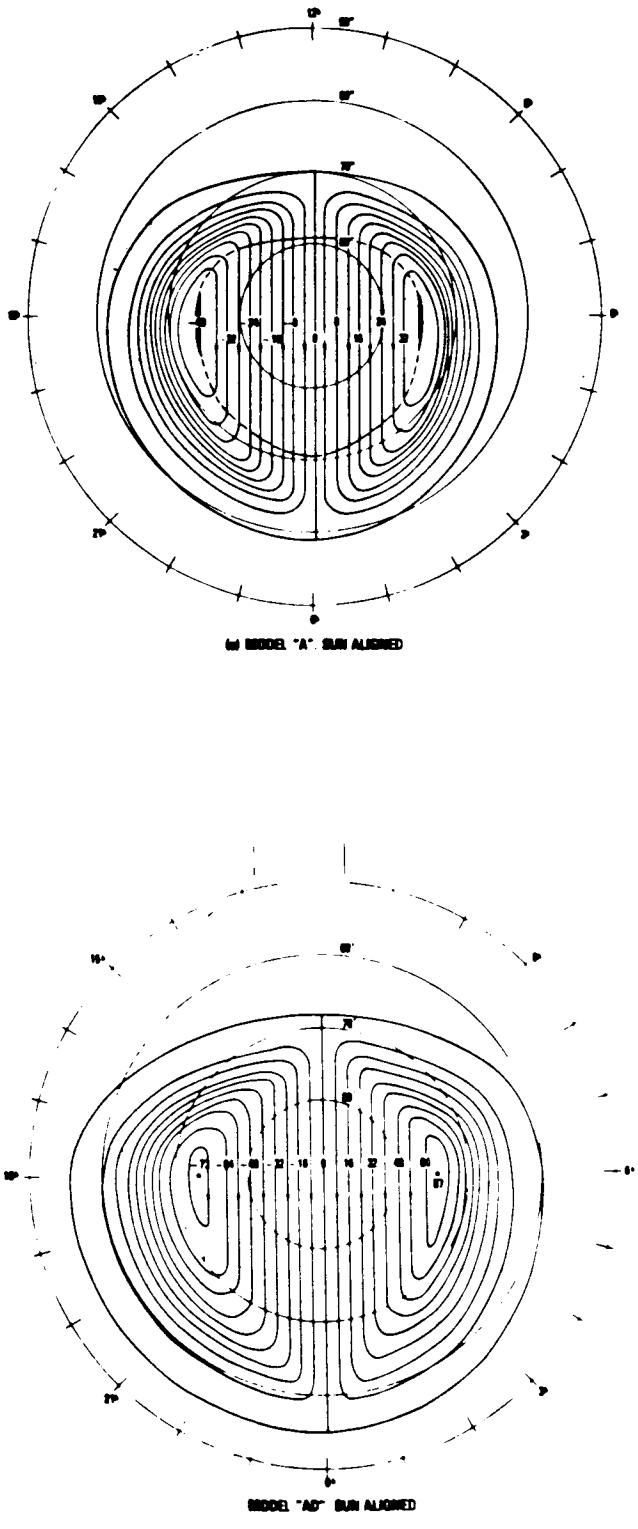

Figure 14. A sun-aligned empirical model of the potential distribution across the magnetic polar cap. Upper figure, is the Geomagnetic quiet model with a 72 kV dawn-to-dusk potential drop, and the lower figure is geomagnetic disturbed model with a 140 kV dawn-to-dusk potential drop (Heppner, 1977).

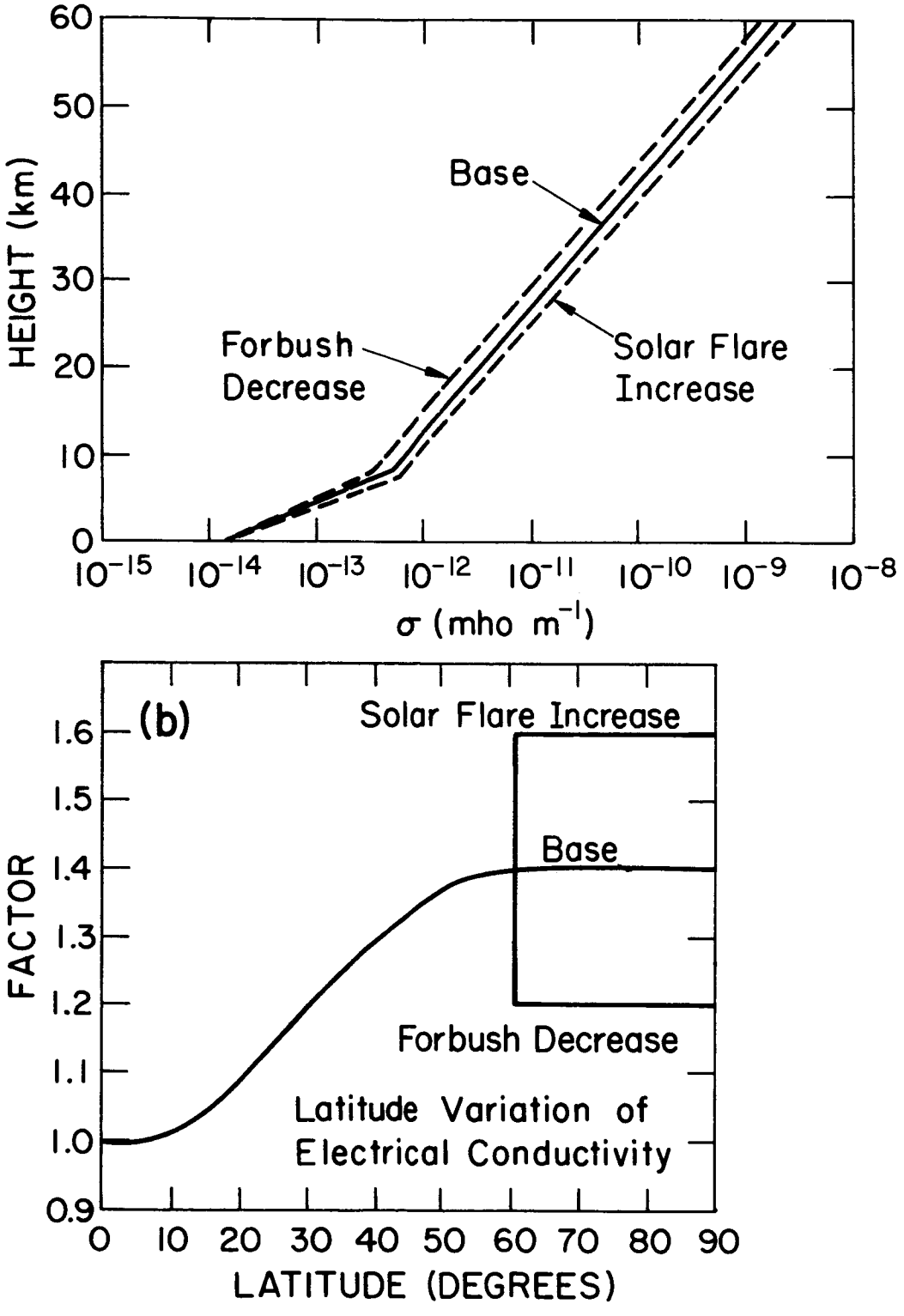

Figure 15. Model electrical conductivity variations with altitude (upper figures) and latitude (lower figure). The assumed variation of electrical conductivity with altitude and latitude for a solar flare ionization increase and subsequent Forbush decrease are also shown.

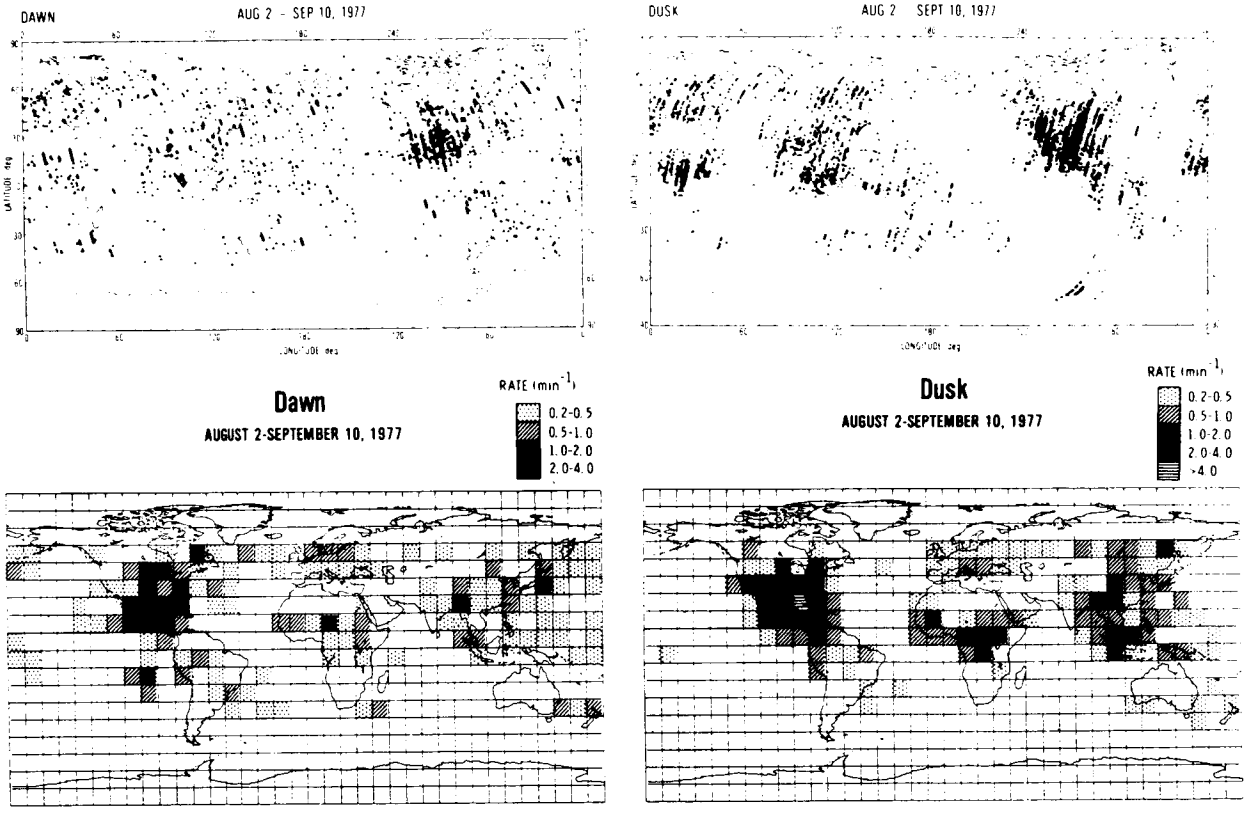

Figure 16. Scatter diagram of satellite lightning observations for the period 2 August-10 September, 1977 at dawn, and dusk. The lower figures give the Occurrence rate for dawn and dusk. (Edgar, 1978).

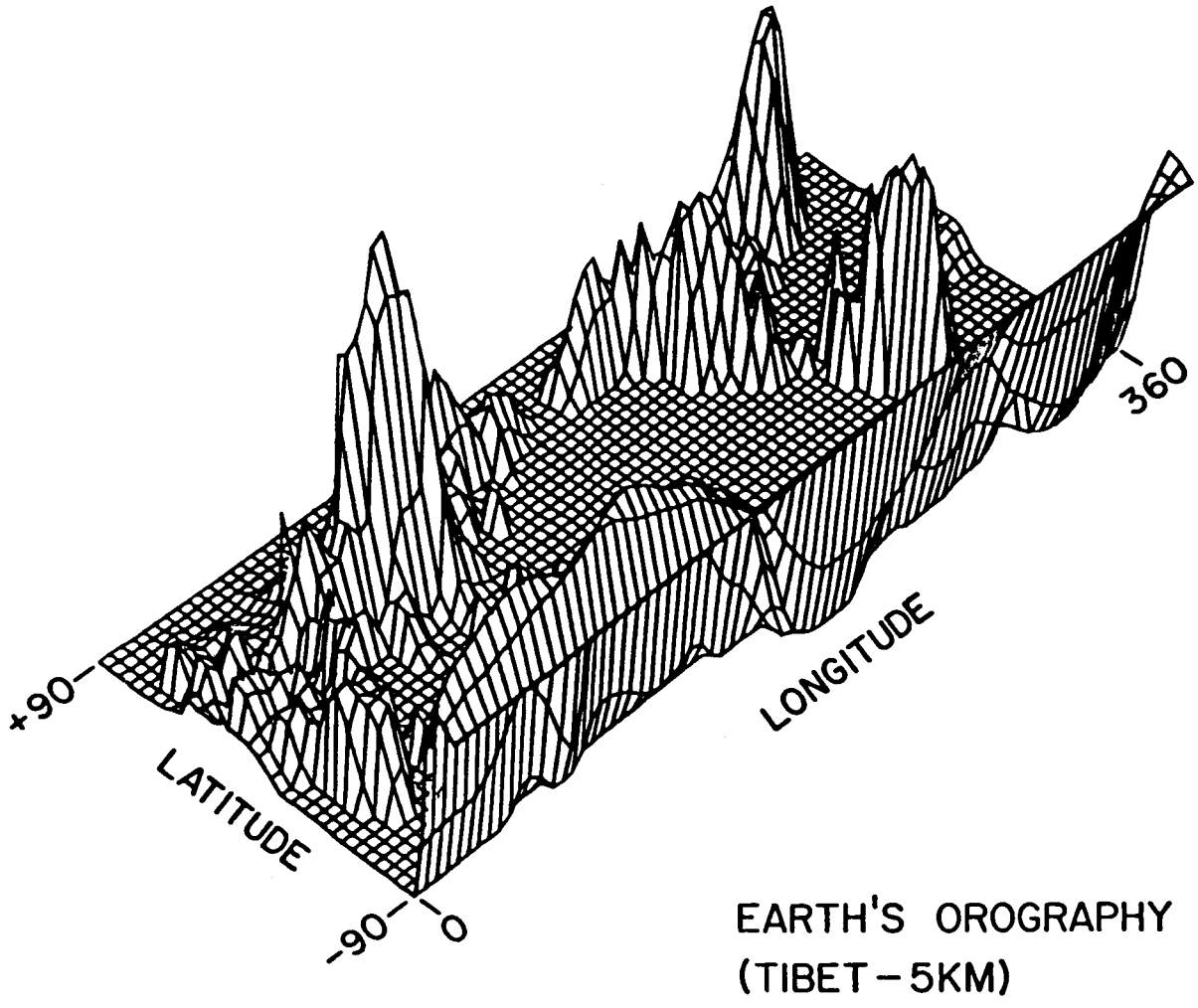

Figure 17. Perspective illustration of the Earth's orographic surface used in the model. The model gives height averages over a 5° grid in latitude and longitude. The highest point is 5 km over the Tibetan plateau.

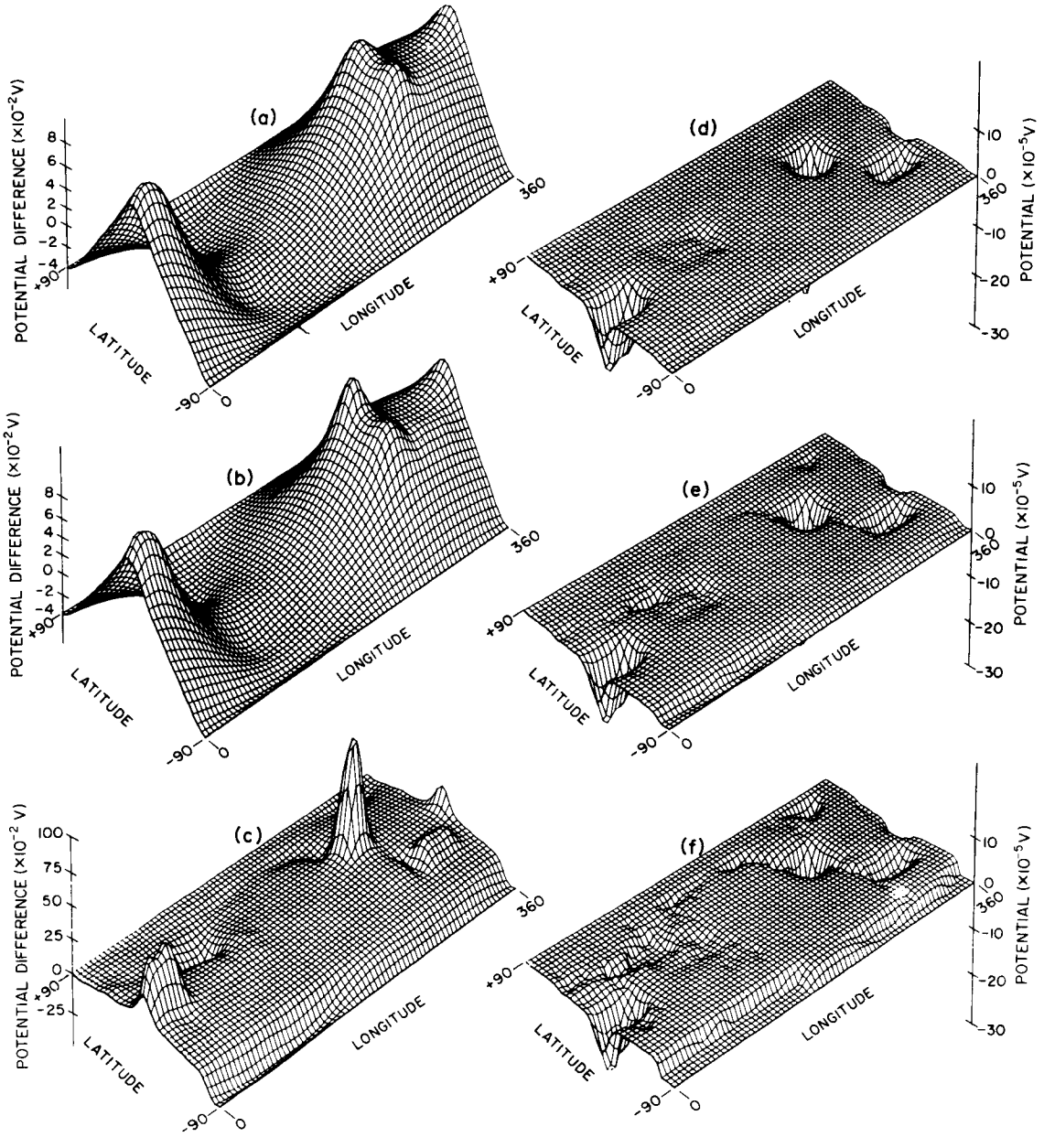

Figure 18. Perspective illustrations of the calculated potential along various constant conductivity surfaces. (a), (b) and (c) illustrate the calculated potential differences (Φ - ϕ_∞) volts along, respectively, the $\sigma = 4.54 \times 10^{-6}$ mho m^{-1} (approximately 105 km at the Equator), $\sigma = 4.74 \times 10^{-10}$ mho m^{-1} (approximately 50 km at the Equator), and $\sigma = 7.3 \times 10^{-12}$ mho m^{-1} (approximately 25 km at the Equator); Φ_∞ is the ionospheric potential. (d) is the potential $\Phi(\sigma_1)$ volts along the $\sigma_1 = 4.3 \times 10^{-13}$ mho m^{-1} (approximately 8 km at the Equator). (e) is the potential Φ(4 km) at a constant 4 km height, and (f) is the potential Φ(2 km) at a constant height of 2 km (Hays and Roble, 1979).

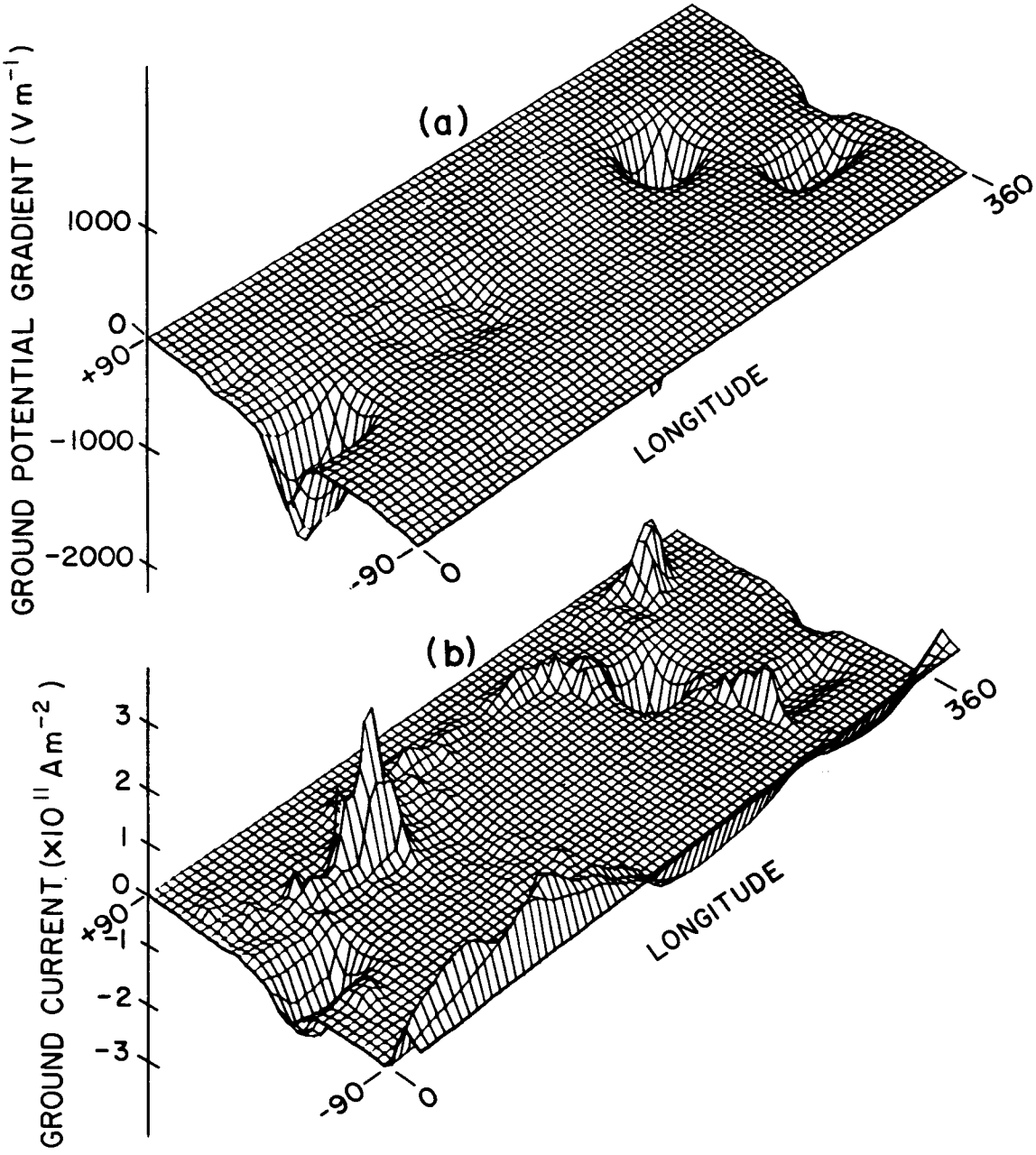

Figure 19. Perspective illustrations of calculated (a) ground potential gradient (V m^{-1}) and (b) ground current (A m^{-2}) along the Earth's orographic surface (Hays and Roble, 1979).

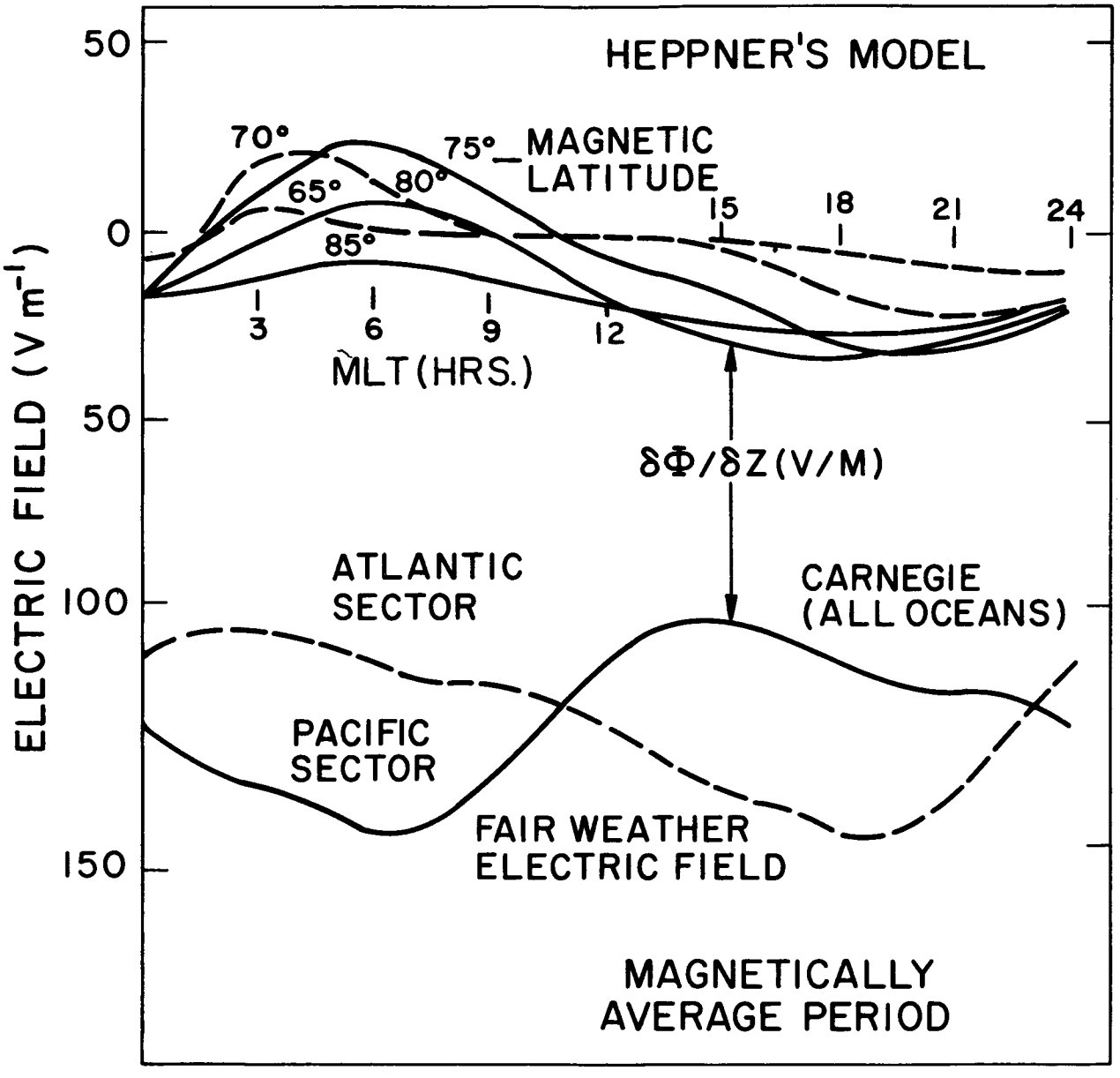

Figure 20. Calculated diurnal variation of ground electric field (V m^{-1}) as a function of magnetic local time. The upper curves are diurnal variations in the effect of the ionospheric potential perturbation, upon the ground electric field at various magnetic latitudes, calculated using Heppner's (1977) model for a magnetically average period. The lower curves are the diurnal (UT) variation of the ground electric field measured during the Carniege expedition in magnetic local time for stations in the Atlantic and Pacific sectors. The total potential gradient variation is determined by the difference between the upper and lower curves as indicated by the vector $\delta\Phi/\delta z$.

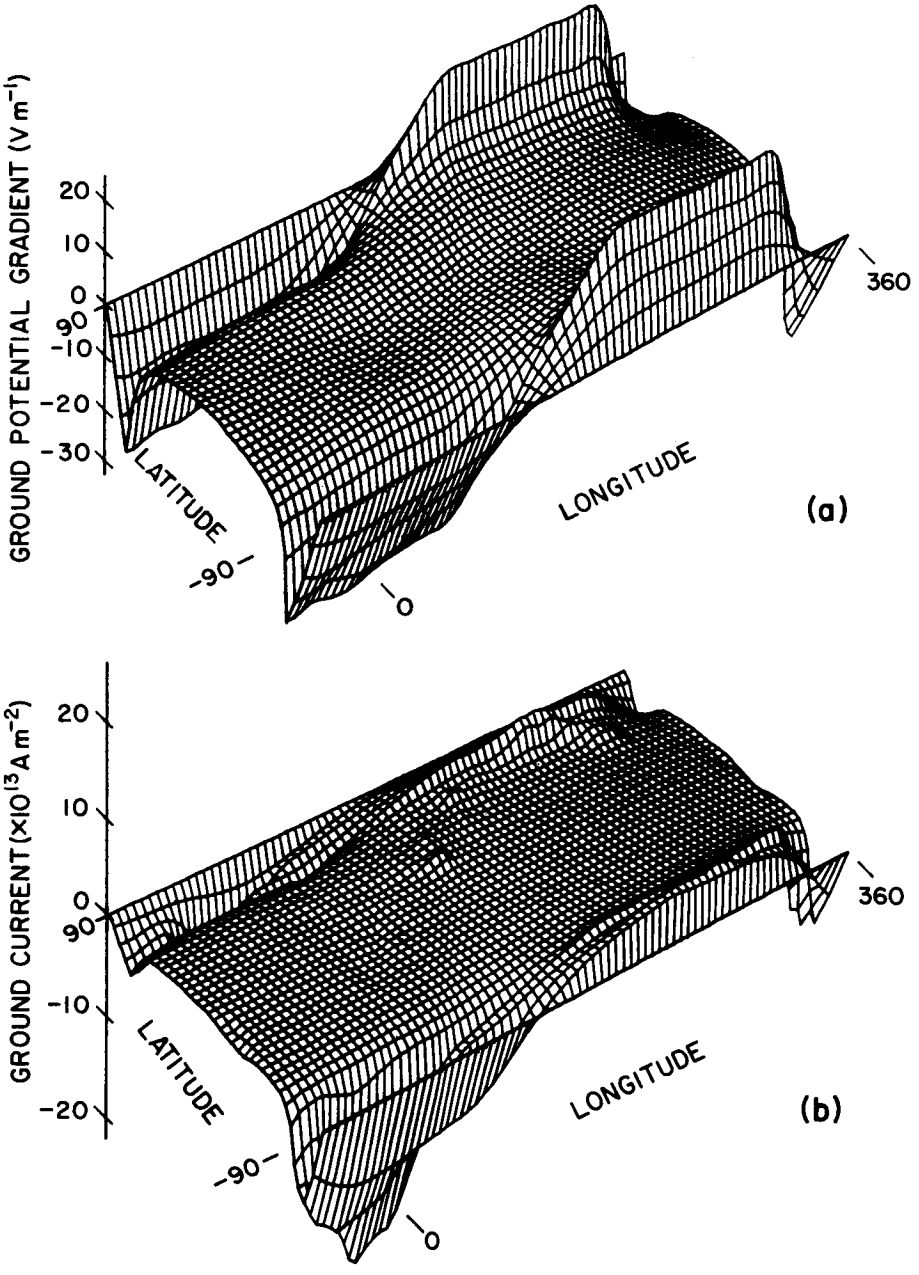

Figure 21. Perspective illustrations of the calculated (a) potential gradient, V m^{-1} and (b) air-Earth current (A m^{-2}) at 1900 UT along the Earth's orographic surface due to the downward mapping of Heppner's (1977) geomagnetic quiet potential pattern over the magnetic polar caps. The plots are in geomagnetic latitude and geomagnetic longitude.

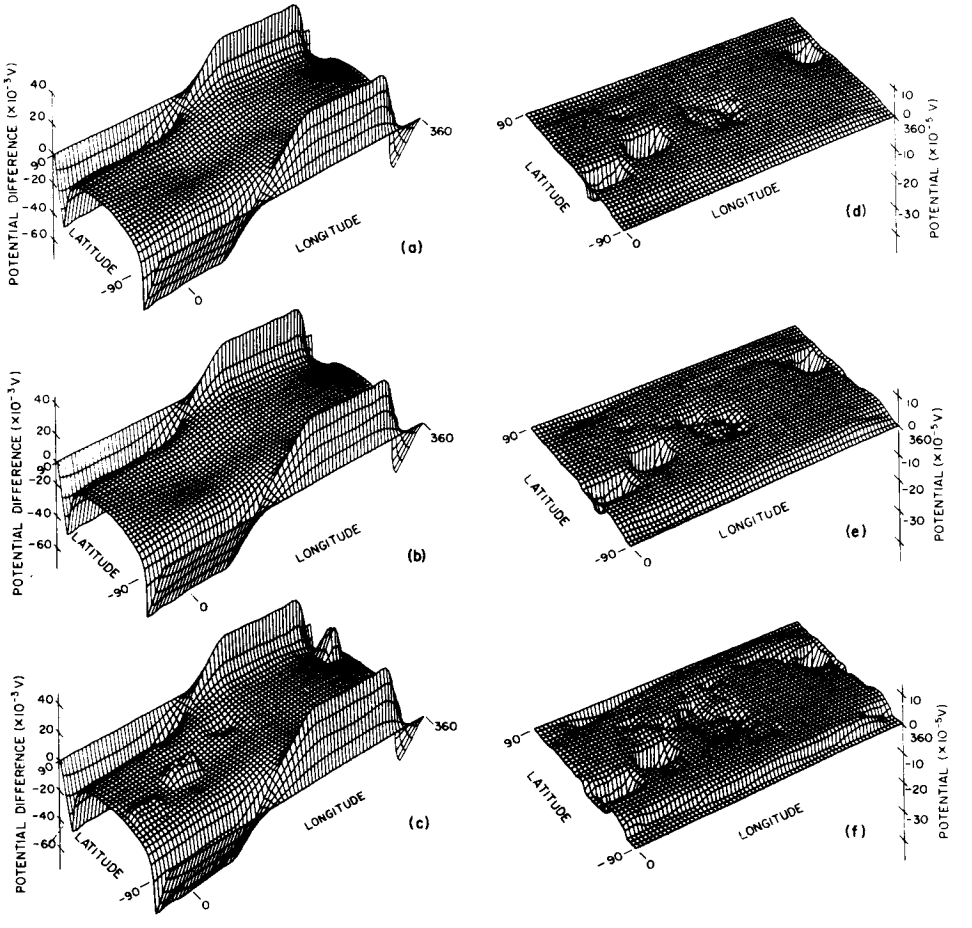

Figure 22. Same as Figure 18, except with the magnetically average period magnetospheric potential pattern over the polar cap superimposed. The plots are also in geomagnetic latitude and longitude at 1900 UT.

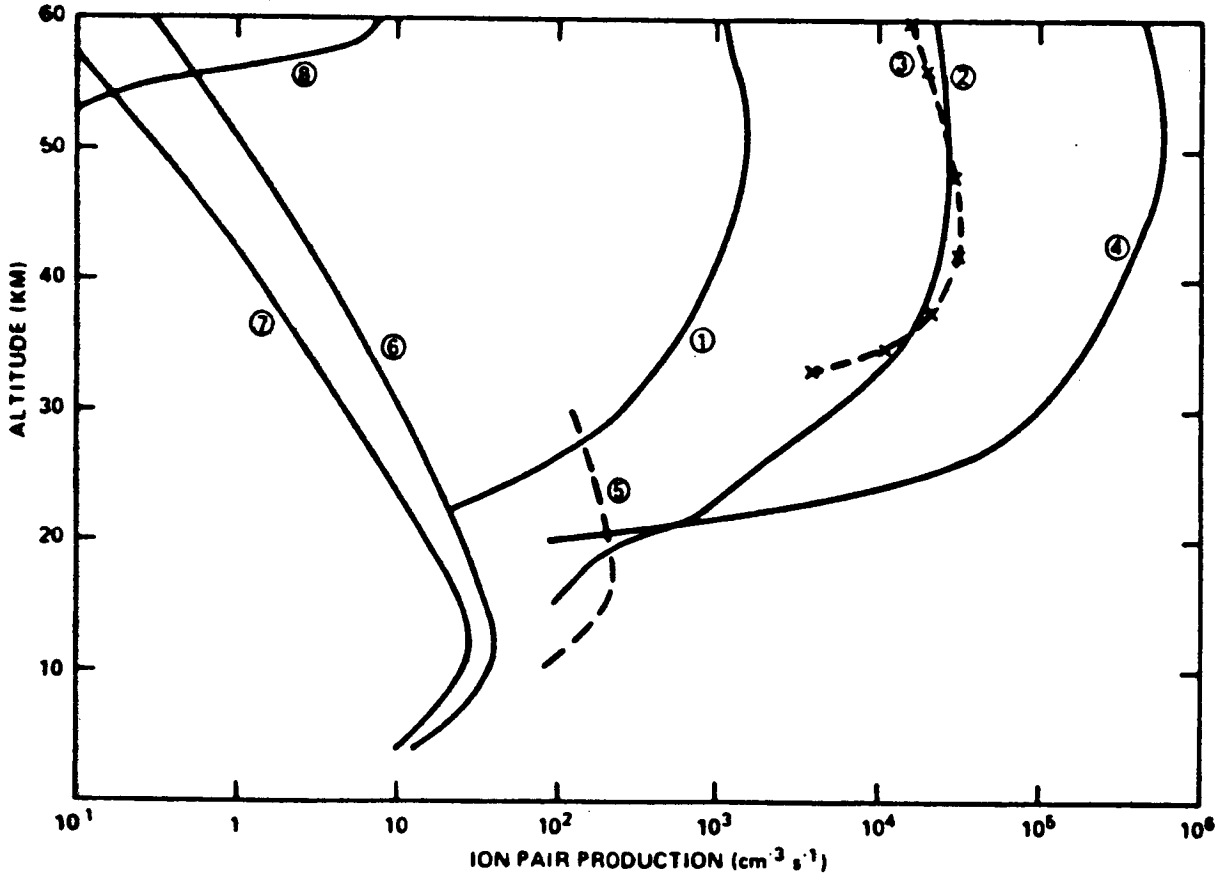

Figure 23. Ion pair production rates due to solar protons: 1-polar cap absorption (PCA), 11/2/69; 2-PCA, 8/4/72, 1500-1600 UT, 3-PCA, 8/4/72, 1508 UT; 4-PCA, 8/4/72, 2200 UT; 5-PCA 9/29/61; 6-SSMIN (sunspot minimum) galactic cosmic rays; 7-SSMAX (sunspot maximum) galactic cosmic rays; 8-precipitating electrons in a hard aurora (Herman and Goldberg, 1978).

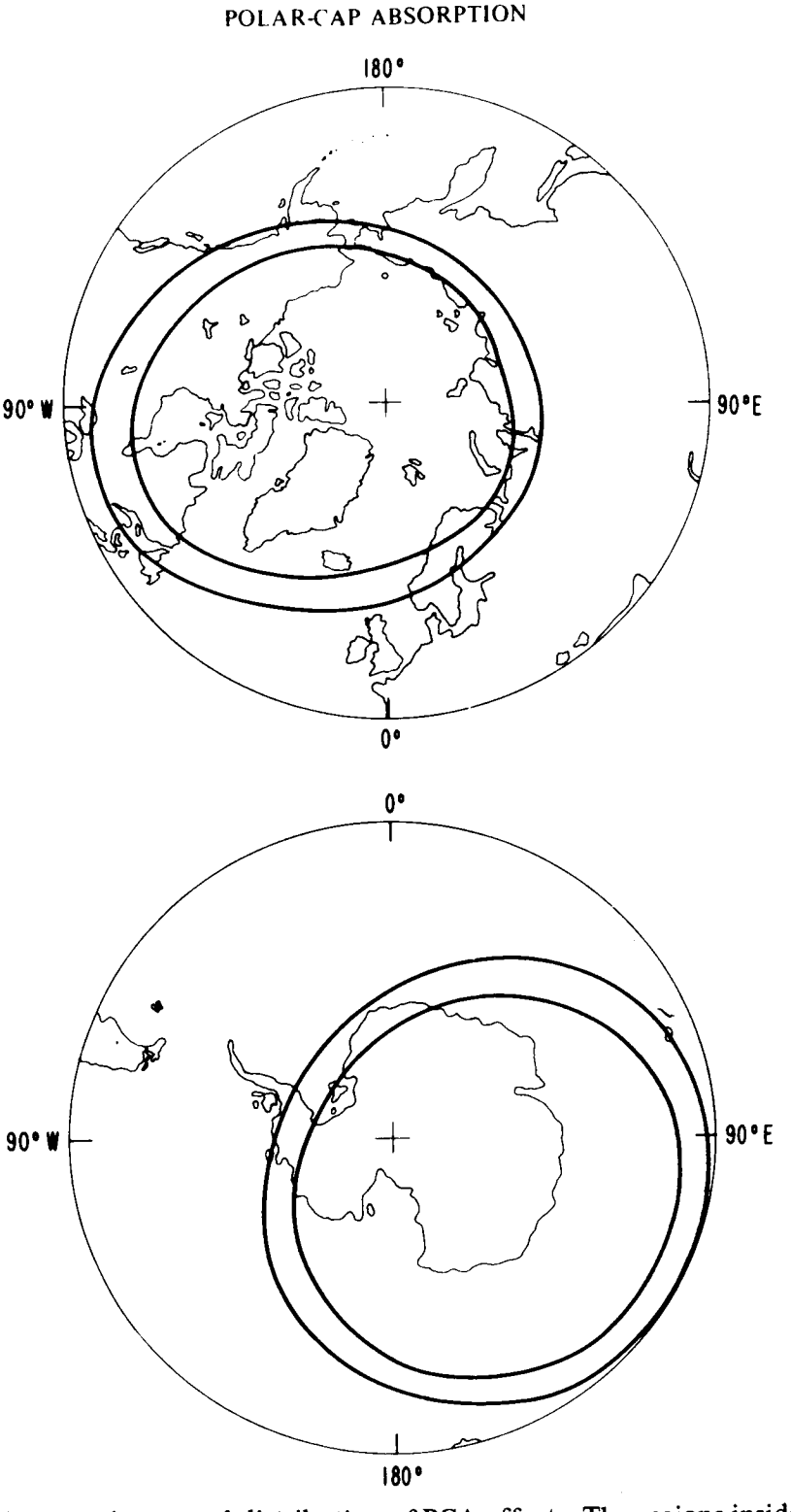

Figure 24. Maps showing the normal distribution of PCA effects. The regions inside the inner curves experience the full intensity, while regions outside of the outer curves are normally unaffected, except during geomagnetic disturbances (Reid, 1974).

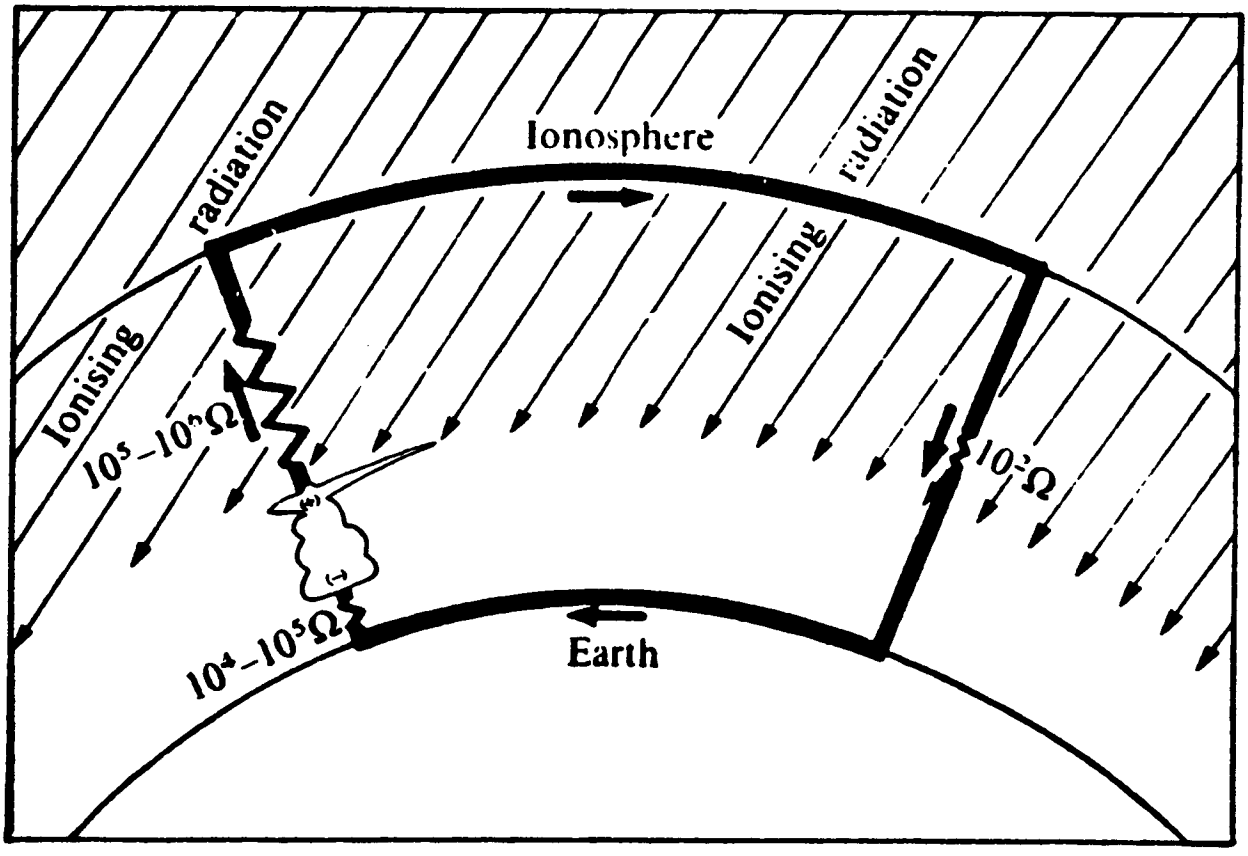

Figure 25. The atmospheric electrical global circuit. Large arrows indicate flow of positive charge. Estimated resistances of circuit elements are given. The thunderstorm depicted represents the global electrical generator, that is, the totality of all global thunderstorms (Markson, 1978a).

Figure 26. Thunderstorm near Boulder, Colorado (NCAR photo).

TABLE 1

Some Approximate Properties of the
Global Electrical Circuit

Number of thunderstorms acting at one time	1500-2000
Currents above thunderstorms	
A) Range	0.1 to 6 A
B) Average	0.5 to 1 A
Currents below thunderstorms (Mühleisen, 1977)	
A) Coronal currents (trees, etc.)	700 A
B) Lightning currents	400 A
C) Precipitation currents	- 200 A
Net current	900 A
Global current	750-2000 A
Ionospheric potential	
A) Range	180-400 kV
B) Mean	240 kV
Columnar resistance at sea level	$1.3 \times 10^{17}\ \Omega\ m^2$
Total resistance (including resistance decrease by mountains)	270 Ω
Current density	
A) Inhabited and industrialized areas	$1 \times 10^{-12}\ A\ m^{-2}$
B) Vegetated ground and deserts	$2\text{-}4 \times 10^{-12}\ A\ m^{-2}$
C) South Pole station	$2.5 \times 10^{-12}\ A\ m^{-2}$
Potential gradient	
A) Equator	$120\ V\ m^{-1}$
B) 60° latitude	$155\ V\ m^{-1}$
C) South Pole	$71\ V\ m^{-1}$
Average charge transfer over the entire world	$+ 90C\ km^{-2}\ yr^{-1}$
Relaxation times	
A) 70 km	10^{-3} s
B) 18 km	4 s
C) 0.01 km	5-40 min
D) Earth's surface	10^{-5} s

TABLE 2

Comparison of Mühleisen (1977) Estimate of Global Circuit Parameters with Model Calculations at 1900 UT. (Hays and Roble, 1979).

	Mühleisen (1977)	Model
Number of thunderstorms	1500-1800	2000 (specified)
Mean value of current intensity over one thunderstorm cell	0.5-1.0 A	0.51 A
Global current	800-1800 A	1065 A
Ionospheric potential	180-400 kV (range 278 kV (mean)	291 kV
Columnar resistance	1.3×10^{17} Ω m^2	1.39×10^{17} Ω m^2
Total resistance	230 Ω	273
Currents below thundercloud A) Corona currents (trees, etc.) 640 A B) Lightning currents 400 A C) Precipiation currents - 200 A total 840	840 A	1065 A
Current density	1×10^{-12} A m^{-2} (inhabited and industrialized areas) $2\text{-}4 \times 10^{-12}$ A m^{-2} (vegetated ground and deserts)	1.52×10^{-12} A m^{-2} @ sea level

TABLE 3

Electrical Response to High-latitude (> 60°) Variations of Conductivity

	Case	Φ_∞(V)	R(Ω)	I(A)	$\partial\Phi/\partial z$ (V m^{-1})	
					Low	High
1.	Base	410,900	310	1325	192	238
2.	Increase	394,900	298	1325	186	260
3.	Decrease	425,000	321	1325	198	217

TROPOSPHERIC EFFECTS ON THE MIDDLE ATMOSPHERE AND VICE-VERSA*

Marvin A. Geller
Division of Meteorology and Physical Oceanography
Rosenstiel School of Marine and Atmospheric Science
University of Miami
Miami, Florida 33149

1. INTRODUCTION

One of the purposes of this paper is to discuss the mechanisms by which phenomena occurring in the troposphere can affect the middle atmosphere, which is defined here as being that atmospheric region lying above the tropopause and below the mesopause. Another purpose, however, is to discuss mechanisms by which middle atmospheric phenomena can affect the tropospheric circulation. A third purpose will be to discuss how the middle atmosphere may act as a medium by which extraterrestrial effects may give rise to changes in tropospheric circulation.

2. CONSIDERATIONS OF ENERGETICS

As a prelude to these discussions, however, I shall first briefly review some aspects of the energetics of the troposphere and the middle atmosphere as well as the energetics of extraterrestrial inputs.

2.1 Tropospheric Energetics

The ultimate energy source for the atmosphere is that portion of the Sun's energy output that is intercepted by the Earth (excepting negligibly small tidal and geothermal effects). This flux of energy is on a yearly averaged basis 1.95 cal cm^{-2} min (1.35×10^3 Wm^{-2}), the "solar constant." The net radiation flux at the top of the atmosphere (F_{TA}) is given by this incoming solar radiation minus the sum of the reflected solar and emitted terrestrial radiation. This can be measured directly from satellite and is shown in Figure 1 (taken from Oort and Vonder Haar, 1976) as a function of latitude and season. Spatial differentials in this net heating is what provides the basic drive for atmospheric motions. Since the atmosphere is rather transparent to solar radiation, most of the solar radiation either heats the Earth's surface or leads to evaporation. Given that the atmosphere is relatively opaque to infrared radiation and that almost all of the water vapor is condensed in clouds and rained out we see that most solar energy leads to heating of the troposphere.

The conversion of this energy into motions can be most easily discussed by referring to the energy cycle for the annually averaged troposphere. This is shown in Figure 2 which is taken from Oort (1964). The latitudinal differential in the zonally-averaged heating of the troposphere gives rise to an energy generation of 3.1 Wm^{-2} which provides the energy source to maintain the available potential energy of the zonally-averaged atmosphere at 40×10^5 Jm^{-2}. Energy is converted from A_z to A_E, the eddy available potential energy, by asymmetric heat transport processes at a rate of 3.0 Wm^{-2}. There is a 0.8 Wm^{-2} rate of energy loss from A_E and a rate of energy conversion of

2.2 Wm^{-2} to K_E, the eddy kinetic energy, by the assymmetric rising of warm air and falling of cool air that maintains the eddy available potential energy at 15×10^5 Jm^{-2}. The eddy kinetic energy is maintained at 7×10^5 Jm^{-2} by a frictional loss of 1.8 Wm^{-2} and a conversion to zonally-averaged kinetic energy by momentum flux convergence of 0.4 Wm^{-2}. Finally, the kinetic energy of the zonally-averaged motions is maintained at 8×10^5 Jm^{-2} by a frictional loss rate of 0.5 Wm^{-2} and a small energy conversion from the zonally-averaged available potential energy by zonally symmetric rising of warm air and falling of cool air.

Before proceeding to the subject of middle atmosphere energetics, a few more remarks should be made on the subject of tropospheric energetics. The calculations of the annually-averaged atmospheric energy cycle that is shown in Figure 2 were made from Northern Hemisphere data polewards of 20°N for altitudes below about 100 mb. The energy conversion processes may be thought of as being due to zonally symmetric processes and assymmetric processes. Thus, a positive energy conversion from A_z to K_z is due to a zonally-averaged rising of warm air and falling of cool air. A positive conversion from A_z to A_E is due to the assymmetric motions transporting heat down the gradient of the zonally- averaged temperature field. It should be mentioned here that these asymmetric motions may arise from two sources. They may be due to the traveling cyclones and anticyclones that arise from hydrodynamic instabilities, and they may be due to the asymmetric flow that is due to asymmetries in both the elevation and thermal properties of the Earth's surface. A positive conversion from A_E to K_E is due to a systematic rising of warm air and falling of cool air within the asymmetric motions. A positive conversion from K_E to K_z is due to a transport of angular momentum by the asymmetric motions so as to maintain the zonally-averaged flow against dissipation. Given the value of the solar constant as 1.35×10^3 Wm^{-2} and the albedo of the Earth-atmosphere system as 0.30 (see Vonder Haar and Suomi, 1971), we see that the average solar flux absorbed by one hemisphere is about 120 Wm^{-2}. Of the absorbed energy, we see from Figure 2 that only about 2.2 Wm^{-2}, or about 2% of the absorbed radiation is used to generate tropospheric motions.

2.2 Middle Atmosphere Energetics

The data from which the information on tropospheric energetics was obtained came from meteorological balloon soundings which have an altitude limit of about 30 km or 10 mb. Recently, high altitude satellite radiance data have begun to be used to study middle atmosphere energetics. For instance, Figure 3 shows the energy budget for three middle atmosphere layers 10 - 100 mb (about 15 - 30 km) 1 - 10 mb (about 30 - 50 km), and 0.2 - 1 mb (about 50 - 60 km). This figure is taken from Hartmann (1976) and includes data from the Southern Hemisphere winter polewards of 15°S obtained using the Selective Chopper Radiometer on Nimbus 5.

One very great difference that we see in the middle atmospheric energetics from that in the troposphere is that in the troposphere there is an external sink for K_E due to frictional dissipation whereas in the middle atmosphere we see an external energy source for K_E due to the convergence of the vertical flux of geopotential energy due to the planetary-scale waves. For instance, Hartmann (1976) found a flux of 0.167 Wm^{-2} through 100 mb, 0.143 Wm^{-2} through 10 mb, 0.027 Wm^{-2} through 1 mb, and 0.004 Wm^{-2} through 0.2 mb. Thus the 10 - 100 mb layer is relatively transparent to this planetary wave energy flux with a convergence of 0.024 Wm^{-2}, or 14% of the incoming flux. There is a convergence of 0.116 Wm^{-2} in the 1 - 10 mb layer which is 81% of the incoming

flux, and there is a convergence of 0.023 Wm^{-2} in the 0.2 - 1 mb layer which is 85% of the incoming flux. In the troposphere, the eddy kinetic energy was supplied by conversion from eddy potential energy whereas above 10 mb the convergence of the vertical flux of geopotential energy is an order of magnitude greater than this conversion.

It should be pointed out that the picture of middle atmosphere energetics that is presented here should rigorously taken to be representative only for the two month period in question for the Southern Hemisphere whereas the tropospheric energetics is representative of the annually-averaged state of the Northern Hemisphere. This point is discussed in Hartmann (1976).

2.3 External Energy Sources

Table (1), which shows the magnitudes of several sources of energy that are external to the atmosphere, is taken from the paper by Willis (1976), and the arguments that he uses in arriving at these values of the energy fluxes can be found there. The solar constant is observed to remain constant to about ±1%, but there have been speculations that it may vary within this range. Of course, within some spectral regions the solar irradiance has been observed to show much larger variations. For instance, there appears to be a solar-cycle change in irradiance by a factor of about 2.5 at some wavelengths in the far ultraviolet according to Heath (1973). The energy at wavelengths which are either known or are thought to vary are deposited in the middle atmosphere and above and in any event comprise a very small fraction of the solar flux. Thus, if temporal changes in the solar flux are to affect the troposphere in a significant fashion they must do so indirectly, possibly operating through changing middle atmosphere parameters that can affect the troposphere. The same is true of the magnetospheric fluxes that are shown in Table 1. They are too small to affect the troposphere directly.

3. MODES OF VERTICAL COUPLING

In a previous section we have seen that the middle atmosphere is strongly coupled to the troposphere by dynamical processes. In this section, we will discuss these dynamical coupling processes as well as those of radiational coupling, chemical coupling, and electrical coupling.

3.1 Upward Dynamical Coupling

The data that were used to make up the pictures of tropospheric and middle atmospheric energetics that were presented used daily nontropical data. This means that only the dynamic effects of extratropical large-scale motions with periods of several days or longer were included. For instance, no effects due to tides and gravity waves are included.

Let us first consider the stationary middle latitude planetary waves as agents for vertical coupling. Extratropical stationary planetary waves are large-scale undulations in the circumpolar flow that are forced by the surface winds blowing over the planetary-scale variations in surface elevation and by the planetary-scale distribution in diabatic heating. Charney and Drazin (1961) showed that such waves cannot propagate energy vertically in the presence of easterly flow in the middle atmosphere such as is present during summer. Dickinson (1969) later showed that as the westerly flow becomes

weaker, such as during the equinox seasons, the dissipative effect of infrared radiation to space becomes greater. Thus, theory is consistent with the observation that the vertical coupling effect of extratropical planetary waves is greatest during the winter season. For instance, Table 2 (from Miller, 1970) shows that the vertical energy flux associated with planetary waves is a maximum in winter. It also shows that there is little vertical coupling from the shorter wavelength planetary waves. Thus, the middle atmosphere acts as a short-wavelength filter for vertical energy propagation (e.g., Charney and Drazin, 1961, and Charney and Pedlosky, 1963).

Matsuno (1971) has shown that increases in the vertical flux of energy associated with tropospheric planetary waves initiate the course of events leading to sudden stratospheric warmings. The studies by Quiroz (1969), Labitske (1972), and Scott (1972) have shown that mesospheric cooling episodes accompany stratospheric warmings. D-region manifestations of planetary waves have been found by Deland and Friedman (1972) and Cavalieri, et al. (1974). Manifestations of planetary waves in the E-region have also been noted by Brown and Williams (1971), Brown (1975) and Cavalieri (1976).

Mean meridional motions also provide a dynamical coupling mechanism between the troposphere and the middle atmosphere. For instance, the numerically modelled mean meridional motions of Cunnold et al., (1975) that are shown in Figure 4 show mean meridional circulation cells that extend from the troposphere to the middle atmosphere.

Finally, shorter period motions such as tides and gravity waves provide a dynamical mechanism for transporting energy and momentum upward from the troposphere. While tidal and gravity waves are no doubt important in influencing the thermosphere (e.g., Lindzen and Blake, 1970, and Hines, 1965), their main influence on the stratosphere and mesosphere is probably to give rise to turbulent mixing through instabilities (e.g., Lindzen, 1968; Hodges, 1967; and Geller et al., 1975).

3.2 Downward Dynamical Coupling

By far the most likely candidate for the middle atmosphere exerting any kind of significant influence on the troposphere through dynamical coupling is through the modulation of the vertical energy flux associated with planetary waves. As Hines (1974) pointed out, since the transmission-reflection properties of planetary waves are strongly influenced by the mean zonal flow in the middle atmosphere, changes in the middle atmospheric flow affects the vertical energy flux out of the troposphere. Given a steady forcing of those waves from below, these changed fluxes would lead to a different equilibrium tropospheric planetary wave structure. Calculations of the type of planetary wave changes to be anticipated have been made by Avery and Geller (1978). Tung and Lindzen (1978) have suggested that changes in the middle atmosphere flow can produce conditions for resonant growth of tropospheric planetary waves which ultimately produce a stratospheric warming.

3.3 Radiational Coupling

The stratosphere is closely coupled to the troposphere by infrared absorption and emission processes. The extent of this coupling can best be appreciated by referring to Table 3 which is taken from the radiation calculations of Ramanathan and Dickinson (1978). Note first that the stratosphere absorbs twice as much longwave radiation from the troposphere as it does solar radiation.

Also, note that the net effect of the stratosphere is to warm the troposphere by about 10 Wm^{-2} and that 2.3 Wm^{-2} of this is a result of ozone in the stratosphere. With these results, we are able to physically interpret the result of Ramanathan et al., (1976) that a percentage depletion of ozone that is uniform in altitude will lead to a lowering of surface temperature such that a depletion of tens of percent leads to a temperature decrease of tenths of a degree Kelvin. Similar changes in surface temperature were also noted by Ramanathan et al., (1976) when the total ozone amount was unchanged but the height distribution is changed. This is due to the dependence of ozone infrared absorption on altitude through pressure broadening.

Ramanathan (1977) has pointed out that the warm polar stratosphere in existence during a sudden warming can play an important role in radiatively warming the polar troposphere. Figure 5, from Ramanathan (1977), indicates that the low latitude troposphere transports heat to high latitudes by mean meridional motions acting together with stationary and transient eddies (see Oort, 1971). It also illustrates another mode of heat transport that occurs when stratospheric warmings take place when there is an enhanced upward flux of eddy geopotential that results in a heating of the polar stratosphere. These higher than normal stratospheric temperatures cause enhanced downward infrared radiation into the troposphere. Ramanathan's (1977) calculations indicate that very strong sudden warmings can give rise to decreases in tropospheric available potential energy of up to 10% and increases in the average winter polar surface temperature of 2°K by this means.

Dickinson (1975), in the course of speculating about possible mechanisms for Sun-weather relationships, raised the possibility that changes in ionization in the vicinity of the tropopause resulting from varying cosmic ray fluxes could modulate the sulfate aerosol layer and that this could affect the energetics of the troposphere through affecting the incoming solar and outgoing infrared radiative fluxes.

Since ozone is the key constituent in the stratosphere, careful consideration of how external factors may change ozone concentrations, as well as the accompanying observational efforts, are needed. For instance, calculations by Ruderman and Chamberlain (1975) have shown that the observed 11-year variation in cosmic ray intensity can possibly give rise to a significant ozone variation, and Chamberlain (1977) has speculated that secular changes in both the Sun's and Earth's magnetic field could have produced secular ozone changes that produced past changes in climate. Also, satellite measurements of an ozone depletion during energetic proton events by Heath et al., (1977) verify the theoretical predictions of Crutzen et al., (1975) that MEV protons from the Sun produce odd-nitrogen in the upper stratosphere, which catalyzes ozone destruction. Such ozone depletions should have both a direct radiative effect on the troposphere as well as an effect on the dynamics in the middle atmosphere (see Schoeberl and Strobel, 1978, for example) in such a manner that might affect planetary wave structure (Geller and Avery, 1977).

3.4 Chemical Coupling

The origin of many of the atmospheric trace constituents lies at the surface of the Earth. Natural biological and anthropogenic processes at the Earth's surface produce, among other constituents, CH_4, N_2O, CO, H_2, CH_3Cl, $CFCl_3$, and CCl_4. These gases have various loss mechanisms in the troposphere, but they all are transported to the stratosphere where destruction by ultraviolet

radiation, O('D) atoms, OH radicals and other processes provide a copious source of free-radical species. Processes that transport these constituents from the ground to the stratosphere thus provide an important link between the troposphere and the middle atmosphere.

3.5 Electrical Coupling

In the last few years, Markson (1975) and Herman and Goldberg (1978) have suggested ways in which solar activity induced changes in the atmospheric electric field may produce modulations in thunderstorm activity. Also, Hays and Roble (1978) and Roble and Hays (1978) have performed calculations of the global electric field that include solar effects on the ionosphere as well as thunderstorm effects. Markson (1975) and Herman and Golberg (1978) both start with the fact that lower atmosphere ionization, and hence conductivity, vary as a consequence of the Forbush decrease in galactic cosmic rays as well as changes in corpuscular radiation. Both, albeit by different mechanisms, then present a sequence of effects which leads to a changed fair weather field on the order of 10 Vm^{-1}. The weakest part of their sequence is coming up with a mechanism by which this relatively small change in the fair weather field can affect the weather. For instance, the electric field in a thunderstorm which results from the active convection dynamics interacting with cloud microphysics is on the order of 10^5 Vm^{-1} (Mason, 1971). Both Markson (1975) and Herman and Goldberg (1978) suggest that these small electric field changes that result from solar activity affect the cloud microphysics in a way that helps to initiate or at least enhance thunderstorms. We will hear more about this in the paper by Dr. Vonnegut. Much remains to be done to show that electrical coupling effects on the troposphere are meteorologically significant, however. Even if the observed lightning frequency is verified to vary with changing fair weather electric field and ion concentrations, as suggested by the results of Stringfellow (1974), it still would remain to be shown that other features of convective storms were influenced, and even if this were demonstrated, it still would remain to be shown how this could significantly affect the large scale distribution of meteorological parameters (Dickinson, 1975).

REFERENCES

Avery, S. K., and M. A. Geller, A modeling study of tropospheric planetary wave response to changes in upper atmospheric reflection and transmission. Paper presented at Conference on the Meteorology of the Upper Atmosphere. October, 1978. Boston, Mass.

Brown, G. M., 1975, Sq Variability and aeronomic structure, *J. Atmos. Terr. Phys.*, **37**, 107 - 117, 1978.

Brown, G. M., and D. C. Williams, Pressure variations in the stratosphere and ionosphere, *J. Atmos. Terr. Phys.*, **33**, 1321 - 1328, 1971.

Cavalieri, D.J., Traveling planetary-scale waves in the E-region, *J. Atmos. Terr. Phys.*, 38, 965 - 977, 1976.

Cavalieri, D. J., R. J. Deland, T. A. Potemra, and R. F. Gavin, The Correlation of VLF propagation variations with atmospheric planetary-scale waves, *J. Atmos. Terr. Phys.*, **36**, 561 - 574, 1974.

Chamberlain, J. W., A mechanism for inducing climatic variations through the stratosphere: Screening of cosmic rays by solar and terrestrial magnetic fields *J. Atmos. Sci.*, **34**, 737 - 743, 1977.

Charney, J. G., and P. G. Drazin, Propagation of planetary scale disturbances from the lower into the upper atmosphere *J. Geophys. Res.*, **66**, 83 - 109, 1961.

Charney, J. G., and J. Pedlosky, On the trapping of unstable planetary waves in the atmosphere *J. Geophys. Res.*, **68**, 6441 - 6442.

Crutzen, P. J., I. S. A. Isaksen, and G. C. Reid, Solar proton events: Stratospheric sources of nitric oxide *Science*, **189**, 457 - 459, 1975.

Cunnold, D., F. Alyea, N. Phillips, and R. Prinn, A three-dimensional dynamical-chemical model of atmospheric ozone *J. Atmos. Sci.*, **32**, 170 - 194, 1975.

Dickinson, R. E., Vertical propagation of planetary Rossby waves through and atmosphere with Newtonian cooling *J. Geophys. Res.*, **74**, 929 - 938, 1969.

Dickinson, R. E., Solar variability and the lower atmosphere, *Bull. Am. Meteor. Soc.*, **56**, 1240 - 1248, 1975.

Deland, R. J., and R. M. Friedman, Correlation of fluctuations of ionospheric absorption and atmospheric planetary scale waves *J. Atmos. Terr. Phys.*, **34**, 295 - 304, 1972.

Geller, M. A., and S. K. Avery, Calculations of solar activity effects on planetary wave propagation Paper presented at Joint IAGA/IAMAP Assembly, Seattle, Wash., August, 1977.

Geller, M. A., H. Tanaka, and D. C. Fritts, Production of turbulence in the vicinity of critical levels for internal gravity waves *J. Atmos. Sci.*, **32**, 2125 - 2135, 1975.

Hartmann, D. L., The dynamical climatology of the stratosphere in the Southern Hemisphere during late winter 1973 *J. Atmos. Sci.*, **33**, 1789 - 1802, 1976.

Hays, P. B., and R. G. Roble, A quasi-static model of global atmospheric electricity: 1, the lower atmosphere (Submitted to *J. Geophys. Res.*), 1978.

Heath, D. F., A. J. Krueger, and P. J. Crutzen, Solar proton event; influence on stratosphere ozone, *Science*, **197**, 886 - 889, 1977.

Herman, J. R., and R. A. Goldberg, Initiation of non-tropical thunderstorms by solar activity *J. Atmos. Terr. Phys.*, **40**, 121 - 134, 1978.

Hines, C. O., A possible mechanism for the production of Sun-weather correlations, *J. Atmos. Sci.*, **31**, 589 - 591, 1974.

Hodges, R. R., Jr., Generation of turbulence in the upper atmosphere by internal gravity waves, *J. Geophys. Res.*, **72**, 3455 - 3458, 1967.

Labitske, K., Temperature changes in the mesosphere and stratosphere connected with circulation changes in winter, *J. Atmos. Sci.*, **29**, 756 - 766, 1972.

Lindzen, R. S., The application of classical atmospheric tidal theory, *Proc. Roy. Soc.*, **A303**, 299 - 316, 1968.

Markson, R., Solar modulation of atmospheric electrification through variation of the conductivity over thunderstorms, *Possible Relationships between Solar Activity and Meteorological Phenomena*, NASA SP-366, 171 - 178, 1975.

Mason, B. J., *The Physics of Clouds*, 2nd edition, Clarendon Press, Oxford, 671 pp., 1971.

Matsuno, T., A dynamical model of the stratospheric sudden warming, *J. Atmos. Sci.*, **28**, 1479 - 1494, 1971.

Miller, A. J., The transfer of Kinetic energy from the troposphere to the stratosphere, *J. Atmos. Sci.*, **27**, 388 - 393, 1970.

Oort, A. H., On estimates of the atmospheric energy cycle, *Mon. Wea. Rev.*, **92**, 483 - 493, 1964.

Oort, A. H., The observed annual cycle in the meridional transport of atmospheric energy, *J. Atmos. Sci.*, **28**, 325 - 339, 1971.

Oort, A. H., and T. H. Vonder Haar, On the observed annual cycle in the ocean-atmosphere heat balance over the Northern Hemisphere, *J. Phys. Oceanogr.*, **6**, 781 - 800, 1976.

Quiroz, R. S., The warming of the upper stratosphere in February 1966 and the associated structure of the mesosphere, *Mon. Wea. Rev.*, **97**, 541 - 552, 1969.

Ramanathan, V., Troposphere-stratosphere feedback mechanism: stratospheric warming and its effect on the polar energy budget and the tropospheric circulation, *J. Atmos. Sci.*, **34**, 439 - 447, 1977.

Ramanathan, V., L. B. Callis, and R. E. Boughner, Sensitivity of surface temperture and atmospheric temperature to perturbations in the stratospheric concentration of ozone and nitrogen dioxide, *J. Atmos. Sci.*, **33**, 1091 - 1112, 1976.

Ramanathan, V., and R. E. Dickinson, The role of stratospheric ozone in zonal and seasonal radiative energy balance of the Earth-troposphere system, accepted for publ. in *J. Atmos. Sci.*, 1978.

Roble, R. G., and P. B. Hays, (Paper to be submitted to *J. Geophys. Res.*), 1978.

Ruderman, M. A., and J. W. Chamberlain, Origin of the sunspot modulation of ozone: Its implications for stratospheric NO injections, *Planet, Space Sci.*, **23**, 247 - 268, 1975.

Schoeberl, M. R., and D. F. Strobel, The response of the zonally averaged circulation to stratospheric ozone reductions, *J. Atmos. Sci.*, **35**, 1751 - 1757, 1978.

Scott, A. F. D., Mesospheric temperatures and winds during a stratospheric warming, *Phil. Trans. R. Soc. London*, **271**, 547 - 557, 1972.

Stringfellow, M. F., Lightning incidence in Britain and the solar cycle, *Nature*, **249**, 332 - 333, 1974.

Tung, K. K., and R. S. Lindzen, A theory of stationary long waves, Part I. A simple theory of blocking, (submitted to *Mon. Wea. Rev.*), 1978.

Willis, D. M., The energetics of Sun-weather relationships: magnetospheric processes, *J. Atmos. Terr. Phys.*, **38**, 685 - 698, 1976.

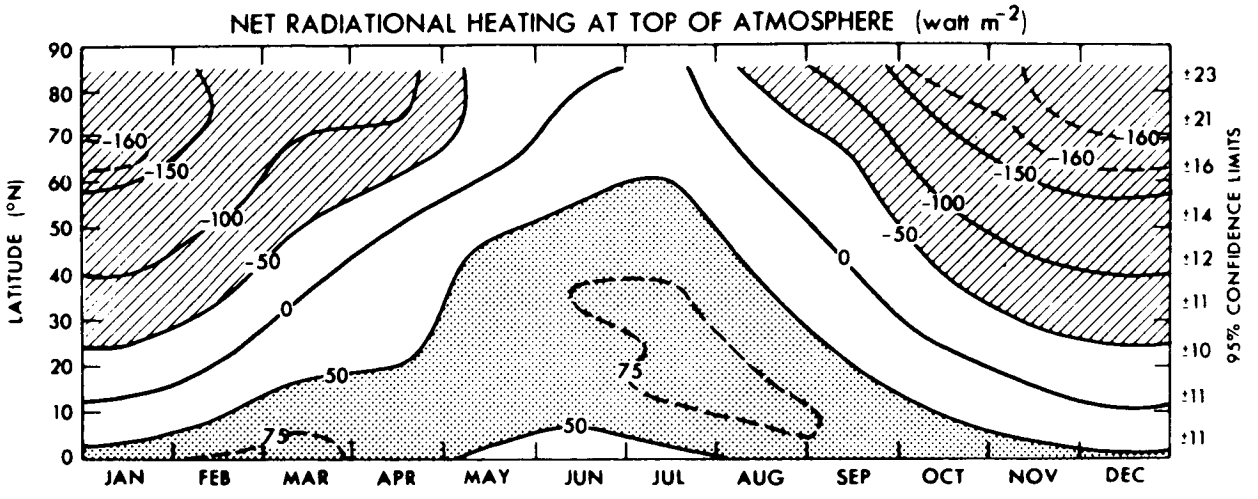

Figure 1. Net incoming radiation flux at the top of the atmosphere (F_{TA}) based on satellite data as a function of latitude and month of the year. Annual mean 95% confidence limits are shown on the right hand side of the diagram.

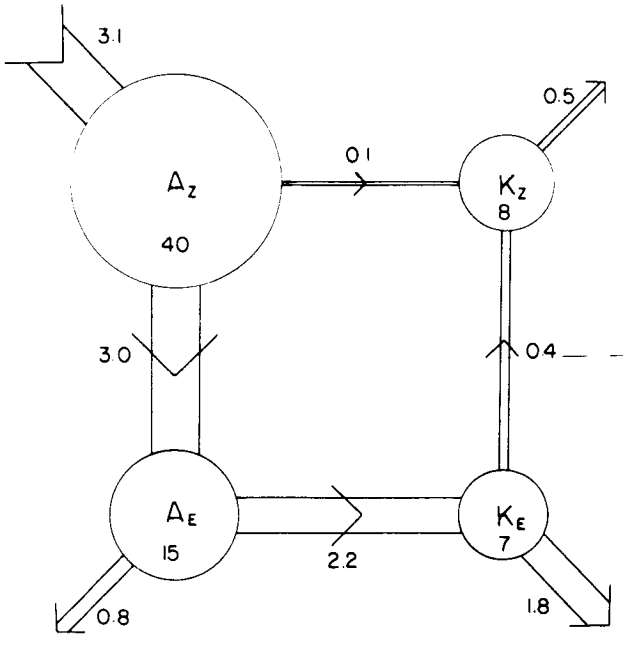

Figure 2. The energy cycle of the atmosphere as estimated by Oort (1964). Values of energy are in units of 10^5 joules m^{-2}, and values of generation, conversion, and dissipation are in watts m^{-2}. The estimated value of conversion from A_z to K_z is smaller than the probable error of the estimate.

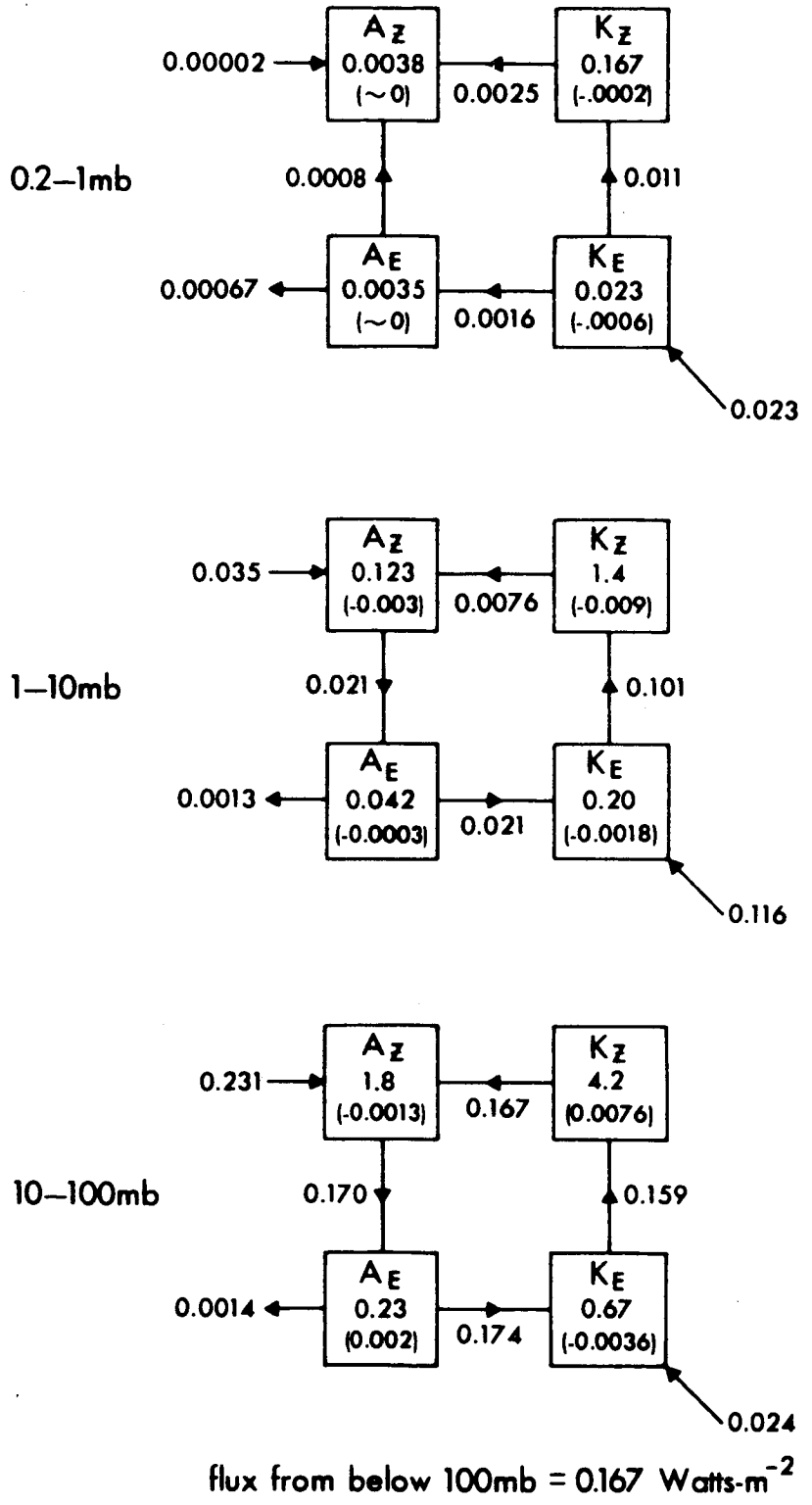

Figure 3. Energy box diagrams for three stratospheric layers: units (amounts, 10^5 J m^{-2}; rates, Wm^{-2}). The values in parentheses are the tendencies. 1 July-6 September.

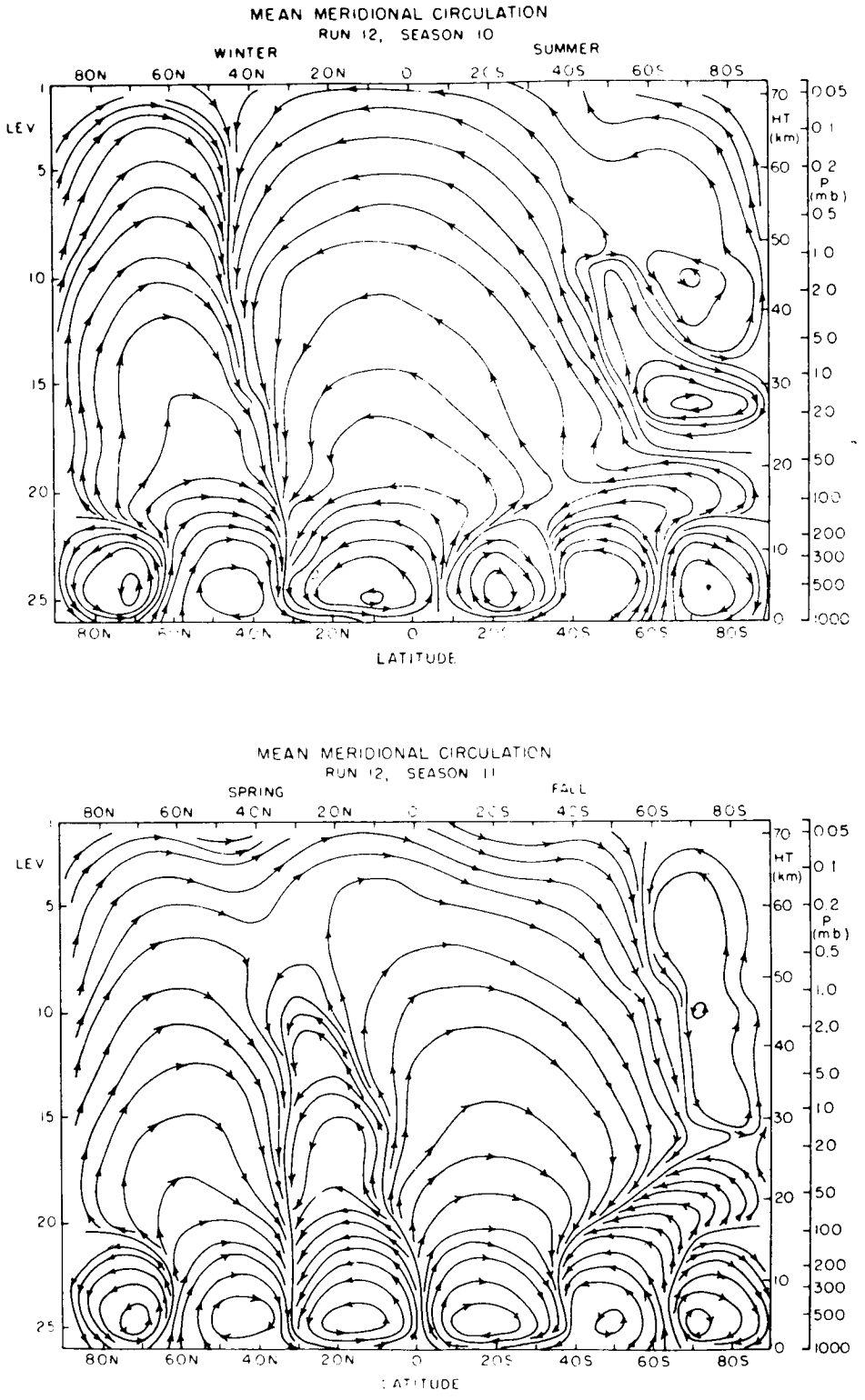

Figure 4. The mean meridional circulation patterns for seasons 10 (solstice) and 11 (equinox).

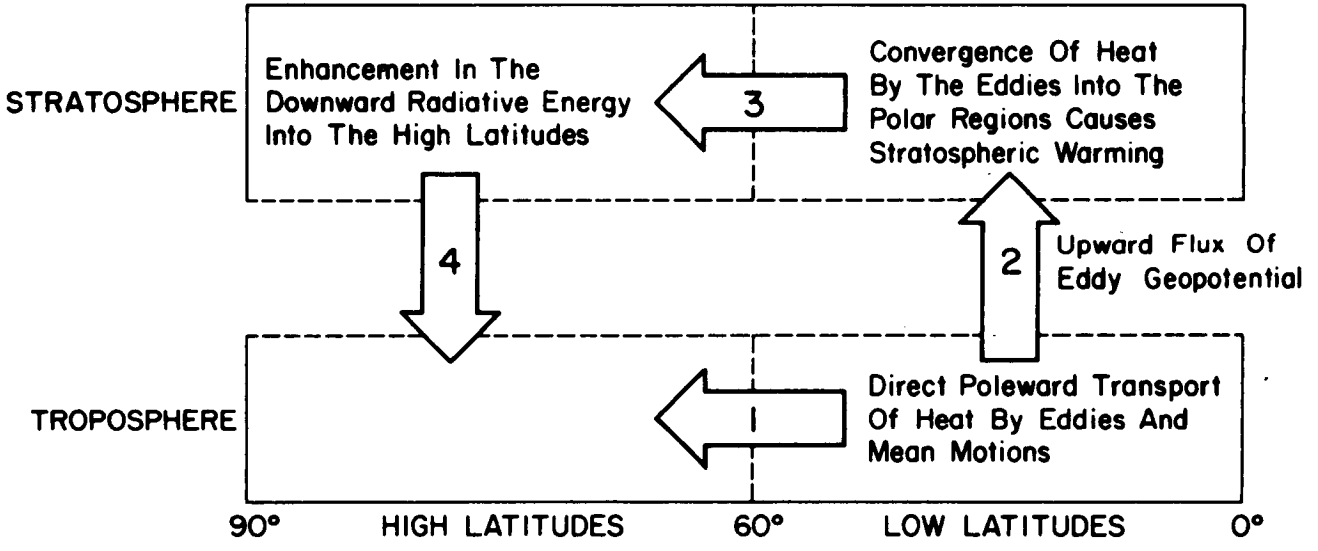

Figure 5. Schematic diagram of the direct and indirect poleward transport of heat by the global circulation. Arrow 1 indicates the direct transport and the events leading from arrow 2 to 4 indicate the indirect transports.

Table 1
Electromagnetic and Magnetospheric Energy Fluxes

Physical Process	Energy Flux ($W\ m^{-2}$)	References
Electromagnetic radiation :-		
Solar constant	1.35×10^{3}	Labs and Neckel (1971), Kondratyev (1972), Allen (1973), Thekaekara (1973), Smith and Gottlieb (1974)
Soft X-rays (0.2 <λ< 50 nm)	8.8×10^{-4}	Smith and Gottlieb (1974)
Extreme ultraviolet (50 <λ< 140 nm)	1.0×10^{-2}	
Far ultraviolet (140 <λ< 210 nm)	2.7×10^{-1}	
Near ultraviolet (210 <λ< 330 nm)	3.9×10^{1}	Thekaekara (1973)
Visible region (330 <λ<1,000 nm)	9.0×10^{2}	
Near infrared (1,000 <λ<2,400 nm)	3.6×10^{2}	
Solar wind	2.7×10^{-4}	Dessler (1975)
Visual aurorae :-		
International brightness coefficient I	6.0×10^{-4}	Dalgarno, Latimer and McConkey (1965)
II	6.0×10^{-3}	
III	6.0×10^{-2}	
IV	6.0×10^{-1}	
Auroral particles :-		
Glow (diffuse) aurora (Nike-Apache rocket)	5.8×10^{-3}	Bryant et al. (1970)
(DAPP satellite)	$\approx 4.0 \times 10^{-3}$	Williams et al. (1975)
Inverted-V precipitation	$<1.0 \times 10^{-2}$	Frank and Ackerson (1971)
Bright auroral arc	$\sim 1.0 \times 10^{0}$	McIlwain (1960)
Proton aurora - quiet conditions	$<1.0 \times 10^{-3}$	Clark and Metzger (1969)
- very disturbed conditions	3.6×10^{-2}	Metzger and Clark (1971)
Stable auroral red arcs	$<2.0 \times 10^{-4}$	Rees and Roble (1975)
Polar cusp electrons	$\sim 1.0 \times 10^{-3}$	Heikkila and Winningham (1971); Paulikas (1971)
Polar cusp protons	$\sim 1.0 \times 10^{-4}$	
Joule heating of the thermosphere :-		
E = 1 mV/m	1.4×10^{-5}	Cole (1975)
E = 10 mV/m	1.4×10^{-3}	
E = 100 mV/m	1.4×10^{-1}	
Solar protons	$<2.0 \times 10^{-3}$	Williams et al. (1975)
Galactic cosmic rays	$\approx 7.0 \times 10^{-6}$	Puppi (1956)
Downward conduction of heat from the magnatosphere	3.2×10^{-5}	Sanatani and Hanson (1970) Cole (1975)

Table 2

Monthly mean values of $[\omega^*z^*]_{100mb}$ by wavenumber based on the period January 1964-December 1968: units, ergs $cm^{-2}\,sec^{-1}$. (Negative values indicate an upward flux of kinetic energy.)

	Wavenumber n			
	1	2	3	4
January	-102	-67	-21	-4
February	-63	-73	-7	-7
March	-54	-39	-25	-9
April	-25	-29	-16	-9
May	-8	-9	-5	-7
June	-0	-5	+0	-1
July	-1	-0	1	-2
August	-4	-2	-1	-4
September	-4	-5	-4	-9
October	-27	-13	-5	-10
November	-78	-48	-26	-8
December	-97	-56	-25	-12
Yearly Mean	-39	-29	-11	-7

Table 3
Global Mean Stratospheric Radiative Energy Balance
Net = Absorption-emission. Units Wm^{-2}

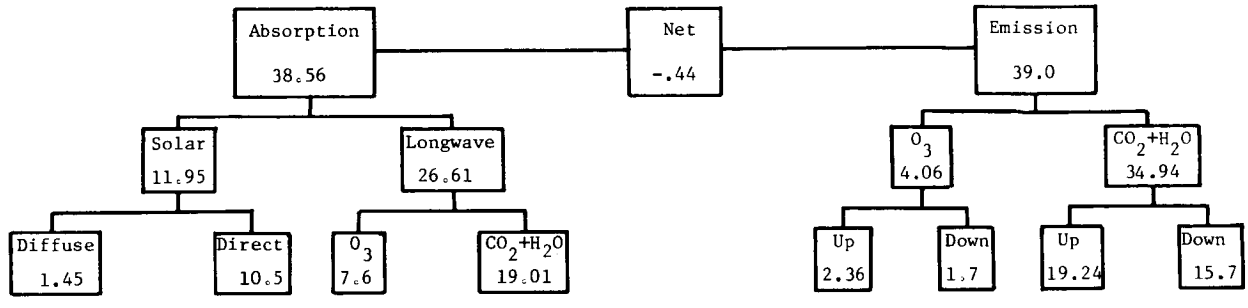

Relative Effects of O_3 and CO_2+H_2O in the Stratosphere

O_3 (=11.95+7.6-4.06)=15.49

CO_2+H_2O(=19-34.94)= -15.94

Stratospheric Effect on the Tropospheric Energy Balance

(a) Total

Solar = -10.5x.69= -7.2

IR = 17.4

Net = (17.4-7.4) 10.2

(b) O_3

Solar = -7.2

Longwave, O_3= 1.7

Longwave, (CO_2+H_2O)=7.8 (15.7/2)

Net 2.3

TROPOSPHERIC ELECTRIFICATION

Bernard Vonnegut
Atmospheric Sciences Research Center
State University of New York at Albany
Albany, New York 12222

1. INTRODUCTION

The solid Earth carries a negative charge of approximately 10^6 C and the lower atmosphere an equal, opposite charge. While a number of charging processes in the lower atmosphere are involved, such as erupting volcanoes, snow, sand and dust storms, and the bubbles bursting from the oceans, the primary cause of the Earth's electrification is activity of the approximately 1,000 thunderstorms that are taking place at any time (Chalmers, 1967). Though we know that the electrification of these clouds is caused by the accumulation of regions of charged water particles, there is no general agreement concerning which of the various processes that have been proposed to account for this is primarily responsible. Not only do we lack a satisfactory explanation of the cause of the electrification within the cloud, but we are also unclear what role this electrification plays in the meteorological processes that take place in the lower atmosphere.

It should be noted that while thunderstorms are undoubtedly the principal source of atmospheric electrification under most conditions, it is possible that extraordinary volcanic eruptions may sometimes play an important role. These have on occasion been observed to cause lightning displays rivaling or surpassing those of the most intense thunderstorms. While measurements are lacking, it is conceivable that because of their great violence and because they rise tens of kilometers higher than thunderstorms and penetrate well into the stratosphere, large volcanic events may produce significant transient perturbations of the global atmospheric electrical circuit.

2. THUNDERCLOUD DEVELOPMENT

The first stage of the development of the thundercloud begins when warm, moist air, because of its lower density, converges and forms an updraft. As a result of adiabatic expansion, the air cools as it rises. Because of this cooling, the relative humidity increases. When the air has risen to the level where its relative humidity is a few percent in excess of saturation, the moisture begins condensing as small water droplets tens of micrometers in diameter. When this happens, the updraft becomes visible as a cloud, the flat base marking the condensation level.

The condensation of water vapor is an important factor in the development of the cloud, for it releases heat into the updraft that increases its buoyancy, and the condensation thus provides much of the energy needed for cumulus development.

During the early stages of convection, large numbers of "fair weather cumulus clouds" develop. Even though they may rise to altitudes of 5 km or more, they exhibit little or no observable electrification. The electrification process is observed to begin when one of the fair weather clouds suddenly grows and becomes larger and taller than its neighbors. For reasons that are not understood, regions of space charge begin to accumulate within the cloud, and the electric field begins to increase exponentially, doubling every few minutes.

Because of the heat being released by the condensation process, the cloud can remain buoyant as it rises for distances of many kilometers, the air experiencing an upward vertical acceleration all the while. Finally, because most of the water vapor has condensed, the rising cloud becomes cooler than its environment and begins to decelerate. In the case of smaller thunderstorms this may occur at inversion layers in the troposphere, but in the case of larger storms the level of neutral buoyancy is usually at the tropopause.

Although the cloud air mass is no longer buoyant at this level, it possesses considerable vertical velocity, many tens of meters per second, as the result of its acceleration in the lower portion of the cloud. Because of its upward momentum, the cloud therefore continues to grow even though because of adiabatic cooling it may be far denser than the surrounding atmosphere. Finally, when the air of the cloud has lost its upward momentum, it reverses its direction and falls back very much like a fountain. It is this upward penetration and falling back that gives rise to the characteristic convective structure that can be seen in the satellite photograph of a thunderstorm cloud shown in Figures 1 and 2. The penetrative overshooting convective towers of the thunderstorm can cool to temperatures as low as -80°C, far colder than the surrounding atmosphere. These unusually cold portions of the upper part of the cloud are clearly evident in satellite infrared imagery and provide the basis of a useful technique for recognizing severe weather from space satellites.

Sometime during the vertical development of the cloud, usually when it reaches altitudes of the order of 9 or 10 km, the growing electric field becomes so large that lightning sparks take place, either within the cloud or between the cloud and ground. While the usual thunderstorm reaches altitudes of 10 or 12 km, as is shown in Figure 3, some smaller storms occurring in the semi-tropics have been observed to produce lightning even though the cloud height never exceeds 5 km. On the other hand, unusual very large thunderstorms of the sort that cause tornadoes have been observed that rise to altitudes in excess of 20 km, well into the stratosphere.

The electrical activity of thunderclouds, as indicated by the frequency with which they produce lightning, increases rapidly with cloud height. Shackford's data on New England thunderstorms (1960) in Figure 4 shows that lightning frequency increases dramatically with height. Ordinary thunderstorms produce lightning at the rate of 10 or 20 flashes per minute, while giant thunderstorms that rise well into the stratosphere are found to produce lightning at rates in excess of 1,000 per minute (Vonnegut and Moore, 1959). If thunderstorms are capable of interacting electrically with the upper atmosphere, it is to be expected that the giant storms should be of the greatest significance, for not only are they the most energetic electrically, but they also reach much higher altitudes than ordinary storms.

3. ELECTRIC FIELDS AND CURRENTS ABOVE THUNDERCLOUDS

Observations of thunderstorms show that most storms approximate a vertical dipole with tens to hundreds of coulombs in the upper part of the cloud and a negative charge of similar magnitude in the lower part of the cloud. It is to be expected that whatever influence the electrification of the cloud may have upon the upper atmosphere, it will arise primarily from the positively charged upper part of the cloud that in large storms can penetrate well into the stratosphere. At these altitudes the electrical conductivity of the atmosphere is two or three orders of magnitude greater than at sea level. We will therefore consider what is known concerning the electrical processes taking place in the upper part of the thundercloud and in the clear air above.

The first atmospheric electrical measurements above an active thunderstorm were made by Gish and Wait (1950) from a B-29 airplane equipped to measure electrical conductivity and electric field intensity. Their results confirmed the prediction of C. T. R. Wilson (1920) that here currents of the order of an ampere were conveying positive charge to the upper atmosphere. Figures 5 and 6 show typical electric field records obtained during flights over the top of the storm.

The record in Figure 6 shows that following a lightning discharge the electric field reverses polarity and briefly is even more intense than it was before the discharge. The field then relaxes and reverses, returning to about its original value at a rate approximating the electrical relaxation time of the air at airplane altitude.

Subsequent measurements made from instrumented balloons by Stergis, et al. (1957), at altitudes of 23 to 30 km MSL show that similar currents flow at higher altitudes.

Observations above thunderclouds from a U-2 airplane equipped with cameras and electrical field measuring equipment reported by Vonnegut, et al. (1966), disclose that the strong electric fields and conduction currents flowing above the cloud are confined to the penetrative cauliflower like convective cells rising above the anvil, such as can be seen in Figure 1.

Although it is clearly evident from the observations that have been made that currents are flowing from the tops of clouds to the upper atmosphere, there are aspects of this process that are not clearly understood. One of these is the manner in which the conduction of charge takes place in the upper part of the cloud. Because there appears to be no process whereby the cloud could serve as a source of fast positive ions, it would appear that at the upper cloud surface the transport of charge to the upper atmosphere is accomplished exclusively by the motion of negative ions moving downward to the cloud surface.

Any adequate description of the charge transfer process must explain what is happening to the approximate one coulomb of negative ions that is arriving at the cloud surface each second. From our knowledge of the behavior of ions and cloud particles it can be calculated that ions moving into the cloud under the influence of electrical forces will rapidly become immobilized by attachment to cloud particles before they have penetrated many tens of meters into the cloud (See Klett, 1972).

There appear to be several possible explanations for what is happening to the negative ions. If the cloud surface remains motionless, it is conceivable that the charge could continue to accumulate on the surface of the cloud under the influence of an ever increasing positive charge within the cloud until dielectric breakdown takes place. Alternatively, it is possible that the accumulating charge is removed from the surface of the cloud through the convective motions of the cloud. This might be accomplished through turbulent diffusion that would act to distribute the negative charge on the cloud surface throughout the positively charged cloud interior. Another possible way that the negative charge could be continuously removed is through large-scale convective movements of the cloud surface, as has been postulated by Grenet (1947) and Vonnegut (1955). According to this idea, there is a large-scale divergence on the top of the penetrative convective cell that would carry away the negative charge down the side of the cloud surface in a manner somewhat analogous to the transport of charge by the belt on the Van de Graaff high voltage generator. An understanding of what is taking place will require that we obtain better measurements than are presently available of the distribution of charged particles in the cloud top.

If the cloud is not a source of fast positive ions, it is evident that there must be an electrode effect of some magnitude in the clear air above the cloud surface, for while fast negative ions are drawn from the upper atmosphere to the cloud, positive fast ions will be repelled. It is therefore to be expected that above the cloud surface there would be a region of negative space charge in the form of negative fast ions and that the negative ion conductivity of the air would be very much larger than that from the positive ions. Probably one would not expect to see an electrode effect in the data taken by Stergis, et al., for their balloons were many kilometers above the cloud, probably well beyond any electrode layer. In the case of the Gish and Wait observations, which in some cases were made within a few kilometers of the cloud top, one might expect to see significant differences in their measured positive and negative ion conductivities. However, such a difference does not appear to exist. There seem to be two possible explanations for the absence of the screening layer during Gish and Wait's flights.

Possibly the electrode layer did not extend or had not yet established itself in the region of Gish and Wait's traverses. Certainly it is desirable to carry out further investigations to establish the existence and extent of electrode layers over active thunderclouds.

The discussion thus far has been concerned with only the simplest of cases above a thunderstorm, such as that shown in Figure 5, in which the electric field approximates that of a simple dipole with no transients of the sort produced by lightning. Figures 6 and 7 show progressively more complicated records in which the electric field changes very rapidly in magnitude and even in direction as the result of lightning discharges taking place within the cloud. It is possible, as has been suggested by Vonnegut, et al. (1966), and as is illustrated in Figure 8, that the reversal in the electric field attending the lightning discharge may be the result of the screening layer on the surface of the cloud when a dipole is destroyed as the result of lightning.

In the steady-state situation, such as illustrated in Figure 5, with no lightning the electric field above the cloud drops off rapidly with height above the cloud because of the dipole nature of the charge distribution in the cloud and because of the rapidly increasing conductivity of the atmosphere with

height. In the case when a lightning discharge occurs in which the field change can take place in a matter of 50 μsec, the transient electric field will undoubtedly be far larger than in the steady-state case. C. T. R. Wilson (1925) has suggested that since the dielectric strength of the atmosphere is proportional to the pressure, which falls off far more rapidly than the electric field of a dipole, it is conceivable that dielectric breakdown may occur at the time of lightning at altitudes many kilometers above thunderstorms. Luminous phenomena have occasionally been reported that may be the result of such a phenomenon. In this case, the electric discharge would be in the nature of a glow discharge rather than the usual lightning-like spark. Should such phenomena occur above thunderstorms, it is possible that the sudden current and ionization phenomena may play a significant role in processes taking place well above the tropopause.

Another ionization phenomenon above the thundercloud is a vertical lightning flash extending above the cloud into the clear atmosphere. This phenomenon reported by Wood (1951) is shown in Figure 9. A similar instance has been reported to the author by a NASA U-2 pilot who described a very similar phenomenon that he saw when flying at an altitude of approximately 20 km MSL above a large active thunderstorm. Although such descriptions of lightning discharges above thunderstorms are rare, the phenomenon may be fairly common, for such an occurrence would be difficult to see from below. Ions, space charge and electric currents and radiation produced by such phenomena may possibly have significant effects on the process taking place in the upper atmosphere.

The lightning discharges of the Earth's thunderstorms taking place at a rate of approximately 100 per second are strong sources of electromagnetic radiation that can possibly influence processes taking place in the middle atmosphere. Vampola (1977) has recently speculated that radiation from high powered VLF transmitters can induce slot electron precipitation and suggested that Bremsstrahlung thus produced could penetrate to the lower atmosphere. Because it is recognized that lightning is a strong source of radiation in the VLF region, it appears reasonable to suppose that it might produce a similar effect.

Although the effects are probably very small, it is worth noting that the coupling of electrical phenomena in the middle atmosphere to the Earth's surface will depend on the electrical conductivity of the lower atmosphere. It is therefore conceivable that fair-weather atmospheric electric phenomena may play a part in influences exerted by the troposphere. For example, natural cloudiness and fog can significantly reduce atmospheric conductivity, and in the case of aerosols produced by volcanoes or nuclear detonations these effects can extend well into the stratosphere. Man-made radioactivity will have the opposite effect and increase the conductivity of the atmosphere. It has been extrapolated from the projected development of nuclear power stations that within decades the electrical resistance between the Earth and the upper atmosphere will decrease significantly as a result of the introduction of Krypton 85 into the atmosphere (Boeck, 1976).

Because we now understand so little about the mechanisms by which thunderstorms become electrified and the role of electrical interactions in the processes taking place within the cloud, it is very difficult to assess the role that middle atmospheric phenomena may play in the meteorological processes taking place in the lower atmosphere. Because the current flowing from the upper atmosphere to the tops of thunderstorms and from the upper atmosphere to the Earth will be influenced

by ionization processes originating or modified in the middle atmosphere, it is reasonable to expect that this could modify the electrification process taking place within the storm. If the conduction current to the storm acts to oppose the electrification process, as would be the case according to electrification mechanisms based on the falling of charged precipitation, increased ionization could be expected to reduce thunderstorm electrification. On the other hand, if the current flowing from the upper atmosphere to the storm is part of the charge generation process, as suggested by Grenet and Vonnegut, then such increases in conductivity might be expected to increase the intensity of electrification. If electrification can play a significant role in cloud microphysical processes, as some have suggested (Vonnegut, 1978), it is conceivable that upper atmospheric processes could exert an effect on tropospheric weather phenomena.

REFERENCES

Boeck, W. L., Meteorological consequences of atmospheric Krypton-85. *Science* **193**, 195-198, 1976.

Chalmers, J. A., *Atmospheric Electricity*, 2nd ed., Pergamon Press (New York), 1967.

Gish, O. H., and G. R. Wait, Thunderstorms and the Earth's general electrification. *J. Geophys. Res.* **55**, 473-484, 1950.

Grenet, G., Essai d'explication de la charge electrique des nuages d'orages. *Anneles de Geophysique* **3**, 306-307, 1947.

Klett, J. D., Charge screening layers around electrified clouds. *J. Geophys. Res.* **77**, 3187-3195, 1972.

Shackford, C. R., Radar indications of a precipitation-lightning relationship in New England thunderstorms, *J. Meteorol.* **17**, 15-19, 1960.

Stergis, C. G., G. C. Rein, and T. K. Kangas, Electric field measurements above thunderstorms, *J. Atmos. Terrest. Phys.* **11**, 83-90, 1957.

Vampola, A. L., VLF transmission induced slot electron precipitation. *Geophys. Res. Letters* **4**, 569-572, 1977.

Vonnegut, B., Possible mechanism for the formation of thunderstorm electricity. *Proc. Conf. Atmos. Electr.*, Geophys. Res. Pap. No. 42, ed. R. E. Holzer, W. E. Smith, AFCRC-TR-55-222, 169-181, 1955.

Vonnegut, B., Electrical Behavior of an Airplane in a Thunderstorm. Technical Report, Contract FA64WA-5151, Arthur D. Little, Inc., Cambridge, Massachusetts, p. 3, 1965.

Vonnegut, B., Atmospheric electricity. *1978 Mc-Graw-Hill Yearbook of Science and Technology*, 99-101, 1978.

Vonnegut, B., and C. B. Moore, Giant electrical storms. *Recent Advances in Atmospheric Electricity*, Pergamon Press (New York), 399-411, 1959.

Vonnegut, B., C. B. Moore, R. P. Espinola, and H. H. Blau, Jr., Electrical potential gradients above thunderstorms. *J. Atmos. Sci.* **23**, 764-770, 1966.

Wilson, C. T. R. Investigations on lightning discharges and on the electric field of thunderstorms. *Phil. Trans. Roy. Soc. London, A*, **221**, 73-115, 1920.

Wilson, C. T. R. The electric field of a thundercloud and some of its effects. *Phys. Soc. London Proc.* **37**, 32D-36D, 1925.

Wood, C. A. Unusual lightning. *Weather* **6**, 64, 1951.

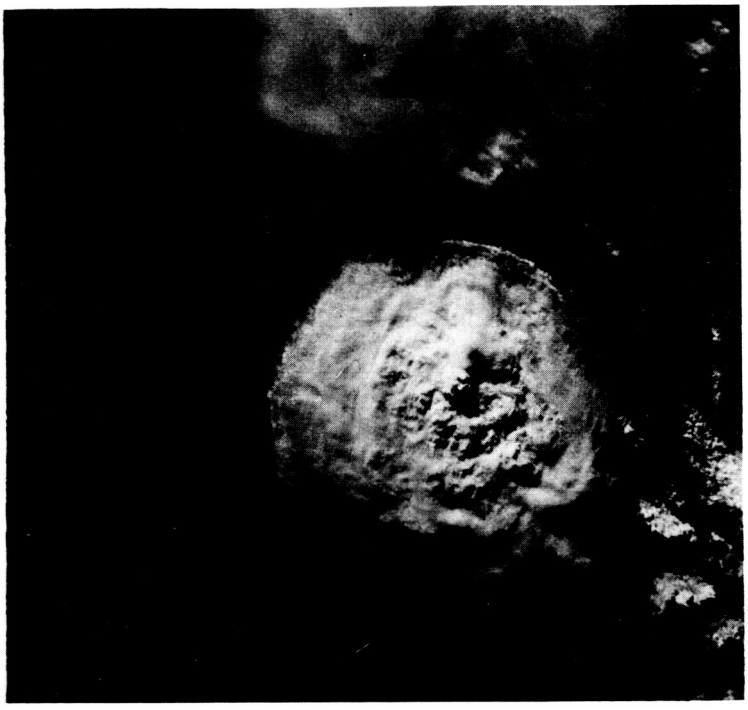

Figure 1. Thunderstorm over South America photographed from Apollo 9 Circular anvil is approximately 100 km in diameter.

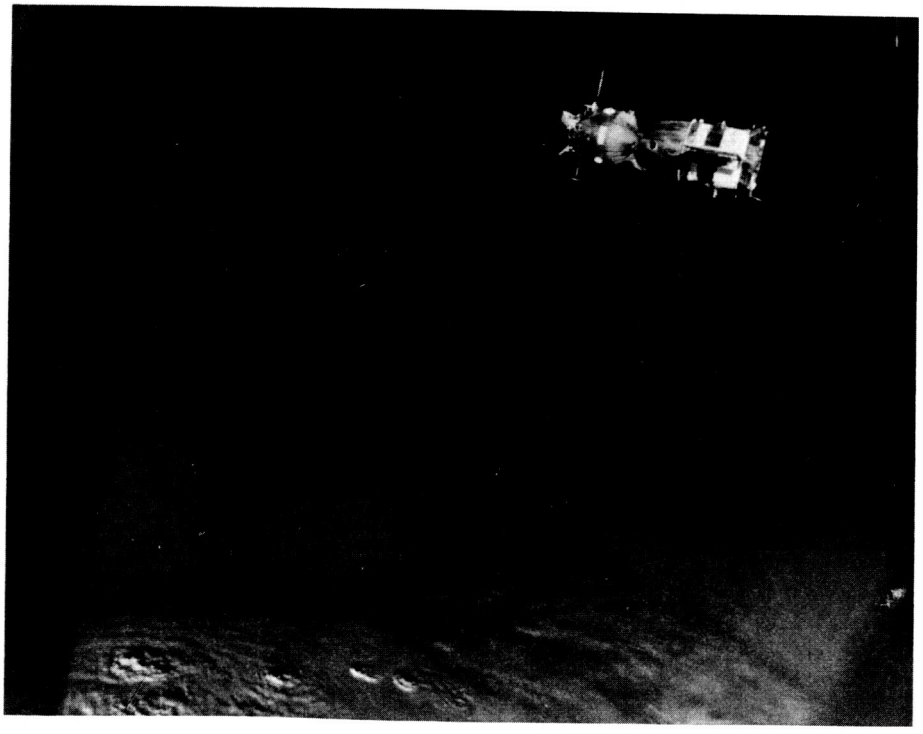

Figure 2. Thunderstorm cells photographed from Apollo/Soyuz mission.

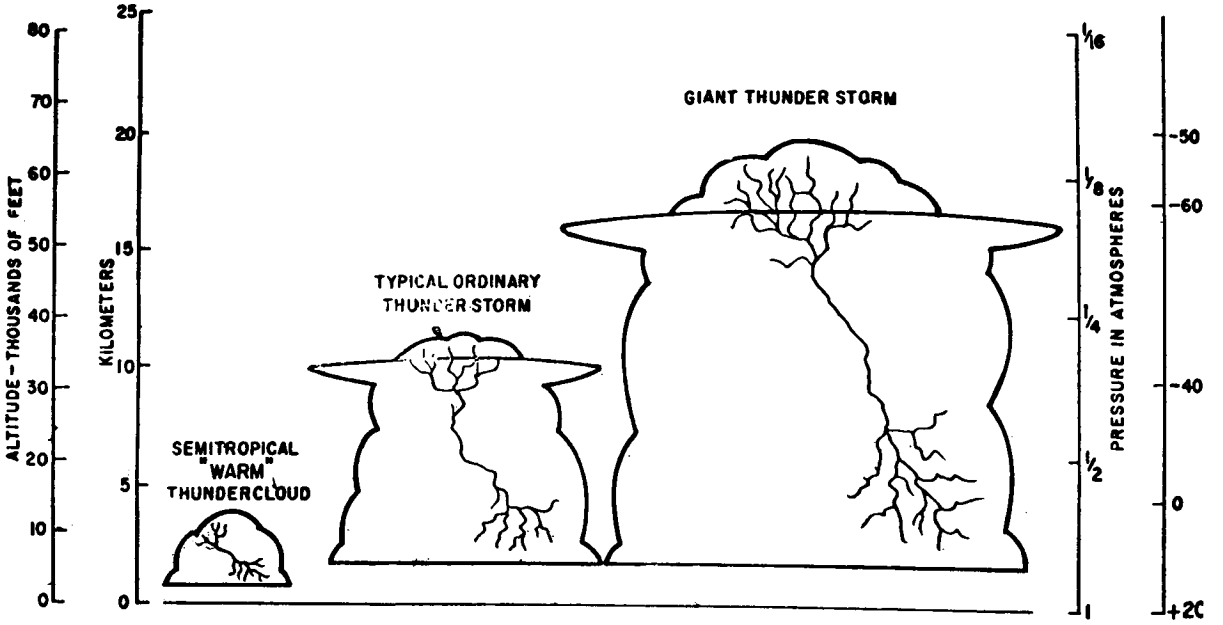

Figure 3. Approximate dimensions of small, ordinary, and giant thunderstorms (Vonnegut, 1965).

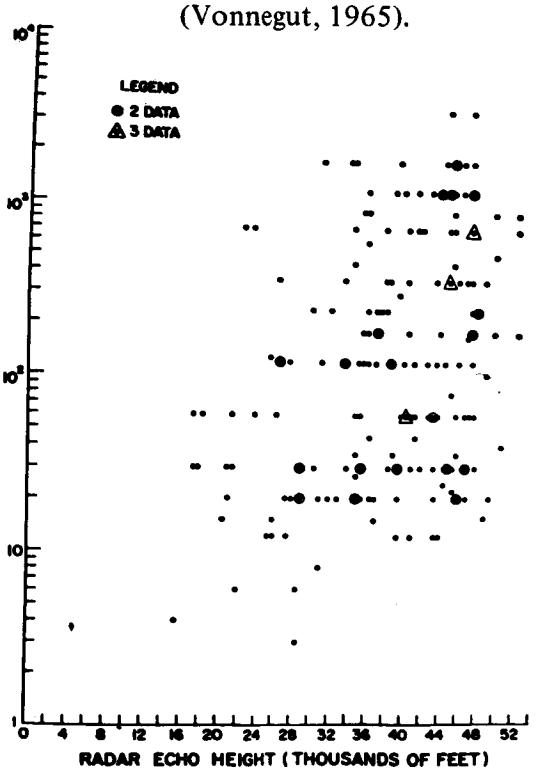

Figure 4. Plot of lightning frequency as function of cloud altitude (Schackford, 1960).

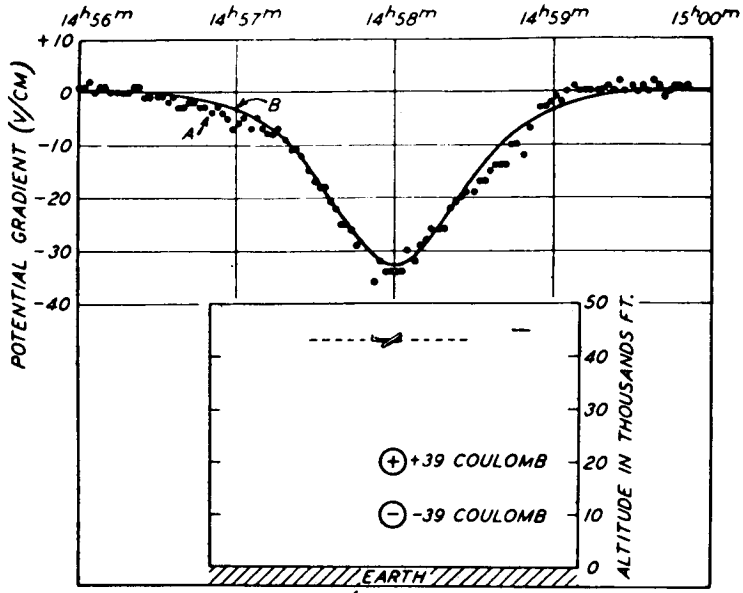

Figure 5. Electric field of thundercloud measured from an airplane (Gish and Wait, 1950).

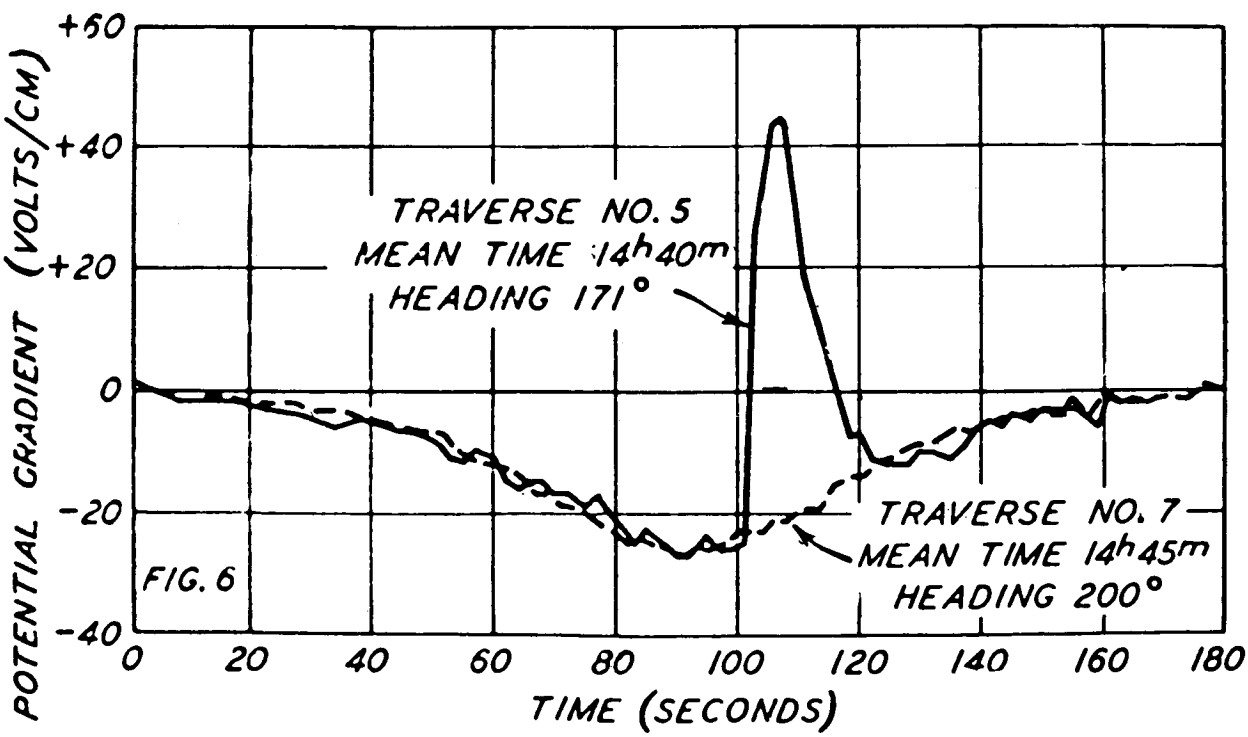

Figure 6. Electric field measured above thundercloud showing effect of lightning discharge within the cloud (Gish and Wait, 1950).

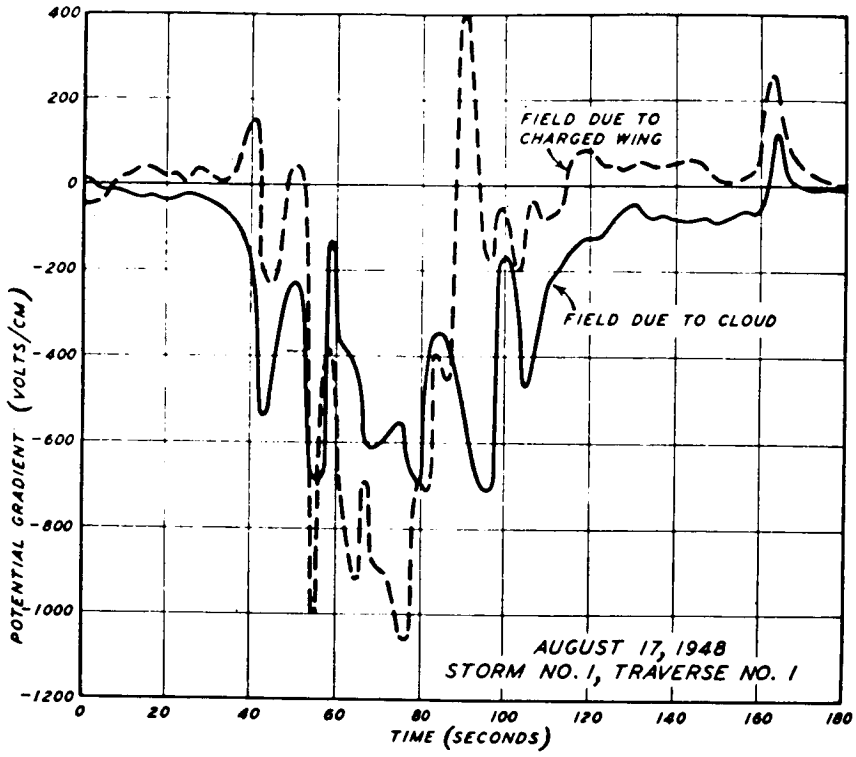

Figure 7. Electric field record above thunderstorm showing more complicated structure (Gish and Wait, 1950).

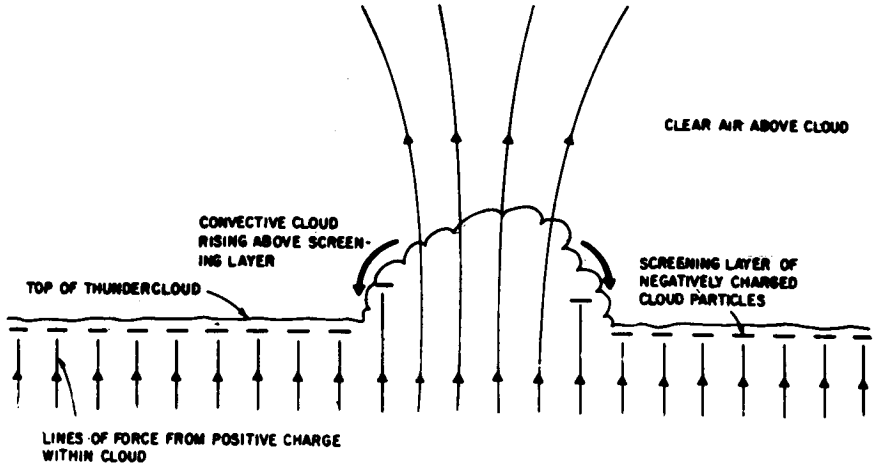

Figure 8. Sketch illustrating how the screening layer of negative charge formed on the upper cloud surface might be carried away as fast as it forms. This screening layer may be responsible for the field reversal observed when lightning occurs within the cloud (Vonnegut, et al., 1966).

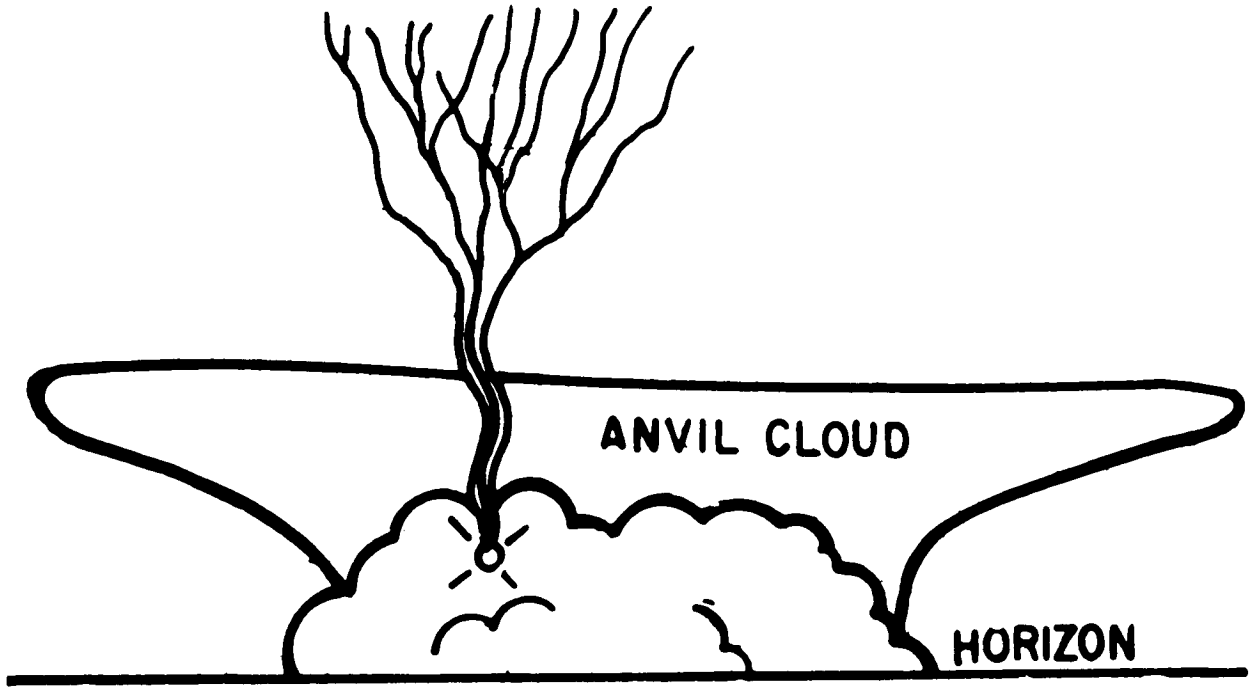

Figure 9. Sketch illustrating lightning display observed above the anvil of a cumulonimbus cloud (Wood, 1951).

ENERGY AND MASS TRANSPORT IN THE THERMOSPHERE

H. G. Mayr, I. Harris and N. W. Spencer
NASA/Goddard Space Flight Center
Laboratory for Planetary Atmospheres
Greenbelt, Maryland 20771

1. INTRODUCTION

The upper atmosphere or thermosphere is referred to as the region above the mesopause (80-90 km) where the neutral gas temperature begins increasing with height to values as high as 2000°K. It harbors a relatively dense plasma population–the ionosphere–which, controlled by electric and magnetic fields, affects the energetics and dynamics of the neutral atmosphere. Through current loads, the ionospheric plasma distribution can also affect the electric fields across the magnetosphere which in turn penetrate into the lower atmosphere (Park and Dejnakariuthra, 1977). The distribution of this plasma is influenced by atmospheric mass and energy transport. In the lower thermosphere, winds are a source for dynamo electric fields.

The average radiative heat input into the atmosphere (down to the tropopause), and the gas temperature are illustrated in Figure 1. Absorption of ultraviolet (UV) radiation with dissociation of O_3 and O_2 dominate in the mesosphere and lower thermosphere respectively. In the upper thermosphere, the extreme ultraviolet (EUV) radiation from the Sun is the principal source of ionization and heating (e.g. Hinteregger, 1976; Stolarski et al., 1975). In absolute terms the thermospheric input is small compared with the energy from UV and visible components of the solar spectrum that are absorbed below 90 km. In general, energy transfer downwards is, therefore, insignificant for the energetics of the lower atmosphere; but for the same reason, even a small leakage of energy due to upward propagating waves may have profound effects on the thermosphere. In terms of the specific heating rate relative to the low ambient density, the EUV source is comparatively large (Figure 1) accounting for the large temperatures in the upper atmosphere. It is believed that the EUV component of the solar spectrum is highly dependent on solar activity and causes large variations in temperature.

The thermosphere also receives solar wind energy through the magnetosphere in the form of precipitating particles and electric fields (Cole, 1971, 1975; Banks, 1977; Ching and Chiu, 1973; Roble and Matsushita, 1975). This energy is comparable to that from EUV absorption at high latitudes and significant for the global energy budget during magnetic storms.

Most of the thermal energy deposited in the upper atmosphere is ultimately carried through vertical heat conduction (molecular and eddy) into the lower atmosphere where radiative cooling becomes important; the large temperature gradients in the lower thermosphere (Figure 1) are a prominent signature of this transport process.

The meager information available on the turbulent properties of the lower thermosphere suggests that the turbopause is located near 110 km. Above that height, molecular diffusion (in contrast to mixing in the lower atmosphere) dominates such that major atmospheric species tend to follow height distributions corresponding to their individual mass and temperature. This diffusive separation in the composition (Figure 1) has profound effects on the formation of the ionosphere which is chemically tied to the neutral atmosphere.

The three major forcing functions due to EUV radiation and magnetospheric and lower atmospheric coupling are different in character, variable in time and highly nonuniform in space. Combined with the fact that nonlocal processes associated with large scale mass, energy and momentum transfer are very important, the dynamic state of the thermosphere is thus complex (illustrated in Figure 2). Thermospheric winds driven by the solar radiative input are typically on the order of 100 m/sec. Associated with these winds are variations in temperature, composition and plasma densities. Electric fields of solar wind-magnetospheric origin produce large scale convection cells with plasma drift velocities as high as a few km/sec (e.g. Cauffman and Gurnett, 1972). The ions accelerate, through ion-neutral drag, the neutral atmosphere and generate wind velocities up to 1 km/sec which are usually much larger than any of the thermally driven winds. These motions produce frictional interactions in the form of Joule heating and viscous dissipation which are important for the energy budget of the thermosphere, in particular during magnetic storms. Precipitating particles from the magnetosphere represent a source of ionospheric plasma at high latitudes and, in part, trigger the transfer of electric field energy to the neutral atmosphere. The ionosphere also plays the important role of damping atmospheric motions which in turn affects the global energy and mass distribution.

The "reverse" of electric field generated wind systems is the atmospheric dynamo. At altitudes below 150 km, the collisional interaction of the ions with the dense neutral atmosphere becomes so important that atmospheric winds eventually dominate the ion motions. While electric and magnetic fields still control the drift of electrons (which are less effective in exchanging momentum with the heavier neutral particles), a polarization or dynamo electric field is generated. This field extends into the F-region where it is responsible for the geomagnetic ionization anomaly and significantly modifies the thermospheric wind field (e.g. Volland, 1976). Dynamo electric fields also reach all the way down into the troposphere (e.g. Volland, 1977).

The generation mechanisms of dynamo electric fields are as varied as the forcing functions of thermosphere dynamics. Analysis indicates that the fundamental diurnal tide, which is excited in situ by UV and EUV radiation, drives the Sq current systems in the altitude range between 120 and 180 km (Richmond et al., 1976; Forbes and Lindzen, 1976a, b; 1977). Semidiurnal tides, excited in the ozone layer of the lower mesosphere, propagate up into the thermosphere. Mode coupling due to prevailing winds can change the tidal structure sufficiently to produce a close match between the height profiles of wind velocities and Hall conductivity. In that event relatively large dynamo currents are generated which may be telltales of dynamic processes in the mesosphere. Wind fields associated with energy and momentum sources of magnetospheric origin are presumably also involved in generating dynamo electric fields.

In the following, we shall discuss a few examples illustrating the effects of large scale energy and mass transport in the thermosphere: (1) The seasonal variations reveal temperature, composition and ionospheric anomalies involving energy exchange between the thermosphere and mesosphere. (2) The midnight temperature maximum in the thermosphere is interpreted as a signature of tidal waves emanating from the mesosphere and momentum coupling associated with ion drag. (3) The ionospheric storm in the F-region illustrates the intricate effects of large scale atmospheric winds driven by magnetospheric energization processes. (4) Atmospheric signatures of Joule heating and electric field momentum coupling are markedly different.

2. SEASONAL VARIATIONS

Some of the most striking anomalies in the upper atmosphere are the winter enhancements in the F2-region ionization, He concentration and gas temperature near the mesopause. The basic ideas that have contributed to an understanding of these phenomena go back to Kellogg (1961) who postulated, from an analogy with the global redistribution of ozone by atmospheric winds in the stratosphere, that the meridional circulation should transport significant amounts of oxygen from the summer toward the winter hemisphere. Kellogg furthermore proposed that accumulation of oxygen in winter and the ensuing three body recombination ($O+O+N_2 \rightarrow O_2+N_2$) could release enough chemical energy to affect the temperature anomaly near the mesopause. King (1964) presented evidence from the F-region winter anomaly (higher peak electron density in winter than in summer) to suggest that the relative abundance of atomic oxygen is enhanced in winter relative to summer. He invoked the circulation concept to explain the changing composition (consistent with a similar suggestion by Johnson, 1964). Johnson and Gottlieb (1970) estimated that meridional winds can account for the large winter He bulge that had been observed from satellite drag and mass spectrometer measurements (Reber et al., 1968; Keating and Prior, 1968).

Figure 3 illustrates in a very simplified geometry the most important transport processes that come into play in the seasonal variations of the thermosphere. We consider the zonal average during solstice conditions. Due to the inclination of the Sun, the summer hemisphere is heated preferentially, setting up pressure gradients across the equator that drive atmospheric winds from the summer toward the winter hemisphere. These winds transport significant amounts of energy and mass. Energy transport is primarily effective in the form of adiabatic cooling (in summer) and adiabatic heating (in winter) thus lowering the temperature contrast between both seasons. Downward heat conduction removes more energy in summer than in winter.

Mass transport takes place in three forms: (a) Thermal expansion and contraction leads to a density increase or decrease in the warmer or cooler regions of the atmosphere respectively; this process is most effective for the heavier constituents. (b) Wind induced diffusion primarily affects the minor species and most of all the lighter ones. Dragged along by the motions of the major constituent, the height integrated horizontal mass transport of He, for example, is proportional to its large scale height (and inversely proportional to its mass). As a result, the He concentration tends to decrease in summer and increase in winter which contrasts the effects of thermal expansion and contraction. (c) Mass transport by exospheric flow (e.g. Hodges, 1973) can be compared with fast diffusion. In this process, particles move in ballistic trajectories from the high-temperature or high-density regions toward the cooler or more tenuous regions on the globe. The resulting flow

velocity is highly temperature dependent ($\alpha T^{5/2}$) and becomes increasingly important for smaller masses so that exospheric transport significantly affects the summer to winter variations of He and essentially governs the H distribution.

The essential elements in the annual variations of the thermosphere are illustrated in results (Figure 4) from a three dimensional multi-constituent model that are in qualitative agreement with observations. Summer to winter variations at the poles are presented which are characterized by a substantial temperature contrast at high altitudes, a winter oxygen bulge below 350 km which is the major cause for the ionospheric winter anomaly in the F_2 - region and a very large (factor of 40) increase in the He concentration from summer to winter. In the lower thermosphere near the mesopause, the winter anomaly in temperature is indicated. Meridional wind velocities of about 40 m/sec at the Equator are shown in the upper thermosphere. As signatures of the mesopause temperature anomaly, the meridional winds reverse direction near 130 km and the zonal winds (at mid latitudes) reverse it near 100 km. Below 80 km, the zonal winds change direction again, consistent with the geostrophic conditions for a temperature maximum in summer.

Figure 5 illustrates in more detail some of the processes that contribute to the seasonal temperature variations in general and the formation of the mesopause temperature anomaly in particular. Results from a theoretical model serve to delineate their significance. Shown are computed relative amplitudes at the poles, plus or minus signs indicating a maximum in summer or winter respectively. Energy from EUV radiation (thin line) is the principle source of the temperature (and density) variations in the upper thermosphere. Atomic oxygen, transported from the summer toward the winter hemisphere recombines and releases energy (Kellogg, 1961) that significantly contributes to the winter anomaly near 90 km (minus sign). This process is in part compensated by the O_2 dissociation and heating from the Schumann-Runge continuum ($UV(O_3)$, in dashed line) which tends to produce a temperature maximum in summer (plus sign). In the mesosphere, where ozone is the principle absorber of solar radiation ($UV(O_3)$), radiative equilibrium (with higher temperatures in summer) and geostrophic conditions prevail. Above 80 km, the meridional circulation driven by this source, however, becomes effective. Thus, both adiabatic heating and recombination energy from O, which is transported toward the winter hemisphere, contribute to increase the gas temperature near the mesopause in winter (dotted line).

The combined effect of these processes which involve thermospheric and mesospheric energization processes reproduces the mesopause temperature anomaly qualitatively—but not quantitatively. Observed temperature amplitudes near 90 km are more than a factor of two larger than those predicted in Figure 5 (CIRA, 1972). Circumstantial evidence from a variety of thermospheric measurements suggest that an important additional energy source is active near the mesopause level. In Figure 6 two computer solutions are presented, the one in solid lines describing the combined effect (in temperature and composition) from the above discussed processes. The second solution in dashed lines includes an additional heat source with a maximum near 90 km in the winter hemisphere, which causes a circulation component schematically illustrated with dashed lines in Figure 5. The results are compared with the empirical MSIS model (Hedin et al., 1977). As postulated, this additional source produces the desired increase in the magnitude of the temperature anomaly near the mesopause. Noting the associated changes in thermospheric temperature

and composition throughout the thermosphere, it is apparent that this source also improves the overall agreement between theory and observations. The magnitudes of the winter oxygen bulge and temperature variation in the upper thermosphere, for example, decrease. Furthermore, the wind velocities above 200 km (shown in Figure 4) tend to increase somewhat, which is in the right direction to accommodate recent radar backscatter measurements (Emery, 1978a, b). In the lower thermosphere the heat source accounts for the observed reversals of the zonal and meridional winds.

At this point, the postulated forcing function is phenomenological in nature. But it is reasonable to speculate that it may actually be due to dissipation of planetary waves that originate in the troposphere and propagate up into the mesosphere during winter (Matsuno, 1975) when the wind shear activity (turbulence) is also observed to be enhanced (Zimmerman et al., 1977).

An important element in understanding the seasonal variations of the thermosphere is the feedback from composition changes (due to wind induced diffusion) on the wind fields and temperature variations. Analysis indicates that the winter oxygen bulge shown in Figure 4 contributes significantly to decrease the pressure gradient that in turn drives the meridional circulation. As a result, the energy transport by thermospheric winds from the summer to the winter hemisphere is reduced and a relatively large temperature variation is maintained. Model calculations show, more specifically, that in the upper thermosphere the relative amplitude of the annual temperature variations would be *reduced* by about a factor of three and the meridional wind speeds would *increase* by about a factor of two if wind induced diffusion of oxygen were neglected. This effect was also shown to be important for the dynamics and energetics of the cytherean thermosphere (Dickinson and Ridley, 1975, 1977).

Due to the difference in time scales, some of the processes discussed above are to a much lesser extent operative in the diurnal variations of the upper atmosphere. To illustrate that, we compare in Table 1 certain parameters that characterize the diurnal and annual variations. Considering the global scale geometries, the relative amplitudes (normalized to the global average) refer to the Equator for the fundamental diurnal tide and to the poles for the annual tide; the wind velocities which tend to maximize in regions of largest pressure gradients, refer to the poles and Equator respectively. More energy (factor of three) goes into the diurnal tide and, correspondingly, the wind velocities are higher. Because of the long time constant for mass transport, the effects of wind induced diffusion on He and O are much larger for the annual component in spite of its comparatively small wind velocities. The winter oxygen bulge, in turn, accounts to a considerable extent for the magnitude of the annual temperature amplitude which, in comparison with the diurnal tide, is disproportionally large for the small annual energy component.

3. THE MIDNIGHT TEMPERATURE ANOMALY

In situ satellite measurements on Atmosphere Explorer-E have revealed pronounced temperature enhancements near midnight (Spencer et al., 1977; Spencer et al., 1979) which are presumably related to similar features that were inferred from radar backscatter (Harper, 1974) and mass spectrometer measurements on OGO-6 (Hedin et al., 1974). The phenomenon is observed most of the

time, but is highly variable and takes on various forms ranging from a flat plateau to a sharply defined maximum in which the temperature occasionally reaches or exceeds daytime values.

Power spectra for the observed diurnal temperature variations (Hedin et al., 1979) show that: (a) the fundamental tide (with zonal wave number m=1) is not significantly affected by the anomaly, (b) the changes in the magnitude of the midnight temperature maxima are proportional to changes in the semidiurnal (m=2) amplitudes, and (c) in general, the midnight anomaly can be adequately described with wave numbers $m \leqslant 3$ and fairly accurately with $m \leqslant 5$. This analysis is the basis of an interpretation that recognizes the unique properties of the semidiurnal tide in the thermosphere. It suggests that coupling processes between mesosphere, upper atmosphere and ionosphere come into play (Mayr et al., 1979).

A block diagram outlining the elements of the model is shown in Figure 7. The fundamental diurnal tide (m=1) is primarily excited in situ by absorption of EUV (and UV) in the thermosphere and it is affected by the global average ion distribution. Both source and ion drag are presumably stable for time periods of several days, and the observed invariance of this tidal component is hence understandable. In contrast, the semidiurnal tide of the upper thermosphere is much more complex. It has three major contributions of which only the EUV source is stable but relatively small. The other two contributions are due to tidal waves originating in the lower atmosphere and nonlinear momentum coupling associated with the diurnal (m=1) variations in the wind field and ion density. Both components are of comparable magnitudes but out of phase; variability of one or both thus translates into lability of the midnight temperature anomaly. Mode coupling associated with prevailing winds in the lower atmosphere, which are variable, significantly affects the structure and propagation properties of the semidiurnal tide (Lindzen and Hong, 1974). The diurnal variation in the ionospheric plasma concentration is strongly influenced by dynamo electric fields which in turn are generated by tidal winds in the lower thermosphere (e.g. Forbes and Lindzen, 1976). For the terdiurnal component (m=3) the contributions from EUV heating and lower atmospheric tidal waves are small, while nonlinear coupling associated with diurnal variations in ion drag dominates. This involves the semidiurnal wind field which is, in parts, excited in the mesosphere. Due to the large diurnal component in ion density the variability of both contributes again to the lability of the midnight temperature anomaly.

Ion-neutral momentum coupling is perhaps the single most important process for generating the midnight temperature anomaly. Its signatures have also been seen in a number of other phenomena such as the apparent geomagnetic field control of the gas temperature that was linked to the equatorial F-region anomaly (Hedin and Mayr, 1973). Figure 8 illustrates the interaction. Thermospheric motions are damped by ion drag, an increase or decrease in ion density thus leads to a decrease or increase in wind velocities. During daytime the atmospheric motions meet significant resistance by the dense ionospheric plasma (controlled by magnetic and electric fields) which contributes to insulation and energy trapping. The low ion concentrations at night, on the other hand, permit an effective energy exchange that can lead to a secondary temperature maximum. One can readily see that the nonlinear interaction between the diurnal components of wind field and ion density is capable of generating a semidiurnal tide (see Figure 7).

Figure 9 illustrates more quantitatively the amplitudes of temperature and N_2 density computed for semidiurnal tides generated (a) in the lower atmosphere by absorption of solar radiation in the water vapor (H_2O) layer near the Earth's surface and in O_3 near 50 km, (b) from UV and EUV absorption in the thermosphere and (c) by ion drag momentum coupling. Plus and minus signs give a crude indication of phases near 00LT (or 1200 LT) and 0600LT (or 1800LT) respectively. The results show that the ion drag component contributes to a temperature enhancement (plus) near midnight (0200 LT). The waves from below dominate in the temperature and N_2 density below 180 and 280 km respectively, thus shifting the phases toward later local times at lower altitudes which is in qualitative agreement with satellite composition measurements (Newton et al., 1975; Hedin et al., 1979). Also shown are the contributions to the terdiurnal tide of the temperature. They result primarily from ion drag coupling with the semidiurnal wind fields excited by O_3 and ion drag. Both components are nearly in phase and tend to produce a narrow temperature maximum (plus) near midnight.

A synthesis of the theoretical results for tides up to order m=4 is shown in Figure 10. It resembles the observed temperature anomaly. Although the maximum occurs almost two hours after midnight it is still within the range of observations. The variations in temperature are similar at 200 and 400 km, but those of N_2 are markedly different. The latter may in part explain the apparent discrepancy between the empirical OGO-6 model (Hedin et al., 1974) for which Tg was inferred from N_2 measurements near 400 km and the recent MSIS model (Hedin et al., 1978) which used a large N_2 data base from lower altitudes.

4. IONOSPHERIC STORMS

Energy deposition from the magnetosphere due to particle precipitation and Joule heating has been shown to be a permanent feature of the thermosphere at high latitudes (e.g. Banks, 1977). Within the auroral oval, Banks observes that the total energy input can reach values as high as 100 ergs/cm^2 sec. Rocket borne electric field, particle and electron density measurements (Maynard et al., 1977; Evans et al., 1977) have indicated that local electric fields and Joule heating rates are anticorrelated with height integrated Pederson conductivity as well as heating rates from auroral electrons. In particular, it was discovered that electric fields inside auroral arcs are depressed relative to the adjacent regions such that the total rate of energy deposition (Joule and particle) varies gradually across auroral boundaries. The measurements thus suggest (Evans et al., 1977) that magnetospheric energy is channeled into particle acceleration at the expense of electric fields. Energetic electrons thereby provide a portion of field aligned or Birkeland currents (within auroral arcs) which in turn are fed by Pederson currents outside auroral arcs (Burch et al., 1976a, b; Evans et al., 1977).

Owing to the localized nature of these energization processes, the large scale heating rates are much smaller than the above quoted value. But even for the global energy budget of the thermosphere these sources are important. In particular during substorms and magnetic storms, the auroral oval expands over time periods of hours and days and produces dramatic effects in the upper atmosphere. From satellite drag measurements it has been known for some time that the mass density (and total pressure) of the thermosphere increase almost uniformly on a global scale during magnetic storms (Jacchia et al., 1967), the polar region being only slightly more affected than the equatorial region (Roemer 1967). Satellite composition measurements reveal that under these conditions large N_2 increases at auroral latitudes are associated with depletions of He and O (at lower

altitudes), while at lower latitudes the abundances of these lighter species are enhanced in relation to those of N_2 and Ar (e.g. Taeusch et al., 1971; Proelss and von Zahn, 1974, Chandra and Spencer, 1975, 1976). Temperature measurements from chemical seeding and airglow observations show large and sometimes localized disturbances during periods of enhanced magnetic activity (e.g. Hays et al., 1969; Blamont and Luton, 1972). Observations of meridional wind velocities at mid latitudes reveal that during magnetic storms either the poleward EUV driven winds are weakened during daytime or the corresponding equatorward winds are enhanced at night (e.g. Hays and Roble, 1971; Brekke et al., 1974; Hernandez and Roble, 1977).

Magnetic storm effects in the F_2-region ionization have been studied extensively with sounding techniques (e.g. Matsushita, 1959; Evans, 1970, 1973; Obayashi, 1972) and satellite in situ measurements (e.g. Proelss et al., 1975; Hedin et al., 1977). The statistical analysis of F_2 peak critical frequencies by Matsushita (1959) reveals some of the fundamental properties of ionospheric storms: At high and mid latitudes, the electron density increases initially during the onset of the storm. As time progresses, this positive phase gives way to a very large, long lasting depression in ionization (negative phase) that persists for some time after the magnetic disturbance has decayed. At low latitudes, the positive phase is observed to persist throughout the entire time period of the ionospheric storm.

Although we are far removed from a quantitative understanding of these phenomena, some of the ingredients in the complex system of interaction processes are known. Since the work of Chimonas and Hines (1970) and Testud (1970), magnetic storm activity in the auroral zones has been recognized as an important source for gravity waves and travelling ionospheric disturbances. The generation mechanisms and propagation properties of such waves and their importance for the global redistribution of energy have been the subject of a number of observational and theoretical studies (Francis, 1975; Yeh and Liu, 1974; Richmond, 1978, 1979; Richmond and Matsushita, 1975). Richmond and Matsushita (1975) and Richmond (1978) have developed sophisticated theoretical models describing the substorm response of thermosphere dynamics driven by auroral zone currents, ion drift momentum sources and precipitating particles. Their analysis shows that such a disturbance will generate gravity waves that propagate equatorwards with speeds of about 750 m/sec, while the amplitudes of temperature and wind fields decay slowly before reaching the Equator. Dynamo action produced by "ringing" in the wind velocities maintains a residual polarization electric field some time after the decay of the substorm activity. While short period waves dominate in the vicinity of the auroral zones, the longer period waves prevail at large distance from the source which substantially agrees with observed wave trains in temperature and vertical velocities (e.g. Spencer et al., 1976). Important as these waves are for the generation of travelling ionospheric disturbances, their role in the transmission of energy from the auroral zones to low latitudes is apparently a very minor one when compared with that of the large scale thermospheric circulation (Richmond, 1979).

The smaller the horizontal dimension of a disturbance, the larger the generated wind velocity, its divergence and rate of horizontal energy transfer. As a consequence of this property, the thermosphere acts like a low pass filter in which the shorter scale disturbances (except for resonance conditions associated with gravity waves, for example) are preferentially damped by wind induced energy transfer (Volland and Mayr, 1971); large scale disturbances thus tend to prevail during

magnetic storms and the global increase in mass density (e.g. Jacchia et al., 1967) is principally understandable. In the diffusive thermosphere, energy and mass transport processes are somewhat more complex and, analogous to Figure 3, are illustrated in Figure 11 for the zonally averaged storm time component. High latitude heating by precipitating particles and Joule dissipation increases the atmospheric temperature (and pressure) and drives winds toward the Equator where adiabatic compression raises the temperature. In parallel, wind induced diffusion takes mass, preferentially O and He, out of the polar region and accumulates them at low latitudes. There is a geometry factor involved in that the area of upwelling near the poles (where mass flow diverges) is much smaller than the horizontal extent near the Equator over which subsidence (convergence) occurs. Flow continuity then requires that the transport effects on the minor species are much less pronounced (and of opposite direction) at low latitudes than at high latitudes.

Figure 12 shows these composition features as inferred from the neutral atmosphere composition experiment (Nace) on Atmosphere Explorer-C (Pelz et al., 1973) during a major magnetic storm in February, 1974 (Hedin et al., 1977). The results were interpreted with a multiconstituent circulation model (Mayr and Volland, 1973), which describes the zonally averaged storm component (analogous to D_{st}). Apart from the apparent 24 hour periodicity in the data, which reflects longitudinal variations that were not considered in the analysis, the theoretical results substantially agree with the observations. The depletions of O and He at high latitudes, coinciding with the observed increase in N_2 and Ar, are reproduced. Data taken at lower latitudes, in particular, provide a crucial test for the validity of the circulation concept. As predicted, the observed density enhancements in O and He are at lower altitudes comparable to or even exceed the equatorial density buildup in N_2 and Ar. Maximum equatorward meridional winds of about 60 m/sec were computed in this analysis.

In the context of the circulation concept, thermospheric winds and composition changes are intimately coupled. Their combined effects on the F2 region ionization are schematically illustrated in Figure 13. With the onset of the magnetic storm, magnetospheric energy deposition increases the atmospheric pressure at high latitudes. Almost instantly, equatorward winds are set up that carry the ionization to higher altitudes where the ionospheric loss rates ($O^+ + N_2 \rightarrow NO^+$, $O^+ + O_2 \rightarrow O_2^+$) are diminished. As ionization is continually produced by photons and electron impact, the density at the F_2 peak should initially increase and thus contribute to the observed positive phase (Kohl and King, 1967; Jones and Rishbeth, 1971). Time progresses, and wind induced diffusion, which is relatively slow, becomes gradually effective in depleting the oxygen population at higher latitudes, while the densities of the heavier species N_2 and O_2 continue to increase. These changes in composition chemically reduce the ionization and eventually overcompensate the wind effects such that they dominate to produce the negative phase in ionospheric storms (Seaton, 1956; Duncan, 1969; Chandra and Herman, 1969). Oxygen transport toward the Equator and wind effects contribute jointly to increase the ionization at lower latitudes.

Results from a self consistent hybrid model (Mayr et al., 1978; Miller et al., 1979) illustrate these effects at 60° and 20° latitudes (Figure 14). For a storm related heat source Q that energizes the thermosphere over a time period of about four days, we show (1) the resulting relative variations of O and N_2 normalized to quiet conditions, (2) the component of the meridional wind velocity parallel to the magnetic field B, (3) the electron density O^+ at various altitudes, and (4) the height

h_{F2} of the F_2 peak. The response time of the wind field (relative to Q) is very short compared with that of the neutral composition; thus the composition changes (O/N_2 ratio, which chemically determines the O^+ concentration) are largest near the time the wind velocity already returned to zero. This time delay, which becomes even more effective for shorter lasting storms, accounts for the characteristic sequence between the positive and negative phases in the ionization responses. At lower latitudes, the composition changes are small, thermospheric winds are relatively more effective and the positive phase prevails at the height of the F_2 peak and above. The variations in h_{F2} closely conform with those of the field aligned velocity component.

5. ELECTRIC FIELD MOMENTUM COUPLING

Neutral wind velocities up to 1 km/sec have been measured at high latitudes (e.g. Hays and Roble, 1971; Wu et al., 1974) and have been attributed to momentum coupling from ExB drifts (e.g. Cauffman and Gurnett, 1972; Fedder and Banks, 1972; Banks and Doupnik, 1975; Heelis et al., 1974; Brinton, 1975; Hanson and Heelis, 1975) that in turn are induced by electrostatic fields of magnetospheric origin (e.g. Heppner, 1977; Volland, 1973). Straus (1978) recently reviewed the observations and theoretical analysis dealing with large scale electrodynamic processes that affect the neutral atmosphere at high latitudes.

In the thermosphere dynamics one is accustomed to associate winds with energy and mass transport. Energization by absorption of solar radiation and magnetospheric processes, for example, drives winds that transport energies comparable to those initiating these motions. The previous three chapters were to illustrate the significance of such processes for the seasonal, diurnal and magnetic storm variations. But important as these winds are for the energetics and mass distribution, their magnitudes are only on the order of 100 m/sec which is usually small compared with the above quoted wind velocities in the auroral zones that are induced by electric field momentum coupling.

The solution for this apparent conflict focuses on an elementary theorem in dynamics stating that any vector field can be described as a superposition of two components, one that has a divergence but no curl (irrotational) and another one that has a curl but no divergence (solenoidal). Mainly the former is responsible for energy and mass transport. In the zonally averaged circulation, these fields happen to coincide with the meridional and zonal velocities respectively. However, that association is not valid in general and it is then, from the standpoint of physical interpretation, advantageous to turn a representation in terms of divergence- and curl-velocities.

We shall briefly discuss here some distinctions between density and temperature signatures (Figure 15) of wind systems driven by Joule heating and Lorentz force. These forcing functions produce two very different classes of wind fields, one with a large divergence and the other one representing primarily a curl field. Although in reality both excitation processes are closely related, it is instructive to describe them separately. Results from a three dimensional model are shown in the form of amplitudes and phases for the diurnal component with a period of 24 hours and a wave number n=9 (corresponding to a characteristic horizontal dimension of 2000 km) which is representative of the convection electric field pattern at high latitudes. For illustrative purposes, both

forcing functions were chosen such that the wind velocities were the same at the poles (250 m/sec). From this comparison the following conclusions are drawn: (a) In the upper thermosphere the wind field driven by the momentum source is more than 20 times less "effective" in producing density variations (and a factor of 100 times less for the temperature) than the winds associated with Joule heating. (b) Under Joule heating the Tg and heavier atmospheric species N_2 and Ar are out of phase with O and He, while for the electric field momentum source the lighter gases O and He vary in phase with N_2 and Ar.

Figure 16a elucidates the mechanism of momentum coupling for an electrostatic field E. Except for the factor B^{-2} the ion velocity $V_i = (ExB)B^{-2}$ is a curl field. By collisional momentum transfer, a corresponding curl component is imposed on the neutral wind velocity, and the Coriolis force in turn couples momentum into a divergence field. This divergence component would be relatively large if it were not for the thermodynamic feedback from adiabatic heating and mass redistribution. Thus induced backpressure, however, counteracts and significantly dampens the divergence field to the degree that its contribution to the total wind velocity becomes actually very small. This situation is in contrast to thermally driven winds where under the influence of ion drag and viscosity the flow can proceed along pressure gradients; the generated divergence component is thus relatively more important and hence the total wind field is much more "efficient" in affecting temperature and density variations. This distinction may be likened to the mixing of paint, where the steady rotation (curl field) is relatively ineffective compared to shaking which produces a divergence field.

The large differences between heat and momentum source signatures in the phase relations of temperature and composition are heuristically discussed in Figure 16b. Given an external heat source Q (e.g. Joule heating), the atmospheric pressure increases and that in turn drives (divergence) winds that act as sinks of energy ($-\Delta Q$) and mass ($-\Delta M$). The net energy change ($Q-\Delta Q$) is usually dominated by the source and remains positive. As a result there is an increase (positive) in the temperature ($\Delta T>0$) and density of the major gas ($\Delta N_2>0$). For the minor and lighter gas (such as He) wind induced diffusion represents a mass sink ($-\Delta M$) (corresponding to the energy loss $-\Delta Q$) that dominates. In the absence of a particle source the density therefore decreases ($\Delta He<0$) bringing forth the inverse relationship between heavier and lighter gases. With a momentum source that (somehow) drives a divergence field, a major distinction is that the external heat source Q is zero. All other conditions being the same as those for the case of Joule heating, the energy sink ($-\Delta Q$) then determines that the temperature ($\Delta T<0$) and major gas ($\Delta N_2<0$) decrease, in phase with the corresponding decrease of the lighter gas ($\Delta He<0$). At higher latitudes, the Joule heating signature rather than the momentum source signature is observed in the composition. This supports the contention that the electric field momentum source drives a wind circulation with a weak divergence field that is incapable of transporting large amounts of mass and energy.

ACKNOWLEDGMENTS

We are indebted to R. E. Hartle for valuable comments and E. M. Coulson for her assistance in preparing the manuscript.

REFERENCES

Banks, P. M., Observations of joule and particle heating in the auroral zone, *J. Atmos. Terr. Phys.*, **39**, 179, 1977.

Banks, P. M., and J. R. Doupnik, A review of auroral zone electrodynamics deduced from incoherent scatter radar observations, *J. Atmos. Terr. Phys.*, **37**, 951, 1975.

Blamont, J. E., J. M. Luton, and J. S. Nisbet, Global temperature distributions from Ogo-6 6300Å airglow measurements, *Radio Sci.*, **9**, 247, 1974.

Brekke, A., J. R. Doupnik, and P. M. Banks, Observations of neutral winds in the auroral E region during the magnetospheric storm of August 3-9, 1972, *J. Geophys. Res.*, **79**, 3773, 1974.

Brinton, H. C., In situ measurements of plasma drift velocity and enhanced NO^+ in the auroral electrojet by the Bennett spectrometer on AE-C, *Geophys. Res. Lett.*, **2**, 243, 1975.

Burch, J. L., S. A. Fields, W. B. Hanson, R. A. Heelis, R. A. Hoffman and R. W. Janetzke, Characteristics of auroral electron acceleration regions observed by Atmosphere Explorer C, *J. Geophys. Res.*, **81**, 2223, 1976a.

Burch, J. L., W. Lennertsson, W. B. Hanson, R. A. Heelis, J. H. Hoffman, and R. A. Hoffman, Properties of spike-like shear flow reversals observed in the auroral plasma by Atmosphere Explorer C, *J. Geophys. Res.*, **81**, 3886, 1976b.

Cauffman, D. P., and D. A. Gurnett, Satellite measurements of high latitude convection electric fields, *Space Sci. Rev.*, **13**, 369, 1972.

Chandra, S., and J. R. Herman, F-region ionization and heating during magnetic storms, *Planet. Space Sci.*, **17**, 841, 1969.

Chandra, S., and N. W. Spencer, Thermospheric storms and related ionospheric effects, *J. Geophys. Res.*, **81**, 5018, 1976.

Chandra, S., and N. W. Spencer, Exospheric temperature inferred from the Aeros-A neutral composition measurements, *J. Geophys. Res.*, **80**, 3615, 1975.

Chimonas, G., and C. O. Hines, Atmospheric gravity waves launched by auroral currents, *Planet. Space Sci.*, **18**, 583, 1970.

Dickinson, R. E. and E. C. Ridley, A numerical model for the dynamics and composition of the Venusian thermosphere, *J. Atmos. Sci.*, **32**, 1220, 1975.

Dickinson, R. E., and E. C. Ridley, Venus mesosphere and thermosphere temperature structure, II, Day-night variations, *Icarus*, **30**, 163, 1977.

Duncan, R. A., F-region seasonal and magnetic storm behavior, *J. Atmos. Terr. Phys.*, **31**, 59, 1969.

Emery, B. A., Neutral thermospheric winds deduced above Millstone Hill, 1. Mathematical model, uncertainties, and representative results, *J. Geophys. Res.*, **83**, 5691, 1978a.

Emery, B. A., Neutral thermospheric winds deduced above Millstone Hill, 2. Seasonal wind variations, 1970-1971, *J. Geophys. Res.*, **83**, 5704, 1978b.

Evans, D. S., N. C. Maynard, J. Troim, T. Jacobsen, and A. Egeland, Auroral vector electric field and particle comparisons 2. Electrodynamics of an arc, *J. Geophys. Res.*, **82**, 2235, 1977.

Evans, J. V., F region heating observed during the main phase of magnetic storms, *J. Geophys. Res.*, **75**, 4815, 1970.

Evans, J. V., The causes of storm time increases of the F-layer at mid latitudes, *J. Atmos. Terr. Phys.*, **35**, 593, 1973.

Evans, J. V., A review of F region dynamics, *Rev. Geophys. Space Phys.*, **13**, 887, 1975.

Fedder, J. A., and P. M. Banks, Convection electric fields and polar thermospheric winds, *J. Geophys. Res.*, **77**, 2328, 1972.

Forbes, J. M. and R. S. Lindzen, Atmospheric solar tides and their electrodynamic effects, 1. The global Sq current system, *J. Atmos. Terr. Phys.*, **38**, 897, 1976a.

Forbes, J. M. and R. S. Lindzen, Atmospheric solar tides and their electrodynamic effects, II. The equatorial electrojet, *J. Atmos. Terr. Phys.*, **38**, 911, 1976b.

Forbes, J. M., and R. S. Lindzen, Atmospheric solar tides and their electrodynamic effects, III. The polarization electric field, *J. Atmos. Terr. Phys.*, **39**, 1369, 1977.

Francis, S. H., Global propagation of atmospheric gravity waves: A Review, *J. Atmos. Terr. Phys.*, **37**, 1011, 1975.

Hanson, W. B. and R. A. Heelis, Techniques for measuring bulk gas motions from satellites, *Space Sci. Instrum.*, **1**, 493, 1975.

Harper, R. M., Nighttime meridional neutral winds near 350 km at low to mid latitudes, *J. Atmos. Terr. Phys.*, **35**, 2023, 1973.

Hays, P. B., A. F. Nagy, and R. G. Roble, Interferometric measurements of the 6300Å Doppler temperature during a magnetic storm, *J. Geophys. Res.*, **74**, 4162, 1969.

Hays, P. B., R. A. Jones and M. H. Rees, Auroral heating and the composition of the neutral atmosphere, *Planet. Space Sci.*, **21**, 559, 1973.

Hedin, A. E., and H. G. Mayr, Magnetic control of the near-equatorial neutral thermosphere, *J. Geophys. Res.*, **78**, 1688, 1973.

Hedin, A. E., H. G. Mayr, C. A. Reber, N. W. Spencer, and G. R. Carignan, Empirical model of global thermospheric temperature and composition based on data from the OGO-6 quadrupole mass spectrometer, *J. Geophys. Res.*, **79**, 215, 1974.

Hedin, A. E., J. E. Salah, J. V. Evans, C. A. Reber, G. P. Newton, N. W. Spencer, D. C. Kayser, D. Alcayde, P. Bauer, L. Cogger and J. P. McClure, A global thermosphere model based on mass spectrometer and incoherent scatter data, MSIS 1, N_2 density and temperature, *J. Geophys. Res.*, **82**, 2139, 1977.

Hedin, A. E., N. W. Spencer and H. G. Mayr, Altitude profiles of the semidiurnal and terdiurnal tides in the equatorial thermosphere from AE-E measurements, to be submitted to *J. Geophys. Res.*, 1979.

Hedin, A. E., P. Bauer, H. G. Mayr, G. R. Carignan, L. H. Brace, H. C. Brinton, A. D. Parks, and D. T. Pelz, Observations of neutral composition and related ionospheric variations during a magnetic storm in February 1974, *J. Geophys. Res.*, **82**, 3183, 1977.

Hernandez, G., and R. G. Roble, Direct measurements of nighttime thermospheric winds and temperatures, 2. Geomagnetic storms, *J. Geophys. Res.*, **81**, 5173, 1976b.

Heelis, R. A., W. B. Hanson, and J. L. Burch, Ion convection velocity reversals in the dayside cleft, *J. Geophys. Res.*, **81**, 3803, 1976.

Heppner, J. P., Empirical models of high-latitude electric fields, *J. Geophys. Res.*, **82**, 1115, 1977.

Hinteregger, H. E., EUV fluxes in the solar spectrum below 2000Å, *J. Atmos. Terr. Phys.*, **38**, 791, 1976.

Jacchia, L. G., J. W. Slowey, and U. von Zahn, Latitudinal changes of composition in the disturbed thermosphere from Esro 4 measurements, *J. Geophys. Res.*, **81**, 36, 1976.

Jacchia, L. G., J. W. Slowey and F. Verniani, Geomagnetic perturbations and upper atmosphere heating, *J. Geophys. Res.*, 72, 1423, 1967.

Johnson, F. S., Composition changes in the upper atmosphere, in Electron Density Distribution in Ionosphere and Exosphere, edited by E. Thrane, p. 81, North-Holland, Amsterdam, 1964.

Johnson, F. S., and B. Gottlieb, Eddy mixing and circulation at ionospheric levels, *Planet. Space Sci.*, **18**, 1707, 1970.

Jones, K. L., and H. Rishbeth, The origin of storm increases of mid latitude F-layer electron concentration, *J. Atmos. Terr. Phys.*, **33**, 391, 1971.

Keating, G. M., and E. J. Prior, The winter He bulge, *Space Res.*, **8**, 982, 1968.

Kellogg, W. W., Chemical heating above the polar mesopause in winter, *J. Meteorol.*, **18**, 373, 1961.

King, G. A. M., The dissociation of oxygen and high level circulation in the atmosphere, *J. Atmos. Sci.*, **21**, 231, 1964.

Kohl, H., and J. W. King, Atmospheric winds between 100 and 700 km and their effects on the ionosphere, *J. Atmos. Terr. Phys.*, **29**, 1045, 1967.

Lindzen, R. S., and S. Hong, Effects of mean winds and horizontal temperature gradients on solar and lunar semidiurnal tides in the atmosphere, *J. Atmos. Sci.*, **31**, 1421, 1974.

Matsuno, T., Weakening of westerly winds due to planetary wave effects in the winter mesosphere, paper presented at IAGA/IAMAP Conference, Int. Ass. of Geomagn. and Aeron., Int. Ass. of Meteorol. and Atmos. Phys., Grenoble, France, 1975.

Matsushita, S. A., Study of the morphology of ionospheric storms, *J. Geophys. Res.*, **64**, 305, 1959.

Maynard, N. C., Electric field measurements across the Harang discontinuity, *J. Geophys. Res.*, **79**, 4620, 1974.

Maynard, N. C., D. S. Evans, B. Maehlum and A. Egeland, Auroral vector electric field and particle comparisons 1. Premidnight convection topology, *J. Geophys. Res.*, **82**, 2227, 1977.

Mayr, H. G. and H. Volland, Magnetic storm characteristics of the thermosphere, *J. Geophys. Res.*, **78**, 2251, 1973b.

Mayr, H. G., I. Harris and N. W. Spencer, Some properties of upper atmosphere dynamics, *Rev. Geophys. Space Phys.*, **16**, 539, 1978.

Mayr, H. G., I. Harris, N. W. Spencer, A. E. Hedin, L. E. Wharton, H. S. Porter, J. C. G. Walker and H. C. Carlson, Jr., Atmospheric tides and the midnight temperature anomaly, submitted *Geophys. Res. Lett.*, 1979.

Miller, N., J. M. Grebowsky, H. G. Mayr, I. Harris, and Y. Tulunay, F-layer positive response to a geomagnetic storm – June 1972, submitted *J. Geophys. Res.*, 1979.

Newton, G. P., W. T. Kasprzak, S. A. Curtis, and D. T. Pelz, Local time variation of equatorial thermospheric composition determined by the San Marco 3 Nace, *J. Geophys. Res.*, **80**, 2289, 1975.

Obayashi, T., Worldwide electron density changes and associated thermospheric winds during an ionospheric storm, *Planet. Space Sci.*, **20**, 511, 1972.

Park, C. G., and M. Dejnakarintra, The effects of magnetospheric convection on atmospheric electric fields in the polar cap, in *Electrical Processes in Atmospheres*, Ed., H. Dolezalek, R. Reiter and H. E. Landsberg, Dr. Dietrich Steinkopf Verlag, Darmstadt, 1977.

Pelz, D. T., C. A. Reber, A. E. Hedin and G. R. Carignan, A neutral-atmosphere composition experiment for the Atmosphere Explorer-C, -D, and -E, *Radio Sci.*, **8**, 277, 1973.

Prolss, G. W., and U. von Zahn, Esro 4 gas analyzer results, 2. Direct measurements of changes in the neutral composition during an ionospheric storm, *J. Geophys. Res.*, **79**, 2535, 1974.

Reber, C. A., J. E. Cooley, and D. H. Harpold, Upper atmosphere hydrogen and helium measurements from the Explorer 32 satellite, *Space Res.*, **8**, 993, 1968.

Richmond, A. D., S. Matsushita, and J. D. Tarpley, On the production mechanism of electric currents and fields in the ionosphere, *J. Geophys. Res.*, **81**, 547, 1976.

Richmond, A. D. and S. Matsushita, Thermospheric response to a magnetic substorm, *J. Geophys. Res.*, **80**, 2839, 1975.

Richmond, A. D., Gravity wave generation, propagation, and dissipation in the thermosphere, *J. Geophys. Res.*, **83**, 4131, 1978.

Richmond, A. D., Thermospheric heating in a magnetic storm: dynamic transport of energy from high to low latitudes, submitted *J. Geophys. Res.*, 1979.

Roble, R. G. and S. Matsushita, An estimate of the global scale Joule heating rates in the thermosphere due to time mean currents, *Radio Sci.*, **10**, 389, 1975.

Roble, R. G., J. E. Salah, and B. A. Emery, The seasonal variation of the diurnal thermospheric winds over Millstone Hill during solar cycle maximum, *J. Atmos. Terr. Phys.*, **39**, 503, 1977.

Seaton, M. J., A possible explanation of the drop in F-region critical densities accompanying major ionospheric storms, *J. Atmos. Terr. Phys.*, **8**, 122, 1956.

Spencer, N. W., H. C. Brinton, H. G. Mayr, and R. F. Theis, The midnight temperature anomaly (abstract), *EOS Trans. AGU*, **58**, 990, 1977.

Spencer, N. W., R. F. Theis, L. E. Wharton and G. R. Carignan, Local vertical motions and kinetic temperature from AE-C as evidence for aurora-induced gravity waves, *Geophys. Res. Lett.*, **3**, 313, 1976.

Spencer, N. W., G. R. Carignan, H. G. Mayr, H. B. Niemann, R. F. Theis, and L. E. Wharton, The midnight temperature maximum, submitted *Geophys. Res. Lett.*, 1979.

Stolarski, R. S., P. B. Hays and R. G. Roble, Atmospheric heating by solar EUV radiation, *J. Geophys. Res.*, **80**, 2266, 1975.

Straus, J. M., Dynamics of the thermosphere at high latitudes, *Rev. Geophys. Space Phys.*, **16**, 183, 1978.

Taeusch, D. R., G. R. Carignan and C. A. Reber, Neutral composition variation above 400 km during a magnetic storm, *J. Geophys. Res.*, **76**, 8318, 1971.

Testud, J., Gravity waves generated during magnetic substorms, *J. Atmos. Terr. Phys.*, **32**, 1793, 1970.

Volland, H., Coupling between the neutral tidal wind and the ionosphere dynamo current, *J. Geophys. Res.*, **81**, 1621, 1976.

Volland, H., Models of global electric fields within the magnetosphere, *Ann. Geophys.*, **31**, 154, 1975.

Volland, H., and H. G. Mayr, Response of thermospheric density to auroral heating during geomagnetic disturbances, *J. Geophys. Res.*, **76**, 3764, 1971.

Wedde, T., J. R. Doupnik, and P. M. Banks, Chatanika observations of the latitudinal structure of electric fields and particle precipitation on November 21, 1975, *J. Geophys. Res.*, **82**, 2743, 1977.

Wu, S. T., S. Matsushita, and L. L. DeVries, An analysis of the upper atmospheric wind observed by Logacs, *Planet. Space Sci.*, **22**, 1036, 1974.

Yeh, K. C. and C. H. Liu, Acoustic gravity waves in the upper atmosphere, *Rev. Geophys. Space Phys.*, **12**, 193, 1974.

Zimmerman, A. P., A. C. Faire, and A. E. Murphy, The measurement of atmospheric stability from 30 to 90 km, *Space Res.*, **12**, 615, 1972.

Table 1

Comparison between atmospheric parameters describing the dirunal (P_1^1) and annual (P_1^0) tides (the horizontal scale of both components is the same but the time scales are different). Note that in comparison to the energy input, the temperature and composition amplitudes are much larger for the annual tide.

Tides	$\Delta Q/Q_o$	$\Delta T/T_o$	Velocity (m/sec)	Δlog 0	Δlog He
Diurnal	1.5	+0.13	100.0	-0.02	-0.15
Annual	0.5	+0.13	35.0	-0.40	-2.00

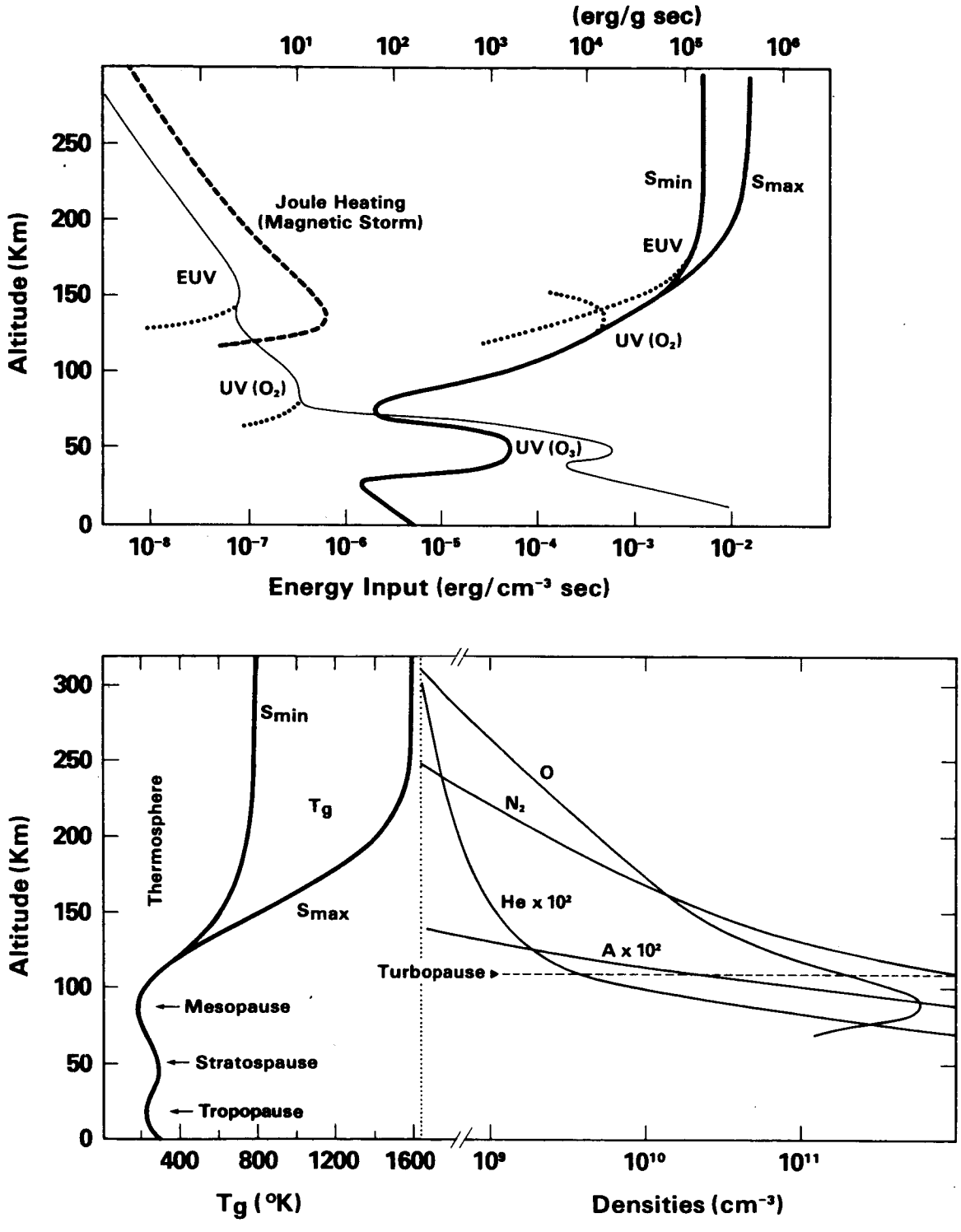

Figure 1. Typical height distribution for the heating rates from solar radiation and Joule dissipation (during disturbed conditions). The heating rate from solar radiation per mass of the absorbing atmosphere is shown in heavy solid lines for minimum (S_{min}) and maximum (S_{max}) solar activity conditions. Temperature and density distributions are also illustrated.

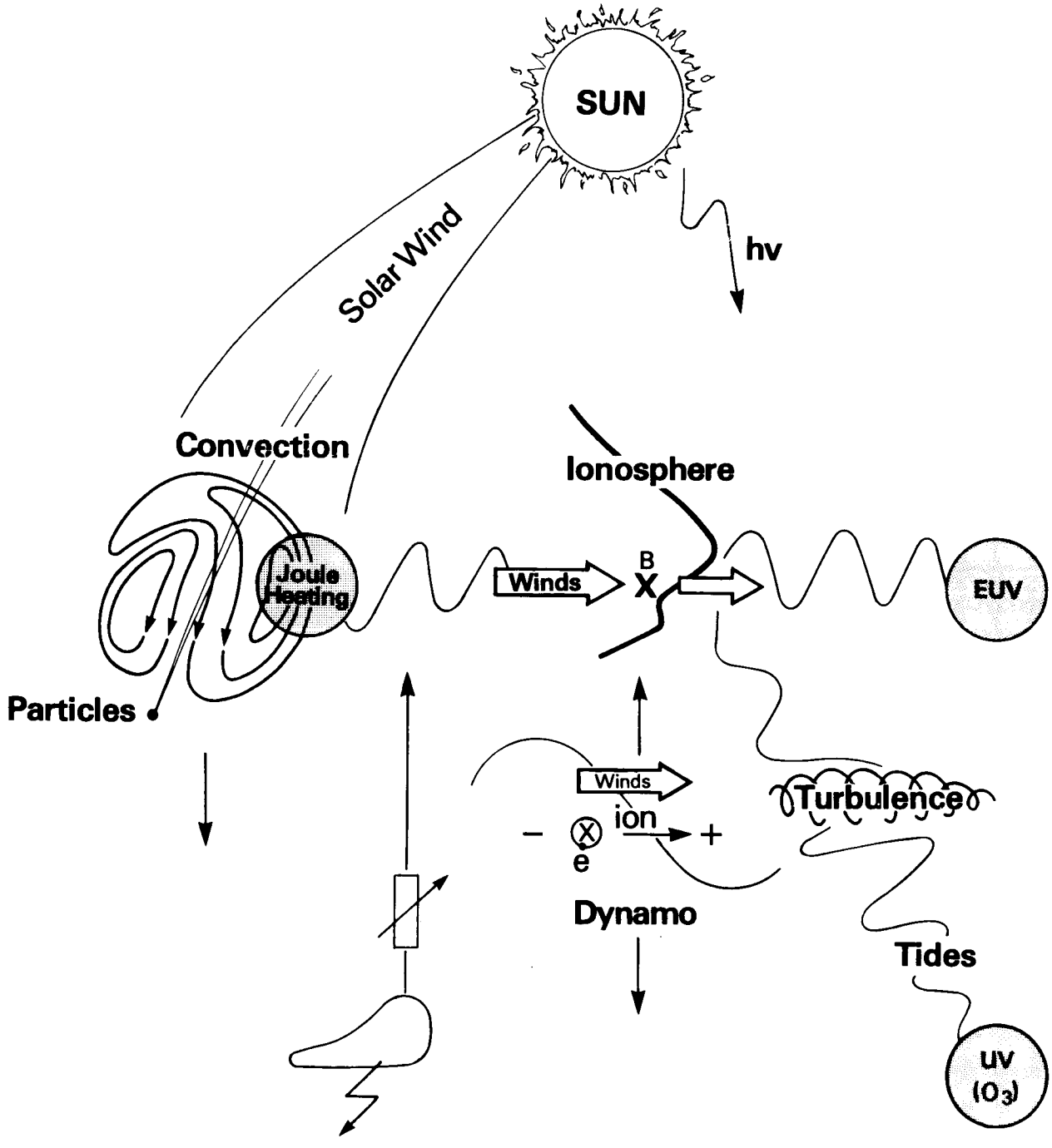

Figure 2. Schematic illustration of dynamic interactions due to absorbed solar radiation and magnetospheric energization processes.

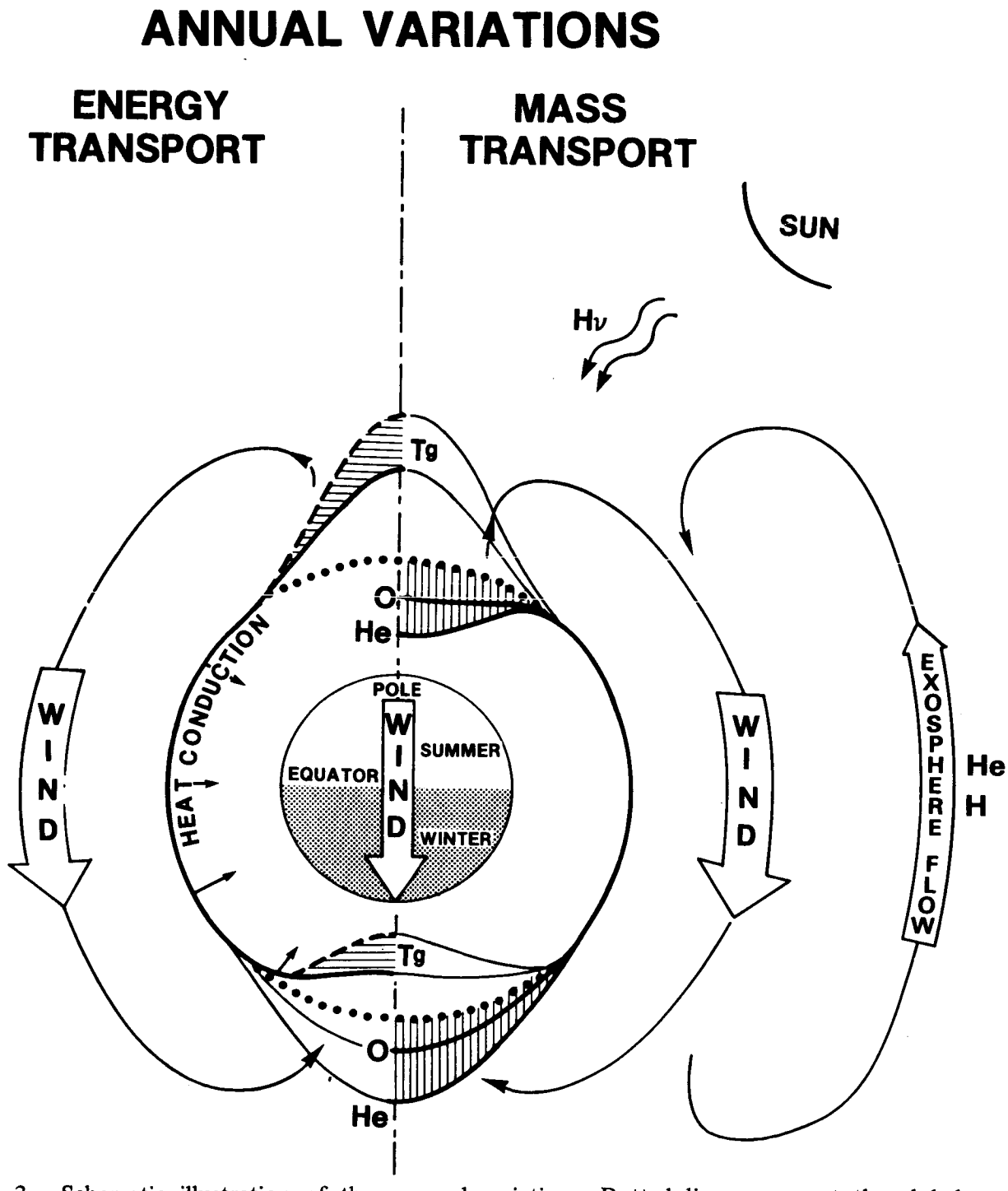

Figure 3. Schematic illustration of the seasonal variations. Dotted lines represent the global average. Dashed lines illustrate temperature and density variations when horizontal transport is neglected; solid lines illustrate distributions under consideration of horizontal transport. The distances from the dashed and solid lines to the dotted line illustrate deviations from the mean. Shaded areas represent the energy (Tg) and mass (O, He) redistribution by winds and exospheric flow.

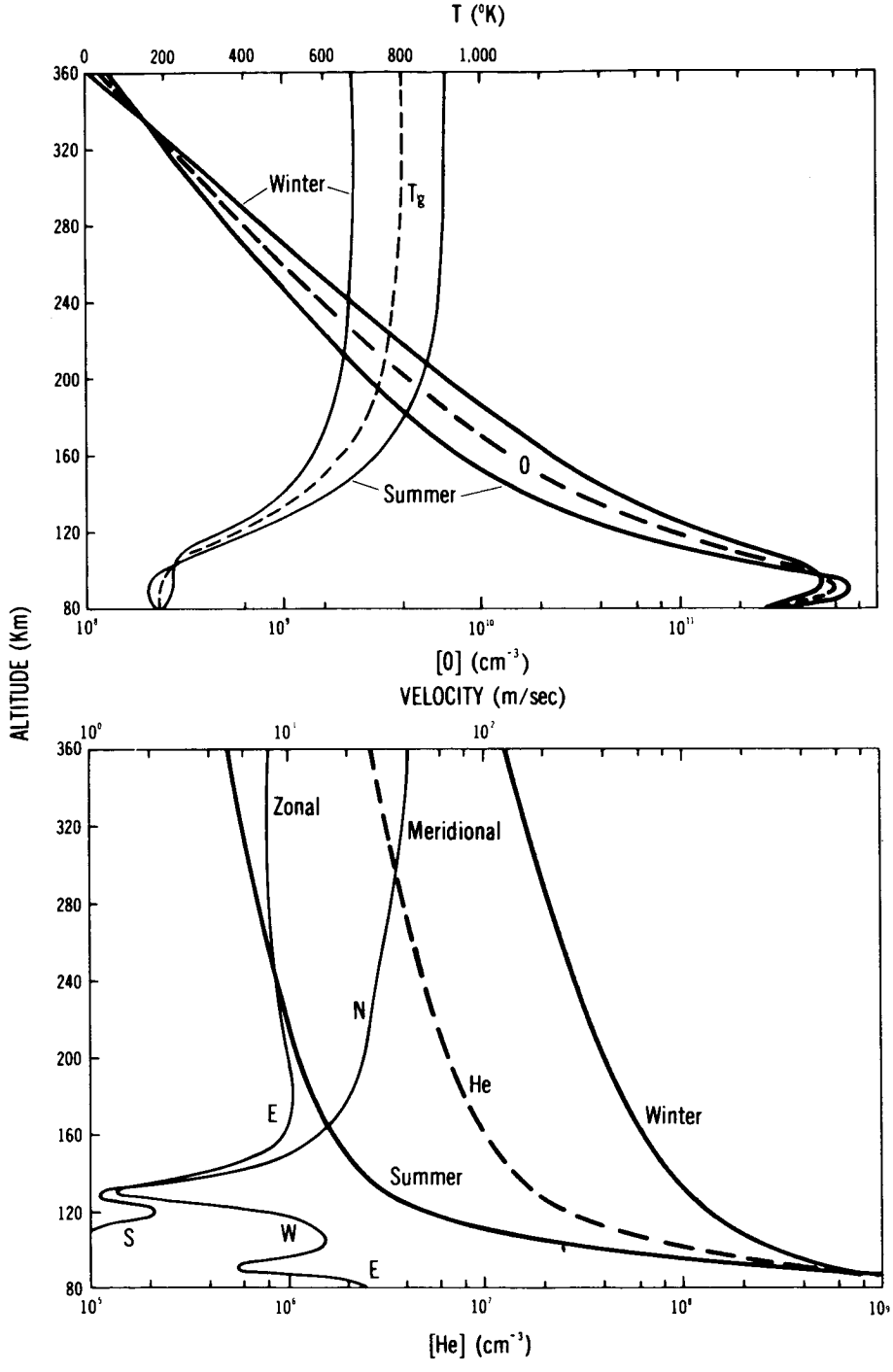

Figure 4. Annual tide computed from a three dimensional theoretical model. Summer and winter distributions refer to the poles. The meridional wind velocity is taken from the equator during June solstice, N and S indicating directions from the north and south, respectively; during that season the zonal wind velocities are taken from mid-latitudes, E and W indicating directions from the east and west, respectively. The results refer to the fundamental asymmetric component P_1^0.

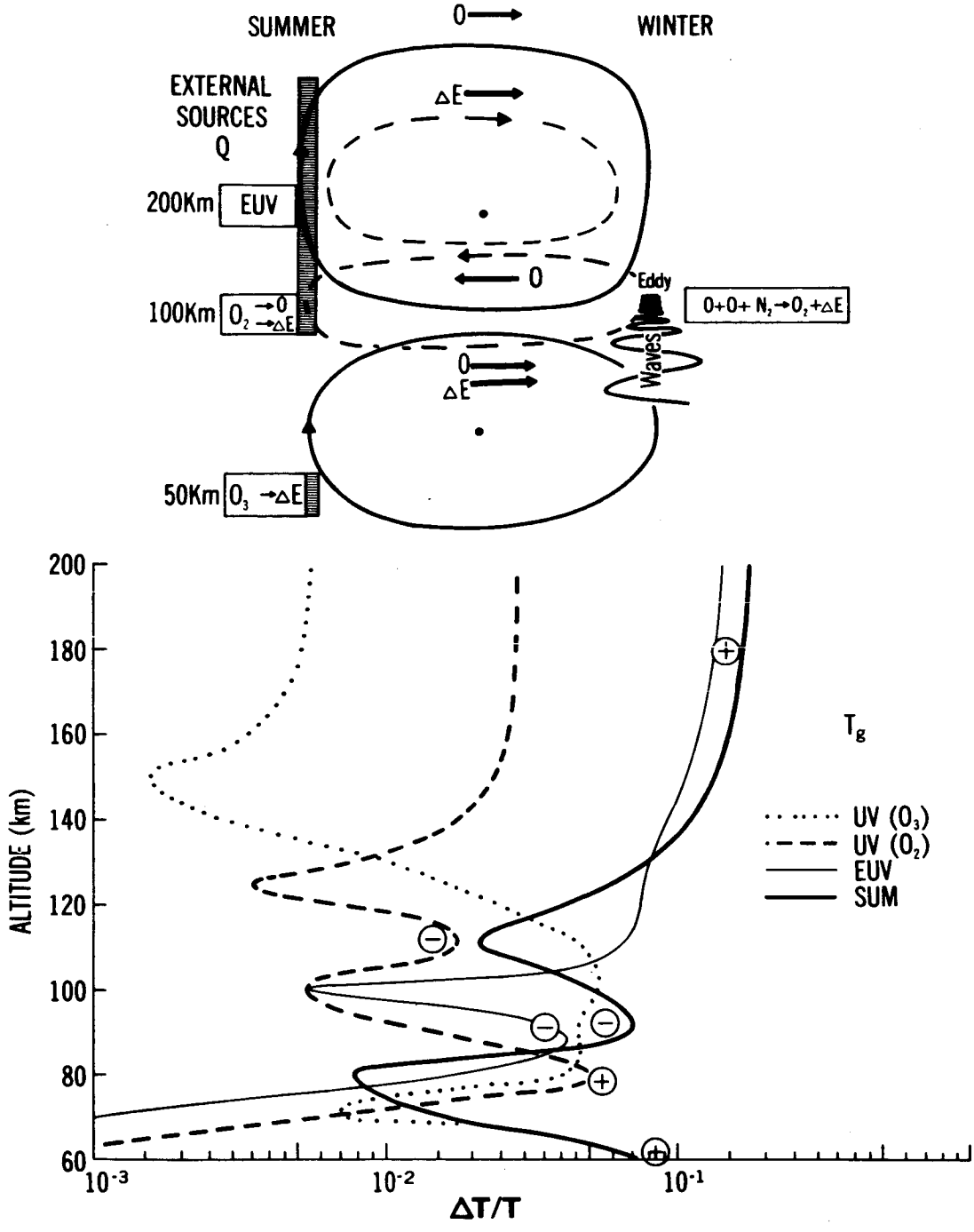

Figure 5. Schematic illustration of the sources that contribute to the annual tide. Wind induced energy advection 'ΔE' and oxygen transport 'O' contribute significantly to the energy budget. Release of chemical energy in three-body recombination is relatively more important in the winter hemisphere. An additional heat source is postulated near 90 km which might be associated with planetary waves. The lower half of the figure shows relative temperature amplitudes (normalized to the global average) for the annual tide due to EUV, UV(O_2) and UV(O_3) excitation. Plus or minus signs indicate a temperature maximum in the summer or winter hemisphere respectively.

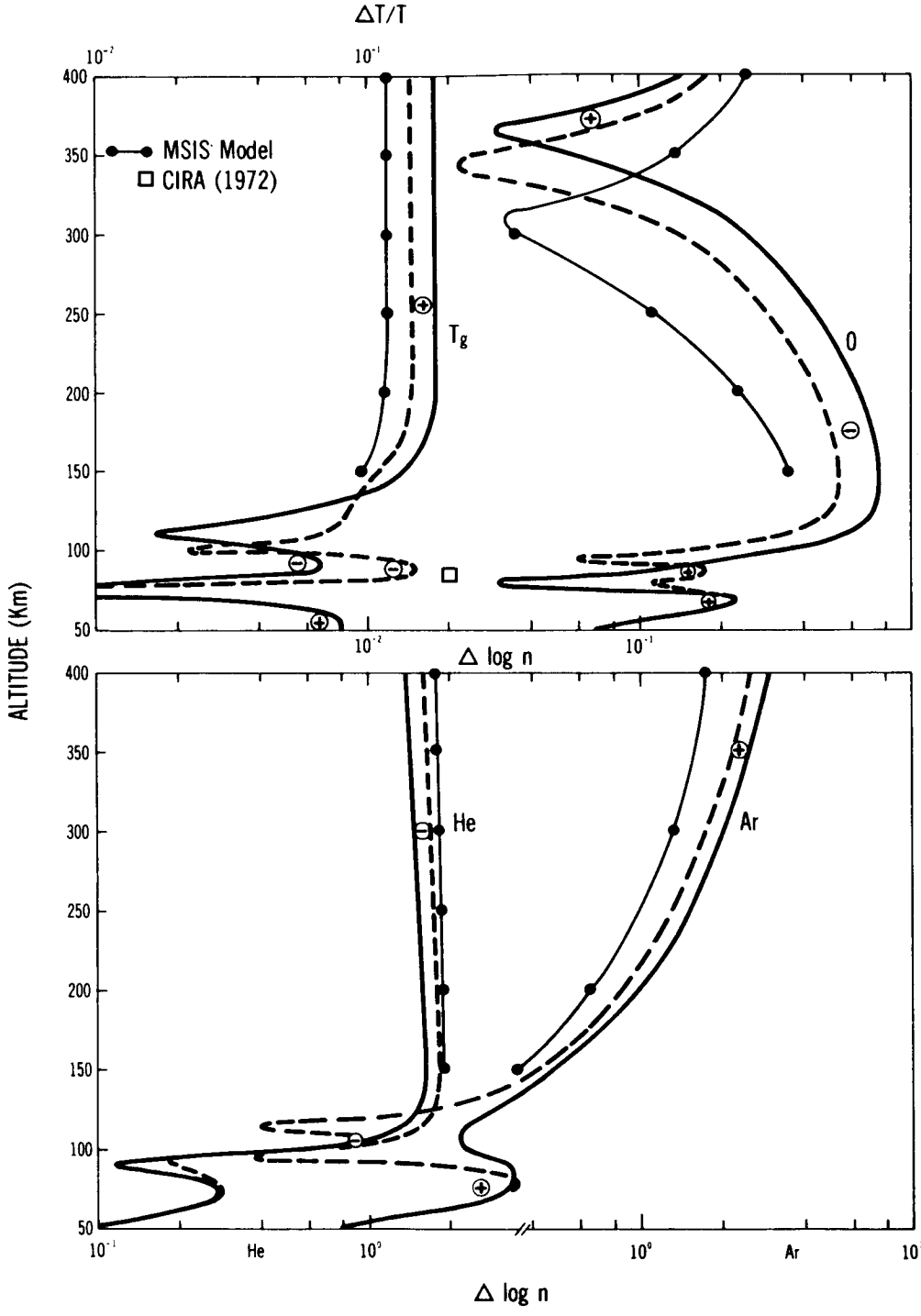

Figure 6. Relative amplitudes of the annual tide at the summer pole. Dashed and solid curves represent solutions with and without "wave source" near 90 km; the former solution was shown in Figure 4. Note that with the wave source the agreement with observations from AE significantly improves. Plus or minus signs indicate an increase or decrease in the summer hemisphere, respectively, and vice versa in the winter hemisphere.

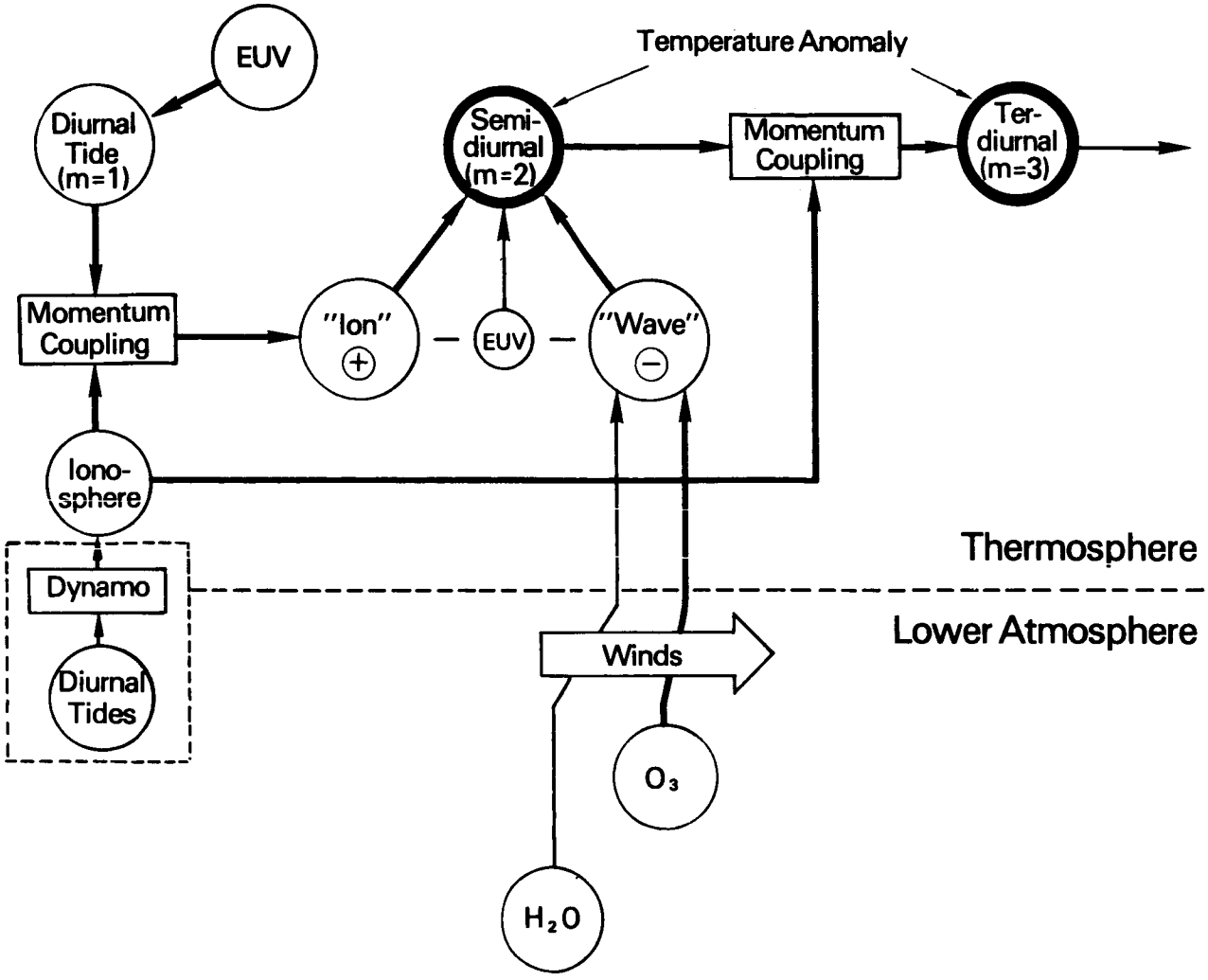

Figure 7. Schematic diagram illustrating the tidal components that contribute to the midnight temperature maximum. The semidiurnal tide in the thermosphere is primarily due to (1) ion drag momentum coupling involving the diurnal (m=1) variations of the wind field and ion density and (2) tidal waves excited in the lower atmosphere. Coupling between that composite semidiurnal tide (m=2) and the diurnal variations in the ionospheric ion density produces a terdiurnal tide and so on.

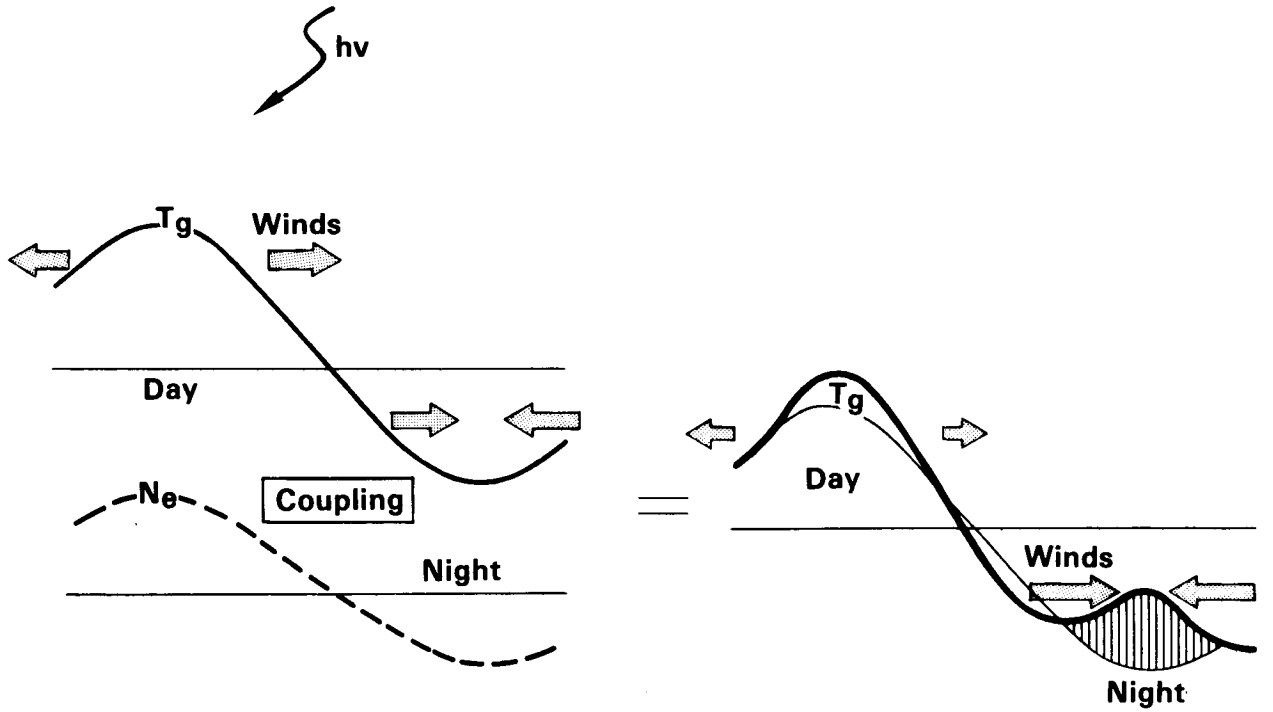

Figure 8. Schematic diagram illustrating the nonlinear interaction due to momentum coupling between diurnal variations in ion drag and wind fields.

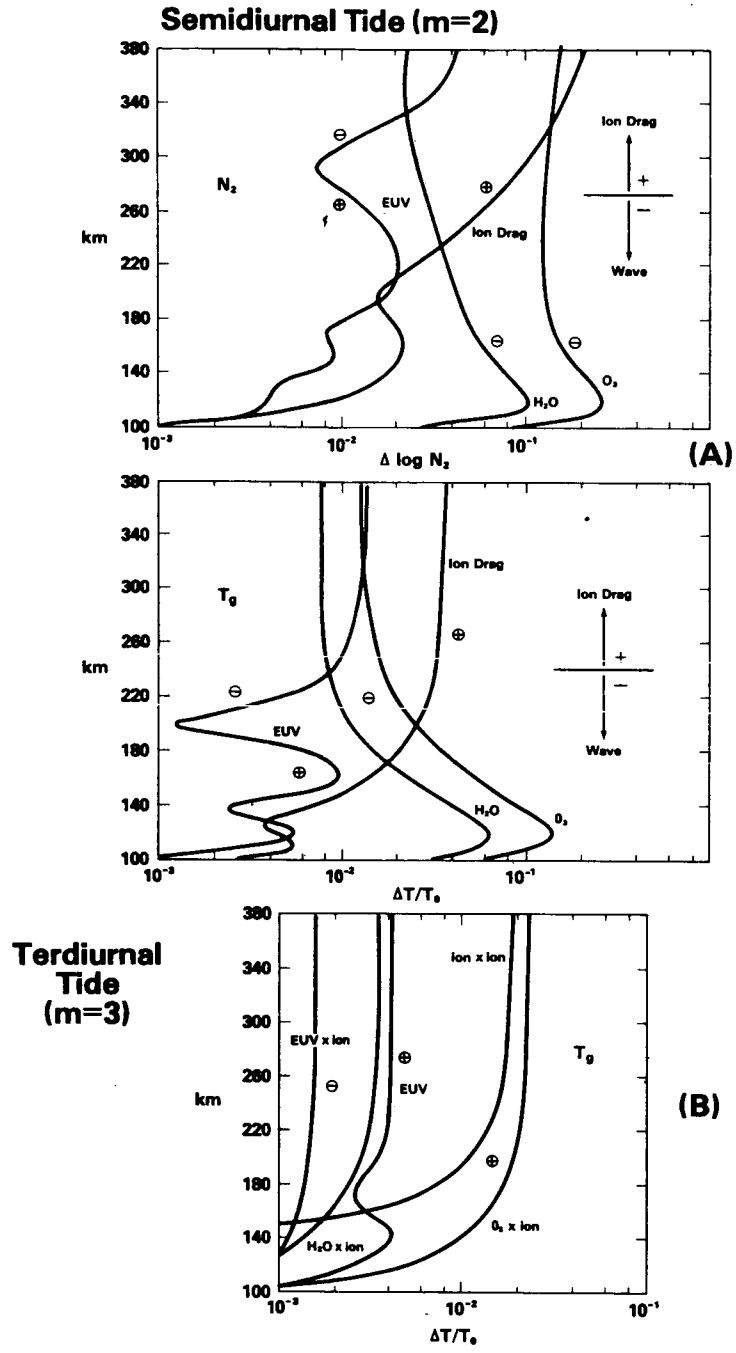

Figure 9. (a) Semidiurnal tides for Tg and N_2 associated with various excitation mechanisms. Plus and minus signs indicate phases in the quadrants near 00(12) and 06(12) local time respectively. (b) The terdiurnal component for the temperature. Plus and minus signs indicate phases in quadrants near 00(8) and 4(12) local time respectively. Except for the direct solar radiative excitation (labelled EUV), the terdiurnal components are the result of nonlinear interaction between semidiurnal wind fields (due to EUV, ion drag, O_3 and H_2O) and diurnal variations in the ion density.

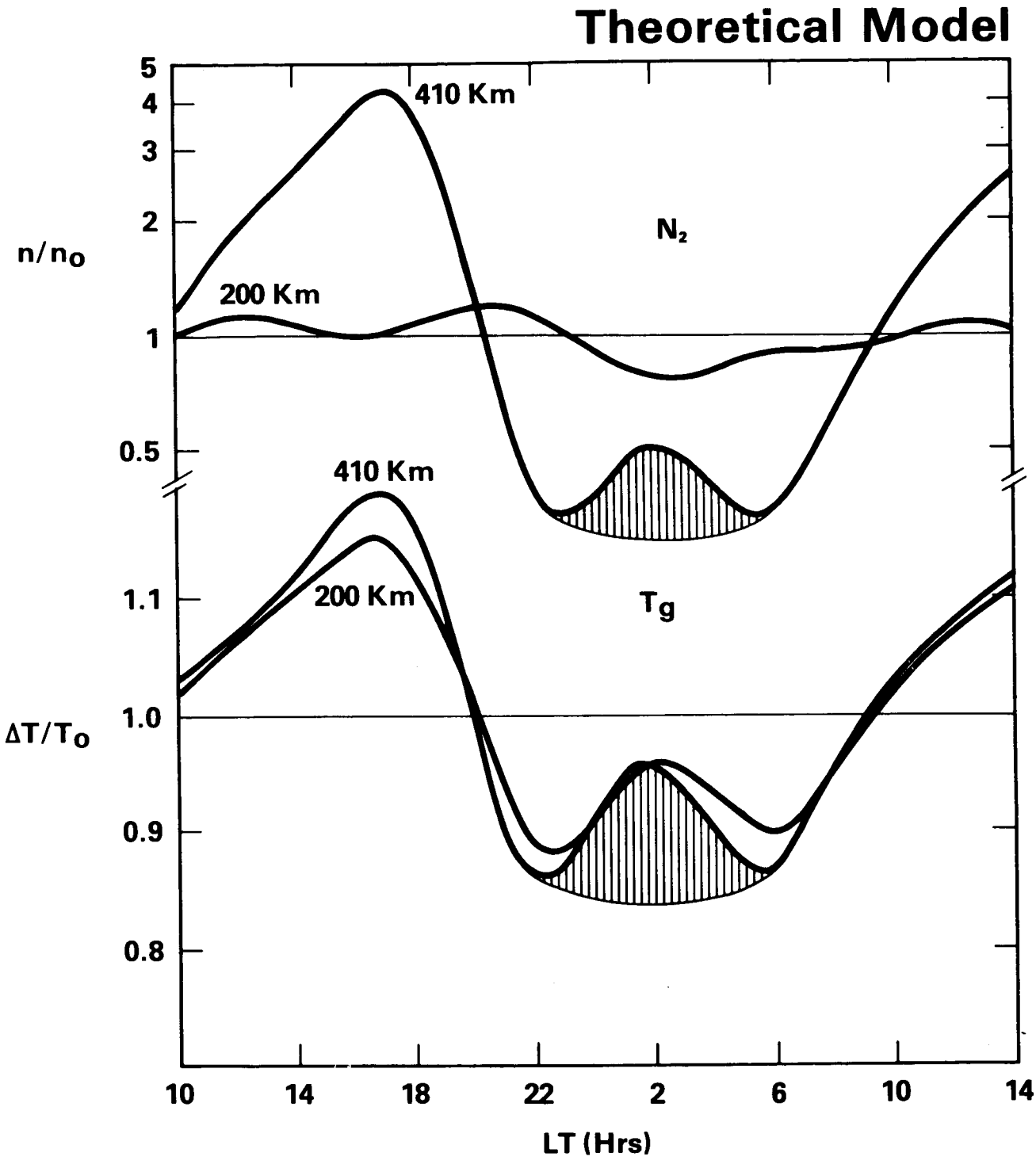

Figure 10. Synthesized diurnal variations of TG and N_2. Note that at 200 km, N_2 does not yet show the signature of a nighttime temperature maximum.

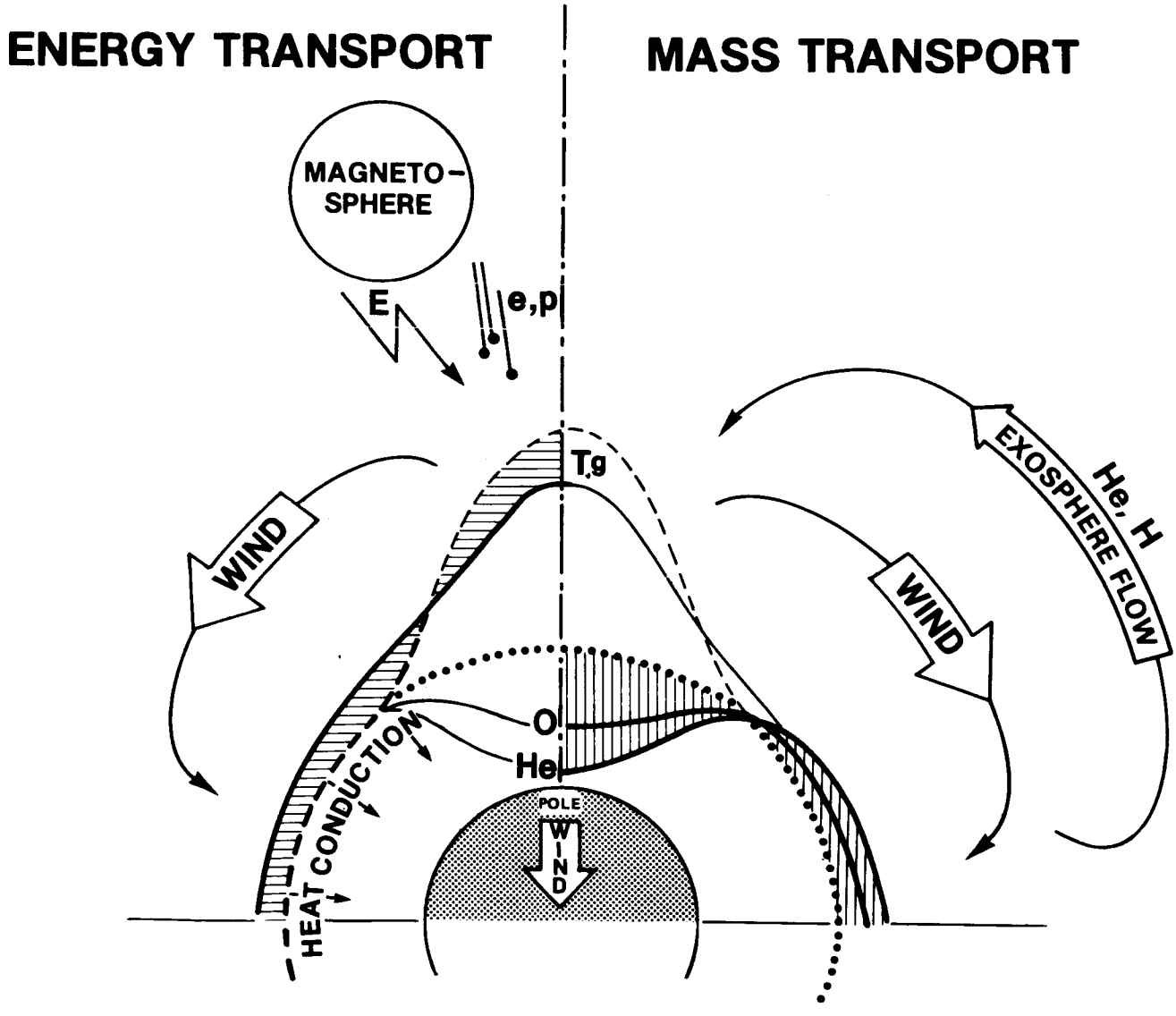

Figure 11. Schematic illustration of the zonally averaged magnetic storm dynamics analogous to Figure 3.

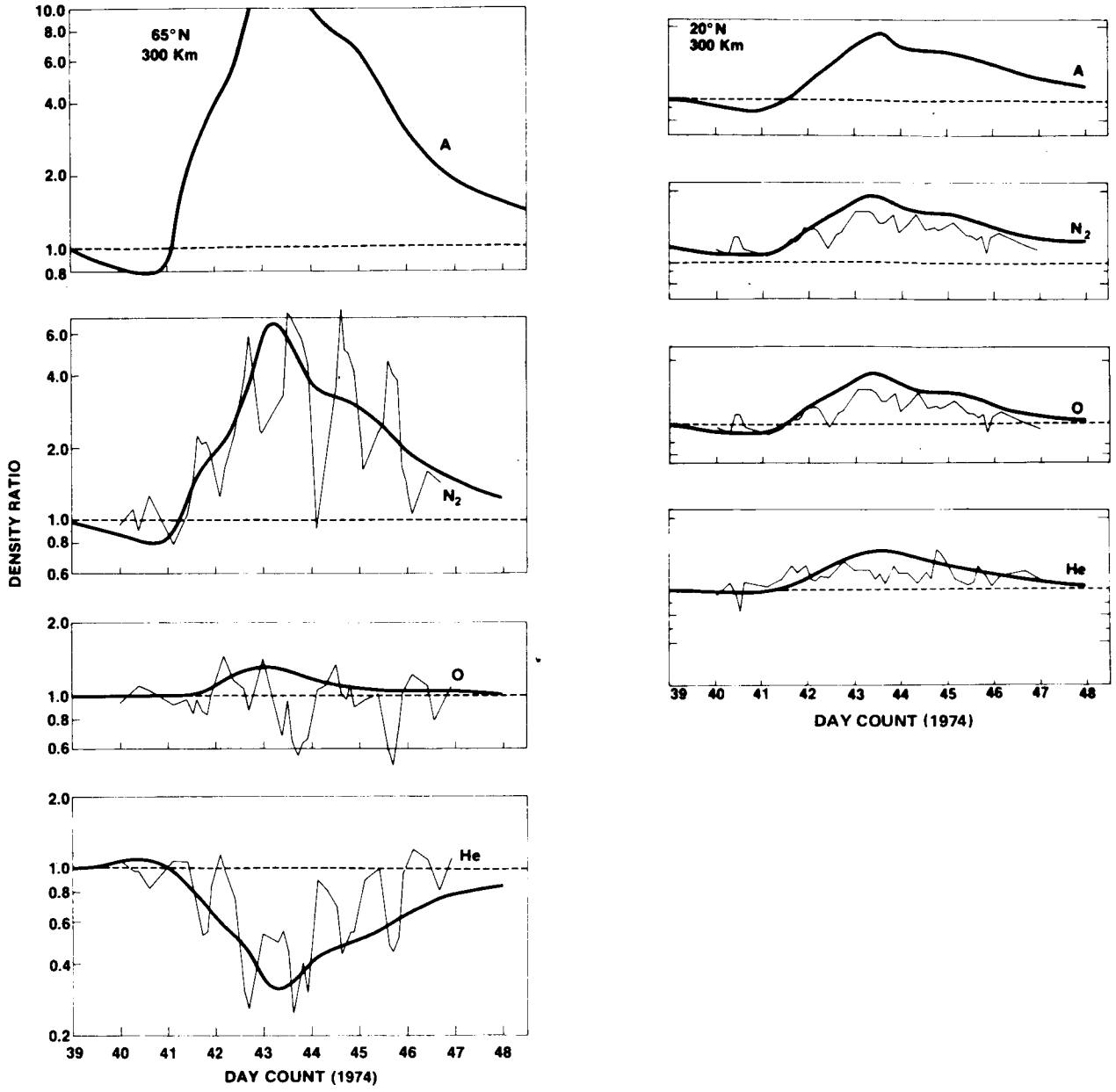

Figure 12. Comparison between theoretical results of composition response (heavy lines) and AE-C data (thin line). Note that the model describes the zonal average while the data display also large longitudinal variations (quasiperiodicity of 24 hours). The density variations are normalized to quiet conditions.

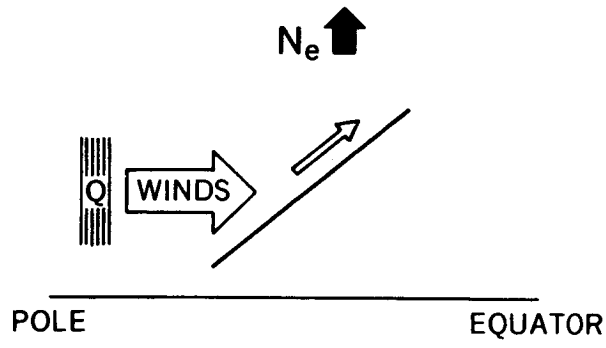

PHASE I

(1) ENERGY DEPOSITION
(2) EXCITATION OF MERIDIONAL WINDS
(3) PLASMA TRANSPORT TO HIGHER ALTITUDES
(4) OVERALL N_e INCREASE

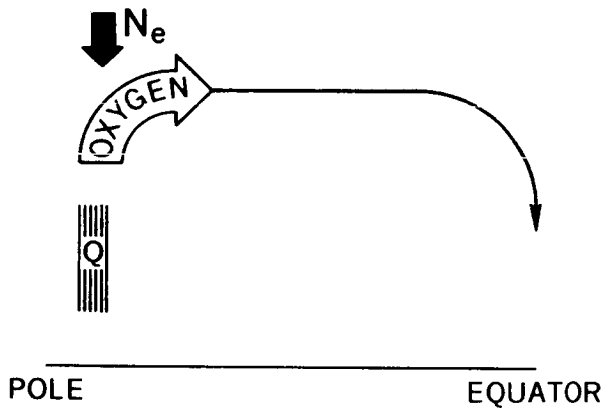

PHASE II

(1) WIND INDUCED TRANSPORT OF OXYGEN
(2) DEPLETION OF O AND INCREASE OF N_2
(3) DECREASE OF N_e AT HIGH LATITUDES

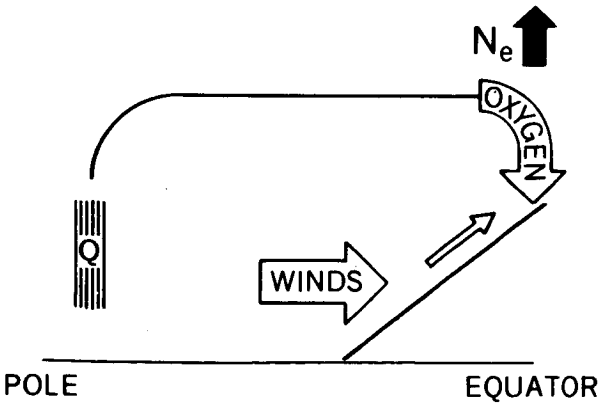

PHASE III

(1) PLASMA TRANSPORT TO HIGHER ALTITUDES
(2) INCREASE OF O AND N_2
(3) INCREASE OF N_e AT THE EQUATOR

Figure 13. Schematic illustration of composition and wind effects in the ionosphere during magnetic storms.

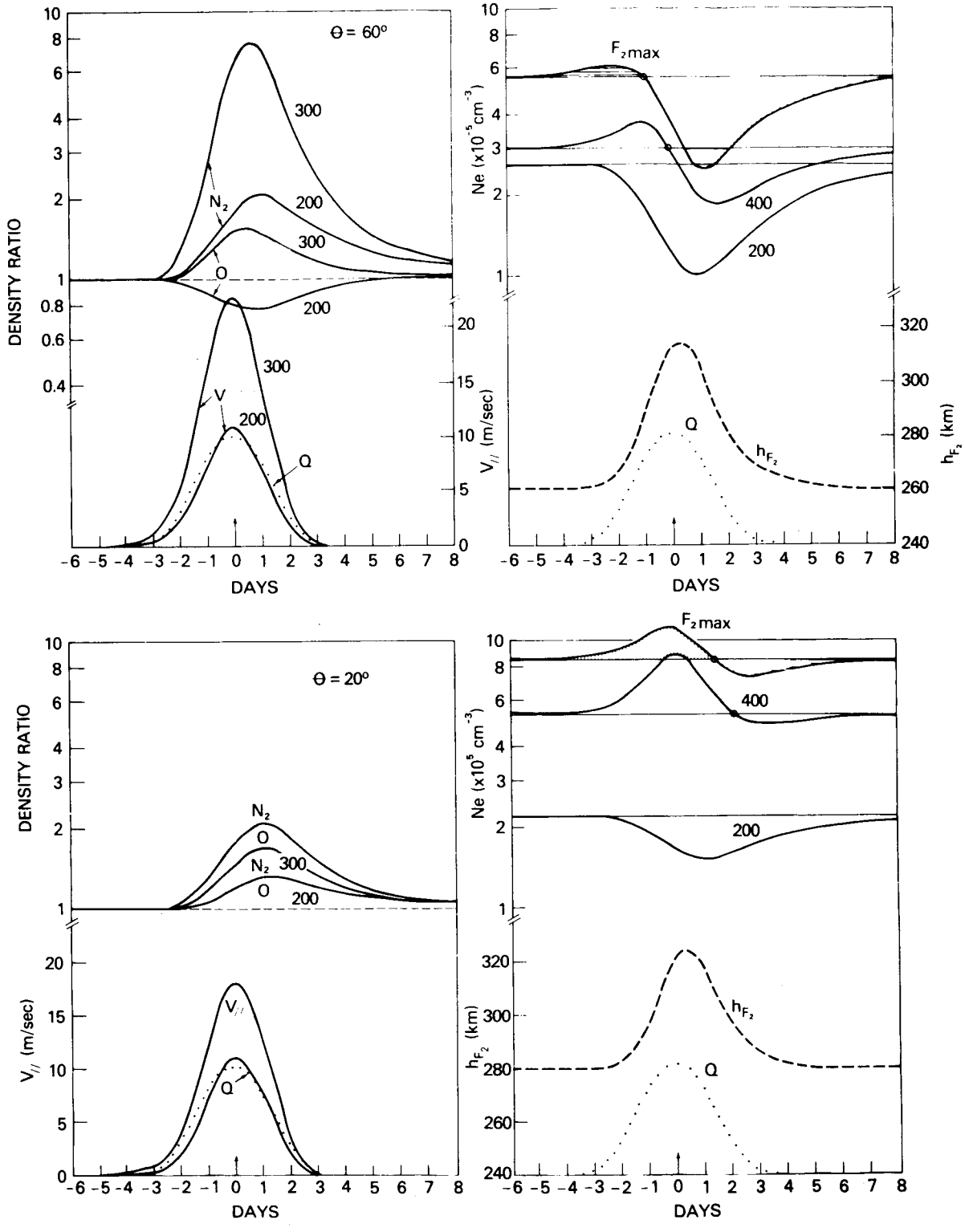

Figure 14. Computer results describing the interaction processes illustrated in Figure 13. The heat source is indicated in dotted lines. Note the delay between the density response of O and N_2 (O/N_2) and the wind velocity which accounts for the characteristic sequence of positive and negative phases. The increase in the height of the F_2 peak is in phase with the wind velocity.

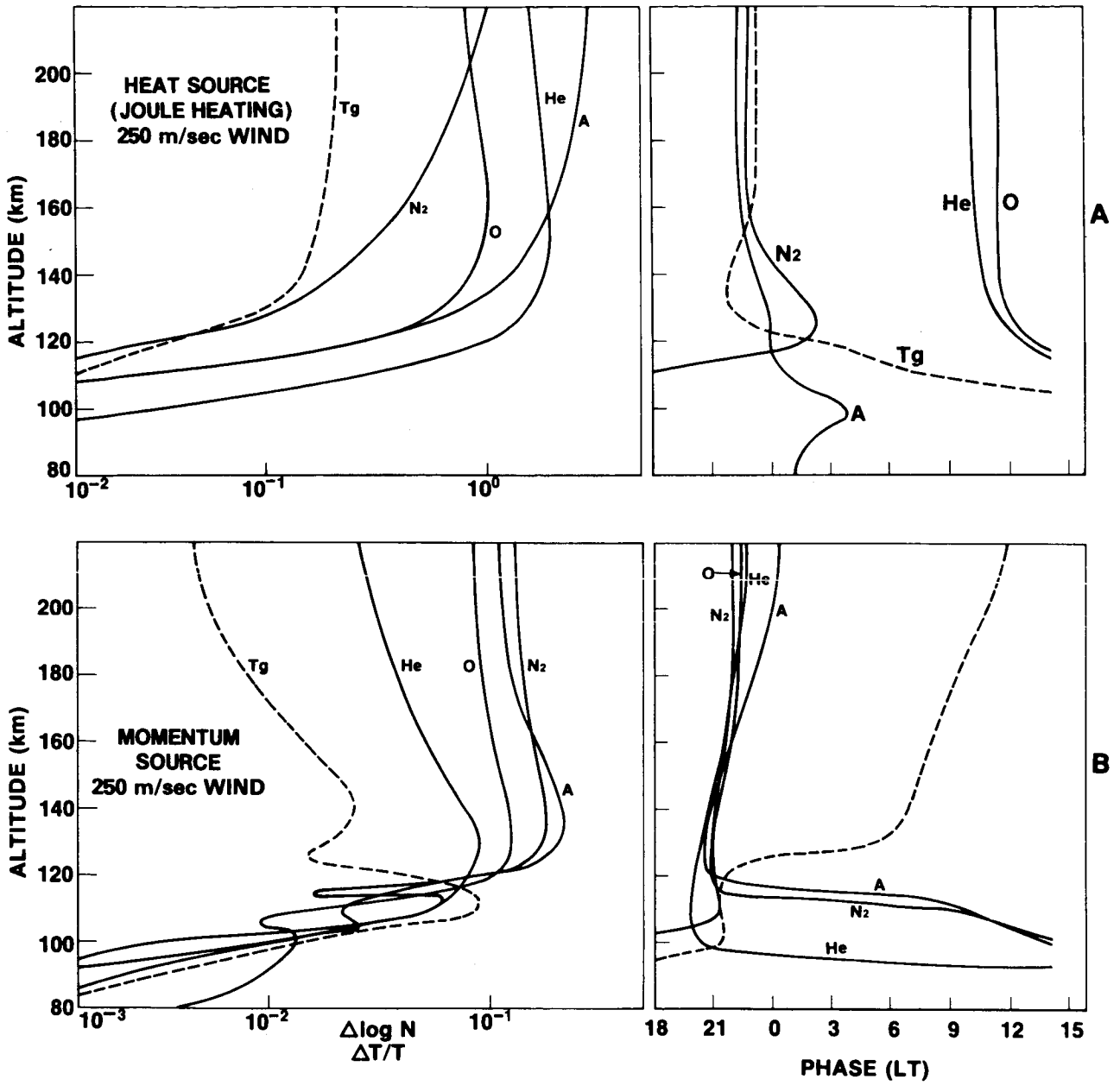

Figure 15. Theoretical results illustrating the differences between temperature and composition signatures due to (a) Joule heating and (b) electric field momentum source. Both source functions were artifically chosen such that the magnitudes of the resulting wind velocities were the same. Because the divergence of the wind field induced by the momentum source is relatively small, it is (in comparison to Joule heating) relatively ineffective in changing the temperature and composition. Note that under the momentum source all gases vary in phase (assumed periodicity is 24 hours) which is in contrast to the Joule heating effects where O and He vary out of phase with N_2 and Ar.

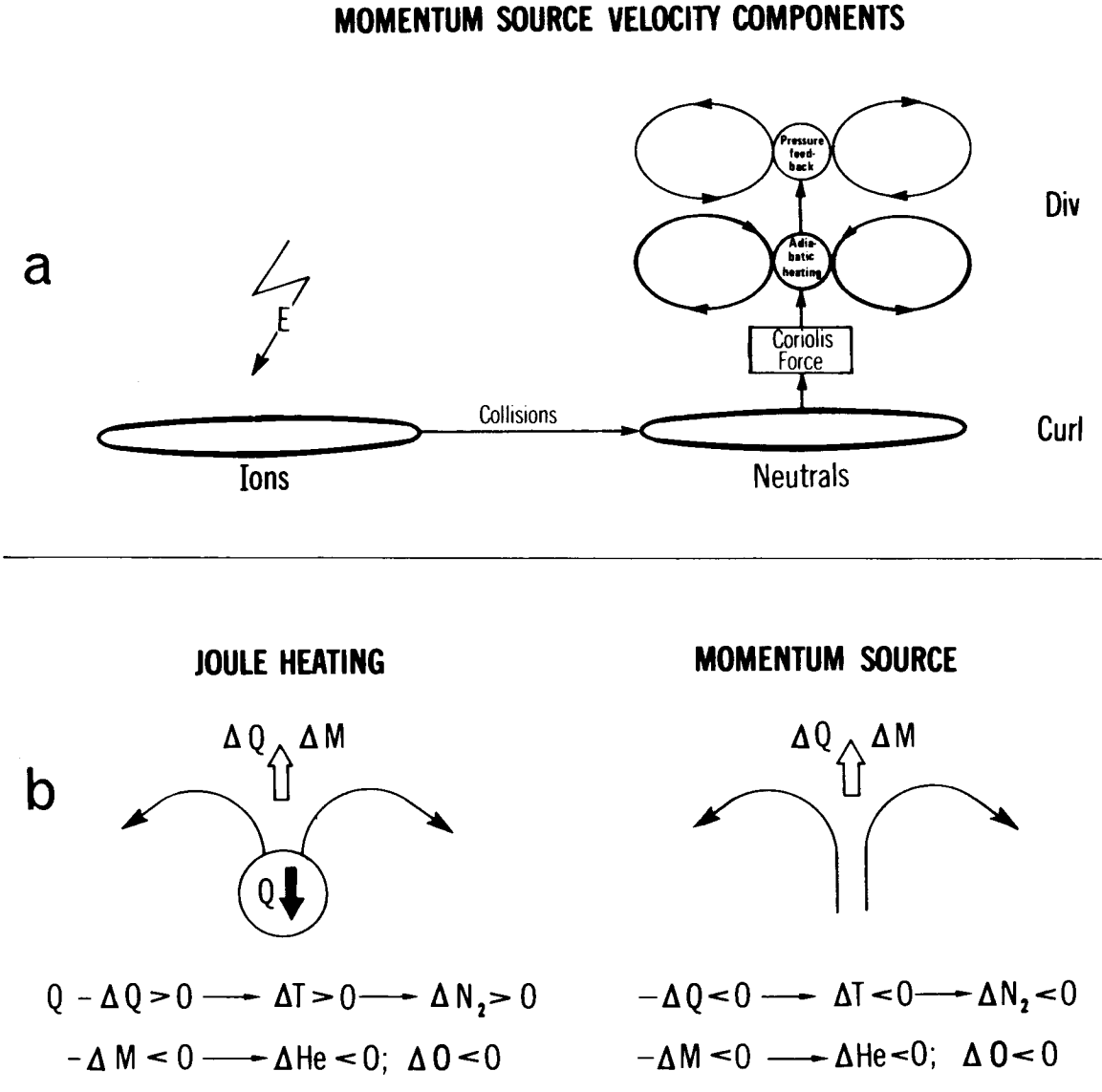

Figure 16. Heuristic explanation of the results shown in Figure 15. (a) Illustration of the coupling between electric field and ion drift (mainly curl component) and the transfer of momentum (via collisions) to the neutral atmosphere. The resultant curl component in the neutral wind field induces, via for example, Coriolis force, a divergence component that causes energy and mass transport resulting in temperature and density variations. (b) Illustration of the differences between Joule heating and momentum source signatures in densities and temperature as discussed in the text.

ELECTRIC GENERATORS IN THE MAGNETOSPHERE-IONOSPHERE SYSTEM

G. Atkinson
Communications Research Centre,
Ottawa, Canada

1. INTRODUCTION

The topic of this discussion is the nature and cause of electric fields in the coupled magnetosphere-ionosphere system and their effects in the middle atmosphere. They can be classified according to cause: Electric fields produced by the solar wind - magnetosphere interaction and electric fields due to neutral winds (winds in the non-ionized atmosphere) at E region heights in the ionosphere. The first dominate at high latitudes where they are typically an order of magnitude stronger than the second, and also an order of magnitude greater than lower latitude fields. For this reason the major part of this discussion will be on electric fields induced by the solar wind.

The equivalence between forces and electric currents and also between current closure and stress balance will be emphasized throughout this discussion. In general, a force in the electrically coupled magnetosphere-ionosphere system is associated with a component of the current perpendicular to magnetic field lines, and the force is equal to $\underset{\sim}{\mathbf{J}} \times \underset{\sim}{\mathbf{B}}$, where $\mathbf{J}$ is the current density and $\mathbf{B}$ the magnetic field strength. The motions of the magnetospheric and ionospheric fluids and hence the electric fields of interest to this workshop, are of course determined by the balance of these forces, or equivalently by the closure of the currents. Thus some time will be spent examining the physical nature of stresses and currents.

2. PROPERTIES OF ELECTRIC FIELDS

First consider the electric field. Because of the very high conductivity in a direction parallel to magnetic field lines, it must be approximately orthogonal to the magnetic field lines throughout the magnetosphere and ionosphere, otherwise very large currents would flow creating problems of current closure. Dejnakarintra (1974) studied the extension of the field to lower altitudes using a model defined by the following: (i) an upper boundary condition of horizontal electric fields at an altitude of 150 km varying periodically in the horizontal direction, (ii) a tensor conductivity from 0 to 150 km which varies with height, (iii) an equipotential surface at the Earth, (iv) the current must be divergence free and (v) the electric field must be curl free.

Figure 1 is a graph (Dejnakarintra, 1974) showing as a function of altitude, the mapping factor (the strength of the horizontal component of the electric field relative to its strength at 150 km) for several different horizontal scale sizes (λ_{eff}) of the field and for two reasonable models of conductivity. It can be seen that for scale sizes greater than 20 km, the horizontal component of the electric field is essentially unchanged above the bottom of the E region. That is, magnetic field lines are electric equipotentials for the scale sizes of interest down to at least 90 km altitude. Further, the electric fields of the large-scale flows discussed in the ensuing sections extend well down into the middle atmosphere. A further result, evident from symmetry in the model, is that the maximum vertical

potential difference between ground and ionosphere is half the maximum horizontal potential difference.

In summary, for the large-scale electric fields to be considered here: magnetic field lines can be regarded as electric equipotentials down to at least the base of the E region ionosphere, the horizontal component of electric field maps unattenuated well down into the stratosphere and maximum vertical potential differences are half the ionospheric horizontal potential differences.

3. EQUIPOTENTIAL CONVECTIVE FLOW

In a collisionless plasma in the presence of orthogonal electric and magnetic fields, the plasma drifts in a direction orthogonal to both as indicated by the equation $\mathbf{E} = -\mathbf{v}_d \times \mathbf{B}$ where $\mathbf{v}_d$ is the velocity of this drift. Particle trajectories are as indicated in Figure 2a. The effect of the electric field on what would otherwise be a circular gyration in the magnetic field, is to maximize the particle velocity and hence the gyrational radius on one side of the gyration and thereby to create a systematic drift motion.

In fact, in the magnetohydrodynamic approximation (cold plasma) and if the magnetic field lines are electric equipotentials, the plasma initially on a given magnetic flux tube drifts in such a way that it always stays connected by magnetic field lines and also contains the same amount of magnetic flux. Under these conditions we can treat flux tubes as fluid elements which convect as a unit. In the steady-state, the motion in the magnetosphere of these banana-shaped fluid elements reduces to a two-dimensional problem and it is sufficient to describe their motion either in the equatorial plane, or in the ionosphere. They convect along electric equipotential surfaces. It is of interest that the Maxwell equation curl E = 0 reduces to div $(\mathbf{B}\mathbf{v}_d) = 0$ for the above two-dimensional flow. Since B is inversely proportional to the flux tube cross-sectional area this is the equation for the conservation of fluid elements.

Figure 3 shows the forces that can act on such a fluid element. First, the magnetic stresses include the pressure from neighbouring flux tubes ($B^2/2\mu_o$) and the shear stress at the ionospheric ends of the flux tubes ($B_n B_t/\mu_o$ where n and t indicate components normal and tangential to the end plane). This latter stress includes the momentum transfer from the neutral atmosphere in the E region. Ions attempting to follow the convective motion collide with neutrals as shown in Figure 2b producing ion drag forces opposing the drift. In referring to the currents, the effect is sometimes called line tying. A further magnetic stress is the tension ($B^2/2\mu_o$) existing along the magnetic field direction. Since the flux tube has a curvature toward the Earth, this results in a force tending to make flux tubes collapse Earthward. An analogy with stretched elastic bands is often used in describing this effect. In a perfectly-dipolar field this inward force is balanced by the magnetic pressure from neighbouring flux tubes.

Now consider the forces due to the plasma on a flux tube. The gyrational motion of the particles produces a current around the surface of a flux tube considered in isolation. This diamagnetic property of the plasma reduces the magnetic field strength inside the flux tube and hence reduces the strength of the Earthward curvature force just discussed. Thus a flux tube containing higher pressure plasma than its neighbours is subject to a force similar to buoyancy in fluid dynamics. It is

labelled 'diamagnetic' in Figure 3. The remaining forces shown in Figure 3 include the solar wind pressure, which serves principally to compress the magnetosphere into the shape shown in Figure 4, and a magnetic shear stress (labelled Maxwell shear stress in Figure 3) acting at the magnetosphere boundary due to connection of the geomagnetic field with the solar-wind magnetic field. According to merging theories (e.g., Atkinson, 1978) of the solar wind-magnetosphere interaction, flux tubes become temporarily connected to the solar wind allowing the solar wind to exert a shear stress through the magnetic fields, which drags magnetospheric flux tubes toward the nightside.

Another possible source of a shear force toward the nightside (not shown in Figure 3) is a viscous interaction between the solar wind and the magnetosphere at the boundary. It is these shear stresses that drive the internal flow of the magnetosphere.

As stated earlier, there is an equivalance between stresses and currents and we now examine the currents corresponding to the above plasma stresses. The currents corresponding to the plasma forces result generally from particle drift due to inhomogeneous magnetic fields. This includes currents associated with the buoyancy force due to the diamagnetic effect, and currents on the boundary of the magnetosphere. The drift motion is similar to that of Figure 2a except that it is oppositely directed for electrons and protons. The difference in the radius of gyration on the two sides of the gyrational orbit in this case results from differences in magnetic field strength on each side of the orbit and also from centrifugal force due to particle motion along curved magnetic field lines. The exception is the ionospheric ion-drag force or line-tying current. The currents here result from (i) electrons convecting faster than ions due to ion-neutral collisions (Hall current) and (ii) ions drifting in the direction of the electric field due to collisions (Pedersen current) as shown in Figure 2b.

In summary, magnetic flux tubes undergo a convective flow and the magnetic flux tube can be regarded as a fluid element. Forces acting on the elements include pressure from neighbouring elements, the ion-drag force due to ionospheric ion-neutral collisions, the curvature force due to magnetic tension along the flux tube, the diamagnetic effect due to plasma pressure on flux tubes, and magnetic and viscous shear stress and solar-wind pressure at the magnetosphere boundary. The currents associated with these forces are generally due to particle drifts where the particles move in non-uniform magnetic fields. The exception to this is the ion drag force in the E region ionosphere where ion-neutral collisions produce Pedersen currents parallel to the electric field and Hall currents orthogonal to the electric and magnetic fields. The solar wind pressure serves to compress the magnetosphere into its shape and the shear stresses at the boundary drive the internal flow.

It should also be noted that for sufficiently energetic plasmas the magnetohydrodynamic approximation breaks down and the particle drifts due to non-uniform magnetic fields become as important in mass, momentum and energy transport as the electric field drift. For magnetic and electric fields typical of the magnetosphere this occurs for energies of a few keV.

4. THE STEADY-STATE MAGNETOSPHERE

Figure 4 represents a noon-midnight cross-section of the magnetosphere showing the features of importance for this discussion. There are three types of magnetic flux tubes: Those that resemble the flux tubes in a dipole field, those that are stretched out into the tail, and flux tubes in the plasma

sheet that are a compromise between the two. Because of their curvature through the plasma sheet, the plasma sheet flux tubes represent an Earthward force on the nightside magnetosphere. If there is a stronger normal component of magnetic field at the plane in the center of the neutral sheet, more of them thread this plane per unit area and the Earthward force is greater.

The model which is to be used to illustrate the forces and currents of importance is a simplified version of the above. It will assume two types of flux tubes only; dipolar and tail like, with a sharp boundary between the two types. An exploded view is shown in Figure 5. The dipole-like region resembles a doughnut and the tail-like region two sausages linked through the hole of the doughnut at C, and pushed back in the antisolar direction to that they wrap around the doughnut and press against and flatten each other at the neutral sheet along BA. The dipole-like region should in fact be flattened in the north-south plane on the nightside and extended north-south on the dayside to give a better indication of the true shape. In this model, the effect of the Earthward force in the plasma sheet will be represented by increasing the size of the dipole-like region on the nightside and hence moving point B of Figure 5 away from the Earth.

As mentioned in the previous section, there are two types of shear forces at the magnetosphere boundary that may be responsible for the internal convective flow. Either of these applies a stress toward the nightside on flux tubes. The resulting imbalance of stresses drives an internal return flow toward the dayside in the dipole-like region. In the simplified model this imbalance of stresses can be pictured as an excess of dipole-like flux tubes on the nightside and a deficiency on the dayside. The Earthward curvature force drives a flow toward the dayside in the doughnut-shaped region. The stresses due to the nightside excess and dayside deficiency are shown schematically in Figure 6 which is an equatorial cross-section of the magnetosphere. A further set of stresses in Figure 6 are labelled 'Alfvén layer shielding' and these are the result of the diamagnetic buoyancy force. They prevent the flow from penetrating very deeply into the magnetosphere. Thus, as seen in the equatorial plane, the flow to the dayside occurs principally in the outer regions of the magnetosphere. The third force shown in Figure 6 is the ion-drag force associated with line-tying currents and this limits the speed of the flow. Generally the three forces balance since inertial effects are usually small. The resulting flow is shown in the top diagram of Figure 7. Figure 7 is a northern polar-cap view (at ionospheric heights) rather than an equatorial section, thus the effects are turned inside-out in comparison with Figure 6 since the outermost magnetic flux tubes map to higher latitudes. The flux tubes in the doughnut shaped region are in the auroral oval (between the heaviest lines) and at lower latitudes. The flow in the auroral oval toward the dayside is consistent with the forces described. The whole flow system, including the nightward flow across the polar cap (innermost circle) results from the shear forces at the boundary.

In Figure 7, the streamlines are identical to electric equipotentials as discussed in the previous section. The resulting Pedersen and Hall currents are shown in the bottom diagrams if the ionosphere has uniform conductivity. The Hall current closes in the ionosphere along the streamlines as shown. The Pedersen current flows across the streamlines parallel to the electric field and then by magnetic-field-aligned currents to the outer magnetosphere where it closes across field lines as current associated with the forces just discussed which determine the flow. The Pedersen currents and their closure tend to be solenoidal and hence produce weaker magnetic fields at the Earth's surface than

the Hall currents. A non-uniform ionospheric conductivity complicates the above picture in that the Pedersen and Hall currents can no longer be treated separately. However, the overall picture is not greatly changed, and the above provides a useful basis for visualization and modelling. The electric field associated with the flow is typically of the order .01 V/m, but sometimes reaches an order of magnitude greater.

Now the stresses are described, for the simplified model in terms of the current and current closure. However, it is not necessary that the reader have a deep understanding of this before proceeding to the rest of this review. The Pedersen currents of Figure 7 are the line-tying currents resulting from the ion-drag force and they close along magnetic field lines to currents shown in Figures 8 and 9 (Atkinson, 1978).

Figure 8 is a view from the evening side of the currents on the evening surface of the northern half of the magnetosphere. Currents are symmetric in the southern hemisphere and reversed on the dawn surface. Figure 9 is an equatorial cross-section showing the currents. Current systems 1 and 6 close entirely on the surface and in the plasma sheet. These two current systems also exist in a non-convecting magnetosphere, and are the result of solar wind pressure and plasma pressure in the plasma sheet.

The remaining current systems are associated with the convective flow. Current systems 5 and 7 can be simply related to the nightside excess and dayside deficiency of flux tubes in the simplified model. The deficiency of dipole-like flux tubes on the dayside moves the cusp, C in Figure 8, closer to the Equator. This decreases the eastward current across the nose of the magnetosphere, since it is physically smaller, and increases the westward current above the cusp. As a result, the additional current system 5, in Figure 8, appears. It closes along magnetic field lines to and from the ionosphere as indicated by the circles with dots in them. Similarly the excess of dipole-like flux tubes on the nightside creates a bulge (Figure 9) in the boundary of dipole-like field lines (that is a bulge relative to the boundary for the non-convecting case) which is associated with the diversion of some of the cross-tail current to the ionosphere along magnetic field lines. The diverted current is shown as system 7 in the figures. Current systems 5 and 7 are contiguous, and the field-aligned flow of the ionosphere occurs at the northern edge of the auroral oval as shown in Figure 7. Possibly they should be regarded as a single system associated with the driving forces for the convective flow. Current system 4 is called the partial ring current. It is associated with the diamagnetic buoyancy forces of the plasma as previously discussed. It closes by field-aligned currents to the low-latitude edge of the auroral oval (see Figure 7).

In summary, the combined current systems 5 and 7 drive the convective flow into the nightside magnetosphere, current system 4 prevents it from entering deeply and confines it to flux tubes rooted in the auroral oval, and finally the north-south ionospheric Pedersen current across the oval limits the flow rate along the oval back toward the dayside. This is illustrated schematically in Figure 6 in terms of forces. Figure 6 is an equatorial section. The nightside excess and the dayside deficiency of dipole-like flux tubes are represented as forces driving the flow in the solar direction. The diamagnetic effect is represented as radial forces at the Alfvén layer (the limit of penetration), and the line-tying force opposing the flow to the dayside is included.

There are other influences affecting the flow that are worth discussing before considering the time-dependent magnetosphere. First, observations (e.g., Heppner, 1977) show that the convective flow across the polar cap from the dayside to the nightside is distorted from that shown in Figure 7. For magnetic fields in the solar wind with a component in a direction antiparallel to the Earth's orbital velocity, the north polar cap flow tends to have maximum on the dawnside and the south polar-cap flow a maximum on the duskside. The situation is reversed for an interplanetary magnetic fields with a component parallel to the Earth's orbital velocity. The simplest explanation of this is based on the merging model. Flux tubes near the dayside edge of the polar cap that are connected to the solar-wind magnetic field (see Figure 3) are subject to a stress towards dawn or dusk depending on the direction of the interplanetary magnetic field to which they are connected. This is in addition to the nightward stress already discussed.

Another effect to be discussed before considering the time dependent case is non-uniform ionospheric conductivity. There are two regions where it has been shown that this is likely to assume some importance. In the polar caps in summer, the day-night conductivity gradient is expected to squeeze the flow toward the dawnside (Atkinson and Hutchinson, 1978), an effect superimposed on those just discussed. In the nightside, near midnight, the enhanced conductivity of the auroral oval produces a lack of symmetry about the midnight meridian. That is, the divider between the two flow cells shown in Figure 7 should slope from north-west to south-east in the near-midnight oval (e.g., Vasyliunas, 1970).

Further influences on the flow include the drift and loss of energetic charged particles. Perhaps the most promising approach to the overall problem is the development at Rice University of a computer simulation of the flow (e.g., Wolf, 1974, Harel and Wolf, 1976). The simulation is gradually being expanded to include various influences. By and large the flow does not vary greatly in its general form from that shown in Figure 7.

5. THE TIME-DEPENDENT MAGNETOSPHERE

The major time-dependent event in the magnetosphere is the magnetospheric substorm. Its major features include: (i) a characteristic development of auroral activity, (ii) a large somewhat localized increase in current system 7 shown in Figures 8 and 9; this implies more-dipolar flux tubes in the neutral sheet or, in the simplified model, a larger bulge in the boundary of dipole-like flux tubes, (iii) intense particle precipitation and a resulting ionospheric conductivity increase, (iv) injection of particles into the inner magnetosphere partial ring current (system 4). The total energy involved can be as high as 10^{15} joules.

The auroral development as first described by Akasofu (1964) and further developed by Montbriand (1971), is shown in Figure 10 as a time-sequence of diagrams of the auroras in the polar cap. Initially quiet auroras first brighten near midnight then move northward leaving behind them a region of active auroras. The brightening and activity spread eastward and also westward by means of a large fold called the westward travelling surge. The region inside the bulge is believed to correspond to more-dipolar flux tubes. Hence the current downward to the east of midnight, westward along the oval and then upward at the westward travelling surge, is the diverted tail current (system 7) that is expected if more-dipolar flux tubes occur on the nightside. Features ii to iv above

correspond to all the forces shown on the nightside, in Figure 6, being enhanced, although the conductivity variations affect the distribution of ionospheric current between Pedersen and Hall currents.

The reason for the substorm is still a subject of debate and there are at least two possible classes of theory at the present time (Atkinson, 1979): (i) the plasma in the plasma sheet for some reason (several have been suggested) becomes unable to maintain the stretched field line configuration (Figure 4) and there is a collapse of plasma sheet and/or tail flux tubes to a more-dipolar state, (ii) there is a feedback effect between ionospheric conductivity and precipitation of particles. As both increase a more-dipolar plasma sheet (a bigger bulge in the simplified model) is necessary to maintain the flow against the increased line-tying force (analogous to the backing up of a river partially blocked by an obstacle until the hydrodynamic head is sufficient to restore the flow rate).

The actual behavior of the flow and electric field are not well known. The flow is expected to be similar to that in Figure 11. Flows of this type, because of their time dependence, are able to penetrate more deeply into the magnetosphere. Thus substorm associated flows have been observed at latitudes where field lines extend out to only two or three Earth radii, unlike the steady state where the major flow is confined to flux tubes which extend outside four or five Earth radii.

6. NEUTRAL WINDS AND LOW LATITUDES

Most of what has been said in section 5 applies to flux tubes outside the plasmasphere; that is, to magnetic latitudes greater than about 60° at ionospheric heights. It has been assumed that magnetospheric forces are the major driving forces for the flow and that the effect of neutral winds at ionospheric heights can be neglected. This is probably true much of the time at high latitudes.

Inside the plasmasphere, the solar-wind induced electric fields are greatly reduced due to the effect of current system 4, as discussed in section 5, in limiting the depth of penetration of the flow. At middle to low latitudes, the electric fields are an order of magnitude less than at high latitudes, being typically .001 V/m. They may be partly due to solar-wind induced effects (Matsushita, 1971), particularly on the nightside, and partly due to neutral winds in the ionosphere. At equatorial latitudes, the electric fields are believed to be due primarily to neutral winds. At low latitudes on the nightside, winds in the F region ionosphere may be more important than in the E region.

The forces of importance acting on these lower-latitude flux tubes are (see Figure 4) the ion-drag force or line-tying effect due to the relative motion of flux tube and neutral gas, the interaction with neighbouring flux tubes, including those transmitted from higher latitudes, and any effects due to the plasma on flux tubes. Thus, at low latitudes it should in principal be possible to calculate the fields from a knowledge of neutral winds and using the curl $\mathbf{E} = 0$ condition as discussed in section 3.

In general, the winds will cause a convective flow and its associated electric fields and current flow should occur along magnetic field lines between hemispheres in response to neutral winds and conductivities which are not symmetric about the equatorial plane. In practice there are a number of complications (Volland, 1976) and more work is needed on models. Further, observations of the neutral wind are rather sparse.

The approach often used (e.g., Forbes and Lindzen, 1977) is to start with known tidal harmonics of the neutral atmosphere, and from the winds associated with these to predict electric fields and currents. These can then be compared with radar measurements of the motion of the ionized component. The reader is referred to the above publication for results, since they are somewhat complex and will not be included here. It should be noted that the tidal harmonics are large scale and should map well down into the stratosphere.

Perhaps it is worth noting that the tidal harmonics lead to a simple behaviour in equatorial regions. Radar measurements show upward drifts in the day and downward at night with velocities ~10 m/s in near equatorial regions (electric fields of .0003v/m).

7. CONCLUDING STATEMENT

In summary, it appears that all the large-scale electric fields discussed here should map well down into the stratosphere. Further, vertical fields should exist with potential differences equal to half of the horizontal potential differences. The fields include: (i) solar-wind induced high-latitude fields with strengths of .01 V/m and greater, and scale sizes of hundreds to thousands of kilometers, (ii) midlatitude and low-latitude fields with strengths of .001 V/m and scale sizes of thousands or tens of thousands of kilometers. It should be noted that smaller-scale electric fields do exist and are at times as strong as the above. None of those observed have been found to conform to a pattern and are believed to be due to turbulence in the flows.

Finally I would like to point out that if it turns out that electrical field measurements in the lower or middle atmosphere can be used to monitor the cross-polar-cap potential difference, an important step will have been made in magnetospheric physics since this quantity enters directly into the energy flow equations for the magnetosphere-ionosphere system.

REFERENCES

Akasofu, S. I., The development of the auroral substorm, *Planet, Space Sci.*, **12**, 273, 1964.

Atkinson, G. and D. Hutchinson, Effect of the day-night ionospheric conductivity gradient on polar cap convective flow, *J. Geophys. Res.*, **83**, 725, 1978.

Atkinson, G., Energy flow and closure of current systems in the magnetosphere, *J. Geophys. Res.*, **83**, 1089, 1978.

Atkinson, G., The expansive phase of the magnetospheric substorm, Proceedings of AGU Chapman Conference: Magnetospheric substorms and related plasma processes, October 1978, *Space Sci. Reviews*, In Press, 1979.

Dejnakarintra, M., A Theoretical study of electric coupling between the troposphere, ionosphere, and magnetosphere, Technical Report No. 3454-3, Radioscience laboratory, Stanford Electronics Laboratories, Stanford University, 1974.

Forbes, J. M., and R. S. Lindzen, Atmospheric solar tides and their electrodynamic effects - III. The polarization electric field, *J. Atmos. Terr. Phys.*, **39**, 1369, 1977.

Harel, M. and R. A. Wolf, Convection, *Proc. of the International Symposium on Solar-Terrestrial Physics*, Editor D. J. Williams, Published by American Geophysical Union, 617, 1976.

Heppner, J. P., Emperical models of high-latitude electric fields, *J. Geophys. Res.*, **82**, 1115, 1977.

Matsushita, S., Interactions between the ionosphere and magnetosphere for S_q and L variations, *Radio Sci.*, **6**, 279, 1971.

Montbriand, L. E., The proton aurora and auroral substorm, in *The Radiating Atmosphere*, ed. B. M. McCormac, Reidel, Dordrecht, 1971.

Vasyliunas, V. M., Mathematical models of magnetospheric convection and its coupling to the ionosphere, in *Particles and Fields in the Magnetosphere*, ed. B. M. McCormac, Reidel, Dordrecht, 60, 1970.

Volland, H., The atmospheric dynamo, *J. Atmos. Terr. Phys.*, **38**, 869, 1976.

Wolf, R. A., Calculations of magnetospheric electric fields, in *Magnetospheric Physics*, ed. B. M. McCormac D. Reidel, Hingham, Mass., 167, 1974.

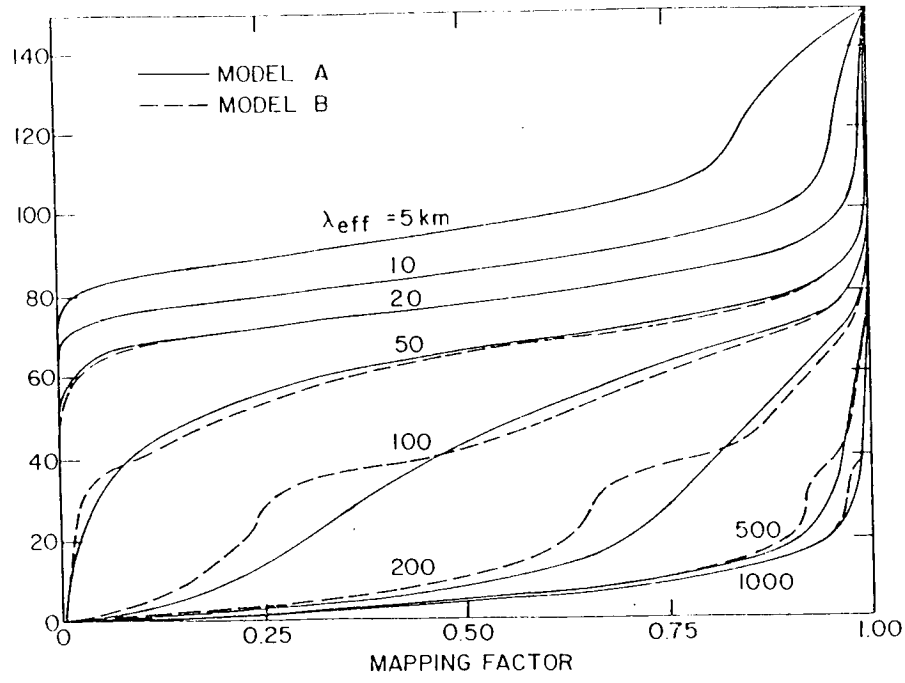

Figure 1. The mapping factor as a function of altitude for different horizontal scale sizes (λ_{eff}) of the electric field (from Dejnakarintra, 1974). The mapping factor is the strength of the horizontal component of the electric field relative to its strength at 150 km altitude.

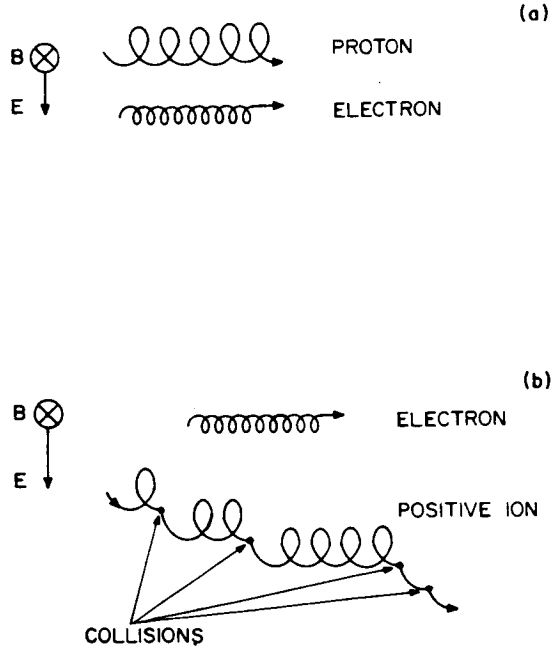

Figure 2. Drift motions of particles in crossed electric and magnetic fields (a) collisionless (b) with ion-neutral collisions.

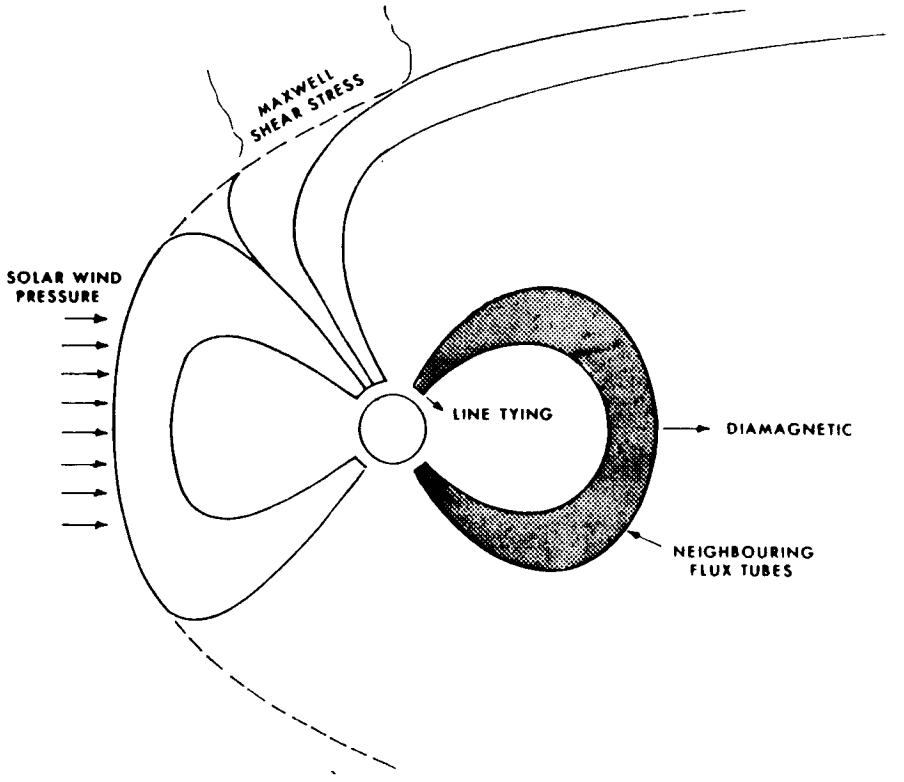

Figure 3. Forces acting on magnetic flux tubes.

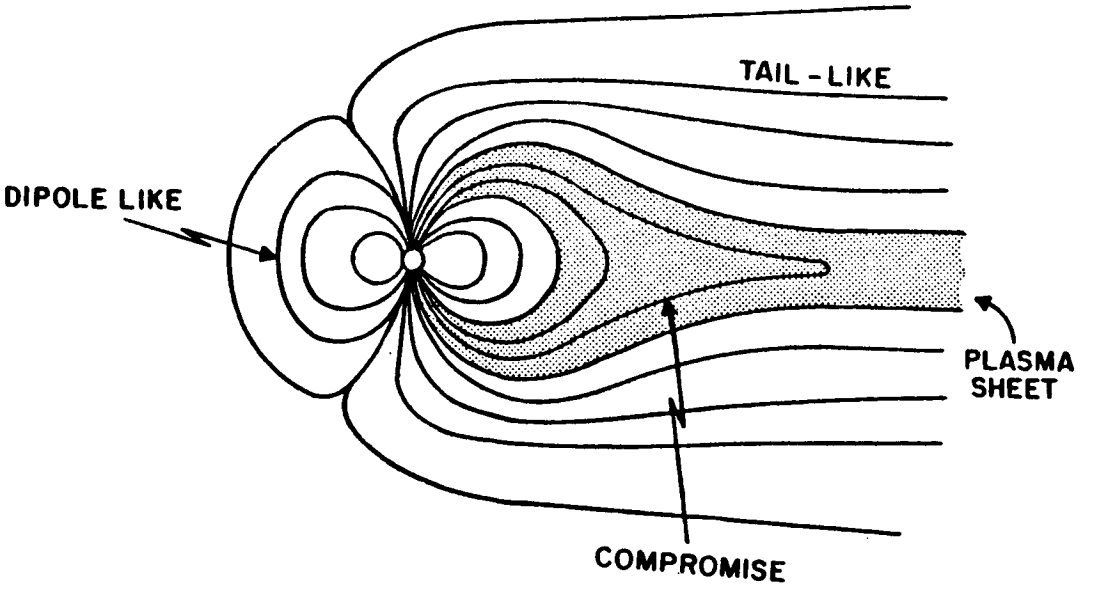

Figure 4. Types of flux tubes in the magnetosphere.

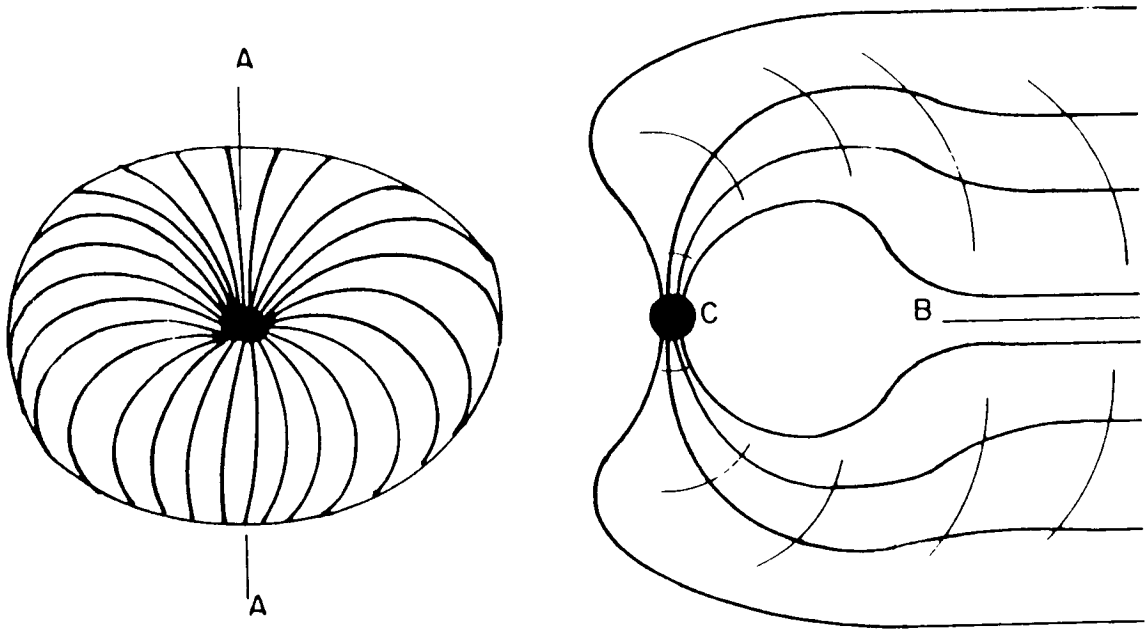

Figure 5. Exploded view of the magnetosphere showing dipole-like and tail-like flux tubes.

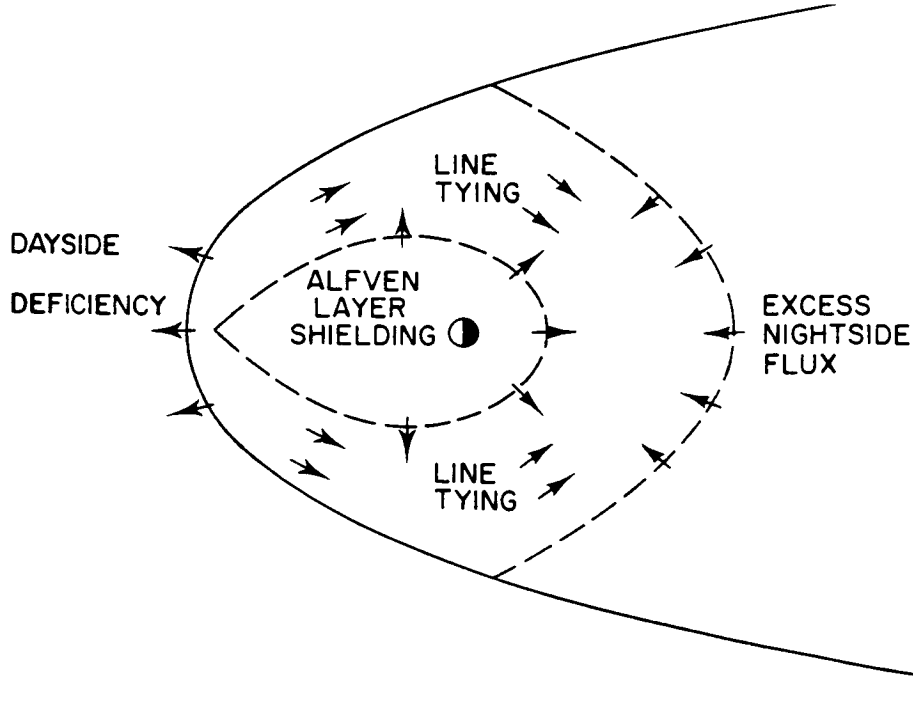

Figure 6. Equatorial section showing the forces of importance in steady-state flow.

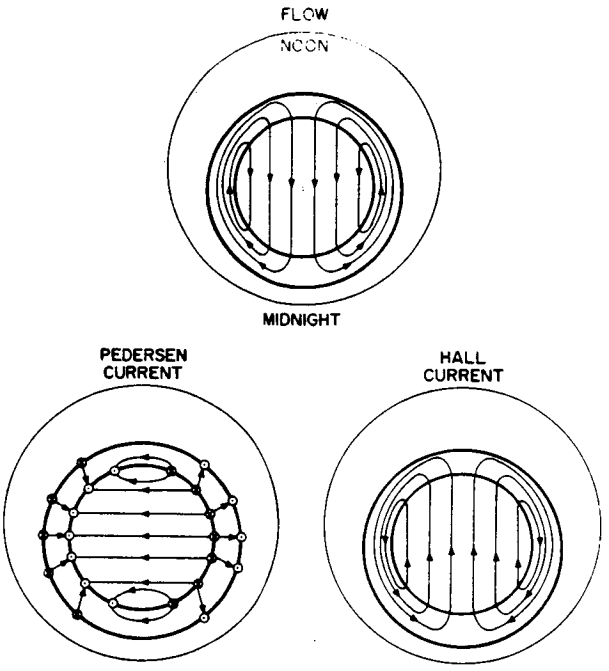

Figure 7. View of northern polar cap showing typical flows and currents. Dots and crosses in small circles indicate upward and downward current flow along magnetic field lines.

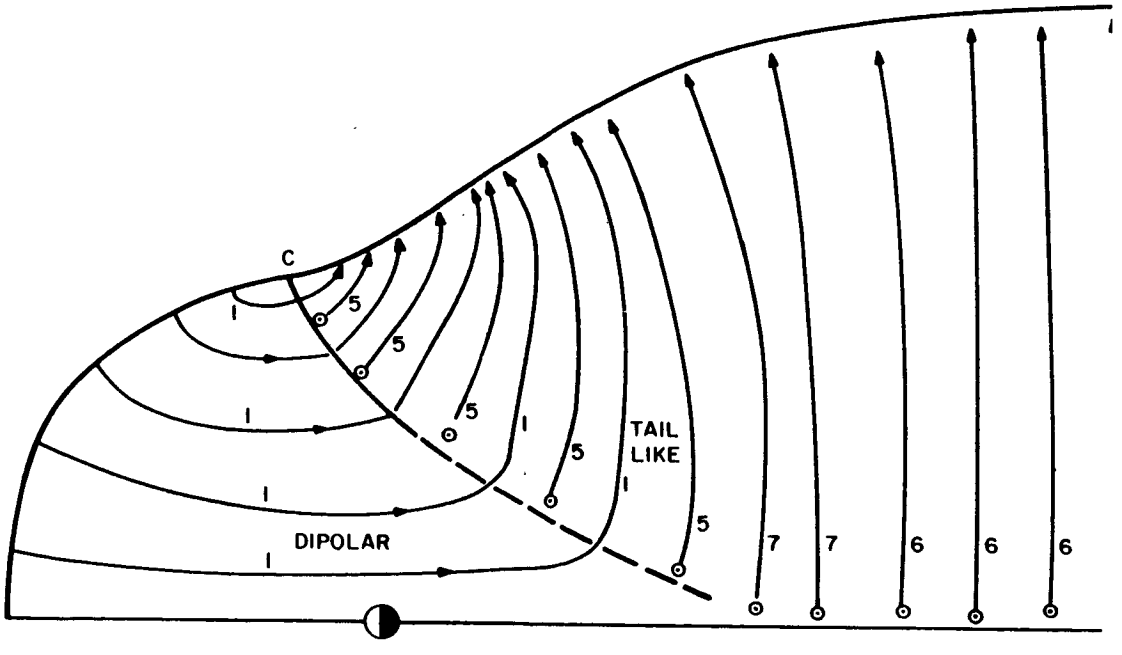

Figure 8. View from the evening side of currents on the magnetosphere boundary in a flowing steady-state magnetosphere.

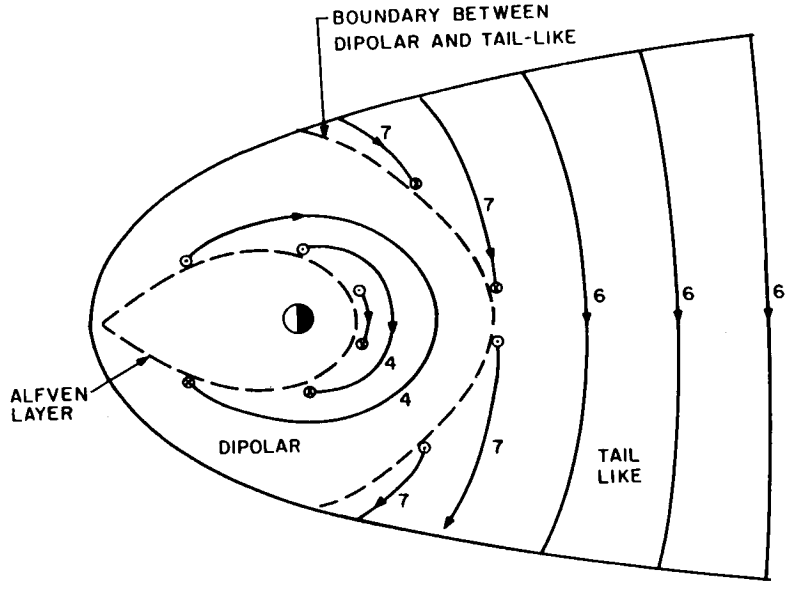

Figure 9. Equatorial section of the magnetosphere showing current systems. Dots and crosses indicate flow along magnetic field lines from and to the ionosphere.

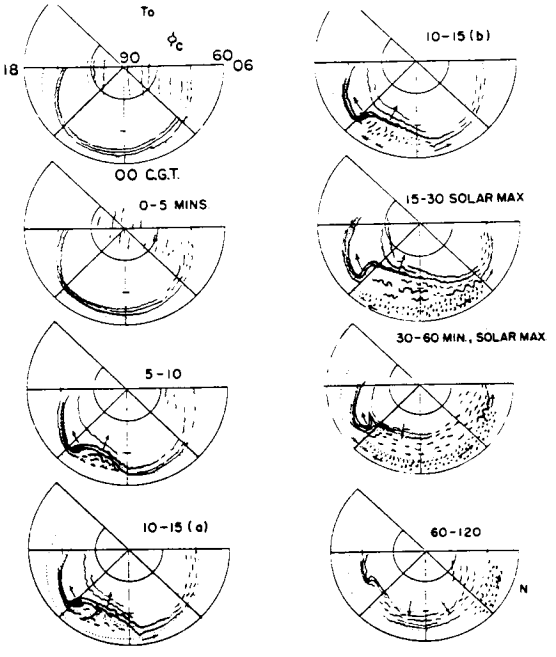

Figure 10. Polar cap view of a typical development of an auroral substorm (Montbriand, 1971). The time development is shown in successive polar cap views. Solid lines are discrete auroras, the dotted lines are the boundaries of proton precipitation. Arrows indicate the motion of auroral structures.

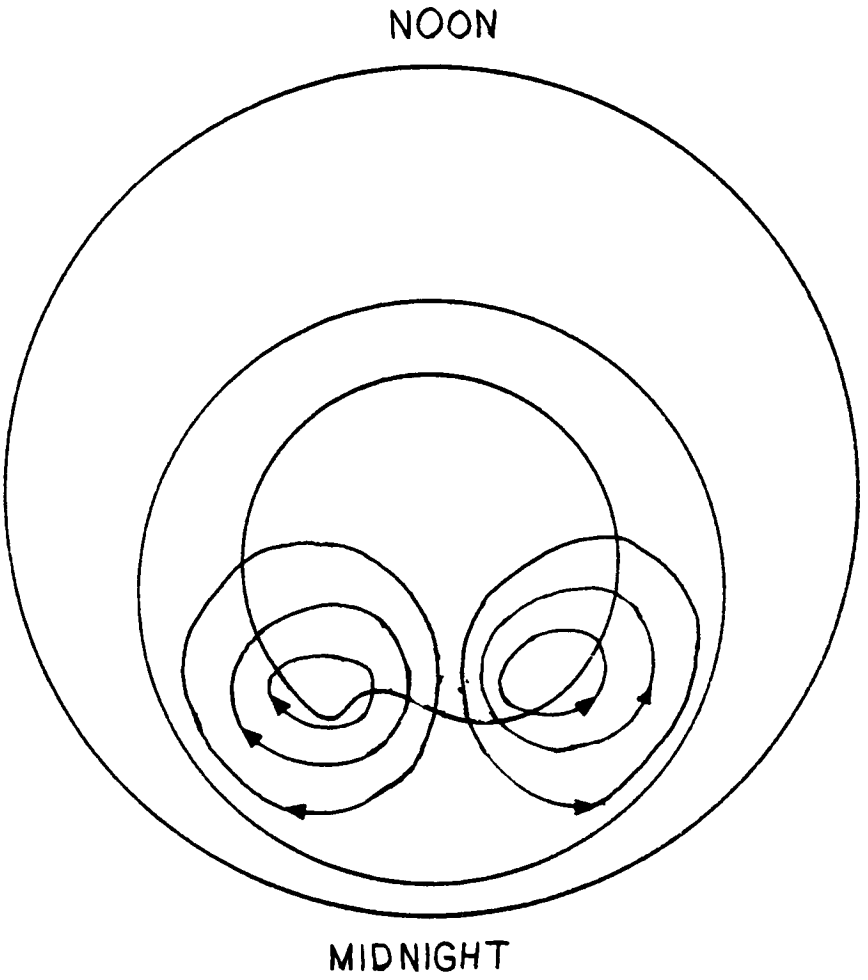

Figure 11. Polar cap view of the expected flow in substorm.

AREAS WHERE SOLAR-TERRESTRIAL COUPLING MAY INFLUENCE OR BE INFLUENCED BY THE MIDDLE ATMOSPHERE

Richard A. Goldberg
Laboratory for Atmospheric Sciences
NASA/Goddard Space Flight Center
Greenbelt, Maryland 20771

1. INTRODUCTION

Traditionally, the charged or ionized components of the atmosphere have been treated independently from the neutral structure. In the upper atmosphere (above 60 km) the ionosphere has been studied to establish its control on radio wave propagation, and to understand atmospheric chemistry. The lightly ionized upper atmosphere has also provided a suitable environment for study of physical processes involving plasma interactions with the Earth's electric and magnetic fields. It is well known that the ionosphere is responsive to long-term and transient phenomena governed by solar activity.

There is now increasing evidence that coupling processes between the upper and lower atmosphere occur, and in large part involve atmospheric electrical properties. Suggestions have also been proposed that such interactive processes may ultimately affect weather and climate. The coupling may occur through changes in localized ionization, which can alter stratospheric and mesospheric chemical processes, thereby affecting ozone and other minor species. The ionization can also affect the production of aerosols and other macroscopic or submacroscopic particulates. The ionizing radiations can affect ion size and mobility, thereby modifying ion-neutral drag and other transport processes. In addition, deviations of the vertical and horizontal atmospheric electric fields from the average quiet norm (fair weather electric field) may also play an important role in processes governing interactions between regions.

This review is concerned with the nature of such suggested interactions, particularly those induced by transient solar and geomagnetic phenomena. Solar activity, in the sense used here, also includes modulations of the galactic cosmic ray flux reaching Earth, as well as solar rotation effects including solar magnetic sector passage by the Earth. Here, we will concentrate on processes involving charged particles and/or atmospheric electric structure. The former also relate to electrodynamical coupling in the sense that the primary source of ionizing radiations below 60 km is corpuscular, and thereby subject to focusing by the Earth's magnetic field. Finally, no discussion of wave coupling interactions is included, since it is covered by other papers in this volume.

2. BACKGROUND AND COMPETITIVE EFFECTS

Figure 1 (Sechrist, 1979) helps exemplify the complexity and nature of the problems relating to solar terrestrial coupling. Solar transient and variable emissions reach the Earth in the form of both electromagnetic and corpuscular radiations. These radiations in turn affect the chemistry and

physical properties of the upper, middle and/or lower atmosphere. Timing for particle arrivals and subsequent magnetic field controls are also important. Electromagnetic radiations travel to the Earth in a few minutes at the velocity of light and affect all sunlit regions; corpuscular radiations arrive from a few hours to a few days following a solar event and are mainly focused to high latitude regions. Other effects are caused by galactic cosmic rays, which do not originate from the Sun but are modulated by short and long-term solar variability. Solar magnetic field effects induced by solar rotation may also couple to the Earth electromagnetic structure. Finally, meteoric ions may be modulated by ionization sources subject to solar variability.

Figure 1 concentrates on processes involving the passage of signals, energy, and other forms of coupling from the upper to lower atmosphere. There is already a large body of evidence demonstrating the reverse influence i.e. tropospheric meteorological disturbances on the upper atmosphere and magnetosphere. These add to the difficulty of analyzing cause and effect, and must be contended with in suitable coupling mechanism concepts.

For example, Gherzi (1950) and Bauer (1958) demonstrated ionospheric F region ionization enhancements above hurricane passages. Apparent ionospheric responses to cold fronts were also noted by Gherzi (1950), Bauer (1957), and Arendt and Frisby (1968). To explain the observational results, Bauer (1957) hypothesized a dynamic coupling process between the troposphere and ionosphere.

Acoustic waves generated by several local storms have been detected in the F region by Georges (1968), and Baker and Davies (1969), and Hung et al. (1975). The waves, whose periods in the ionosphere are in the range 2-5 minutes, are detected by CW doppler techniques. Most recently, Hines and Halevy (1977) have proposed a gravity wave feedback mechanism, whereby energy produced in the troposphere by meteorological phenomena propagates upward via gravity waves. Under certain assumed conditions which could be modulated by solar activity, the upper atmosphere will reflect the waves downwared to interfere constructively or destructively.

In addition, there is evidence that lightning can induce effects in the middle atmosphere and above. For example, whistlers, which are VLF waves thought to be induced by lightning discharges, are guided along the Earth's magnetic field between conjugate points for path length exceeding 30,000 to 50,000 km (e.g. Davies, 1965). Recently, Bering et al. (1979) have measured microbursts of electron precipitation from the magnetosphere, stimulated by VLF spherics generated by lightning in a thunderstorm cell. Since the precipitating particles can ionize and dissociate molecules in the upper atmosphere, a lightning induced mechanism for perturbation of the upper atmosphere is created.

A direct effect on stratospheric ozone has also been suggested by Dubin and Zipf (1977). They have determined enhanced production rates for N_2O under lightning discharge conditions, and offer the suggestion that large quantities of N_2O, NO_x, and other trace species are produced within the tropical zone, where thunderstorm activity is highest. Injection of such species into the lower stratosphere, particularly within large convective thunderstorm cells that penetrate the tropopause, could significantly deplete stratospheric ozone in time (Noxon, 1976; Chameides et al., 1977).

Man induced effects in the troposphere also affect the upper domains. The most famous topic under discussion in recent years has been depletions in stratospheric ozone induced by hydrofluorocarbons, which occur in many products such as aerosol sprays. SST transports have also been considered as significant candidates for ozone modification in the stratosphere. Man may also affect the upper atmospheric environment in electrodynamic ways. For example, Park and Helliwell (1978) have shown correlative data to suggest that power lines, particularly at high latitudes, generate VLF waves which propagate to the outer magnetosphere. There they can induce particle precipitation which affects ionization, etc. within the lower thermosphere (Figure 2). Finally, Boeck (1976) has considered the gradual increase in the troposphere of radioactive Krypton 85 discarded during nuclear power plant operation. He suggests that this is rapidly becoming the dominant ionization source in the lower troposphere, and will soon have a profound effect on the global electrical circuit.

The above provides both transient and long term examples of effects that must be considered in any studies involved with the determination of atmospheric coupling processes. The evidence for upward coupling is established. We must now determine if downward coupling can play as significant a role.

3. RADIATION SOURCES - A BRIEF SYNOPSIS

Solar electromagnetic radiations are predominantly in the visible, and affect the lower troposphere. There is some evidence (Heath and Thekaekara, 1977) that solar UV, especially toward the more energetic portion of the spectrum, shows a solar cycle dependence, but this has not been observed for the total solar output (solar constant). Solar flares and other active phenomena exhibit enhanced emissions of UV and X-rays which cause ozone production and ionization respectively, but such emissions are short lived and do not cause sustained effects.

Solar active events cause the deposition of energetic corpuscular streams into the Earth's atmosphere at high latitudes, where geomagnetic shielding effects are weakest. These energetic particles can directly or indirectly affect the middle atmosphere, depending on their type, energy, and flux. They include solar protons which produce polar cap radio absorption events (PCA), and relativistic electron precipitation events (REP) whereby relativistic electrons created by plasma interactions in the magnetosphere precipitate to stratospheric depths. Furthermore, most high latitude geomagnetic disturbances lead to energetic electron precipitations which cause x-ray aurorae by the bremsstrahlung process near 100 km. The converted energy can reach to stratospheric depths, and can dominate over the effects of galactic cosmic rays to altitudes below 40 km. Finally, galactic cosmic rays are modulated by the individual geomagnetic events and by sunspot cycle, and these have bearing on the ozone distribution in the mesosphere, stratosphere, and troposphere. Characteristic penetration depths for the various corpuscular radiations as a function of energy are illustrated in Figure 3 (Thorne, 1977).

4. COUPLING PROCESSES AND MECHANISMS

Two major categories of interaction have emerged which apply to electrodynamic coupling. First, in the search for identification of physical processes to explain the statistical correlations of sun/weather and climate, the stratosphere and mesosphere must be regarded as an important atmospheric domain within which coupling might occur. Ozone plays a major role in the radiative and photochemical processes of this region, and therefore must be considered a key parameter for study. It is also extremely important to understand the natural variability of ozone and its response to geophysical phenomena before one can assess the impact of man induced influences on the same environment. Because the variability of ozone may be influenced by ion-neutral chemistry induced by energetic charged particles, it is appropriate to consider such effects here. Aerosols and particulates must also be considered here, since some variation in these constituents can also be related to solar activity. Noctilucent and nacreous clouds, as well as sub-macroscopic particles, have been offered as modifiers of tropospheric weather and climate. Hence, this category considers the middle atmosphere as a buffer region, within which energy undergoes reflection, transmission, filtration, amplification, absorption, and/or some other form of conversion.

Second, there is newly emerging experimental evidence that atmospheric electric fields, especially at high latitudes and in the upper atmosphere, are responsive to solar and geomagnetic phenomena. The corpuscular radiations previously discussed are known to strongly enhance the local atmospheric electrical conductivity and ionization at stratospheric and mesospheric altitudes. However, the electric field perturbations are not easily explained by conventional atmospheric electricity considerations. Several new theories have now postulated that some electric field perturbations are regulated by solar activity and may be responsible for the observed statistical correlations between solar activity and tropospheric disturbances, e.g., thunderstorms. They include the concept that cosmic rays and/or solar protons can both affect the global electrical circuit and the local field near thunderstorms. These can then alter the rate of lightning formation and possibly, thundercloud buildups.

Both categories contain established results relating to middle atmospheric and tropospheric response to the radiation sources. However, extrapolations to short-term (weather) or long-term (climate) affects in the troposphere all suffer from one or more speculative components. The electrical connection has made more progress toward a full explanation, because it may bypass the stratosphere as an intermediary, and because it causes instantaneous reactions.

4.1 PROCESSES INVOLVING MIDDLE ATMOSPHERIC RESPONSES TO SOLAR ACTIVITY - OZONE

To pass from the upper atmosphere to the troposphere, energy may undergo one or more intermediate changes, possibly affecting relevant meteorological parameters. Recent observations of stratospheric variability in connection with particle injection events have already suggested some possible candidates. A depletion of ozone during a PCA event was first observed in the mesosphere by Weeks et al. (1972) and later interpreted by Swider and Keneshea (1973) to be caused by enhanced HO_x production during this event. More recently, a 20 percent depletion above 4 mb was observed during the great PCA event of August 1972, using ozone data from the BUV experiment

on Nimbus IV (Figure 4, Heath, et al. 1977). Most remarkable is the persistence, whereby the O_3 depletion was maintained long after the termination of the responsible source. The high latitude depletions observed were explained by production of odd nitrogen through proton bombardment as a loss agent. It has also been argued by Thorne (1977) that REP events could cause similar magnitude changes when the cumulative effect of these more frequent events are combined. Rocket data evidence for ozone depletions during auroral x-ray events has been reported by Goldberg (1979). Preliminary findings showed a 25% depletion of ozone above 1 mb, cf. Figure 5, (Hilsenrath, pvt. communication 1979) following each of two nighttime x-ray auroral substorms. These results have been verified with two additional comparisons during March 1978. The observed maximum in x-ray energy deposition occurred in the region of ozone depletion. However, x-ray and particle data showed that nighttime relativistic electrons were also present in adequate quantities to override the x-ray energy deposition above 55 km by as much as a factor of 100. Nighttime relativistic electrons have also been detected on a regular basis during auroral storm conditions by satellite (cf. Reagan, 1977). This newly measured nighttime radiation may help account for the observed ozone depletion, which is too large to be explained by conventional means from the x-rays alone.

Long-term response of stratospheric ozone over a solar cycle (e.g. Angell and Korshover, 1973, 1975) has also been seen from statistical studies based on data from the global network of ground based Dobson stations. If true, this longer response may be more indicative of solar UV variability over a solar cycle, as indicated in the work of Heath and Thekaekara (1977), since solar UV is the primary control for atmospheric ozone production. The results are controversial, because of absolute and intercalibration errors between stations, gaps in data acquisitions and a host of additional problems. The conflicts may further be explained by the fact that total ozone (Dobson) measurements are dominated by the maximum density of ozone found below about 25 km altitude. In this height regime the residence time of atmospheric ozone is about 2 years, and its distribution and concentration are controlled by transport processes. The effects of production and loss processes related to solar variability are thus obscured in total ozone data.

In searching for physical mechanisms based on ozone to improve the forecastibility of weather and climate, total ozone data bases are the wrong place to look. Rather, variations in ozone above the transport region should be investigated. Frederick (1977) has in fact theoretically modelled O_3 response to solar UV changes over several solar rotations using the data of Heath (1973) and found 22% fluctuations about the norm in mesospheric ozone. Even the auroral effect produces approximately 7% change in mesospheric ozone. For the eleven year solar cycle both Callis and Nealy (1978) and Penner and Chang (1978) have calculated significant changes in stratospheric ozone, with the latter case showing agreement with Angell and Korshover (1973, 1975). Although solar UV variability presents a major influence on natural ozone response, we concentrate on corpuscular effects to maintain our context with electrodynamical coupling. Here, numerous calculations have been published demonstrating the feasibility for ozone depletion by corpuscular bombardment (e.g. Frederick, 1976; Thorne, 1977; Heath, et al. 1977).

Thus, there are apparent changes to stratospheric and mesospheric ozone induced by both transient and long-term solar variability. The question to be asked is if such ozone variability can affect tropospheric behaviour. There are several new ideas linking ozone changes to stratospheric heating, alteration of the stratospheric circulation pattern, and eventual modification of the troposphere.

Fritz and Angell (1976) have suggested an auroral mechanism, whereby auroral IR heating may affect stratospheric temperatures as much as 2°K. Others have looked at the effects of solar UV variability and corpuscular radiations. Stratospheric temperature variations due to changing solar UV flux intensities are substantial at heights above about 10 km, according to modeling results of Callis and Nealy (1978). At solar maximum, the greater heating of O_3 by solar UV leads to calculated temperature increases up to a maximum of 18°K in the 40-55 km height range in three model cases and 45°K in the other two. Most recently, Penner and Chang (1978), with a more comprehensive model, have found the effects to be much smaller but still significant. Both papers have not attempted however, to calculate how temperature changes of this magnitude, induced globally by solar UV, could affect circulation patterns. Schoeberl and Strobel (1978) have considered circulation effects caused by corpuscular radiations, which deplete ozone to induce temperature changes on a more local scale. They conclude that even for the great PCA events of August 1972, the measured ozone depletion would be inadequate for cause significant change in the global mean circulation.

Using a different approach, Avery and Geller (1979) have investigated the effects of changing middle atmospheric winds on tropospheric planetary waves. The Avery and Geller calculations, based on a steady-state linear, quasi-geostrophic planetary wave model extending from the ground up to 100 km altitude with spherical geometry, indicate that the planetary wave amplitude can change significantly as its phase shifts east or west (i.e., ridges of highs and lows move E or W) mainly in response to jet stream amplitude changes. Here, variations in solar UV flux intensity over the 11-yr sunspot cycle and the 27-day solar rotation period, or in solar corpuscular emissions, could alter the stratospheric ozone structure and produce changes in the temperature gradient through ozone heating. The temperature changes would then affect the strength of the polar night jet stream near the stratopause, causing amplitude variations and phase shifts in the planetary wave structure. Finally, variations in planetary wave structure could alter the position of principal storm tracks, with an attendant change in weather patterns.

Turning to the very long-term, Reid et al. (1976) have considered PCA's during Earth magnetic field reversals. During such periods (at intervals of order 10^6 years) the Earth's field is sufficiently weak to permit solar proton bombardment globally, following solar proton flares. They have considered how such bombardment on this more extensive scale might affect the biosphere, but also indicate possible influences on climate.

4.2 PROCESSES INVOLVING MIDDLE ATMOSPHERIC RESPONSES TO SOLAR ACTIVITY– CLOUDS AND AEROSOLS

Clouds and aerosols may also respond to solar variability. Noctilucent clouds (NLC) are the highest in our atmosphere and occur near the summer polar mesopause ($\sim$85 km) in polar summer. Satellite data (Donahue et al., 1972) have shown NLC to be continuous over the polar cap (>80° latitude) for several weeks during polar summer. This is in contrast to ground based measurements, which have historically indicated temporally varying and spatially discontinuous structure, especially toward lower latitudes within the auroral zone. Little is known about the structure and composition of NLC. However, Hummel and Olivero (1976) have calculated radiative temperature changes at the Earth's polar surface on the basis of the satellite observations and conclude that changes of up to 1°C are possible, depending on particulate shape, size and concentration.

Statistical correlations of NLC with solar activity have been reported. For example, one observation claims that NLC rapidly dissipate following the onset of aurorae, and D'Angelo and Ungstrup (1976) postulated that this may be due to joule dissipation of large ionospheric electrical fields. Experimental evidence with a rocket-borne ion mass spectrometer (Goldberg and Witt, 1977) shows that metallic species of meteoric origin (especially Fe^+) may be nucleation agents for NLC formation. Since the production of Fe^+ ions is enhanced by precipitating particles this may lead to increased NLC formation when other meteorological conditions are satisfied.

Within the stratosphere, nacreous (mother of pearl) clouds are occasionally observed, always near 30 km. They are most often sighted in northern latitudes during local winter, and can only be seen during the unique sunlight reflection conditions provided by sunrise and sunset. Meteorologists consider such clouds to be induced orographically, but this does not explain an absence of sightings at mid- and low- latitudes. The impact of such clouds on coupling processes, through frequency of occurrence and spatial coverage, remains to be demonstrated, although effects originating through nucleation by solar proton events and other geomagnetic phenomena cannot be discounted at this time.

Solar and geomagnetic influences on cirrus clouds, highest in the troposphere, have also been postulated. These relatively frequent and well observed clouds can modulate the intensity of visible radiation reaching the lower atmosphere and surface. Roberts and Olsen (1973 a,b) have claimed that a cirrus cloud deck near 300 mb could cause local heating up to 1°C per day at high latitudes over a relatively warm ocean surface. The strong temperature gradients induced would then lead to significant circulation patterns within the troposphere. Roberts and Olsen also postulated that cirrus clouds are subject to solar activity effects through interaction with ionizing energetic corpuscular radiation, either directly or through secondary bremsstrahlung x-ray radiations. Johnson and Imhof (1975) have criticized this concept however, by arguing that the nearly constant ion pair production rate up to 28 km due to cosmic rays is rarely perturbed by x-ray radiations, even during major geophysical events.

Finally there is some evidence for submacroscopic aerosols within the middle atmosphere. These particulates have been deduced largely from the data of rocket-borne Gerdien and blunt probes. These data have exhibited huge order of magnitude changes of ion conductivity within the middle atmosphere as a function of latitude, time of day, season, and geomagnetic or solar disturbances. Our lack of knowledge concerning such particulates is evidenced by the recently reported results of Mitchell et al., (1977). They conducted a series of four soundings to measure ion conductivity through sunrise from White Sands, New Mexico (Figure 6). The large enhancements between 40 to 65 km are attributed to increases in ion mobility (reduction in ion size), since solar ionizing radiations have small effect below 65 km. This could be observed directly on the latter two flights in 1975, which used Gerdien probes capable of evaluating mobility from independent measurements of ion concentration and conductivity. The paper argues that the solar UV radiation must dissociate heavy ions or particulates to form smaller mass species during daytime, but a closer study of the profiles seems to indicate that the effect progressed from lower to higher altitudes, in conflict with that explanation. It is also not clear what effect the time separation ($\sim$4 years) between soundings may present.

More measurements are required to determine the character, distribution, size, and morphology of submacroscopic particulates within the middle atmosphere. If they exist in reasonable quantities, they may affect the transport and circulation properties of the middle atmosphere. For example, Hale (1977) has recently speculated a scavenging process whereby a few charged particulates of appropriate size, set in motion by electric field forces, could drag the neutral atmosphere and cause accumulation of trace constituents in localized regions. A knowledge of charged particulates and heavy ions is also important for the electrical considerations of the next section.

4.3 THE ELECTRICAL CONNECTION

In most classical texts on atmospheric electricity, e.g., Israel (1970, 1973), it is specified that the global electrical current is driven by global thunderstorm activity (about 1500 to 2000 storms at any given instance of time). This conclusion is largely deduced from indirect measurements (e.g., Figure 7) wherein the observed daily (UT) variation in vertical potential gradient appears as the envelope of the peaked activity for the three major continental thunderstorm regions. This assumption has not been verified with a suitable global mapping study. At present, there is no adequate technique employed for establishing the variation of thunderstorm activity on a spatial and temporal basis, both of which are required to evaluate the total electrical budget. In the classical sense, the basic circuit cannot be subject to perturbations from external sources, since the ionosphere acts as an "infinitely" conducting spherical shield. However, recent comparisons of the magnetospheric and atmospheric electric fields show them to be of comparable magnitude (Sugiura, private communication, 1979). Since the ionosphere is not an infinite conductor in actuality, one might suspect penetration of the external magnetospheric fields into the middle and lower atmosphere, and vice versa. Furthermore, solar and magnetospheric fields connect in outer space, providing the possibility of a direct physical connection between solar active phenomena and the atmosphere.

4.3.1 Electric Field Response

The mapping of solar related phenomena to the atmospheric fair-weather electric circuit has been observed through correlative studies relating on the short term, to solar sector boundary passages and solar flares, and on the long-term to the 11-year sunspot cycle. The parameters studied are the return current (air-Earth current density, J_c), the atmospheric vertical potential gradient (or electric field, E), and the total ionospheric potential (potential difference between the ionosphere and ground, V_i). Fair-weather measurements of E and J_c over the 11-year period May, 1964, to February, 1975, at Zugspitze (47.4°N, 11.0°E, elevation 2962 m) exhibit response to sector boundary crossings (Reiter, 1976; 1977). The results of Reiter's superposed epoch analysis, show that both E and J_c increased by 20% or more on the two days following a -/+ sector boundary crossing in maximum solar activity years. An increase also occurred for +/- boundaries, but on the same day as the crossing date. A superimposed epoch study based on a shorter data span (March - November, 1974) by Park (1976) indicates that the potential gradient at Vostok (78°S, 107°E) increased sharply by 20-30% beginning 3 days after boundary passages, and the effect was more pronounced in the astral winter months than the equinox months. The response was similar for +/- and -/+ boundary crossings. The difference in response time for the Vostock and Zugspitze electric fields remains unclear, although new modeling results by Hays and Roble (1979) may account for geographical differences in temporal lag.

Next turning to solar flares, Cobb (1967) found at the Mauna Loa, Hawaii observatory (19.5°N, 204.4°E, elevation 3400 m), that E and J_c increase significantly after solar flare eruptions. The potential gradient maximized 3-4 days after the flare day, while the air-Earth current density reached maximum after 1 day; both quantities remained above normal for several days thereafter. In a series of studies, Reiter (1969, 1971, 1972) has shown that E and J_c measured at Zugspitze also responded to solar flare eruptions.

Potential gradient enhancements have been observed to be correlated with solar radio noise bursts (associated with flares) at Zugspitze (Reiter, 1972), and at stations within the Arctic Circle (Sao, 1967). Märcz (1976) has found enhancements in E of 30-50% in Poland (approx. 51°N) associated with geomagnetic storms (which generally follow solar flare eruptions).

Long-term measurements of the fair-weather electric field in the first two decades of this century suggested a stronger average field strength in years of maximum sunspot activity compared to minimum years at some European stations, but no apparent influence at others (c.f., the review by Herman and Goldberg, 1978b, p. 139). According to Mühleisen (1971), the total ionospheric potential measured over Germany for a complete solar cycle exhibits a positive correlation with annual mean sunspot number. To the extent that the total potential is proportional to global thunderstorm activity, one might therefore expect the latter quantity to be correlated with the 11-yr. sunspot cycle.

4.3.2 Disturbed Weather (Thunderstorm) Response

In contrast to the classical electrical picture that thunderstorms drive and control the fair weather electrical circuit, there is some emerging evidence that external influences may help modulate thunderstorms. At this time, the results are largely statistical and in many cases, questionable or controversial (Pittock, 1978; Herman and Goldberg, 1978b). The current techniques for counting thunderstorms and/or lightning are quasi-subjective, dependent on good observing techniques and station location. They normally ignore factors such as storm intensity, lightning frequency, or storm areal extent.

Markson (1971) was the first to observe solar sector boundary response and based his study on U.S. thunderstorm data collected during the solar minimum period covering approximately 52 sector boundary crossings (November, 1963-December, 1964, inclusive). There seemed to be a definite preference for thunderstorms to occur from about 1 day before to one day after a +/- crossing, but no statistically significant response to -/+ crossings.

A more detailed analysis has now been made by Lethbridge (1979), who used data from 102 weather stations in the U.S. extending from the Atlantic Coast to 102°W longitude and from 30°N to 45°N latitude to derive a thunderstorm index. The daily index was corrected for seasonal effects, and compiled for the total area as well as for three latitude bands (30-35°, 35-40°, 40-45°). In a superposed epoch analysis of three separate sets of data (1947-1956; 1957-1965; 1966-1976), she found the strongest solar signal in the thunderstorm index for the winter months (November-March) in the latitude band 40-45°N, with peak activity occurring 1 day after +/- boundary crossings. With the index combined for all seasons and latitudes, and for both polarity crossings, Lethbridge could find no discernible response to sector boundaries.

Several different measures of thunderstorm activity have been utilized in studies of the response to solar flare eruptions, and all seem to show a positive response but with varying lag times. For example, Reiter (1969) used sferics counts in Germany (indicative of lightning flashes in thunderstorms within a 300-mile radius) for the years 1964-1967. He found a 57% increase in count rate peaking about 4 days after the eruption of solar flares with importance ≥ 2. Markson (1971) used the number of thunderstorms reported daily in the United States in 1964-1965, and claims a 63% increase approximately 7 days after flare occurrences.

Other results include Bossolasco et al. (1973), who used the number of long-range radio direction-finding fixes recorded in the Mediterranean area as a measure of thunderstorm activity in that area for the 1961-1971 period, and showed a 50% increase in the daily number of fixes beginning one day and peaking 4 days after solar flare occurrences. VLF whistler counts were used by Holzworth and Mozer (1979) as an indicator of high-latitude thunderstorm activity during the August, 1972, solar-terrestrial events. They found a strong increase in count rate beginning about 12 hours after the class 3 flares of August 4 and August 7.

Finally, long-term studies of the variability of the annual number of thunderstorm days in different regions with the 11-yr. solar cycle are replete with contradictions. The analysis of Siberian thunderstorms by Septer (1926) has been cited often as proof that middle-to-high latitude thunderstorm occurrence is directly correlated with annual mean sunspot number (correlation coefficient = +0.9). This result, however, has been severely criticized by Pittock (1978). Brooks (1934) listed correlations coefficients for 22 regions of the world including Siberia, England/Wales, and seven subdivisions of the USA. His analysis from 57 years of England and Wales data suggests that annual mean sunspot numbers and annual number of thunderstorm days are uncorrelated. On the other hand, Stringfellow (1974) found a strong positive correlation for the same region based on English thunderstorm occurrence in the years 1930-1973, as shown in Figure 8.

4.3.3 Causal Mechanisms for Thunderstorm Triggering

No fewer than five separate theories have been recently proposed to seek an explanation for thunderstorm (lightning) response to solar activity. However, none of these bridge the final gap to explain how modifications in the electrical structure of thunderstorms can affect local or global meteorological structure. One concept considers the effects that external influences may have on the global electrical circuit. Ney (1959) suggested that thunderstorm activity may be modulated by solar variability through alteration of the electrical state of the middle and lower atmosphere. Markson (1971, 1975, 1978) amplified this idea to evolve a theory which in its present state (1978) assumes that the electrical resistance of the atmosphere above thundercloud tops (the charging resistor, see Figure 9) will be lowered by enhanced ionization associated with incoming cosmic particles. The charging current is thereby increased leading to an enhanced ionospheric potential and fair-weather electric field which must adjust globally to the increased charging current. The enhanced electric field is also thought to somehow produce increased lightning within thunderclouds. One question with this idea concerns the magnitude of cosmic ray fluctuations reaching thunderstorm heights in the tropical zone, where thunderstorms predominate; are the fluctuations near the equator sufficiently large to induce the required effect?

D'Angelo (1978) has modified the global circuit by introducing a variable emf source representing the ionospheric potential at high latitudes. Fluctuations in this second driver forces readjustment in the global circuit including the fair-weather electric field. He argues that the ionospheric potential is sensitive to solar wind electric fields, magnetospheric fields, etc., thereby introducing a coupling link within the solar-terrestrial system. These results are also consistent with the recent analysis of Sugiura (1979, pvt. communication) which demonstrates the equivalent magnitudes of the fair-weather and magnetospheric electric fields, and help justify the concept of magnetospheric electrical field mapping into the stratosphere (Figure 10). New experimental results of Hale and Croskey (1979) also suggests that middle atmospheric electric fields in the auroral zone are sensitive to auroral phenomena. Hays and Roble (1979) have provided the most quantitative and sophisticated modeling effort to date. They have developed a global model for electrical parameters, which includes as input parameters orographic effects from the Earth's surface, the global thunderstorm distribution as observed from the DMSP satellite, and the latitudinal distribution of cosmic ray flux. They too, have calculated high latitude effects induced by solar active and/or magnetospheric phenomena, and have found significant perturbations on the global circuit properties. Finally, we note that care must be taken in each of the above cases to separate electric field disturbances of solar origin from those induced by tropospheric storms. According to Cole (1976), the latter can develop a feedback phase relationship giving the appearance of magnetospheric origin.

In a more localized approach, Herman and Goldberg (1976, 1978) have considered how cosmic rays and solar protons affect the local environment near thunderstorms, and if modifications in the local conductivity and electric fields can assist lightning generation. For the case of cosmic rays, the changes appear quantitatively reasonable based on the school of thought (c.f., Chalmers, 1967), that an increase in the fair-weather field enhances the probability of thunderstorm formation under appropriate meteorological conditions. Thus, solar-controlled variation in cosmic ray intensity, especially over the 11-yr. cycle, may modulate the fair-weather field and hence the rate of thunderstorm occurrence. The more difficult question concerns how solar protons, which typically are absorbed above 20-25 km, could affect tropospheric electrical structure. Figure 11 shows penetration depths for protons during several large PCA events of the last decade, and compares the effect of cosmic rays over a solar cycle. Ion transport cannot carry charge to lower altitudes because of short ion lifetimes and slow vertical transport in that part of the atmosphere. One possible exception is illustrated in Figure 12, wherein large vertical motions induced by ion-neutral drag may exist near the tropospheric gap caused by the polar jet stream. Also, charges attached to particulates can have longer lifetimes; this adds further justification for increased study of aerosols as discussed earlier. Alternatively, Herman and Goldberg have suggested that flare-produced solar protons penetrating to the stratosphere may effectively lower the height of the electrosphere. The boundary region for proton cutoff would increase the magnitude of the vertical fair-weather field and also induce a horizontal field component at thunderstorm heights, as shown in Figure 13. Triggering of lightning would again be accomplished by the modified potential gradient.

Follin et al. (1977) have taken a different approach to explain lightning generation in thunderstorms. Beginning with the premise of a pre-existing thundercloud, they argue that meteorological dynamics cannot generate sufficient electric potential to equal or exceed the breakdown voltage of the atmosphere. If however, the cascading muons from a high energy cosmic ray pass through the

thundercloud they can provide an ionized path for a lightning bolt to follow. If there is any solar control of the occurrence rate of cosmic ray air showers, the incidence of lightning should correlate with solar variables.

The final scenario, what happens to the meteorology by changes in atmospheric electrification, is open to speculation. Here, various suggestions have postulated improved conditions for hail formation, water droplet growth and enhanced rain, etc. These concepts await physical validation.

5. SUMMARY AND CONCLUSIONS

We have briefly considered the various radiations reaching the middle atmosphere in response to solar activity, and their known effects on neutral and ionic species of that region. Those responses have then been evaluated as possible coupling mechanisms connecting the upper and lower atmosphere. Two general categories emerge. First, we have discussed the role of the stratosphere and mesosphere as a buffer region, wherein small perturbations of local parameters can be amplified into major effects affecting the transport or conversion of energy from external sources reaching the region. The constituents include ozone, aerosols, and to a lesser extent, charged species. The major effects involve heating, circulation patterns, and possible long term effects on climate in both the stratosphere and troposphere.

The electrical connection involves changes in the global and local electrical structure of the atmosphere induced by solar activity. These effects are more direct and may possibly bypass the stratosphere altogether. The responses in the atmospheric circuit to local changes are nearly instantaneous, and therefore are looked on with more promise for possible influences on weather systems. Newly emerging experimental evidence indicates that atmospheric electric fields, especially at high latitudes and in the upper atmosphere, are responsive to solar and geomagnetic phenomena. The corpuscular radiations previously discussed are known to strongly enhance the local atmospheric electrical conductivity and ionizations at stratospheric and mesospheric altitudes. However, the electric field perturbations are not easily explained by conventional atmospheric electricity considerations.

Theories now postulate that the electric field perturbations regulated by solar activity may be responsible for the observed statistical correlations between solar activity and thunderstorms. They include the concept that modulations in stratospheric electric fields induced by cosmic rays and/or solar protons can in turn affect the local field near thunderstorms, and change the rate of lightning formation. This is offered as an example of how atmospheric coupling may occur electrically.

The various ideas presented here are partially established, but primarily hypothetical. Experiments are needed to investigate the more promising concepts and establish the importance of each conceived idea. The electrical environment in particular needs further study, to establish its response to energetic radiations, the mapping of magnetospheric fields into the middle atmosphere, the influence of tropospheric electrical disturbances on the middle atmosphere, localized effects induced by auroral activity, etc. Since most electrical reactions are instantaneous, properly designed experiments can seek cause and effect simultaneously. Early field experiments should therefore relate to

electrical coupling processes, and should concentrate on atmospheric electrical properties, with an appropriate coordination between rocket, balloon, aircraft, and ground based experiments under both solar quiet and disturbed conditions.

REFERENCES

Angell, J. L. and J. Korshover, Quasi-biennial and long-term fluctuations in total ozone, *Monthly Weath. Rev.*, **101**, 426, 1973.

Angell, J. L. and J. Korshover, Global analysis of recent total ozone fluctuations. Rept. of NOAA Air Resources Laboratory (Reviewed in *EOS*, **56**, 584, 1975).

Arendt, P. R. and E. M. Frisby, Possible relation of a specific ionospheric event to simultaneous meteorological data, *Nature*, **219**, 475, 1968.

Avery, S. K. and M. A. Geller, Effects of middle atmosphere winds on planetary waves in the troposphere, submitted to *Geophys. Res. Let.*, 1979.

Baker, D. M. and K. Davies, F2-region acoustic waves from severe weather, *J. Atmos. Terr. Phys.*, **31**, 1345, 1969.

Bauer, S. J., A possible tropospheric-ionospheric relationship, *J. Geophys. Res.*, **62**, 425, 1957.

Bauer, S. J., An apparent ionospheric response to the passage of hurricanes, *J. Geophys. Res.*, **63**, 265, 1958.

Bering, E. A., J. R. Benbrook, D. Detrick, T. J. Rosenberg, M. J. Rycroft, M. A. Saunders and W. R. Sheldon, Electric fields, energetic electron precipitation and VLF radiation during a simultaneous magnetospheric substorm and atmospheric thunderstorm, submitted for publication, 1979.

Boeck, W. L., Meteorological consequences of atmospheric krypton-85, *Science*, **193**. 195, 1976.

Bossolasco, M., I. Dagnino, A. Elena and G. Flocchini, The thunderstorm activity over the Mediterranean area, *Revista Italiana di Geofisica*, **12**, 21, 1973.

Brooks, C. E. P., The variation of the annual frequency of thunderstorms in relation to sunspots, *Quart. J. R. Meteorol. Soc.*, **60**, 153, 1934.

Callis, L. B. and J. E. Nealy, Solar UV variability and its effect on stratospheric thermal structure and trace constituents, *Geophys. Res. Let.*, **5**, 249, 1978.

Chalmers, J. A., "Atmospheric Electricity," 2nd edition, Pergamon Press, Oxford, 1967.

Chameides, W. L., D. H. Stedman, R. R. Dickerson, D. J. Busch, and R. J. Cicerone, NO_x production in lightning, *J. Atmos. Sci.*, **34**, 143, 1977.

Cobb, W. E., Evidence of a solar influence on the atmospheric electric elements at Mauna Loa Observatory, *Monthly Weather Rev.*, **95**, 12, 1967.

Cole, K. D., Physical argument and hypothesis for sun-weather relationships, *Nature*, **260**, 229, 1976.

D'Angelo, N., Thunderstorms, ionosphere-to-ground potential drop, and the solar wind sector structure, U. of Iowa Report, 78-24, 1978.

D'Angelo, N. and E. Ungstrup, On the occurrence of widely observed noctilucent clouds, *J. Geophys. Res.*, **81**, 1777, 1976.

Davies, K., "Ionospheric Radio Propagation," National Bureau of Standards Monograph *L*80, 1965.

Donahue, T. M., B. Guenther, and J. E. Blamont, Noctilucent clouds in daytime; circumpolar particulate layers near the summer mesopause, *J. Atmos. Sci.*, **29**, 1205, 1972.

Dubin, M. and E. P. Zipf, Nitrogen fixation from atmospheric discharges as the prime source of atmospheric nitrous oxide and soil nitrates, *EOS*, **58**, 464, 1977.

Follin, Jr., J. W., E. P. Grey and K. Yu, The connection between cosmic rays and thunderstorms, *EOS*, **58**, 1220, 1977.

Frederick, J. E., Solar corpuscular emission and neutral chemistry in the Earth's middle atmosphere, *J. Geophys. Res.*, **81**, 3179, 1976.

Frederick, J. E., Chemical response of the middle atmosphere to changes in the ultraviolet solar flux, *Plant. Space Sci.*, **25**, 1, 1977.

Fritz, S. and J. K. Angell, Temperature and wind variation in the tropical upper stratosphere and lower mesosphere during a sunspot cycle, *J. Geophys. Res.*, **81**, 1051, 1976.

Georges, T. M., HF doppler studies of travelling ionospheric disturbances, *J. Atmos. Terr. Phys.*, **30**, 725, 1968.

Gherzi, E., Ionosphere and weather, *Nature*, **165**, 38, 1950.

Goldberg, R. A., An experimental search for causal mechanisms in sun/weather-climatic relationships in "Proceedings of the Symposium/Workshop on Solar Terrestrial Influences on Weather and Climate," Columbus, Ohio, July 1978, ed. by B. M. McCormac and T. Seliga, (in press) 1979.

Goldberg, R. A. and G. Witt, Ion composition in a noctilucent cloud region, *J. Geophys. Res.*, **82**, 2619, 1977.

Hale, L. C., Particulate transport through the mesosphere and stratosphere, *Nature*, **268**, 710, 1977.

Hale, L. C. and C. L. Croskey, An auroral effect on the fair weather electric field, submitted to *Nature*, 1979.

Hays, P. B. and R. G. Roble, A quasi-static model of global atmospheric electricity I. The lower atmosphere, in "Proceedings of the Symposium/Workshop on Solar Terrestrial Influences on Weather and Climate," July, 1978, Columbus, Ohio, ed. by B. McCormac and T. Selega, (in press), 1979.

Heath, D. F., Space observations of the variability of solar irradiance in the near and far ultraviolet, *J. Geophys. Res.*, **78**, 2779, 1973.

Heath, D. F., A. J. Krueger, and P. J. Crutzen, Solar proton event influence on stratospheric ozone, *Science*, **197**, 886, 1977.

Heath, D. F. and M. P. Thekaekara, Measures of the solar spectral irradiance between 1200 and 3000A, in "The Solar Output and its Variations," ed. by O. R. White, Colorado Associated University Press, Boulder, Colorado, 1977.

Herman, J. R. and R. A. Goldberg, Solar activity and thunderstorm occurrence, *EOS*, **57**, 971, 1976.

Herman, J. R. and R. A. Goldberg, Initiation of non-tropical thunderstorms by solar activity, *J. Atmos. Terr. Phys.*, **40**, 121, 1978a.

Herman, J. R. and R. A. Goldberg, "Sun, weather and climate," NASA SP426, 1978b.

Hines, C. O. and I. Halevy, On the reality and nature of a certain sun-weather correlation, *J. Atmos. Sci.*, **34**, 382, 1977.

Holzworth, R. H. and F. S. Mozer, Direct evidence of solar flare modification of stratospheric electric fields, *J. Geophys. Res.*, **84**, 363, 1979.

Hummel, J. R. and J. J. Olivero, Satellite observation of the mesospheric scattering layer and implied climatic consequences, *J. Geophys. Res.*, **81**, 3177, 1976.

Hung, R. J., G. L. Rao, R. E. Smith, G. S. West and B. B. Hensen, Ionospheric disturbances during severe weather activity, in "Proc. Symp. Effects of the Ionosphere on Space Systems and Communications," Naval Research Laboratory, Jan. 1975.

Israel, H., "Atmospheric Electricity, Volume I: Fundamentals, Conductivity, Ions," Israel Program for Scientific Translations, Jerusalem NTIS Doc. TT-67-51394/1, 1970.

Israel, H., Atmospheric Electricity, Volume 2: Fields, Charges, Currents," Israel Program for Scientific Translations, Jerusalem, NTIS Doc. TT-67-51394/2, 1973.

Johnson, R. G. and W. L. Imhoff, Direct satellite observations on bremsstrahlung radiation as a technique to investigate its role in meteorological processes, NASA SP366 (ed. by W. R. Bandeen and S. P. Maran), 1975.

Lethbridge, M., Thunderstorm frequency and solar sector boundaries in "Proceedings of Symposium/Workshop on Solar Terrestrial Influences on Weather and Climate," July 1978, Columbus (ed. by B. McCormac and Selega), (in press), 1979.

Märcz, F., Links between atmospheric electricity and ionospheric absorption due to extraterrestrial influences, *J. Geophys. Res.*, **81**, 4566, 1976.

Markson, R., Considerations regarding solar and linar modulation of geophysical parameters, atmospheric electricity, and thunderstorms, *Pure Appl. Geophys.*, **84**, 161, 1971.

Markson, R., Solar modulation of atmospheric electrification through variation of the conductivity over thunderstorms, in NASA SP-366 (ed. by W. R. Bandeen and S. P. Maran), 1975.

Markson, R., Solar modulation of atmospheric electrification and possible implications for the Sun-weather relationship, *Nature*, **273**, 103, 1978.

Mitchell, J. D., R. S. Sagar and R. O. Olsen, Positive ions in the middle atmosphere during sunrise conditions, *Space Res.*, **17**, P. 199, Pergamon Press, Oxford, 1977.

Muhleisen, R., Neue Ergebnisse und Probleme in der Luftelektrizitat, *Zs. Geophysik*, **37**, 759, 1971.

Ney, E. P., Cosmic radiation and the weather, *Nature*, **183**, 451, 1959.

Noxon, J. F., Atmospheric nitrogen fixation by lightning, *Geophys. Res. Let.*, **3**, 463, 1976.

Park, C. G., Solar magnetic sector effects on the vertical atmospheric electric field at Vostok, Antarctica, *Geophys. Res. Let.*, **3**, 475, 1976.

Park, C. G. and R. A. Helliwell, Magnetospheric effects or power line radiation, *Science*, **200**, 727, 1978.

Penner, J. E. and J. S. Chang, Possible variations in atmospheric ozone related to the eleven year solar cycle, *Geophys. Res. Let.*, **5**, 817, 1978.

Pittock, A. B., A critical look at long term Sun-weather relationships, *Rev. of Geophys. & Space Sci.*, **16**, 400, 1978.

Reagan, J. B., Ionization processes in "Dynamical and Chemical Coupling of the Neutral and Ionized Atmosphere," ed. by B. Grandal and J. A. Holtet, P. 145, D. Reidel Publishing Co., Dordrecht, Holland, 1977.

Reid, G. C., T. E. Holzer, I. S. A. Isaaksen and P. J. Crutzen, The influence of ancient solar proton events on the evolution of life, *Nature*, **259**, 177, 1976.

Reiter, R., Solar flares and their impact on potential gradient and air-Earth current characteristics at high mountain stations, *Pure Appl. Geophys.*, **72**, 259, 1969.

Reiter, R., Further evidence for impact of solar flares on potential gradient and air-Earth current characteristics at high mountain stations, *Pure Appl. Geophys.*, **86**, 142, 1971.

Reiter, R., Case study concerning the impact of solar activity upon potential gradient and air-Earth current in the lower troposphere, *Pure Appl. Geophys.*, **94**, 218, 1972.

Reiter, R., The electrical potential of the ionosphere as controlled by the solar magnetic sector structure, *Die Naturwissenschaften*, **63**, Part 4, 192, 1976.

Reiter, R., The electrical potential of the ionosphere as controlled by the solar magnetic sector structure, result of a study over the period of a solar cycle, *J. Atmos. Terr. Phys.*, **39**, 95, 1977.

Roberts, W. O., and R. H. Olson, New evidence for effects of variable solar corpuscular emission on weather, *Rev. Geophys. Space Phys.*, **11**(3), 731, 1973a.

Roberts, W. O. and R. H. Olson, Geomagnetic Storms and wintertime 300-mb trough development in the North Pacific - North America Area, *J. Atmos. Sci.*, **30**, 135, 1973b.

Sao, K., Correlations between solar activity and the atmospheric potential gradient on the Earth's surface in the polar regions, *J. Atmos. Terr. Phys.*, **29**, 213, 1967.

Schoeberl, M. R. and D. F. Strobel, The response of the zonally averaged circulation to stratospheric ozone reductions, *J. Atmos. Sci.*, **35**, 1951, 1978.

Sechrist, C., Workshop Report on the role of minor atmospheric constituents in solar-terrestrial influences on weather and climate in "Proceedings of Symposium/Workshop, Solar Terrestrial Influences on Weather and Climate," Columbus, Ohio, July 1978, ed. by B. McCormac and T. Selega (in press).

Septer, E., Sonnenflecken und Gewitter in Siberien, *Meteorol. Z.*, **43**, 229, 1926.

Stringfellow, M. F., Lightning incidence in Britain and the solar cycle, *Nature*, **249**, 332, 1974.

Swider, W. and T. Keneshea, Decrease of ozone and atmic oxygen in the lower mesosphere during a PCA event, *Planet. Space Sci.*, **21**, 1969, 1973.

Thorne, R. M., Energetic radiation belt electron precipitation: a natural depletion mechanism for stratospheric ozone, *Science*, **195**, 287, 1977.

Weeks, L. H., R. S. Cuikay and J. R. Corbin, Ozone measurements in the mesosphere during the solar proton event of 2 November 1969, *J. Atmos. Sci.*, **29**, 1138, 1972.

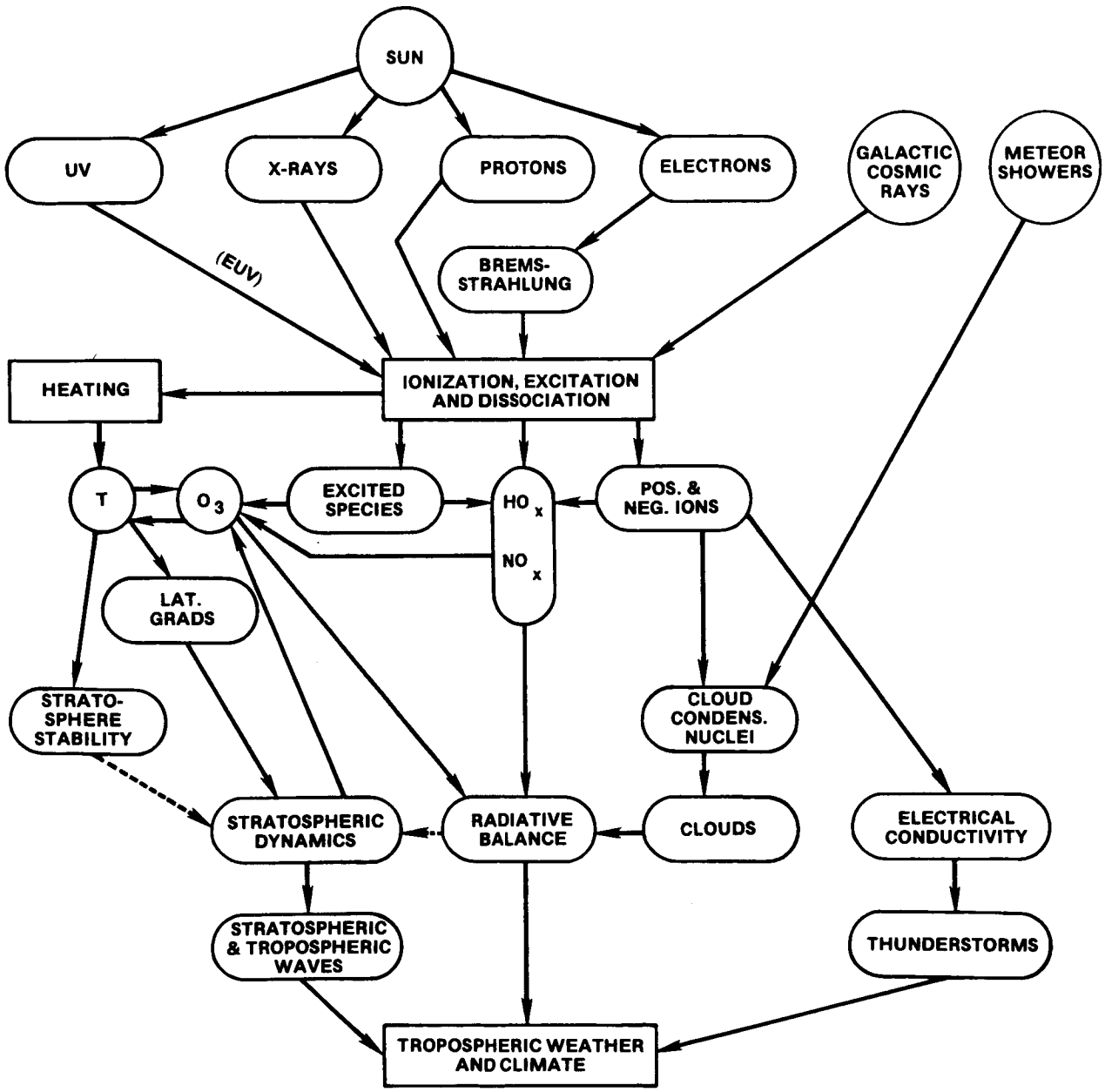

Figure 1. Schematic depiction of extraterrestrial radiation sources modulated by solar activity, and their subsequent effects and interactions with various parts of the middle and lower atmosphere. (After Sechrist, 1979.)

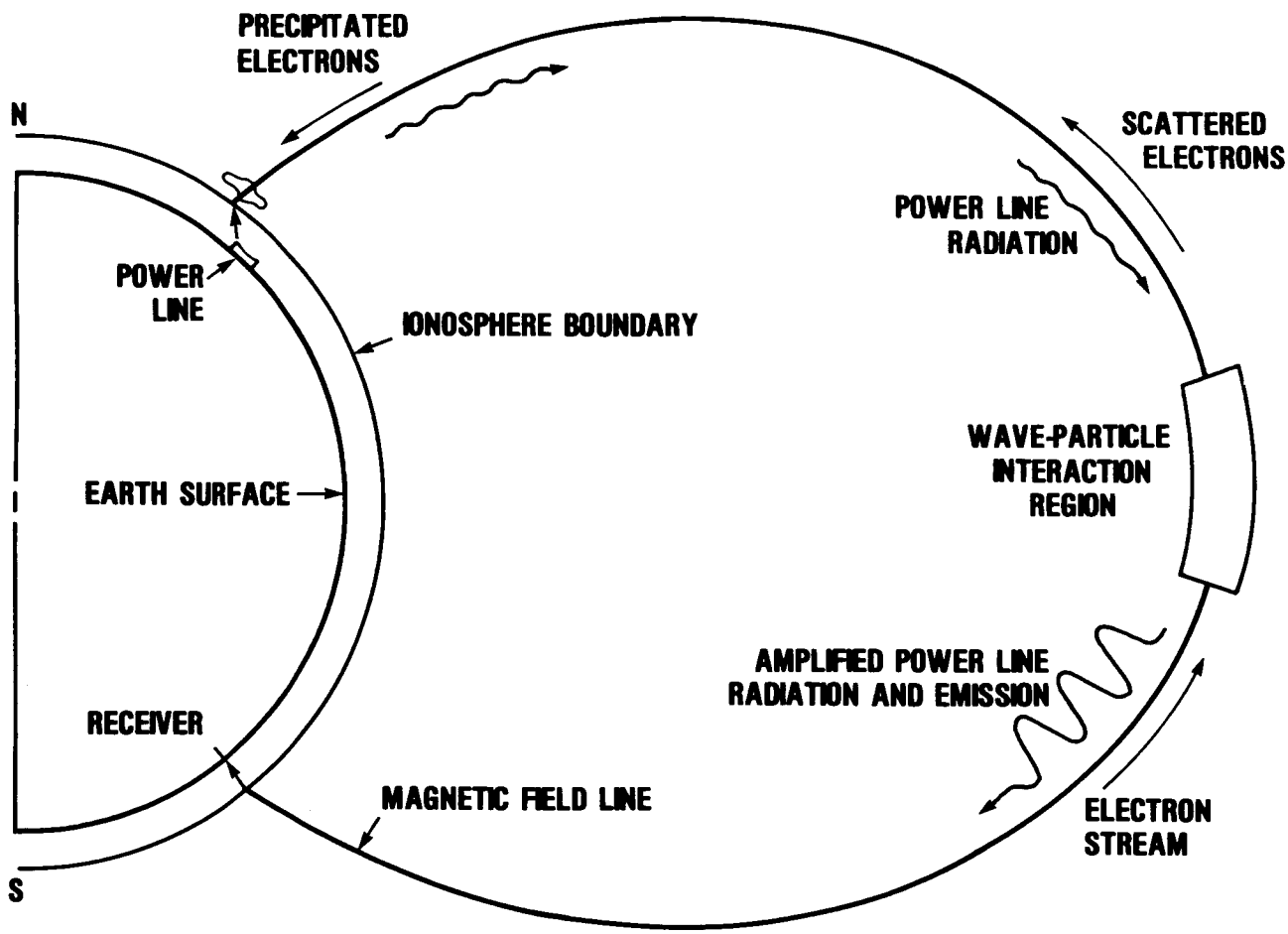

Figure 2. A schematic diagram illustrating the effects of power line radiation (PLR). Harmonic radiation from power lines ($\sim$ several kHz), is guided to the Equatorial magnetosphere where it interacts with counterstreaming energetic electrons. The wave particle interaction amplifies the PLR, triggering emissions of order 10^3 greater than the input level. Scattered electrons precipitate into the upper atmosphere with estimated energy fluxes 10^6 or more times the input wave power. (After Park and Helliwell, 1978.)

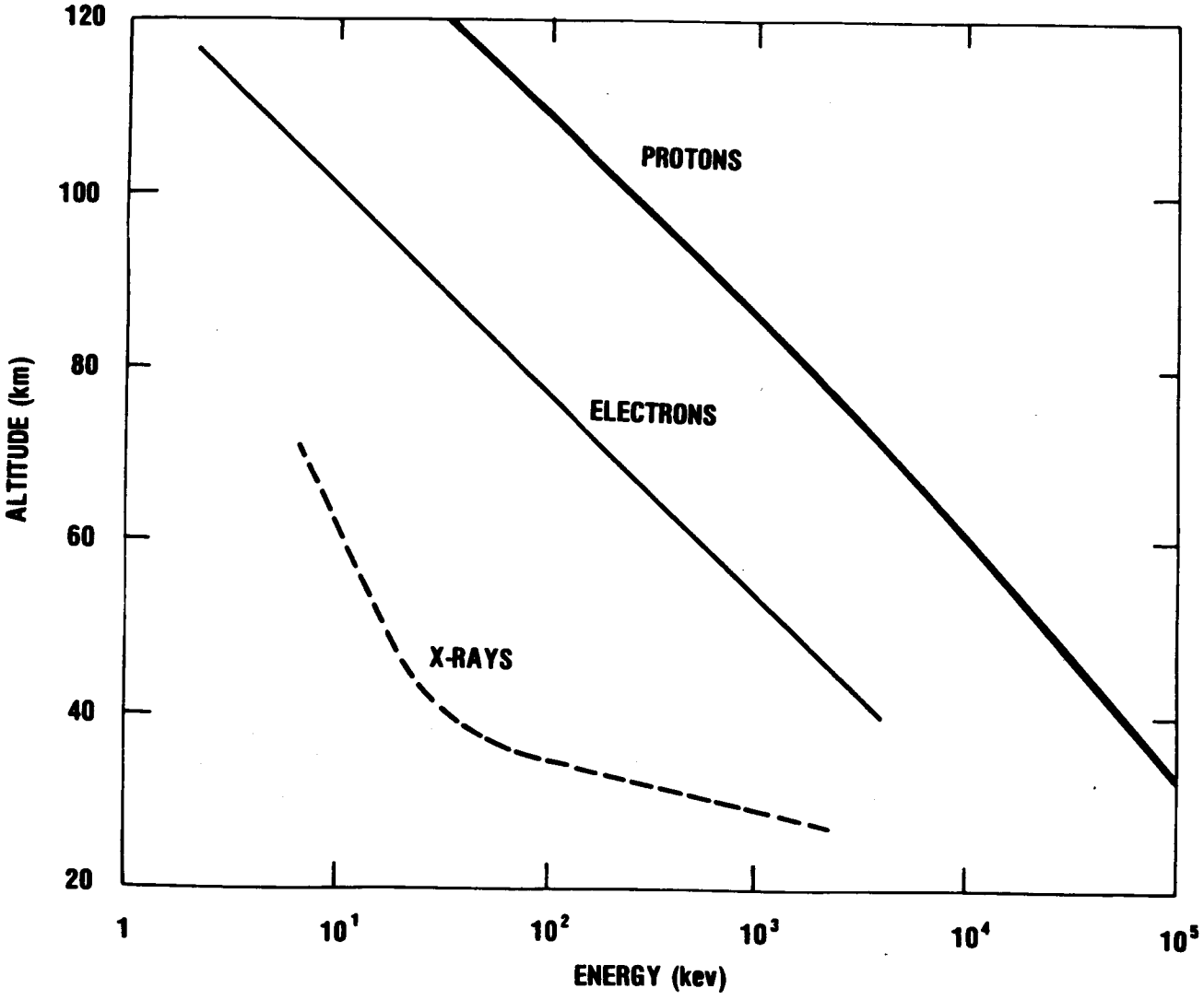

Figure 3. The nominal penetration depth for energetic electrons, protons, and X-rays normally incident at the top of the Earth's atmosphere. (After Thorne, 1977.)

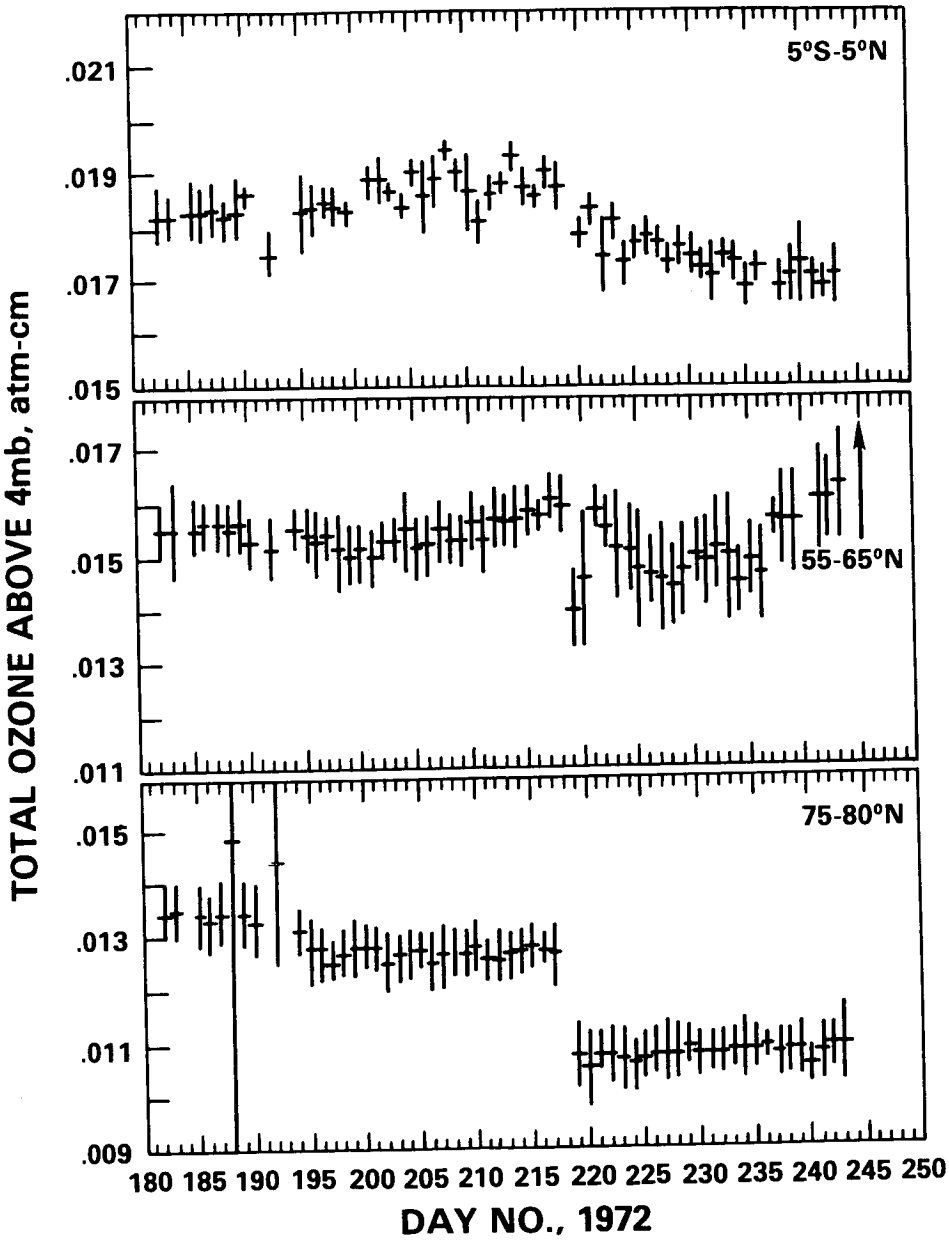

Figure 4. Daily zonally averaged total ozone (Nimbus 4 BUV experiment) above 4 mb pressure level (about 38 km) for Equatorial (top panel) middle (middle), and high (bottom) latitudes during July and August, 1972. (From Heath, et al., 1977.)

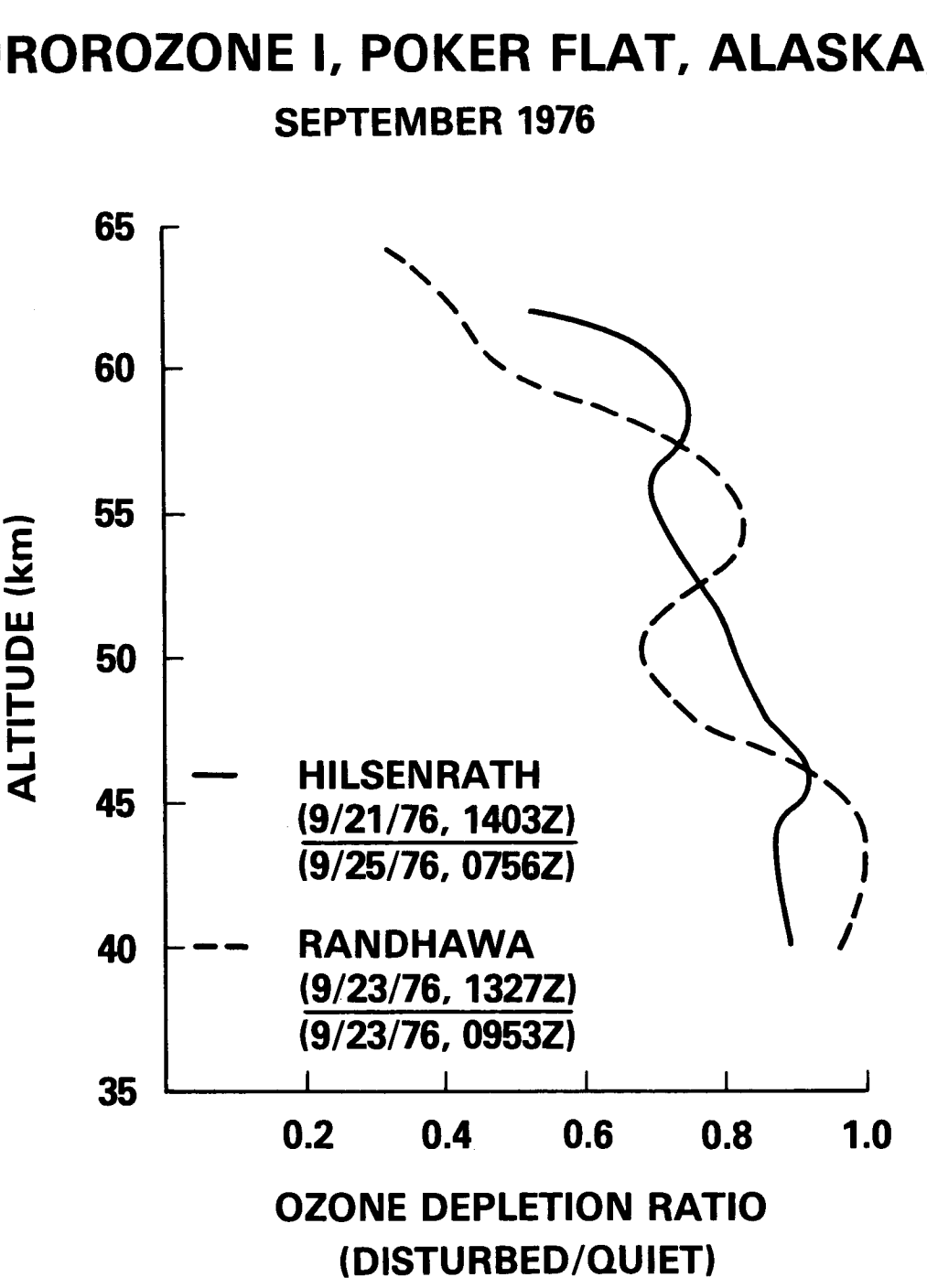

Figure 5. Ratio of nighttime vertical ozone distributions comparing post auroral disturbance values to quiet time profiles preceding each event. The ratios were calculated from four independent rocket chemiluminescent detector soundings from Poker Flat, Alaska at the times shown. One comparison (Randhawa technique) was obtained on a single night. The second comparison (Hilsenrath technique) was obtained by comparison of quiet and post disturbance values on separate nights (Hilsenrath, pvt. communication.)

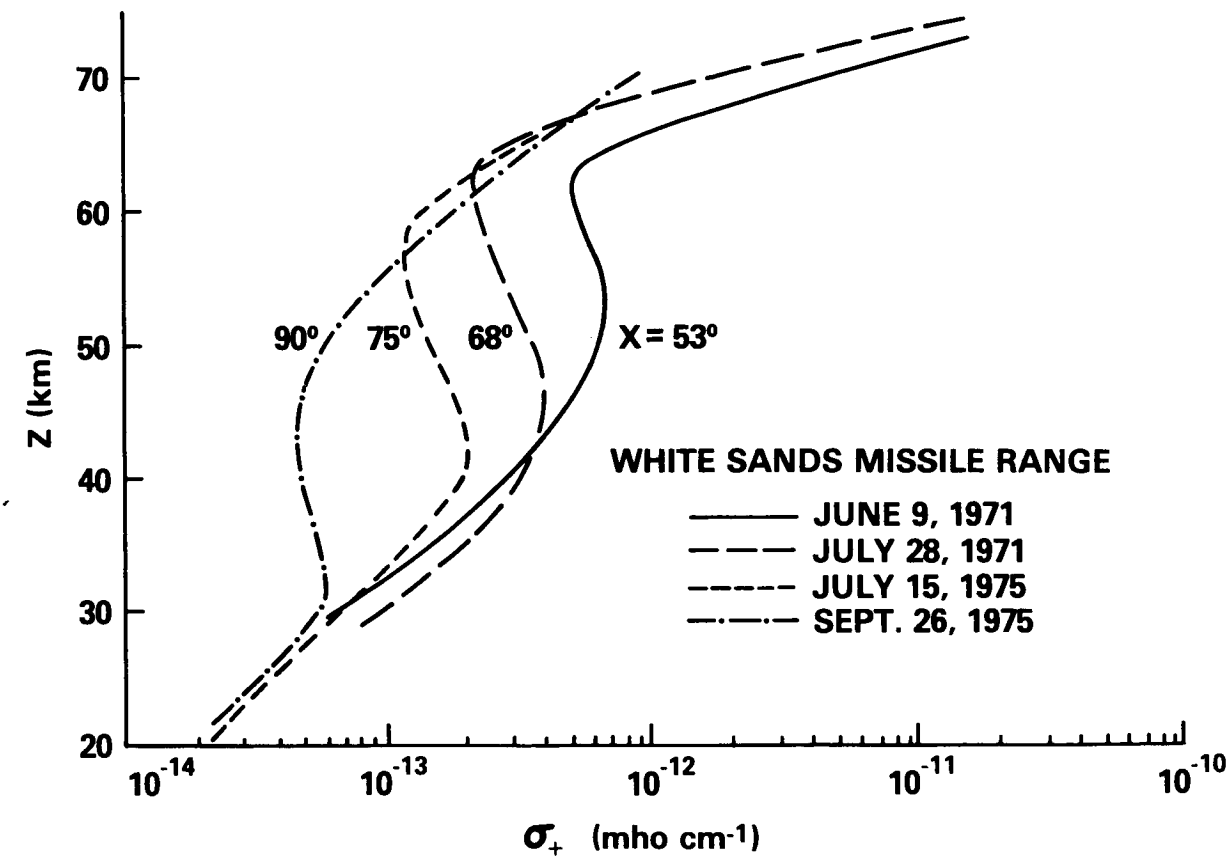

Figure 6. Positive ion conductivity (σ_+) profiles with altitude for four solar zenith angles following sunrise. Rocket soundings occurred at White Sands Missile Range, New Mexico. (After Mitchell et al., 1977.)

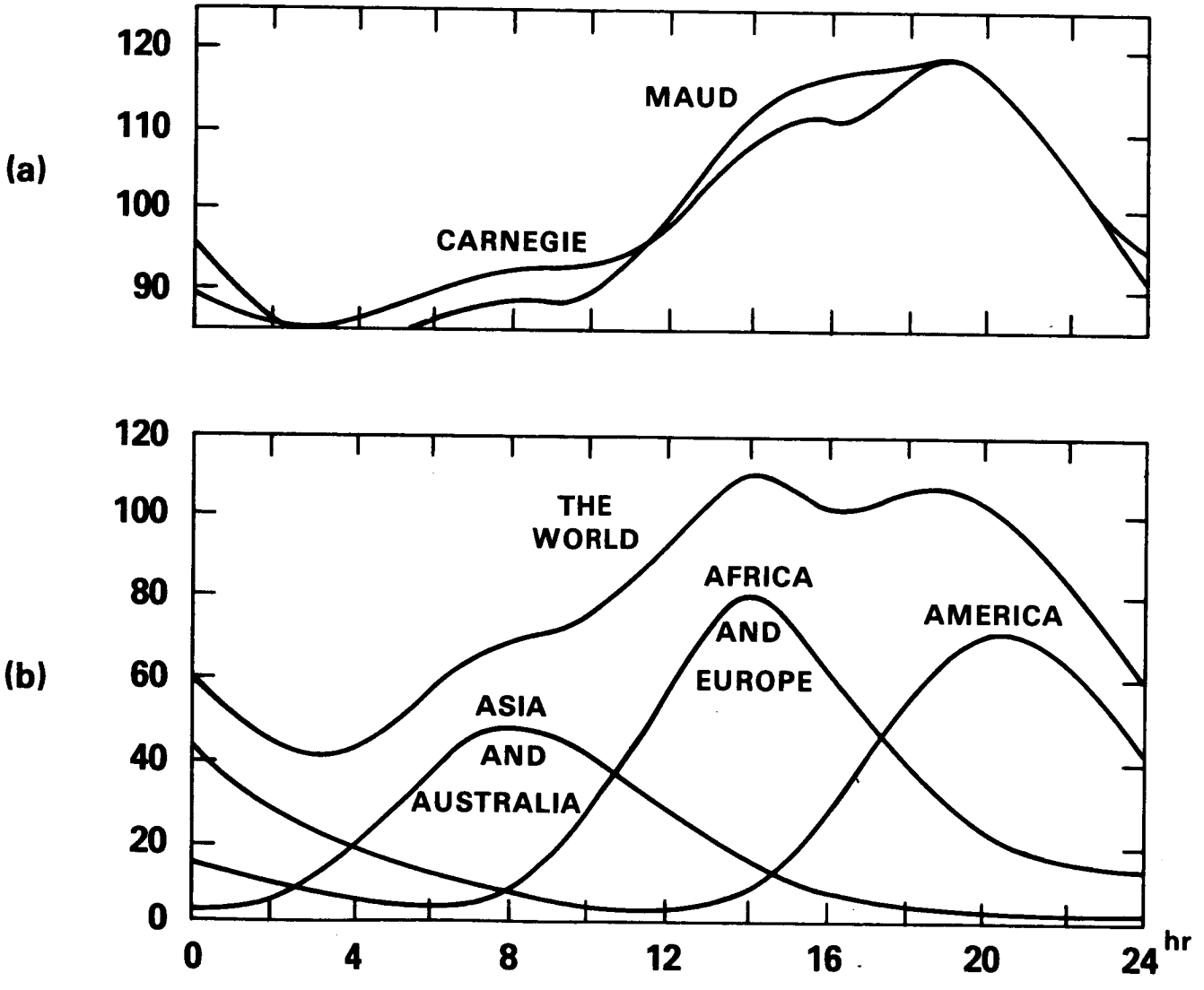

Figure 7. (a) Diurnal variation of the atmospheric vertical potential gradient. (b) Diurnal variation of thunderstorm expectation for individual continents and for the world envelope. The area covered at any time by thunderstorms is in units of 10^4 km^2. (After Israel, 1973, p. 366.)

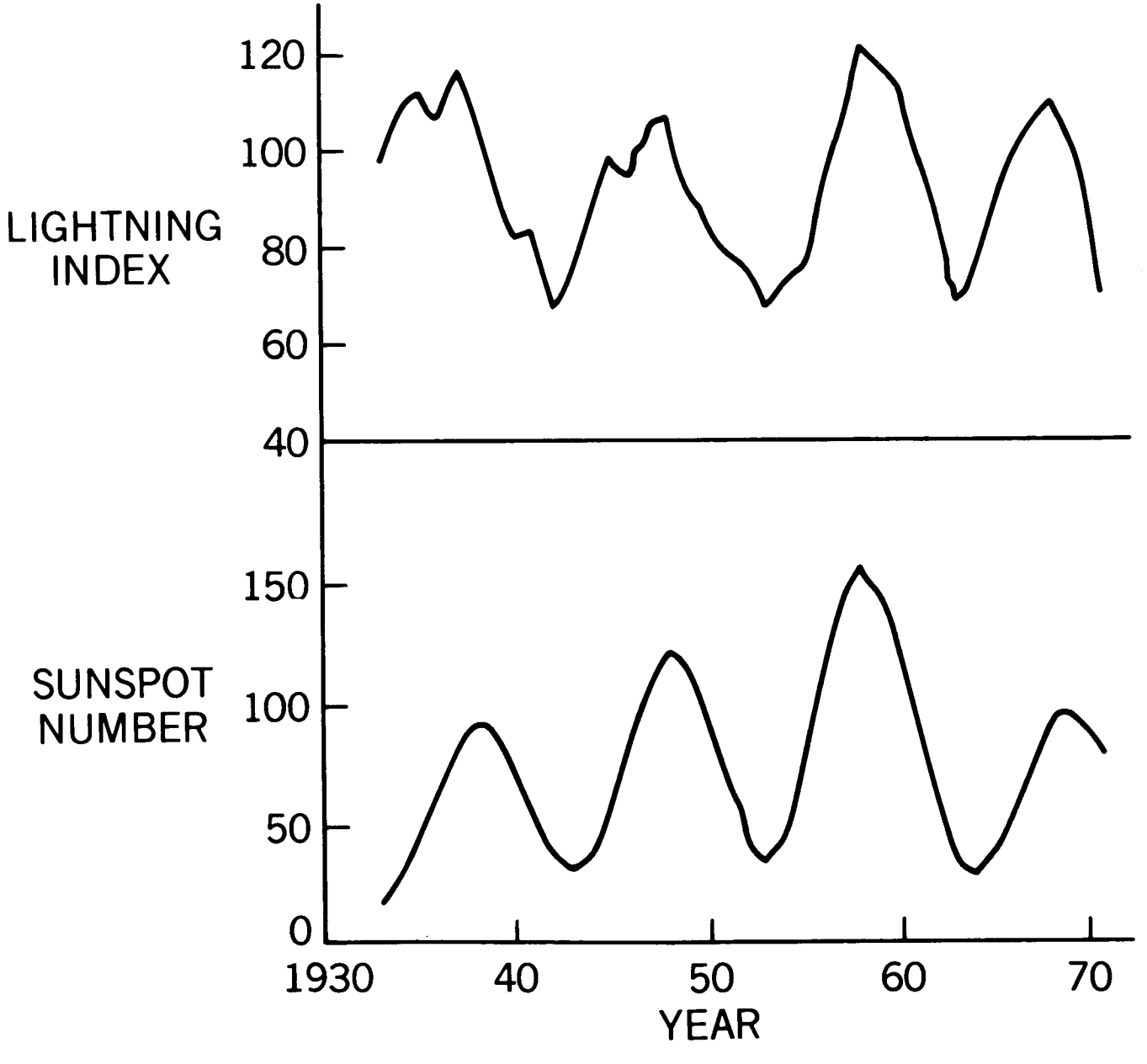

Figure 8. Five-year running means of average annual sunspot number (lower curve) and average annual lightning index. (From Stringfellow, 1974.)

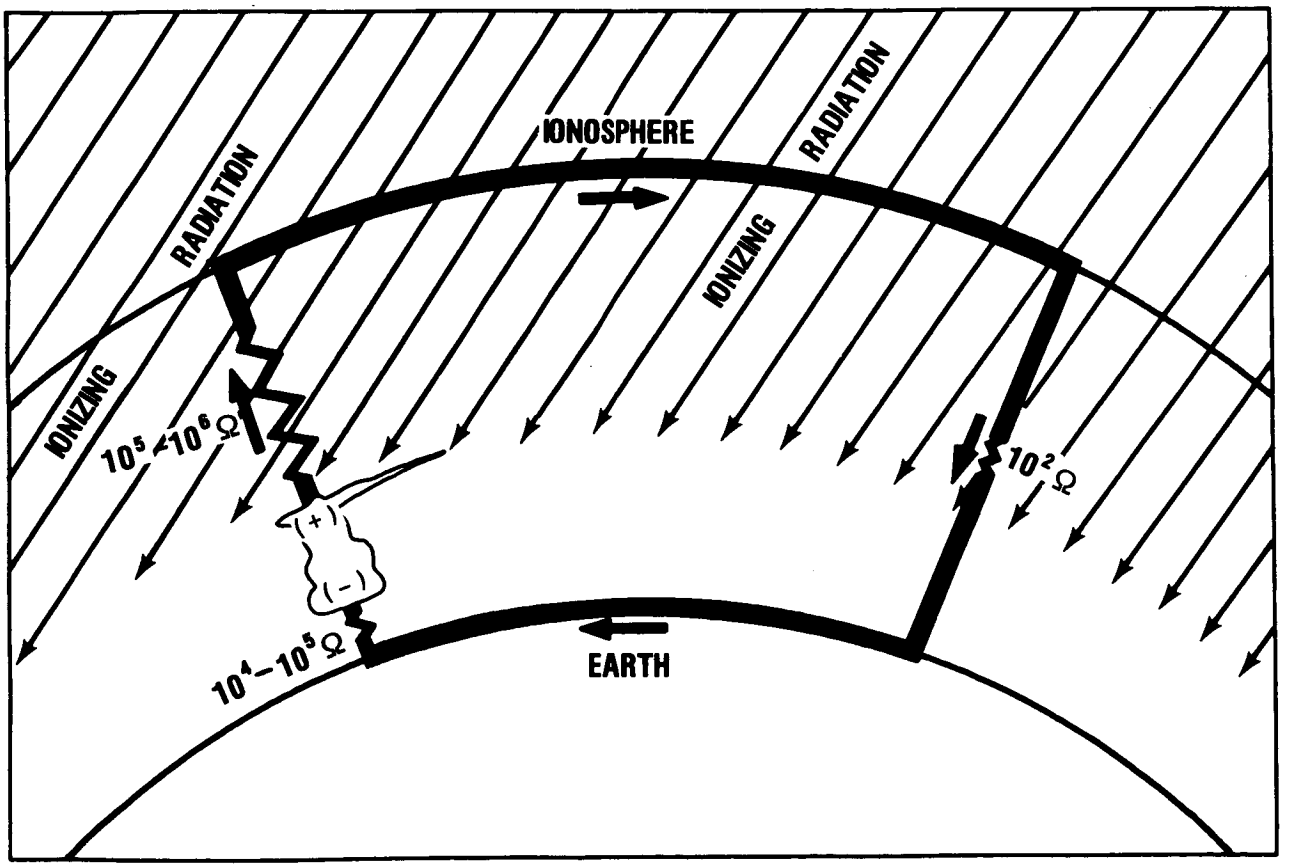

Figure 9. The atmospheric global electrical circuit. Large arrows indicate the flow of positive charge. Estimated resistances of circuit elements are given. The thunderstorm depicted represents the global electrical generator, i.e., the totality of all thunderstorms, and sends current through the charging resistor (10^5 - $10^6\,\Omega$) to the ionosphere. The cumulative effect of the global return current passes through the load ($10^2\,\Omega$) resistor. (After Markson, 1978.)

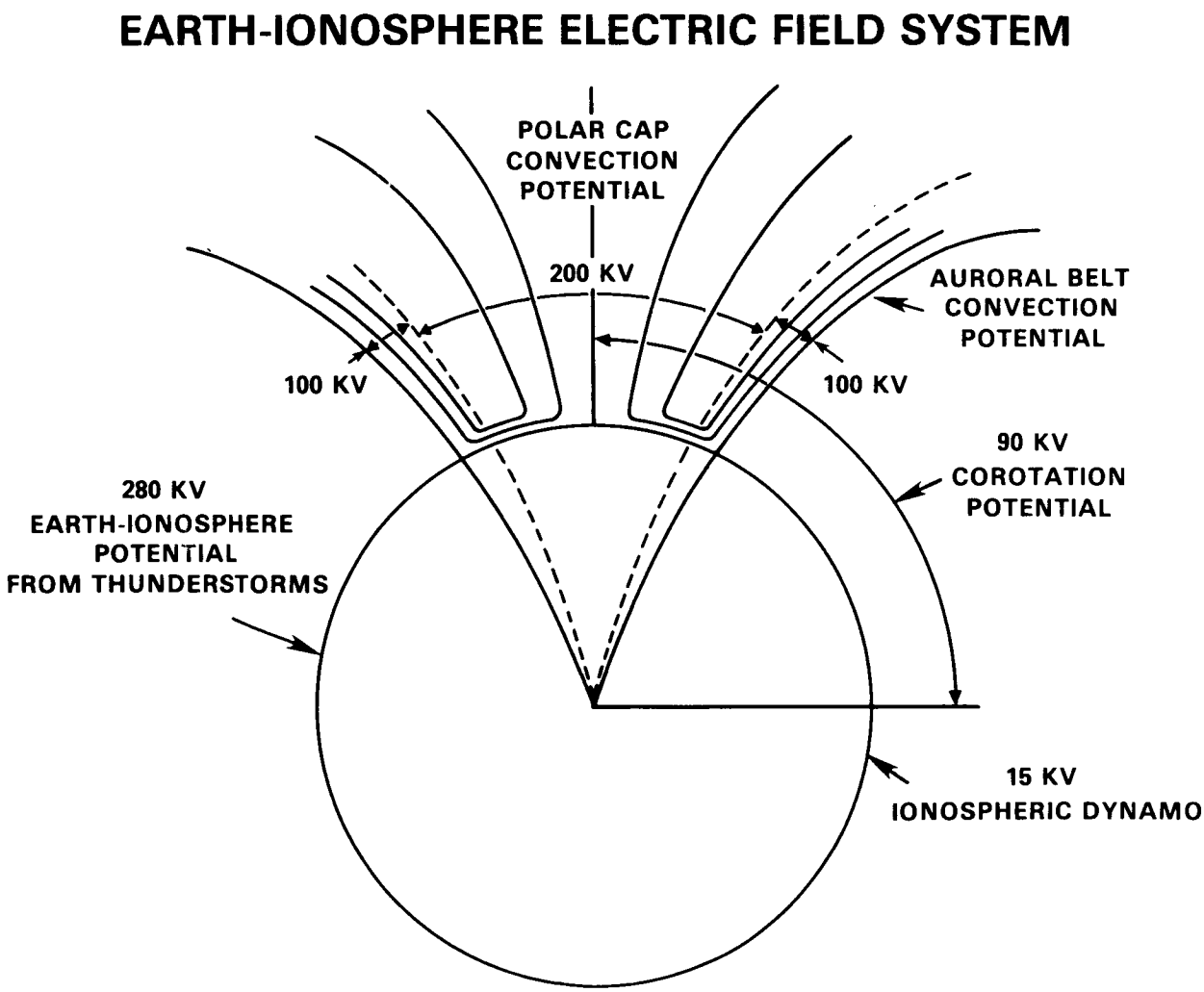

Figure 10. Schematic illustrating sources and magnitudes of electric fields in near Earth space. (Suguira, pvt. communication.)

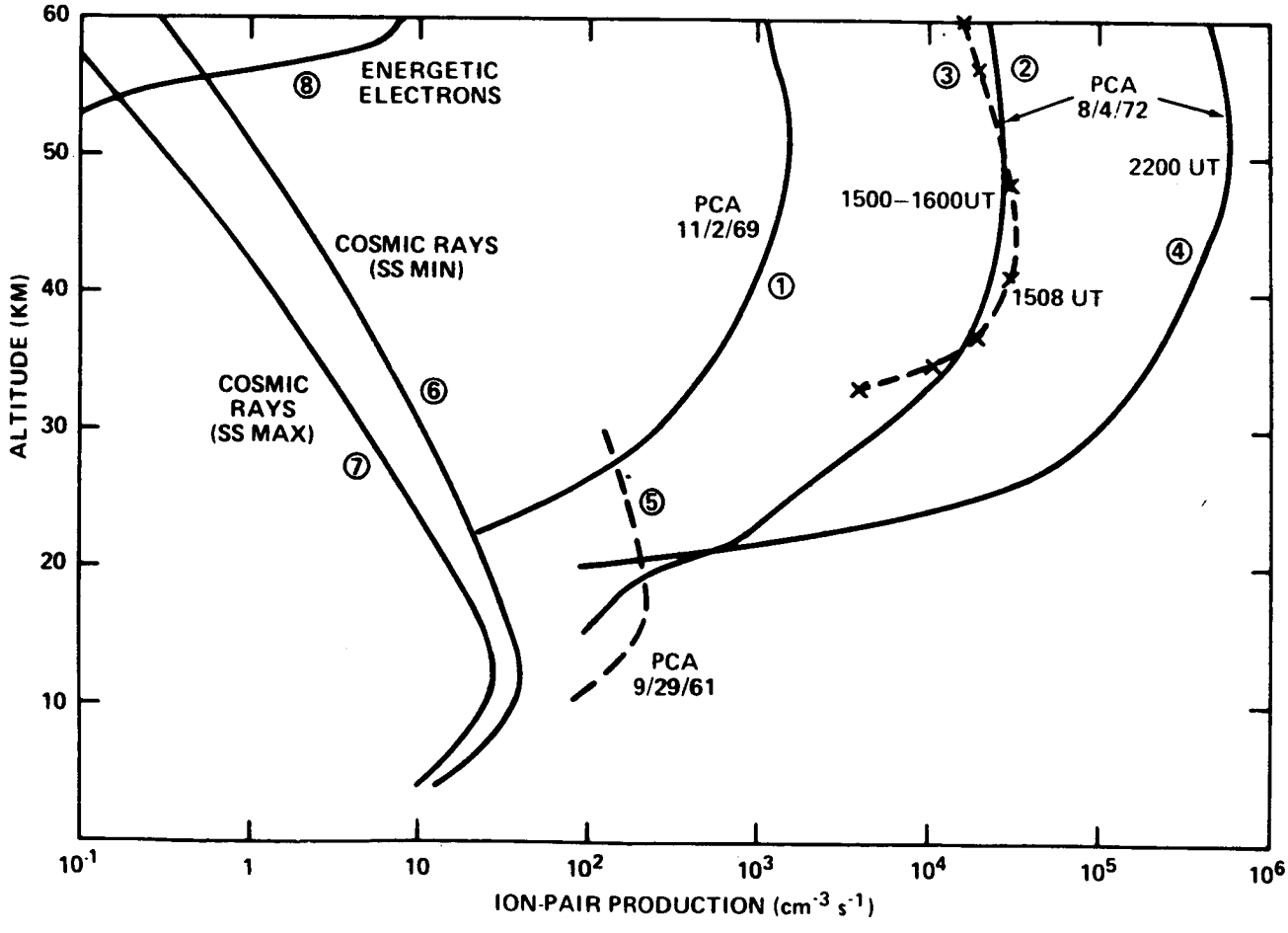

Figure 11. Ion pair production rates due to solar protons (curves 1-5), galactic cosmic rays at sunspot minimum (curve 6) and sunspot maximum (curve 7), and energetic electrons (curve 8). These curves are based on calculations from various sources as given in Herman and Goldberg (1978a).

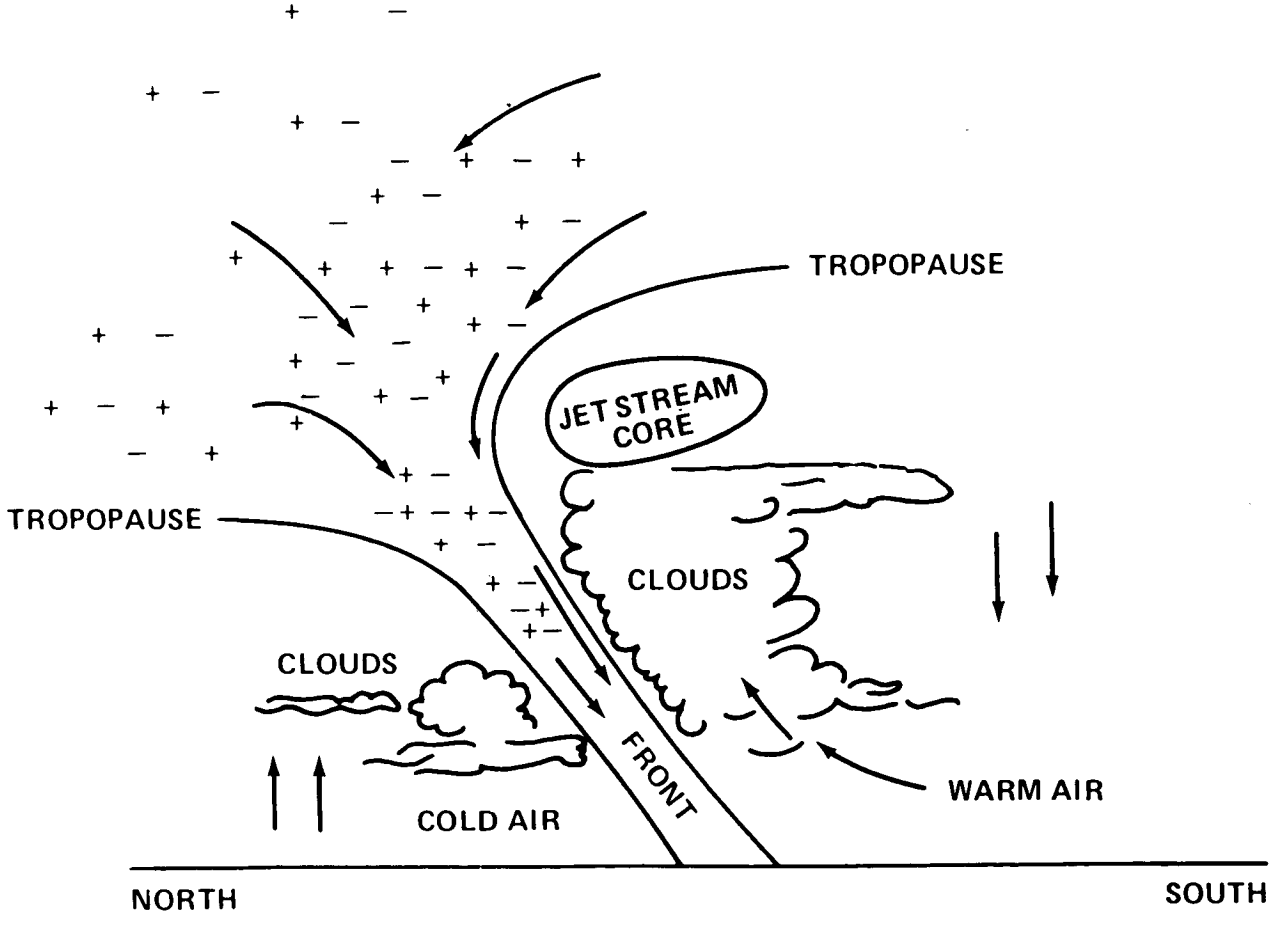

Figure 12. Penetration of stratospheric air and ions to tropospheric heights near a jet stream, (cf. Herman and Goldberg, 1978a).

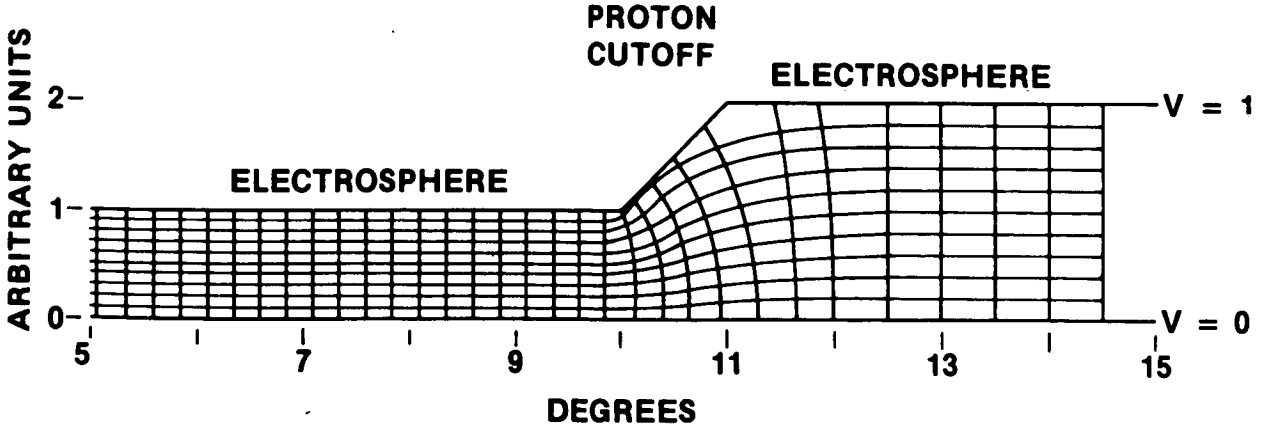

Figure 13. Model of proton effects on the electrosphere and potential gradient (electric field) in the vicinity of the proton cutoff latitude. Horizontal lines with perturbations are equipotential surfaces, and vertical lines are electrical field lines between the electrosphere at a relative potential of V = 1 and the ground with a relative potential of V = 0. (From Herman and Goldberg, 1978b, p. 261.)

APPENDIX B

WORKSHOP LOGISTICS

APPENDIX B

WORKSHOP LOGISTICS

PROGRAM AND ORGANIZING COMMITTEE

Dr. Nelson Maynard (Chairman), Goddard Space Flight Center
Dr. David Cauffman (Liaison), NASA Headquarters
Dr. Arthur Few (Thunderstorm Electric Fields), Rice University
Dr. Richard Goldberg (Stratosphere), Goddard Space Flight Center
Dr. Paul Hays (Modelling), University of Michigan
Dr. Laurence Jones (Cosmic Rays, Air Showers), University of Michigan
Dr. Michael Kelley (Ionospheric Electric Fields), Cornell University
Dr. Janet Luhmann (Atmospheric Effects of X-Rays), Aerospace Corporation
Dr. Volker Mohnen (Stratosphere), State University of New York, Albany
Dr. Rocco Narcisi (D Region Chemistry), Air Force Geophysics Laboratory
Dr. Chung Park (Coupling Theory), Stanford University
Dr. Leslie Smith (D Region Electrons), University of Illinois
Dr. Masahisa Sugiura (Atmospheric and Ionospheric Currents), GSFC
Dr. William Vaughan (Troposphere), Marshall Space Flight Center
Dr. Bernard Vonnegut (Lightning, Atmospheric Electricity), SUNY, Albany

SELECT REVIEW PANEL

Dr. Sidney Bowhill	University of Illinois
Dr. William Hanson	University of Texas at Dallas
Dr. George Reid	NOAA
Dr. Hans Volland	University of Bonn

WORKSHOP ON THE ROLE OF THE ELECTRODYNAMICS OF THE MIDDLE ATMOSPHERE ON SOLAR TERRESTRIAL COUPLING

Sheraton International Conference Center
Reston, Virginia
January 17-19, 1979

Wednesday, January 17: Tutorial

Morning:

9:00	Conference Logistics	
9:05	Welcome	
	Dr. Siegfried J. Bauer	NASA/GSFC
9:10	Expectations	
	Dr. David P. Cauffman	NASA Headquarters

Conference Theme

9:25	The Middle Atmosphere	
	Dr. George C. Reid	NOAA
10:30	Coffee	

The Middle Atmosphere

10:45	Direct Energy Inputs to the Middle Atmosphere	
	Dr. T. J. Rosenberg	University of Maryland
	Dr. L. J. Lanzerotti	Bell Laboratories
11:30	Ion Chemistry of the Middle Atmosphere	
	Dr. Eldon Ferguson	NOAA
12:15	Lunch	

Afternoon:

1:15	Solar Terrestrial Coupling through Atmospheric Electricity	
	Dr. R. G. Roble	NCAR
	Dr. P. B. Hays	University of Michigan

Lower Atmospheric Influences

2:00 Tropospheric Effects on the Middle Atmosphere and Vice-Versa
Dr. Marvin Geller — University of Miami

2:35 Tropospheric Electrification
Dr. Bernard Vonnegut — State University of New York

3:10 Coffee

Upper Atmosphere Influences

3:25 Energy and Mass Transport in the Thermosphere
Dr. H. G. Mayr — NASA/GSFC
Dr. I. Harris — NASA/GSFC
Mr. N. W. Spencer — NASA/GSFC

4:00 Electric Generators in the Magnetosphere-Ionosphere System
Dr. Gerald Atkinson — Communications Research Center-Ottawa

Coupling Phenomena

4:35 Areas where Solar-Terrestrial Coupling may Influence or be Influenced by the Middle Atmosphere
Dr. Richard Goldberg — NASA/GSFC

5:15 Discussion

Evening:

7:00 Dinner-Social

9:00 Experimental Programs having Impact on the Middle Atmosphere
NASA/Headquarters-Sciences
NASA/Headquarters-Applications
NSF
ONR

Thursday, January 18: Workshops

Morning:

9:00 Workshop Groups

A. Electrical Coupling through the Middle Atmosphere

Chairman:	Dr. Chung Park	Stanford University
Reporters:	Dr. Arthur Few	Rice University
	Dr. Michael Kelly	Cornell University

B. Middle Atmosphere Conductivity and Currents

Chairman:	Dr. Paul Hays	University of Michigan
Reporters:	Dr. Richard Goldberg	NASA/GSFC
	Dr. Laurence Jones	University of Michigan
	Dr. Les Smith	University of Illinois

C. Ion Composition, Chemistry, and Dynamics

Chairman:	Dr. Rocco Narcisi	AFGL
Reporters:	Dr. Janet Luhman	Aerospace Corp.
	Dr. Volker Mohnen	State University of New York

12:15 Lunch

Afternoon:

1:15 Workshop Groups

3:15 Coffee

3:30 Joint Session
Reporters' reports and discussion.

Friday, January 19: Workshops

Morning:

9:00 Workshop Groups

12:30 Lunch

Afternoon:

1:30 Joint Session
Chairmen's reports of recommendations.

Review Panel Discussion

Dr. Sidney Bowhill	University of Illinois
Dr. William Hanson	University of Texas at Dallas
Dr. George Reid	NOAA
Dr. Hans Volland	University of Bonn

NASA WORKSHOP ON THE ROLE OF THE ELECTRODYNAMICS OF THE MIDDLE ATMOSPHERE ON SOLAR TERRESTRIAL COUPLING

January 17-19, 1979
Reston, Virginia

Registrants

Arthur C. Aikin
NASA Goddard Space Flight Center
Greenbelt, Maryland 20714

Robert V. Anderson
137 Cree Drive
Oxon Hill, Maryland 20021

Etienne Arijs
Belgian Institute for
Space Aeronomy
3 Ringlaan
B1180 Brussels, Belgium

Gerald Atkinson
P.O. Box 11430, Station H.
Department of Communications
Communications Research Center
Ottawa, Ontario
Canada K2H8S2

S. J. Bauer
7 David Court
Silver Spring, Maryland 20904

James R. Benbrook
Physics Department
University of Houston
Houston, Texas 77004

S. A. Bowhill
Department of Electrical Engineering
University of Illinois
Urbana, Illinois 61801

Henry C. Brinton
Code 621
Goddard Space Flight Center
Greenbelt, Maryland 20771

Hsiao-hua K. Burke
E.R.T. 696 Virginia Road
Concord, Massachusetts 01742

Herbert C. Carlson, Jr.
Division for Atmospheric Sciences
National Science Foundation
1801 G. Street, N.W.
Washington, D.C. 20546

D. P. Cauffman
Code ST-5
NASA Headquarters
Washington, D.C. 20546

S. Chandra
NASA Goddard Space Flight Center
Greenbelt, Maryland 20714

Samuel C. Coroniti
3305 Mill Spring Drive
Fairfax, Virginia 22031

M. H. Davis
Universities Space Research Association
P.O. Box 3006
Boulder, Colorado 80307

James C. Dodge
600 Independence Avenue, N.W.
Code EBT-8
Washington, D.C. 77004

Hans Dolezalek
Office of Naval Research, 462
Arlington, Virginia 22217

Bruce C. Edgar
Box 92957
Los Angeles, California 90009

Eldon Ferguson
Aeronomy Laboratory
NOAA
Boulder, Colorado 80303

Arthur A. Few, Jr.
Department of Space Physics
Rice University
P.O. Box 1892
Houston, Texas 77001

James W. Follin, Jr.
Johns Hopkins University
Applied Physics Laboratory
Johns Hopkins Road
Laurel, Maryland 20810

Stuart Gathman
6218 Colchester Road
Fairfax, Virginia 22530

Marvin A. Geller
Rosenstiel School of Marine
and Atmospheric Science
Miami, Florida 33149

Richard Goldberg
NASA/GSFC
Code 912
Greenbelt, Maryland 20771

Joseph M. Grebowsky
Code 621
NASA Goddard Space Flight Center
Greenbelt, Maryland 20771

Wolfgang E. Gringel
Department of Physics and Astronomy
University of Wyoming
Laramie, Wyoming 82071

Leslie C. Hale
IRL-PSU
University Park, Pennsylvania 16802

R. E. Hartle
NASA Goddard Space Flight Center
Greenbelt, Maryland 20771

Paul B. Hays
University of Michigan
Space Physics Research Laboratory
2455 Hayward
Ann Arbor, Michigan 48109

William Hanson
University of Texas at Dallas
Box 688
Richardson, Texas 75080

Donald Heath
Code 912
NASA Goddard Space Flight Center
Greenbelt, Maryland 20771

John R. Herman
624 Tulane Avenue
Melbourne, Florida 32901

Walter R. Hoegy
12029 Bayswater Road
Gaithersburg, Maryland 20760

R. A. Hoffman
14005 Beth Page Lane
Silver Spring, Maryland 20906

Robert Holzworth
Building A6/Room 2447
P.O. Box 92957
Los Angeles, California 90009

James Hughes
Code 465
Office of Naval Research
Arlington, Virginia 22217

William G. Johnson
E.S. 01
Marshall Space Flight Center
Huntsville, Alabama 35801

Lawrence Jones
Department of Physics
University of Michigan
Ann Arbor, Michigan 48109

Michael C. Kelley
School of Electrical Engineering
Phillips Hall
Cornell University
Ithaca, New York 14853

Paul Kintner
119 Phillips Hall
Cornell University
Ithaca, New York 14853

Derek R. Lane-Smith
Barringer Research
304 Carlingview Drive
Rexdale Ontario
Canada M9W5G2

David M. LeVine
10608 Meadowhill Road
Silver Spring, Maryland 20714

Janet Luhmann
A6/2447 Aerospace Corporation
P.O. Box 92957
Los Angeles, California 90009

Malcolm MacLeod
AFGL
Hanscom Air Force Base, Massachusetts 01731

Billy McCormac
12861 Alta Tierra
Los Altos Hills, California 94122

Robert H. Manka
Atmospheric Sciences Section
National Science Foundation
1800 G Street
Washington, D.C. 20550

Ralph Markson
46 Kendal Common Road
Weston, MA 02193

Truls E. Moe
Code 625
NASA Goddard Space Flight Center
Greenbelt, Maryland 20771

Nelson C. Maynard
Code 625
Goddard Space Flight Center
Greenbelt, Maryland 20771

Hans Mayr
Code 621
NASA Goddard Space Flight Center
Greenbelt, Maryland 20771

John D. Mitchell
Department of Electrical Engineering
The University of Texas at El Paso
El Paso, Texas 79968

Volker A. Mohnen
E.S. 324
State University of New York
1400 Washington Avenue
Albany, New York 12222

M. P. Nakada
Code 682
NASA Goddard Space Flight Center
Greenbelt, Maryland 20771

R. S. Narcisi
AFGL/LKD
Hanscom Air Force Base, Massachusetts 01731

George Newton
Code ST
NASA Headquarters
Washington, D.C. 20546

Dirk Offermann
Physics Department
Wuppertal University
Gauss Strasse 20
56 Wuppertal, Germany

Donald E. Olson
Physics Department
University of Minnesota
Duluth, Minnesota 55812

Ernest J. Ott
Code 740.1
NASA/GSFC
Greenbelt, Maryland 20771

Chung G. Park
Radioscience Laboratory
Stanford University
Stanford, California 94305

Dennis Peacock
National Science Foundation
Washington, D.C. 20006

Thomas A. Potemra
APL/SHU
Laurel, Maryland 20810

Joseph B. Reagan
Lockheed Research Laboratory
D/52-12 B 205
3251 Hanover Street
Palo Alto, California 94304

George C. Reid
Aeronomy Laboratory, NOAA
Boulder, Colorado 80302

George R. Ricker
M.I.T. Center for Space Research
Room 37-527
77 Massachusetts Avenue
Cambridge, Massachusetts 02139

Raymond G. Roble
NCAR, Box 3000
Boulder, Colorado 80307

James M. Rosen
Department of Physics & Astronomy
University of Wyoming
Laramie, Wyoming 82071

T. J. Rosenberg
IPST - University of Maryland
College Park, Maryland 20742

Lothar H. Ruhnke
NRL Code 8320
Washington, D.C. 20375

J. Doyne Sartor
NCAR
Box 3000
Boulder, Colorado 80307

E. R. Schmerling
Code ST-5
NASA Headquarters
Washington, D. C. 20546

Jan C. Siren
I.P.S.T. University of Maryland
College Park, Maryland 20742

Leslie G. Smith
2305 Southmoor Drive
Champaign, Illinois 61820

N. W. Spencer
12013 Remington Drive
Silver Spring, Maryland 20902

Masahisa Sugiura
Code 625, Goddard Space Flight Center
Greenbelt, Maryland 20771

Edward P. Szuszczewicz
Naval Research Laboratory
4555 Overlook Avenue, S.W.
Washington, D.C. 20375

Richard M. Thorne
Department of Atmospheric Science
U.C.L.A.
Los Angeles, California 90024

Shelby G. Tilford
8805 Church Field Lane
Laurel, Maryland 20811

H. Volland
Radioastronomisches Institut
University of Bonn
5300 Bonn-Endenich
Auf dem Hugel 71
Germany

Richard Vondrak
Radio Physics Laboratory
SRI International
Menlo Park, California 94025

Bernard Vonnegut
Atmospheric Sciences Research Center
State University of New York
Albany, New York 12222

James W. Warwick
283 South Lake Avenue 218
Pasadena, California 91101

Andrew J. Weinheimer
Space Physics Department
Rice University
Houston, Texas 77025

Eugene Wescott
Geophysical Institute
Fairbanks, Alaska 99701

T. D. Wilkerson
IPST University of Maryland
College Park, Maryland 20742

Roger Williamson
Physics Department UMC - 41
Utah State University
Logan, Utah 84322

John C. Willett
Code 8325
Naval Research Laboratory
Washington, D.C. 20375

Michael Wiskerchen
175 South Reynolds Ap K101
Alexandria, Virginia 22304

ACKNOWLEDGEMENTS

The accomplishments of the meeting are attributable to the diligent efforts of the program committee, most of whom also served as Group Chairman or Reporters. The Group Chairmen, C. G. Park, P. B. Hays, and R. Narcisi, were effective in amalgamating the discussions from diverse scientific disciplines into a coherent program. The Select Panel of S. A. Bowhill, W. B. Hanson, G. C. Reid and H. Volland helped to focus the recommendations to the critical issues. The Select Panel, C. G. Park, R. Narcisi, L. G. Smith (for P. B. Hays), D. P. Cauffman, and M. Sugiura assisted in the review and editing process. C. G. Park and R. Narcisi drafted significant portions of Chapter II. Helpful comments were also received from M. Dubin and A. C. Aikin.

I thank the authors of the tutorial papers for the timely completion of their comprehensive works.

Thanks also go to the American Geophysical Union who, under the guidance of Ms. Merideth Compton expertly managed the logistics of the meeting.